



AMERICAN UNIVERSITY OF BEIRUT

A NOVEL IN-SITU TEST SETUP FOR MEASURING THE  
INTERFACE RESISTANCE BETWEEN PIPELINES AND SOILS

by  
ROBA DARWICH HOUHOU

A dissertation  
submitted in partial fulfillment of the requirements  
for the degree of Doctor of Philosophy  
to the Department of Civil and Environmental Engineering  
of the Maroun Semaan Faculty of Engineering and Architecture  
at the American University of Beirut

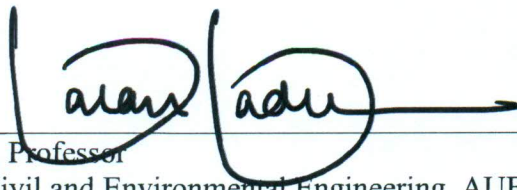
Beirut, Lebanon  
April 2021

AMERICAN UNIVERSITY OF BEIRUT

A NOVEL IN-SITU TEST SETUP FOR MEASURING THE  
INTERFACE RESISTANCE BETWEEN PIPELINES AND SOILS

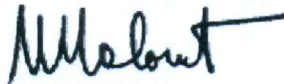
by  
ROBA DARWICH HOUHOU

Approved by:



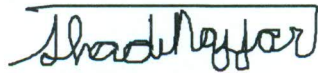
Dr. Salah Sadek, Professor  
Department of Civil and Environmental Engineering, AUB

Advisor



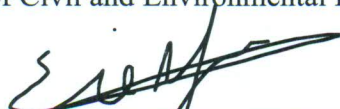
Dr. Mounir Mabsout, Professor  
Department of Civil and Environmental Engineering, AUB

Chair of Committee



Dr. Shadi Najjar, Associate Professor  
Department of Civil and Environmental Engineering, AUB

Member of Committee



Dr. Elie Shammas, Associate Professor  
Department of Mechanical Engineering, AUB

Member of Committee



Dr. Muhsin Rahhal, Professor  
Civil Engineering Department of the Faculty of Engineering, USJ

Member of Committee



Dr. Hussein Mroueh, Professor  
Department of Civil Engineering, Université de Lille

Member of Committee

Date of dissertation defense: April 1, 2021

# AMERICAN UNIVERSITY OF BEIRUT

## DISSERTATION RELEASE FORM

Student Name: \_\_\_\_\_ Houhou \_\_\_\_\_ Roba \_\_\_\_\_ Darwich \_\_\_\_\_  
Last First Middle

I authorize the American University of Beirut, to: (a) reproduce hard or electronic copies of my dissertation; (b) include such copies in the archives and digital repositories of the University; and (c) make freely available such copies to third parties for research or educational purposes:

- As of the date of submission
- One year from the date of submission of my dissertation.
- Two years from the date of submission of my dissertation.
- Three years from the date of submission of my dissertation.



13/04/2021

---

Signature

Date



## ACKNOWLEDGEMENTS

Suffering from one of the worst economic crises globally, along with a severe spread of the COVID-19 virus and a Blast that wiped out half of Beirut, the Lebanese community has been severely challenged, mentally physically and psychologically over the past two years. Working towards a PhD degree under such circumstances was very troubling and would have never been possible without the support, and assistance of the kind people around me, only some of whom I am giving particular mention here.

Firstly, I wish to express my sincere appreciation to my supervisor, Professor Salah Sadek, who is definitely the best mentor anyone could have ever asked for while pursuing a PhD. Your guidance and encouragement have helped me grow professionally and have set me on the path of taking the right decisions and committing to them no matter how tough things become. I will always be grateful for the unique opportunities you have granted me, and for always believing in me even when I did not believe in myself. I would have never imagined getting a job in one of the Top 10 universities globally without your help and insight. Not only have you shown me how to be better professionally in my career, but you have set an example of how I can be a better person. You are a true inspiration!

My genuine thanks also go to Dr. Shadi Najjar, my co-advisor for his guidance, encouragement, and insightful comments. Without your persistent help, the goal of this PhD would have not been realized. You have been incredibly generous with your time and energy, two things that can never be repaid. Thank you for always keeping a smile on your face and the faces of the people around you. I hope that I could be as lively, enthusiastic, and energetic as you are.

In addition to my advisors, I would like to thank Dr. Elie Shamma for his help with overcoming all the challenges related to the mechanical engineering field.

My experience at AUB has been nothing but amazing. Since my first day in the CEE labs, I have felt at home as I was surrounded by the greatest team. Mr. Helmi El Khatib, our lab manager, thank you for your patience and cooperation in helping me design and perform all lab experiments. You are the kindest person I know and I feel worry free whenever you are around. Our assistant lab manager, Dima Hassanieh, you have become more than a teammate; you are a sister that I can rely on. Thank you for being there whenever I needed emotional support or a helping hand. I know I have been very demanding during the last two years, but you and Mr. Helmi were the best support that I could have ever had. Also, I would like to thank Mr. Abed El Rahman El Sheikh, our lab supervisor, for his help with all of my experimental work.

Additionally, many appreciations go to my colleagues, Mohamad Antar, Marwa Saleh, Hiba Bashir, Sarjoun Hassan, Abed Mikati, Joseph Ghanem, Mohamad El Ahmad, Mirna Kassem, Abir Awad, and Amir Arab for the interesting and fun times we had over the last 4

years. In particular, I am grateful for Mohamad Antar and Imad El Chiti for helping me during my long nights of testing and experimentations. Without your effort, I could not have finished my Thesis on time. Your insightful comments were crucial towards enhancing the experimental procedure and thus reaching better results.

Getting through my dissertation required more than academic support. I have many people to thank for being there and having to tolerate me during the hardest times over the past 4 years. I cannot finish expressing my gratitude and appreciation for my dearest friends Rawan and Jana. Rawan, you have been unwavering in your personal and emotional support not only during my PhD, but also for the past 10 years since I first knew you. You make me feel seen and heard and I love you and thank you for that. Jana, we have overcome together the difficulties of our undergraduate studies, and I am very grateful for you having been standing by side during all the rough times even if you were living abroad. My sincere thanks go to Ali and Reem for always being there and for all the memorable moments that we created together.

Most importantly, none of this could have happened without my family. To my parents and my sisters, you have always believed in me, supported me and never doubted or questioned my abilities. You have given me the strength to keep moving forward. This dissertation stands as a testament to your unconditional love and encouragement.

# ABSTRACT OF THE DISSERTATION OF

Roba Darwich Houhou

for

Doctor of Philosophy

Major: Geotechnical Engineering

Title: A Novel In-Situ Test Setup for Measuring the Interface Resistance between Pipelines and Soils

Offshore hydrocarbon transport pipelines operate at relatively high pressures and temperatures. These operation conditions lead to their expansion and/or contraction and may ultimately result in pipeline buckling or “walking” after multiple cycles of operation. Such movements are typically resisted by the pipe-soil axial resistance at the interface, which controls the compressive forces within the pipeline itself. Any errors in establishing the interface resistance will lead to either an over-estimation of pipeline extension or of high compressive stresses possibly leading to buckling. Such erroneous assumptions/outcomes will have significant impacts as to the necessary costs to mitigate their effects. The actual axial interface response whether in the short or longer terms is a function of many factors such as the pipe laying process, the consolidation periods, the shearing rate, the interface roughness, and the weight of the pipeline itself. Reliable and efficient design methodologies are thus needed to optimize the engineering performance of the pipelines while minimizing testing and construction costs. To date, different testing techniques have been adopted in the quest for an accurate estimation of the axial pipe-soil resistance throughout the operational life of the pipeline. These include laboratory soil element testing, laboratory model testing, and in-situ testing using specialized, complex and costly apparatuses. Given their nature and the fact they involve seabed soils in their actual/real conditions, in-situ tests provide the most reliable results. However, they are limited by the very small number of available specialized field equipment, e.g. the Fugro SMARTPIPE, and recently developed “pipe-like” penetrometers, both of which suffer from many draw backs related to their high cost, practicality and testing conditions. The work presented in this thesis presents an attempt at addressing most of the limitations that were identified in the currently available methods, leading up to the development of a new in-situ, cost-effective apparatus for measuring the axial pipeline resistance. The new proposed, designed, built and lab-validated setup directly targets the limitations of currently available systems. The new apparatus was conceived with a particular focus on eliminating the problem of passive stresses generated at the pipe ends, and delivering a cost-effective and reliable solution for conducting in-situ interface tests. A laboratory proof of concept

experimental setup that could be adapted/automated in future work to become an autonomous field apparatus was thus designed, produced, and tested on a clay bed and under different testing conditions. The tested prototype reliably captured the effect of drainage conditions, normal stress, and rate of loading on the interface resistance. It produced accurate drained interface friction factors that are comparable to the ones obtained from the direct shear tests on the same soil and interface. Under undrained conditions, the measured interface response was realistic but the test section exhibited slight rotations in all directions that affected the pore pressure readings. The results obtained are very promising and confirmed the practicality and functionality of the proposed setup/prototype. Furthermore, these results revealed the need for some improvements that we intended to apply in future work and that would enhance the testing effectiveness and reliability. Part of the background validation work that was done in this thesis was dedicated to compare the interface test results obtained using the two most common laboratory testing methods: the tilt table and the interface direct shear test apparatus. Both sets of laboratory equipment were used to test the drained clay-solid interface response for different soil composition (high and low plasticity clay), interface roughness (smooth and rough), and the applied normal stress. The comparison suggested that using the Interface Direct Shear machine for determining the drained residual pipe-soil interface resistance is a practical and reliable testing alternative, provided that the conventional direct shear setup is properly modified to reduce mechanical friction and make it amenable to low pressure testing.

# TABLE OF CONTENTS

ACKNOWLEDGEMENTS .....	1
ABSTRACT .....	3
ILLUSTRATIONS .....	9
TABLES .....	16
1. INTRODUCTION .....	17
2. BACKGROUND REVIEW .....	24
2.1 Fundamental Aspects of pipe-soil interaction: .....	24
2.1.1 Pipeline Embedment: .....	25
2.1.2 Axial and Lateral Pipeline Movement: .....	27
2.2 Seabed Characterization .....	29
2.2.1 In Situ testing .....	29
2.2.2 Soil Sampling .....	33
2.3 Available methods for predicting the axial pipe-soil interaction .....	35
2.3.1 Soil Element Tests: .....	37
2.3.2 Model Tests .....	49
2.3.3 In-situ Tests .....	57
2.4 Design approaches .....	64
2.4.1 $\alpha$ and $\beta$ approaches .....	65
2.4.2 Pipe-Soil Interaction Framework .....	66

### 3. DRAINED AXIAL PIPE-SOIL RESISTANCE USING TILT

#### TABLE AND DIRECT SHEAR TESTS ..... 73

3.1	Introduction .....	73
3.2	Testing Materials .....	76
3.2.1	Soils .....	76
3.2.2	Interfaces.....	78
3.3	Interface direct Shear Testing.....	79
3.3.1	Modified Direct Shear Apparatus .....	79
3.3.2	Testing Procedure .....	81
3.4	Tilt Table Testing .....	83
3.4.1	Tilt Table Apparatus .....	83
3.4.2	Testing Procedure .....	83
3.5	Testing Program .....	86
3.6	Experimental Results and Discussion .....	87
3.6.1	Direct Shear Tests .....	87
3.6.2	Discussion of Direct Shear Results.....	94
3.6.3	Comparison between Tilt Table and Interface Direct Shear.....	106
3.7	Conclusions .....	112

#### 4. A NOVEL IN-SITU SETUP: DESIGN AND PROOFING .... 114

4.1	Introduction .....	114
4.2	Design of the in-situ setup.....	116
4.2.1	Concept .....	116
4.2.2	Design Model.....	116
4.3	Instrumentation.....	122
4.3.1	Load Cell.....	122
4.3.2	LVDT.....	123
4.3.3	Pore Pressure Sensor.....	123
4.3.4	Digital Camera and Computer vision approach.....	126

4.4	Data Acquisition .....	129
4.5	Validation Tests .....	130
4.5.1	Preparation of the Clay Test Bed .....	131
4.5.2	Testing Procedure .....	133
4.5.3	Preliminary Results .....	134
4.5.4	Setup Improvements .....	137
4.6	Shear strength of soft clay using miniature ball penetrometer, vane shear, UU triaxial tests and direct shear tests.....	138
4.6.1	Preparation of Element Soil Samples .....	139
4.6.2	Miniature ball penetrometer apparatus .....	140
4.6.3	Vane shear apparatus .....	142
4.6.4	Testing Procedure .....	144
4.6.5	Estimation of the undrained shear strength of clay and c/p ratio.....	147
4.6.6	Evaluation of the resistance factor .....	152
4.7	Conclusion.....	154

## 5. PIPE-SOIL RESISTANCE USING A NOVEL TEST

SETUP .....	157	
5.1	Introduction .....	157
5.2	Experimental Program.....	157
5.2.1	Test Soil .....	157
5.2.2	Test Sequences.....	163
5.3	Results from tests using the Stainless Steel Interface .....	166
5.3.1	Penetration and Consolidation Response.....	166
5.3.2	Clay/Pipe Interface Resistance .....	173
5.4	Results of Sandpaper interface testing .....	198
5.4.1	Penetration and Consolidation response: .....	198
5.4.2	Interface Response during Shear (Sandpaper).....	202
5.5	Post-test penetration tests .....	209
5.6	Comparison between smooth and rough interface responses .....	210

5.7	Evaluation of the new test setup (comparison with interface direct shear) ..	211
5.8	Conclusion and Recommendations .....	218
<b>6.</b>	<b>CONCLUSIONS AND RECOMMENDATIONS .....</b>	<b>222</b>
6.1	Thesis findings.....	222
6.2	Suggestion for future research.....	225
6.2.1	Setup Improvements: .....	226
6.2.2	Uncovered Aspects .....	227
	<b>APPENDIX A.....</b>	<b>228</b>
	<b>REFERENCES .....</b>	<b>232</b>



# ILLUSTRATIONS

## Figure

1.	Global crude oil production: (a) between onshore and offshore and (b) by water depth (US Energy Information Administration, October 2016).....	25
2.	Global offshore oil and natural gas production by water depth in the New Policies Scenario (IEA, 2018).....	25
3.	Lateral Buckles from Side-scan Surveys ( Bruton et al., 2010) .....	29
4.	Ball and T-bar penetrometer : (a) Schematic and Image of ball and T-bar penetrometer with typical dimensions and (b) Typical penetration results (Dejong et al 2010).....	33
5.	(a) The box core rigging system – (b) DMS on the Box corer (H. E. Low et al., 2008) .....	35
6.	Modified Direct shear device in the University of Western Australia (White et al., 2012). .....	41
7.	Typical (a) Shear stress - displacement and (b) Settlement – displacement response at 0.1 mm/s shearing rate (White et al.,2012).....	42
8.	Drained Interface response: (a) Shear Stress - Displacement and (b) Residual Stress - Normal Effective Stresses (Boukpeti & White, 2017) .....	43
9.	Undrained Interface Response: (a) (a) Shear Stress - Displacement and (b) Shear Stress – Cumulative displacement (Boukpeti & White, 2017b) .....	43
10.	General view of ring shear apparatus (Eid et al., 2015) .....	46
11.	Tilt table frame and sliding of the plate at failure ( Najjar et al., 2007).....	47
12.	Photograph of Cam-shear test setup (Ganesan et al.,2014) .....	48
13.	Peak friction coefficient in function of OCR for:(a) Smooth Interface and (b) Rough Interface (Ganesan et al., 2014).....	48
14.	Photograph and Schematic diagram of the Cam-Tor machine (Kuo et al., 2015).....	49
15.	Schematic diagram of the model test in the University of Cambridge (White et al., 2011) .....	51
16.	Schematic diagram of Smith and White (2014) setup. ....	53

17. Assembled model pipe, S-shaped axial load cell and loading arm.....	54
18. Residual axial friction: (a) Constant rate tests and (b) variable rate tests (Boylan et al. 2014).....	55
19. Photograph of the macro-scale interface direct shear test device (Wijewickreme et al., 2014).....	56
20. Schematic Detailing of SMARTPIPE (Hill & Jacob, 2008) .....	59
21. The interface axial response from (Ballard & Jewell, 2013): (a) Axial resistance vs displacement and (b) axial friction factor vs normal stress. ....	61
22. - Schematic of ROV-based drag test concept. ....	61
23. The "Pipe -like" penetrometer apparatus detailing (Schneider et al., 2020).....	63
24. Mechanism controlling axial pipe-soil resistance (Boukpeti & White, 2017) .....	67
25. Shear strength ratio variation with interface roughness under: (a) undrained conditions and (b) drained conditions (Westgate et al., 2018).....	68
26. Power law function developed by Boukpeti & White (2017) .....	69
27. (a) Critical state model to capture the effective stress variation with shearing cycles and (b) The residual axial resistance change with number of cycles (Low et al., 2017). ....	71
28. Residual stress ratio variation with shearing rates for : (a) Normally consolidated clay (White et al., 2012) and (b) Overconsolidated clay (Boylan et al., 2014).....	72
29. Tested soils: (a) Low Plasticity Clay, (b) High Plasticity Clay, and (c) Kaolinite.....	77
30. Gradation curves of the tested soils .....	77
31. SEM images of (a) LPC, (b) HPC, (c) Stainless Steel, and (d) Sandpaper .....	78
32. The 90x60 mm interfaces: (a) Plexiglass, (b) Stainless Steel, and (c) Sandpaper, fitted into the lower shear box of the interface direct shear apparatus.....	79
33. Modification made to the standard direct shear testing machine .....	80
34. (a) Tilt table test setup, (b) 2mm clay specimen, and (c) Additional loading .....	84
35. Slipping phase at failure .....	86
36. Consolidation curves for (a): clay-clay and clay-interface tests: (b): clay-stainless steel, and (c): clay-sandpaper at a $\sigma'_n$ of 4.26 kPa.....	89

37. Variation of coefficient of consolidation with effective normal stress for (a): LPC, (b): HPC, and (c) KAO.....	89
38. Results of the clay-clay direct shear tests on LPC and HPC soil .....	91
39. Results of the clay-solid direct shear tests on LPC and HPC with stainless steel .....	92
40. Results of the clay-solid direct shear tests on LPC and HPC with Sandpaper .....	93
41. Variation of the drained secant residual friction angle with the logarithm of the normal stress for (A) HPC and (B) LPC.....	96
42. The nonlinear failure envelopes and the corresponding best-fit <i>a</i> and <i>b</i> parameters for the power-law function for all interfaces.....	97
43. The variation of the drained residual friction ratio with the roughness.....	99
44. Failure mechanism of HPC on the (a) Stainless Steel and (b) Sandpaper.....	99
45. Comparison between peak and residual interface efficiencies .....	101
46. Internal and Interface Shear Stress Responses for LPC, HPC and KAO for (a): soil-soil, (b): rough sandpaper and (c): smooth steel.....	102
47. Effect of Plasticity Index on (a) residual clay and (b) residual interface strength .....	103
48. Contrast between the smooth and rough interfaces and the LPC and HPC.....	104
49. Variation of the residual interface efficiency with the normalized roughness .....	105
50. Failure mechanism of the Low Plasticity Clay on: (a) the Stainless Steel and (b) the Sandpaper .....	106
51. Drained residual friction angles of (a): LPC, (b): HPC, and (c): KAO sheared against all interfaces using the tilt table .....	108
52. Comparison between the residual friction angles measured in the tilt table and direct shear setups for (a) LPC, (b) HPC, and (c) Kaolinite.....	109
53. Comparison between the failure envelopes from tilt table and direct shear setups.....	110
54. Comparison between the interfaces residual angles from tilt table and interface direct shear tests.....	111
55. 3D view of the in-situ setup.....	117
56. In- situ setup model using SOLIDWORKS.....	118

57. 3D Printed mid-section: (a, b) top view, (c) bottom view and (d, e) front view. ....	121
58. Schematic of the in-situ setup.....	122
59. Pore pressure sensor and cap .....	124
60. Calibration setup of the pore pressure sensor. ....	125
61. Calibration curves of the pressure sensor. ....	125
62. Flowchart of computer vision-based displacement measurement. ....	128
63. Validation Test: Patterns on the frame and detection procedure .....	129
64. Clay Bed Preparation Steps: (a) Empty bed, (b) Gravel layer, (c) Filled with clay,(d) Covered with geotextile and (e) loaded by steel plates .....	132
65. Consolidation curves of (a) the clay slurry under 1.4 kPa and (b) the pipe section under an estimated normal stress of about 3.55 kPa.....	133
66. The setup inside the clay bed before shearing initiation.....	134
67. Time histories for (a) axial displacement and (b) axial resistance during test .....	136
68. Variations of the mobilized interface friction angle and coefficient with displacement .....	136
69. Comparison between interface direct shear and tilt table results and the model results .....	137
70. Ball Penetrometer Apparatus: (a) Fixed on the tank's frame to test the clay bed and (b) Testing a clay sample.....	142
71. Vane shear apparatus and various testing stages. ....	144
72. Stress-rotation responses from vane shear tests.....	150
73. Undrained direct shear results: (a) Shear-stress responses and (b) Settlements. ....	151
74. Deviatoric stress vs axial strain for UU-triaxial tests. ....	151
75. Penetration resistance for a 1D consolidated sample to 49 kPa. ....	152
76. (a) Penetration Resistance Profiles and (b) undrained shear strength profiles with $N_{ball} =$ 13.5 .....	154
77. Theoretical $N_{ball}$ factors. ....	154

78. Consolidation with time after re-forming and loading the clay bed. ....	159
79. Measured penetration resistance at (a) Location 1, (b) Location 2, and (c) Location 3. .....	161
80. (a) Effective vertical stresses, (b) Water content and (c) Undrained shear strength variation with depth. ....	161
81. Compression curves of the tested clay.....	162
82. Cyclic curves: (a) Penetration resistance and (b) normalized penetration resistance..	163
83. (a) Pore pressure measurements during pipe laying process, (b) dissipation of pore pressure post-lay, and (c) consolidation post lay.....	167
84. Setup after consolidation .....	168
85. Variation of the pipe settlement and excess pore pressure with time during the second penetration and subsequent consolidation under dead weights of 27 kgs. ....	169
86. Variation of the pipe swelling and excess negative pore pressure with time upon pipe unloading. ....	169
87. Undrained penetration stage of the setup using a hydraulic jack. ....	171
88. Pore pressures generation and dissipation during and after (a) undrained penetration and (b) application of dead weights in Stage 3.....	172
89. (a) Soil swelling and (b) pore pressure dissipation due to dead weight unloading in stage 3. ....	172
90. Soil berms around the setup and the created shearing path in Stage 3. ....	172
91. Dissipation time-histories of excess pore pressure at the pipe invert normalized by the initial excess pore pressure under applied load plotted against the time factor, T after pipe penetration in each stage.....	173
92. The axial response during F1-S1: (a, b) shear-stress variation, (c, d) excess pore pressures at the pipe invert and side. ....	174
93. Net Pore Pressures during F1-S1 at the setup: (a) invert and (b) side.....	178
94. The accumulated soil pushed by the test section during shearing in a previous sweep .....	179
95. Rotation angles of the test section during F1-S1. ....	181

96. Position of the Center of rotation.....	181
97. (a) Rotation displacement and (b) Net displacement of the test section (F1-S1) .....	181
98. The normal stress distribution under the test section for the maximum applied load.	182
99. Shear response during undrained cycles F2, F3 and F4. ....	184
100.Pore pressures during F2, F3, and F4 at: (a) invert and (b) side of the test section. ...	184
101.Drained clay/steel interface response during sequence 1. ....	185
102.(a) Variation of peak friction factor with waiting period prior shearing cycle and (b) the Peak to minimum resistance ratio with shearing cycles. ....	186
103.Undrained response in Stage 2: (a, b) shear stress variation and pore pressure generation at (c) the invert and (d) the side. ....	188
104.Drained interface response in Stage 2 ( $\sigma_n = 3.0$ kPa).....	190
105.Undrained response in Stage 3: (a, b) shear stress variation and Pore pressure generation at (c) the invert and (d) the side. ....	192
106.Drained interface response in Stage 2 ( $\sigma_n = 2.1$ kPa).....	193
107.Visual of the Pipe Embedment for the three Stages of Testing .....	194
108.Comparison between the Undrained Interface Responses of the Smooth Pipe at Different Embedment Levels (Stage 1 to Stage 3).....	195
109.Comparison between the Drained Interface Responses of the Smooth Pipe at Different Embedment Levels (Stage1 to Stage 3).....	195
110.Variation of peak and minimum friction factors with shearing cycles during (a) Stage 1, (b) Stage 2 and (c) Stage 3.....	197
111.Effect of normal stress on: (a) peak friction factor and (b) minimum friction factor for Undrained Shearing Cycles .....	198
112.The setup placed in the middle of the clay bed during the second test and the sandpaper interface fixed around the test section. ....	199
113.The settlement of the setup following pipe laydown in Stage 1.....	200
114.The settlement and the excess pore pressure observed during Stage 2 and the subsequent consolidation.....	201

115.(a) Soil swelling and (b) negative pore pressure dissipation during unloading in Stage 2. .....	201
116.The setup settlement and the excess pore pressure during loading and the subsequent consolidation in Stage 3.....	202
117.(a) Soil swelling and (b) pore pressure dissipation during unloading in Stage 3. ....	202
118.Embedment of Rough sandpaper interface in Stages 1 to 3 .....	202
119.Undrained shear cycles results during Stage 1: (a, b) shear stresses, (b) pore pressure and (c) settlements .....	203
120.(a) Rotation angle in the z-direction, (b) sheared soil, and (c) dragged soil in S1. ....	205
121.Drained response of the sandpaper-clay interface during Stage 2 and Stage 3 (a) shear stress versus displacement, and (b) rotation angle versus displacement. ....	208
122.Comparison between the interface shear response in the “fast” test of Stage1 with the responses observed in the drained tests of Stages 2 and 3.....	209
123.Ball penetrometer profiles before and after testing with (a) Smooth Interface and (b) Rough Interface. ....	210
124.Friction factors variation for the sandpaper and stainless steel interfaces during (a) drained cycles and (b) undrained cycles. ....	211
125.Comparison between the interface direct shear results and the novel pipe model interface test results. ....	213
126.Comparison between the clay/clay internal strength (direct shear) and the interface tests with the novel rough pipe model. ....	216
127.Peak and residual drained friction factors from interface direct shear and the novel pipe model tests. ....	216

## TABLES

### Table

1. Applicability- reliability of interpreted soil parameters (Lunne et al., 2011).....	31
2. Element tests for measuring interface shear resistance (Westgate et al. 2018) .....	39
3. Summary of published experimental studies that are based on laboratory scale pipe-soil element interface tests.....	40
4. Properties of clays used in the experimental program.....	77
5. Measured percent reduction in normal stress due to friction in the box.....	82
6. Comparison between the LVDT and patterns displacements.....	129
7. Properties for Vane and Ball Penetrometer Soil Specimens .....	140
8. Summary of vane shear, direct shear and UU tests. ....	150
9. Shearing sequence for the case of the stainless steel interface. ....	165
10. Shearing Sequence parameters in case of sandpaper interface.....	165



# CHAPTER 1

## INTRODUCTION

The high demand on hydrocarbons has led to an ever-increasing development of offshore fields that are now approaching very deep water sites (3000 m). In deep water, the cost of flowlines and pipelines that export hydrocarbon products to offshore and onshore storage facilities constitutes a significant portion of the overall project cost. Reliable and efficient design methodologies are thus needed for offshore pipelines to optimize their engineering performance while minimizing construction and testing costs. A main parameter that has been shown to govern the engineering response of pipelines against operational loads is the soil-structure interaction at the interface between the pipeline and the surrounding soil. Modeling this interaction with realistic/robust methodologies is key for optimizing the design of pipelines and reducing their cost.

Offshore pipelines operate at high pressure and high temperature which cause the pipeline's expansion and contraction and ultimately the pipeline's buckling or walking after cycles of operations. Such movements are resisted by the pipe-soil interface axial resistance which in turn dictates the buildup of compressive forces within the pipeline walls. Underestimation of the axial resistance may lead to low predicted compressive forces and excessive pipeline expansion which requires costly mitigation solutions for the termination structures at the ends of the pipeline. In contrast, overestimation of the axial resistance may lead to high predicted compressive forces and thus numerous lateral buckles which require expensive restraining structures for mitigation.

A complicating factor in modeling the response of offshore pipelines is the dependency between the mobilized interface resistance and the drainage conditions at the pipeline-soil interface. The drainage conditions have been reported to shift from fully undrained to fully drained conditions during the pipeline's operational life (Ballard & Jewell, 2013; Boukpeti & White, 2017; White et al., 2012 and Boylan et al., 2014). Such transition is expected to have a significant effect on the mobilization of the interface strength which has been shown to be controlled by (1) the lay process which generally remolds the soil, (2) the pore pressure dissipation after laying the pipeline, and (3) consolidation due to either the pipe weight or the following shearing events. Therefore, an accurate characterization of the axial pipeline response under each of these conditions is crucial for a robust pipeline design.

Many researchers have tried to quantify the key parameters of the axial pipe-soil resistance using laboratory soil element testing, laboratory model testing, and in-situ test apparatuses. The main parameters that were varied in these studies are the roughness of the pipe-soil interface, the shearing rates, the consolidation periods and the loading history.

Since shallow seabed sediments are generally soft with relatively low shear strengths (less than 10 kPa), conventional laboratory apparatuses such as the interface direct shear and ring shear are not naturally designed and constructed for testing in this relatively low pressure range. In the literature, several attempts have been made to modify conventional laboratory test apparatuses and adapt them to the conditions of low pressure testing. These attempts targeted correcting for the effect of friction in the test device and increasing the sensors' sensitivity to measure relatively small forces (Boukpeti & White,

2017; Hill et al., 2012; Westgate et al., 2018; White et al., 2012 and Eid et al., 2015).

Results from the modified element test setups showed that they can sufficiently capture the interface response under different test conditions in the low pressure range. In parallel to modifying existing test setups, several attempts have been made to design and construct laboratory testing methodologies that specifically target interface testing in the low pressure range. Examples include the tilt table test setup and the cam-tor device ( Najjar et al., 2003; Najjar et al., 2007 and Pedersen et al., 2003; De Brier et al., 2016; and Kuo et al., 2015).

The main limitation in laboratory interface test setups is that they are conducted with remolded soil specimens that are reconstituted in the lab after being extracted from offshore sites typically using box core samplers. Such sampling and testing techniques do not reflect the in-situ structure of the soil, which is generally disturbed and remolded in the sampling procedure and the preparation of the test specimens.

This limitation in laboratory testing instigated several efforts that targeted measuring the axial pipe-soil resistance in-situ. Such in-situ testing tools are very few, the most important of which is the Fugro SMARTPIPE testing system which is associated with relatively high testing costs and complicated testing methodologies ( Ballard & Jewell, 2013; Hill & Jacob, 2008; Schneider et al., 2020; Stanier et al., 2015; White et al., 2011). Recently, novel “pipe-like” penetrometers have been designed by Schneider et al. (2020) and introduced as viable field testing systems that have yet to be tested and deployed in actual offshore projects.

The selection of realistic design values for the pipe-soil interface resistance is important given the significant impact on the cost of the pipeline system. The uncertainty in

the soil/pipe interface resistance (particularly at the early stages of design) may necessitate the adoption of highly conservative design values (lower-bound interface friction coefficients) that will eventually lead to oversized pipes. In addition to the increase in material costs, there are significant installation costs that will be incurred given the compounded challenges that are associated with installing large diameter pipes.

Based on the above, it could be stated with confidence that there is a clear need for efficient cost-effective methodologies that will allow for a characterization of the seabed/pipe interface interaction with a high level of confidence, while reflecting the spatial variability in the interface interaction along the pipeline route. A study of the state-of-practice experimental testing options shows clearly that available options do not fulfill this need due to the following two reasons.

First, laboratory-based approaches for measuring the interface resistance between pipeline and soils are generally conducted after the concept stage and in many cases after the front end engineering design (FEED) stage. At this late stage of the project, many important decisions would have already been made and many resources would have already been exhausted, reducing the ability of the designer to fully optimize the design of the pipeline. There is a need for a testing technique/methodology that would allow for quantifying the interface resistance between the pipe and the soil in the FEED stage, if not at the concept stage of the project. This need cannot be fulfilled using the laboratory-based model interface tests since they all require that the site investigation and sampling be already initiated/implemented.

Second, the argument above points to the need for conducting in-situ tests to measure the interface resistance possibly at an early stage in the project, whereby the value of the measurements could be maximized in the context of pipeline design. This need was the impetus for FUGRO to design and implement the smartpipe field testing system. The main limitation in the FUGRO testing system is its implementation cost. The smartpipe test setup is relatively complicated and consists of a pipe section that is suspended underneath a frame by means of a hydraulically activated trolley system. The system is deployed via a lifting cable from vessels equipped with a 20-tonne capacity frame that is 5m wide and 7m tall. Given the complexity of the mechanisms involved and the need for the vessel to be present, conducting a test using the smartpipe system at any given location is relatively costly. If multiple tests are to be conducted at several locations along the pipeline route to characterize the variability in the interface characteristics, the associated costs of testing may become prohibitive. As a result, there is a clear need for an alternative testing methodology that would allow for conducting multiple tests to characterize the spatial variability in the interface friction characteristics in the field while minimizing cost and time.

This thesis aims at designing and constructing an innovative, cost-effective, and reliable mechanism to quantify the interface resistance between offshore pipelines and soils in-situ. The work focused on implementing a laboratory proof of concept experimental setup that could be adapted/automated in future work to become an autonomous field test setup for measuring the interface resistance between pipes and soils in the field in their undisturbed state. The proposed mechanism have the capacity to be deployed on the seabed

and displaced in a controlled environment while measuring the soil-artifact interface resistance.

In the following chapters, a literature review on the offshore pipelines behavior was first presented (Chapter 2). The fundamental aspects of the pipe-soil interface resistances were initially highlighted to explain the importance of a reliable estimation of this resistance. An accurate estimation of the interface resistance requires first an understanding of the seabed types, behaviors and strength and thus the different testing methodologies used to characterize a seabed were reported. As for the interface resistance predication methods, all the adopted testing techniques were discussed along with their main outcomes, advantages, and disadvantages. The design approaches of offshore pipeline based on the outcomes of all the experimental tests were also included. This comprehensive background review indicated that the two most common laboratory testing approaches used for measuring the interface strength between pipelines and clays are the tilt table test and the interface direct shear test but there no published efforts that show a direct comparison between their results. This comparison was established in Chapter 3 of this thesis. This chapter includes the design and fabrication of a tilt table and an interface direct shear setups capable of accurately estimating the drained interface resistance at low normal stresses in addition to comparing their results under identical testing conditions. Both setups tested the drained clay-solid interface response varying the soil composition (high and low plasticity clay), the interface roughness (smooth and rough), and the normal stress range. In addition, these results were used to assess the quality of the novel setup outputs. In Chapter 4, the detailed design of the novel setup was presented that mainly addresses the limitations of

previously studied systems with particular focus on eliminating the passive stresses at the pipe ends and establishing a cost-effective mechanism for conducting the in-situ interface test in the most economical way possible. The results of a validation test performed on soft clay were also reported. In addition, the design and calibration of a ball penetrometer apparatus used to measure the clay's undrained shear strength were incorporated. The efficiency and functionality of the proposed in-situ setup were checked in Chapter 5 where the setup was tested under different testing conditions inside a soft clay bed.

## CHAPTER 2

### BACKGROUND REVIEW

#### **2.1 Fundamental Aspects of pipe-soil interaction:**

Global offshore oil production has expanded rapidly in the last decade and accounted for nearly 30% of total oil production by the end of 2015 (Figure 1a). Most of the offshore production is in shallow waters since it is relatively cheaper and technically easier than in deep waters. However, there is a move towards deepwater projects reflected by the 25% increase of deepwater production from 2005 to 2015 (Figure 1b) owing to the exhaustion of shallow offshore resources, economic changes and technology advancements. . The oil and gas production from deepwater and ultra-deepwater is expected to increase in the next 20 years as predicted by IEA (2018) in Figure 2. The larger the distance to shore, the longer the pipelines needed to export oil and gas and thus the higher their installation cost. This has urged researchers to improve the pipeline design models as an attempt to reduce project costs without compromising safety. The most critical design issues are the pipeline deformation known as the pipeline buckling and walking due to the thermal expansion and contraction of pipelines during operations. In order to mitigate such issues, the pipe-soil interface forces must be reliably quantified while considering the pipeline embedment, the laying process, and the axial and lateral interactions along with an accurate seabed characterization.



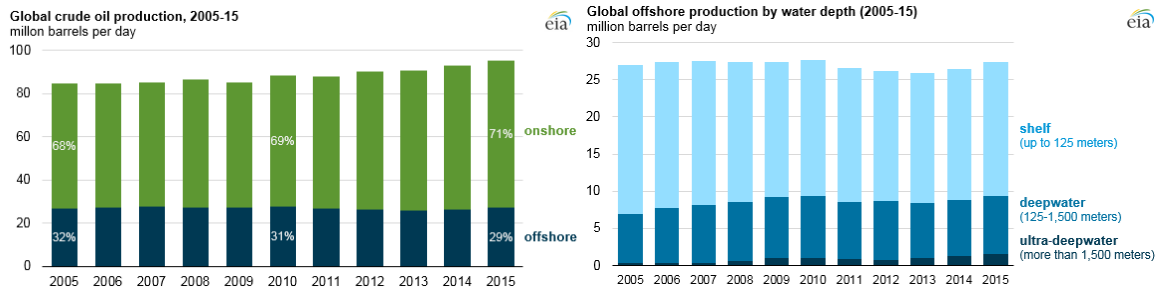


Figure 1. Global crude oil production: (a) between onshore and offshore and (b) by water depth (US Energy Information Administration, October 2016)

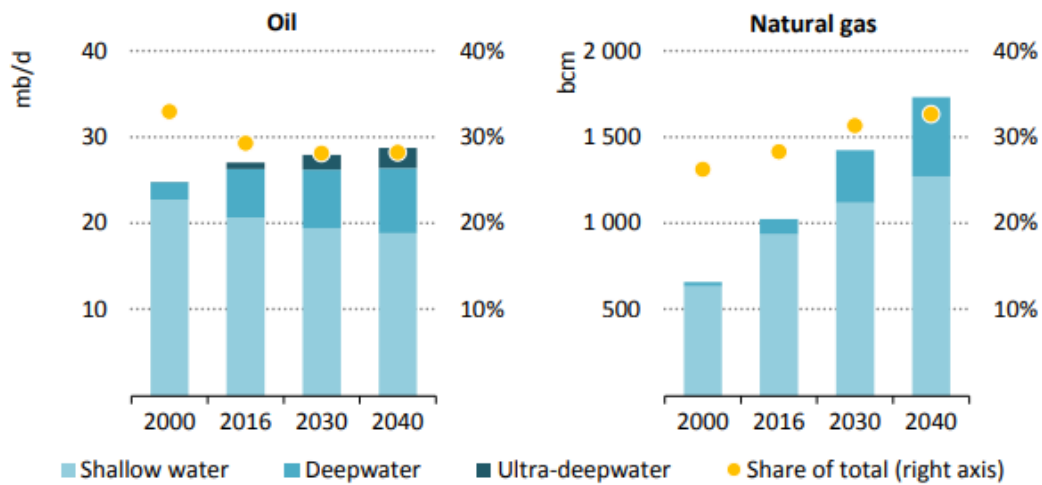


Figure 2. Global offshore oil and natural gas production by water depth in the New Policies Scenario (IEA, 2018)

### 2.1.1 Pipeline Embedment:

In deep water, the high temperature high pressure pipelines (HTHP) are directly laid on the seabed forming a certain embedment based on their self-weight, the applied forces during laying process, the soil type, and the dynamic effects due to the lay vessel's motion. In granular soils, the embedment will be minimal and usually changes during the operation

life due to sediment transport during storms or sediment build up. In soft soils, the pipeline embedment will mainly be governed by the laying forces.

Many methods are available to estimate the pipeline embedment under different conditions, which is a fundamental factor for the assessment of the lateral and axial soil resistance. The first method focuses on the estimation of the static penetration resistance,  $V$ , which is expressed as the sum of the geotechnical resistance and the resistance representing the buoyancy force of the submerged unit weight,  $\gamma'$  of the displaced soil (Equation (2.1))

$$\frac{V}{D} = aS_{u,invert}\left(\frac{w}{D}\right)^b + f_b \frac{\gamma' A'}{D} \quad (2.1)$$

Where  $D$  is the pipeline diameter,  $w$  the pipe invert embedment,  $A'$  the embedded cross-sectional area of the pipe and  $S_{u,invert}$  the shear strength at the invert level. The constants  $a$  and  $b$  vary with the shear strength and the pipe roughness (Aubeny et al., 2005; Chatterjee et al., 2012). The buoyancy factor,  $f_b$ , denotes the enhancement of the buoyancy force due to the soil heave and a typical value of 1.5 is usually used (Chatterjee et al., 2012).

Field observations show that the as-laid embedment of pipelines is higher than that estimated from only the static penetration. Such differences result from the two other mechanisms occurring during laying process which are the stress concentration at the touchdown point and cyclic embedment due to dynamic effects. During the laying process and upon pipe touch down, the contact stresses exceed the submerged weight of the pipe,  $W'$ , by a certain amount depending on the water depth, the stiffness of the seabed,  $K$ , the

bending rigidity of the pipeline, EI, and the effective tension in the pipeline in the touchdown zone,  $T_0$ . Randolph & White (2008) developed the analytical solution (2.2) to estimate the maximum vertical load,  $V_{max}$ , within the touch zone which is valid for

$$\frac{T_0^{1.5}}{((EI)^{0.5}W')^{0.25}} > 1.$$

$$\frac{V_{max}}{W'} = 0.6 + 0.4 \left( \frac{EI K}{T_0^2} \right)^{0.25} \quad (2.2)$$

The second mechanism that affects the pipe embedment is the pipe dynamic movement during lay caused by the vessel motion and hydrodynamic loading of the hanging pipe. Such movements will lead to seabed sediment softening, a reduction of its strength and thus an increase in the pipe penetration. The dynamic amplification may also enhance the vertical load at the pipe invert and the lateral pipe motion will scrape the sediments and, hence change the expected embedment. Westgate et al. (2013) proposed models to account for such dynamic movement based mainly on results from centrifuge model tests. However, White et al. (2017) discussed a base-level approach that was validated using field observations of pipeline embedment, and consists of two basic steps: (1) evaluation of the maximum vertical force using equation (2.2) and (2) evaluation of the pipeline embedment using equation (2.1) but using the remolded shear strength for the seabed sediments.

### **2.1.2 Axial and Lateral Pipeline Movement:**

HPHT pipelines are designed with a range of flexibility allowing some pipeline movement during operation under either hydrodynamic loading or under thermal and

pressure loadings which generally induce the pipeline expansion and contraction. This flexibility is permitted to avoid the generation of high thermal stresses as the pipeline temperature changes. However, the thermal and pressure loadings must be controlled as they lead to the pipeline walking and buckling after repeated cycles of startup and shutdown.

The pipeline walking is the phenomenon of axial movement accumulation of pipelines with cycles of operation due to the asymmetry of either the thermal loadings or the mobilized axial pipe-soil resistance caused by the presence of a seabed slope or end-of-line tension (Carr et al., 2006; White & Cathie, 2011). Such phenomenon will induce overstressing of connections, the loss of tension in steel catenary risers and an increase of loading within a lateral buckle (Bruton et al., 2010). To prevent these issues, rock-dumping and large hold-back anchors are usually required.

The pipeline buckling is triggered by the excessive compressive forces within the pipeline and mainly depends on the soil resistance and the pipe weight. As a result, axial forces will decrease within the buckled section permitting the accumulation of high bending strains. Figure 3 shows real footage of lateral buckles of an offshore pipeline. The considered measures to minimize lateral buckling differ from laying the pipeline in a snake profile to the use of additional supports.

All the required measurements to mitigate the pipeline walking and buckling are expensive and increase the safety hazards. Thus, one of the design solutions is to control the pipeline movement and this only can be done by an accurate estimation of the pipe-soil response. Consequently, the pipe-soil interaction must be well understood and the effect of

pipeline weight, roughness, embedment and the seabed properties must be reliably captured.

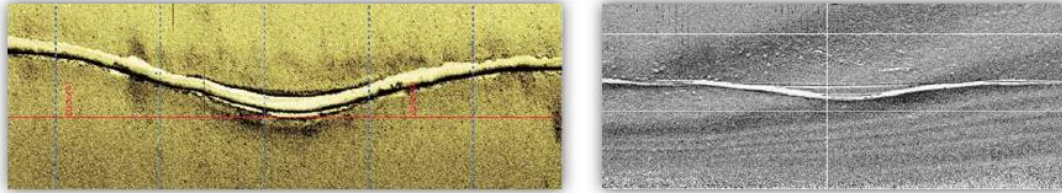


Figure 3. Lateral Buckles from Side-scan Surveys ( Bruton et al., 2010)

## 2.2 Seabed Characterization

The evaluation of intact properties of near surface sediments is critical for an accurate estimation of the pipe-soil resistance. Uncertain soil properties will result in uncertain estimation of the pipe embedment and the pipe-soil interaction parameters and thus invalid potential mitigation solutions, erroneous designs of pipeline and total project costs. However, it is a challenging task since seabed sediments are usually very soft having typical shear strengths between 0 to 5 kPa. In some case such as the West African coast, a pipelines may be supported on a crust having a higher strength of 10 to 15 kPa (Kuo & Bolton, 2013). In general, conventional testing methodologies are not applicable at such a low pressure range and alternative methods are adopted.

### 2.2.1 *In Situ testing*

Different in-situ tests are available to characterize the seabed sediments. T-bar penetrometer, ball penetrometer, piezocone and vane shear tests are utilized the most in

offshore applications. Lunne et al. (2011) suggested some recommendations on the design of these techniques and the interpretation of the penetration resistances in order to get reliable and consistent results from different operators. In addition, the usage of each technique was found to be project dependent in the sense that not all techniques are suitable to all soil types and all the encountered geotechnical conditions. Lunne et al. (2011) proposed a guide to regulate the usage of in-situ tests based on the most relevant geotechnical problems found in deepwater field developments (Table 1).

The full flow penetrometers (T-bar or Ball-penetrometer) are nowadays widely used to characterize the seabed sediments by generating a continuous profile for the sediments' undrained shear strength. This technique has several advantages that make it suitable for offshore applications more than the conventional cone penetrometer as it requires a minimal correction for overburden and pore pressures, provides a simple deduction of the shear strength based on the available theoretical solutions and allows for cyclic tests from which the remolded strength can be estimated (Randolph, 2004).

Table 1. Applicability- reliability of interpreted soil parameters (Lunne et al., 2011).

Geotechnical problem	Depth below seabed (m)	Comment	Soil parameters required <sup>d,f</sup>	Applicability-reliability		
				Piezocone	T-bar, ball	Vane
Backfilled trenches: upheaval buckling	0-1	Extremely soft material may be encountered	Soil profile	1-2	3	—
			Classification	2	—	—
			Soil density	2-3	—	—
			Undrained shear strength	2-3	1-2	2-3
Pipeline-riser soil interaction	0-3	Very soft material may be encountered	Soil profile	1-2	3	—
			Classification	2	—	—
			Undrained shear strength	2	1-2	2-3
			Remoulded shear strength	5	1-2 <sup>b</sup>	2-3 <sup>e</sup>
Skirted foundations: penetration, bearing capacity	0-15/40	—	Soil profile	1-2	3	—
			Classification	2	—	—
			Undrained shear strength	2	1-2	2-3
			Remoulded shear strength	5	1-2 <sup>b</sup>	2-3 <sup>e</sup>
Seabed templates, penetration, stability, settlements	0-10	—	Soil profile	1-2	3	—
			Classification	2	—	—
			Undrained shear strength	2	1-2	2-3
			Remoulded shear strength	5	1-2 <sup>b</sup>	2-3 <sup>e</sup>
Geohazards; slope stability	0-10/100 <sup>c</sup>	Use of T-bar-ball and vane may be limited to 40 m depth	Soil profile	1-2	3	—
			Classification	2	—	—
			Undrained shear strength	2	1-2	2-3
			Remoulded shear strength	5	1-2 <sup>b</sup>	2-3 <sup>e</sup>
			Settlements	(3-4) <sup>d</sup>	(—) <sup>d</sup>	(—) <sup>d</sup>
			Soil profile	1-2	3	—

<sup>a</sup>Scale of relative applicability-reliability: 1, high; 5, very low; —, no applicability. The values indicate to some extent NGI and COFS's view on the potential tool to derive a certain parameter.  
<sup>b</sup>Require cyclic T-bar (or ball) penetration tests.  
<sup>c</sup>This study mainly covers the interpretation of parameters at depths up to say 30 m below seabed.  
<sup>d</sup>Settlement parameters have not been covered in this study.  
<sup>e</sup>Requires at least 10 quick rotations.  
<sup>f</sup>Parameters for evaluating cyclic behaviour not included in the above table.

Many researchers proposed a correlation between the penetration resistance measured by the full flow penetrometer and the intact or remolded shear strength, but, in the case of shallow depths, White & Randolph (2007) proposed an additional reduction factor to account for the shallow penetration mechanism while estimating the undrained shear strength using T-bar penetrometer. Dejong et al. (2010) recommended practices regarding the penetrometer design, testing procedure and data analysis. Typical dimensions for a T-bar are a length of 250 mm and a diameter of 40 mm and for a ball penetrometer, 113 mm diameter when a standard size cone rod is used (35.6 mm) as shown in Figure 4(a). In offshore applications, smaller ball diameters (60-80 mm) can be used (Peuchen et al., 2005). These dimensions can be altered while preserving a penetrometer area ratio of 10:1 to ensure full-flow conditions with a penetration rate of 0.5 diameters per second for T-bar and 0.2-0.3 diameters per second for the ball. For the standard penetrometer size, the rate

should be 20 mm/s. Special care should be made regarding the accuracy of the used load cell, the surface roughness and the incorporation of a pore pressure sensor while designing a penetrometer. Other recommendations on the testing procedure including system calibration, monotonic and cyclic testing and rate effects can be found in Dejong et al. (2010). In general, the net penetration resistance of a full flow penetrometer,  $q_{T-bar}$  or  $q_{Ball}$ , can be expressed as

$$q_{T-bar} = q_{Ball} = q_m - \frac{[\sigma_v - u(1 - a)]1}{A_R} \quad (2.3)$$

Where  $q_m$  is the measured penetration resistance;  $\sigma_v$  is the total vertical overburden stress;  $u$  is the pore water pressure acting at the connection between the full flow probe and the push rod;  $a$  is the area ratio that accounts for water pressure acting on the back of the full flow probe and  $A_R$  is the penetrometer area ratio which is the ratio between the projected area of the push rod over that of the probe. Figure 4 (b) shows the typical results of T-bar penetration tests during penetration and extraction at shallow depths.

The undrained shear strength can be thus deduced by using equation (2.4)

$$S_u = \frac{q_{T-bar}}{N_{Su-T-bar}} = \frac{q_{Ball}}{N_{Su-Ball}} \quad (2.4)$$

Where  $N_{Su-T-bar}$  and  $N_{Su-Ball}$  are the undrained shear strength factors that can be estimated by a direct calibration against site specific laboratory or field vane data.

Another in-situ testing technique was proposed by Aubeny et al. (2005) to estimate the shear strength of the surficial seabed sediments which is the expendable bottom penetrometer (XBP). In brief, the XBP measures acceleration during impact penetration



over a large area which can be related to the undrained shear strength of soft clays using the proposed analysis by Aubeny et al.(2005). However, the results are limited to the first order estimation of the shear strength of clay since many simplifications were assumed to come up with the proposed analysis. Another device's limitation is the uncontrolled impact location which will not account for the special variability of the shear strength profile and thus result in uncertainties in the pipeline design.

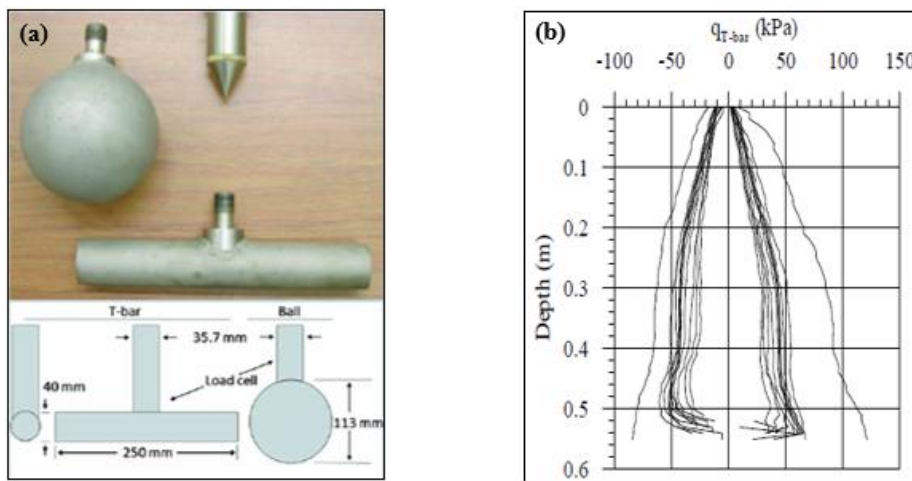


Figure 4. Ball and T-bar penetrometer : (a) Schematic and Image of ball and T-bar penetrometer with typical dimensions and (b) Typical penetration results (Dejong et al 2010).

### 2.2.2 Soil Sampling

Instead of performing in-situ tests, seabed sampling can be used as an alternative to estimate the seabed sediments properties by extracting either undisturbed samples or box core samples from the seabed and testing them directly in the vessel or in the laboratory. Undisturbed samples can be obtained by piston core technology (Young et al., 2000) directly from the seabed but it is still difficult to prevent any disturbance and has a

relatively high cost. A better solution is box core samples in which either miniature vane shear tests or penetrometer tests can be performed to measure the strength profile ( Low et al., 2008). The miniature vane size depends on the strength of the tested soil, Low et al. (2008), for example, used a blade of 25.4 mm height and 25.4 mm diameter. The blade should be as thin as possible to minimize the soil disturbance during vane penetration. The vane shear tests must be performed in accordance with ASTM-D4648 to control the penetration and rotation rates before measuring the residual shear strength of the tested soil. The limitations of this test are disturbing the soil during penetration, inducing a soil consolidation while waiting before the initiation of the test and generating only discrete shear strength values instead of continuous shear strength profiles.

Low et al. (2008) presented a new manually operated penetrometer DMS as a substitute of the miniature vane shear tests to get a continuous strength profile inside a box core sample (Figure 5). DMS is a portable testing device that can be fitted with a cone, T-bar or ball penetrometers and a microcomputer to store all the testing data. The setup was tested with a T-bar having a diameter and length of 8 and 42 mm, respectively in a box core recovered from a site in the Gulf of Mexico. The results were reliable and time effective when compared to the results of a miniature vane shear test. But some improvements have been made to maximize the performance of DMS by incorporating a motor to get a better control of testing and by increasing the box corer size so that multiple characterization tests can be done.

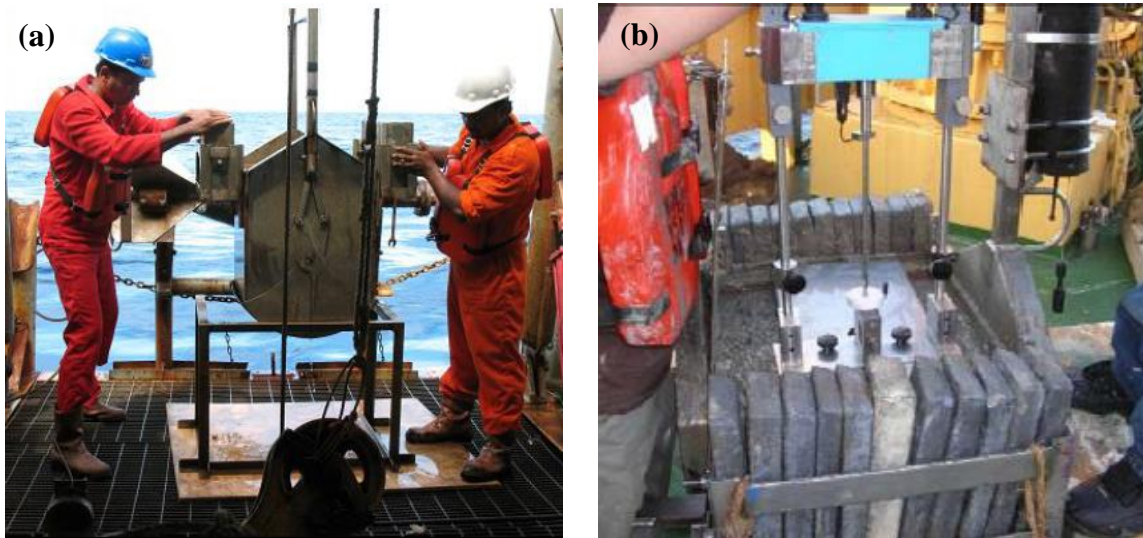


Figure 5. (a) The box core rigging system – (b) DMS on the Box corer (H. E. Low et al., 2008)

### 2.3 Available methods for predicting the axial pipe-soil interaction

The interaction between the HPHT pipelines and soft seabed sediments in deep water is extremely complex. An accurate prediction of the pipe-soil interaction response requires identifying all the factors that can affect the response throughout the laying process, hydrostatic testing and cycles of operations. The main challenge in understanding and quantifying the soil-pipe interaction is the low contact effective stresses range (generally below 10 kPa), imposed by the weight of the pipeline. Another challenge is the uncertainty in predicting the pipeline embedment as discussed in Pipe Embedment Section. From a loading perspective, variability of loading rates due to variations in temperature and pressure during cycles of start-up and shut down also play a role in understanding the response. The typical maximum movement rate of pipelines was reported by Bruton et al. (2007) to be around 0.5 mm/s. This fast rate only occurs at the beginning of shutdown or

startup when the temperature drops or increases quickly. The actual movement rate is around 0.005 mm/s over a complete shutdown (White et al., 2011). However, this rate will vary with the pipeline geometry and type, the flow conditions, the temperature ranges and the induced soil resistance. Such variability will control the drainage conditions during the pipeline movement. Different testing methods have been used to estimate the axial pipe-soil interaction taking into consideration all these parameters which cover all the available tools in engineering such as model tests, soil element tests, numerical models and in-situ tests.

For the model and in-situ tests, a specific framework is usually adopted to interpret the results. As these methods can reproduce the real pipeline movement, the interpretation should thus take into consideration the pipe shape and the generation of excess pore pressure during fast shearing tests. Since the pipe will be embedded in soil, the normal stress around the pipe surface,  $N$ , will exceed the pipe's submerged weight,  $V$ . The enhancement of the normal stress is known as the wedging factor,  $\xi$  expressed as:

$$\xi = \frac{N}{V} \quad (2.5)$$

White & Randolph (2007) suggested a simple method to estimate the wedging factor:

$$\xi = \frac{2 \sin \theta}{\theta + \sin \theta \cos \theta} \quad (2.6)$$

Where

$$\cos \theta = 1 - 2 \frac{z}{D} \quad (2.7)$$

Where  $z$  is the pipe embedment, and  $D$  the pipe diameter. The maximum wedging factor in Equation (2.6) is valid for 1.27 which corresponds to a  $z/D = 0.5$ . If the embedment

exceeds this value, the wedging factor remains constant (1.27). Therefore, the friction coefficient between the pipe and the soil beneath it can be estimated through the following steps:

1. *As-measured pipe friction coefficient*: which is calculated as a function of the measured shear force  $F$  divided by the pipe's submerged weight,  $V$ .

$$\mu = \frac{F}{V} \quad (2.8)$$

2. *Planar friction coefficient*: which is calculated from Equation (2.9) while incorporating the wedging factor in the calculation.

$$\mu_{\xi} = \frac{\mu}{\xi} = \frac{F}{\xi V} = \frac{\tau}{\sigma_n} \quad (2.9)$$

3. *Planar effective friction coefficient*: which incorporates the measured pore pressure in the calculation.

$$\mu' = \frac{\tau}{\sigma'_n} \quad (2.10)$$

where  $\sigma'_n = \sigma_n - u_{average}$

$$\sigma_n = \frac{\xi V}{\theta D} \text{ and } \tau = \frac{F}{\theta D}$$

### 2.3.1 Soil Element Tests:

The typical normal stress that acts at the pipe-soil interface in the offshore environment is much smaller than the typical range of normal stresses that is generally encountered in other conventional geotechnical applications. Conventional laboratory devices are not designed to perform tests at such low normal stresses. Over the past

decades, new devices have been developed to target low stress applications such as the tilt table, the cam-shear, the cam-tor and the macro-scale direct shear test device (Najjar et al., 2003; Najjar et al., 2007 and Pedersen et al., 2003; De Brier et al., 2016;and Kuo et al., 2015). Other efforts were invested in modifying available testing setups to account for the low stress range by reducing the inherent system friction (Boukpeti & White, 2017; Hill et al., 2012; Westgate et al., 2018; White et al., 2012 and Eid et al., 2015). The modified direct shear and the ring shear devices are the most known examples. Extracted seabed samples can thus be tested in the laboratory against pipeline interfaces to accurately study the interface response. Westgate et al. (2018) summarized all the available element testing devices stating their advantages and disadvantages as shown in Table 2. A compilation of the different element tests that were published in the literature in reference to the axial soil-pile interaction is presented in

Table 3, with details on the test properties (soil and pipe properties), test procedures and design conditions that were investigated.

Table 2. Element tests for measuring interface shear resistance (Westgate et al. 2018)

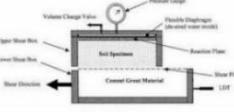
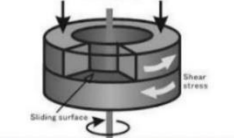
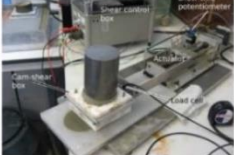

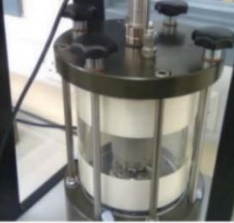
Device	Example Image	Mechanical Description	Advantages	Limitations	References
Direct interface shear box (ISB)		Interface surface sliding below a fixed square or circular specimen	Controlled displacement rate; simple apparatus; wide experience.	Short horizontal displacement range; no pore pressure measurement; potential box friction errors	Potyondy 1961, Tsubakihara and Kishida 1993
Ring shear		Interface surface rotating under fixed annular specimen	Unlimited displacement achievable	Slight variation in strain rate radially across specimen; no pore pressure measurement	Bishop et al. 1971, Bromhead 1979, Yoshimi and Kishida 1981, Stark and Eid 1993
Cam-shear		Circular specimen sliding above a fixed interface surface (similar to ISB)	Controlled displacement rate; simple apparatus	Short horizontal displacement range; no pore pressure measurement	Bolton et al. 2007, Kuo 2011, Ganesan et al. 2013
Tilt table		Thin specimen sliding along titled interface surface	Simple apparatus, machine friction eliminated	Uncontrolled displacement rate; no pore pressure measurement; cyclic capability depends on set-up.	Pedersen et al. 2003, Najjar et al. 2003, Najjar et al. 2007
Cam-Tor		Circular interface rotating under fixed circular specimen	Less machine friction than ring shear and smaller specimen (can use intact samples); globally undrained testing possible (membrane surrounds sample); unlimited displacement achievable	Significant variation in strain rate radially across specimen	Kuo et al. 2015, De Brier et al. 2016

Table 3. Summary of published experimental studies that are based on laboratory scale pipe-soil element interface tests

Reference	Device	Soils					Speeds mm/s	Normal Stress kPa	Shearing Cycles	Interface		Studied Parameters
		Type	C <sub>v</sub> (m <sup>2</sup> /year)	LL (%)	PI(%)	D <sub>50</sub> (mm)				Type	Roughness (μm)	
White et al. (2012)	Direct Shear	Carbonate silt with mud	NA	57	25	0.02	0.001 0.01 0.1	2.5 - 5	20 (continuous)	Rough steel	NA	Shearing rate Consolidation periods
		Carbonate sandy silt	NA	65	30	0.07						
		Carbonate silty sand	NA	NA	NA	0.19						
Boukpeti & White (2017)	Direct shear	Marine clays A	0.5	129	110	NA	0.001 0.1 0.03	2, 4, 8	Slow/Intermediate Tests: 2 cycles 20 fast cycles with 30 min of consolidation	3 layers of polyethylene Smooth	2	Normal Stress Interface Roughness Drainage during and in between shearing
		Marine clays B	0.6	42	63	NA			3 layers of polyethylene Rough	80		
Eid et al. (2014)	Torsional ring-shear and Macro Direct shear device	Fraser river silt	17.19	21	3	0.024	0.0030.0008	3-6	1 cycle	Green epoxy	0.16	Plasticity Index Interface Roughness Low Normal stresses
		Gray Silt	2.98	34	17	0.0096						
		Nile deposit 1 kaolinite	2.61	36	12	0.017						
		Gulf deposit 1	1.95	48	22	0.0027						
		Gulf deposit 2	1.16	53	19	0.035						
		Nile deposit 2	0.84	54	32	0.0019						
		Nile deposit 3	0.51	69	34	0.002						
		Gulf deposit 3	0.53	77	49	0.005						
Eid et al. (2019)	Torsional ring shear test	kaosand	16.02	22	4	80.1	0.0047 0.0015 0.0005 0.0002	10-25	1 cycle	Green epoxy	0.16	Interface Roughness Intermediate Normal stresses Plasticity Index
		redstone	4.89	34	14	9.1						
		kaolinite	1.95	48	22	2.7						
		nile deposite	0.51	69	34	2						
Gansen et al. (2014)	Cam-shear apparatus.	Samples from west Africa	0.04	160	100	NA	0.5, 0.05, or 0.001	1 - 4.5	20 with pause periods prior to shear reversal	Smooth interface	1.64	Overconsolidation ratio Shearing rate Interface Roughness
									Rough Interface	67.44		
De brier et al. (2016)	Cam-Tor	Samples from West Africa	NA	100	NA	10	0.5 0.1 0.0001	2 and 4	1 cycle	Rough interface	3.7	Low Normal stresses Overconsolidation ratio Shear Displacement Shearing rate
Najjar et al.(2007)	Tilt Table	Golf of Mexico Sample 1	0.3-1.2	116-123	82-87	NA	NA	1.7 to 5.7	Repeated cycles until reaching the residual	Smooth fusion-bonded epoxy coating	<10	Interface Roughness Low Normal stresses Clay Composition Rate of loading
		Golf of Mexico Sample 2	0.3	95-102	57-62	NA				Smooth polyurethane	<10	
		Golf of Mexico Sample 3 -1	0.3	86-98	55-60	NA				Polyurethane	<10	
		Golf of Mexico Sample 3 -2	0.3	86-89	55-60	NA				Polypropylene	<10	
		Golf of Mexico Sample 3 -3	0.3	68	42	NA				Rough fusion-bonded epoxy coating	50	
		Kaolinite	0.5-1	54-58	20-27	0.3-5.2						



Most of the published interface tests using a modified direct shear device were carried in the University of Western Australia (Boukpeti & White, 2017; Hill et al., 2012; Westgate et al., 2018; White et al., 2012). Testing methodologies were adopted to mimic the response at the pipe-seabed interface while varying the stress history, consolidation periods, normal stresses, interface roughness and shearing rates. Published databases were then used to develop a theoretical framework for axial pipe-soil interaction which. The conventional direct shear device was first modified to minimize its friction. Normal stresses were imposed by adding compact dead weights of anodized steel directly on the sample as shown in Figure 6. The remaining system friction was then quantified by performing a shear test without soil and was found to be 0.5 kPa which was subtracted from the soil-interface results. The device was computer controlled so all the sequential testing can be automated.

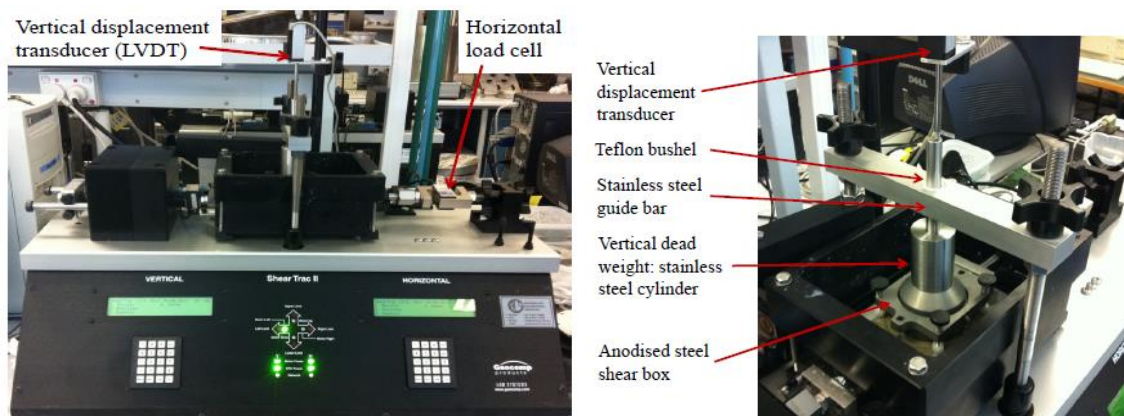


Figure 6. Modified Direct shear device in the University of Western Australia (White et al., 2012).

White et al., (2012) studied the effect of loading history and consolidation experienced by the soil beneath the pipeline due to intermitted startup and shutdown over their operation using this device. The axial interface resistance was measured

between a rough steel and normally consolidated carbonate soils by either performing continuous drained cycles or undrained cycles separated by 30 minutes of consolidation period. The typical response of carbonate sandy silt consolidated to 2.5 kPa and then sheared at 0.1 mm/s against steel is presented in Figure 7. The shear stress increased with shearing cycles accompanied with continuous settlement indicating sample contraction under partially drained or undrained conditions. The excess pore water pressure dissipated with time and the interface strength increased until reaching the critical state where the drained and undrained strengths converged. This is known as the cyclic hardening effect.

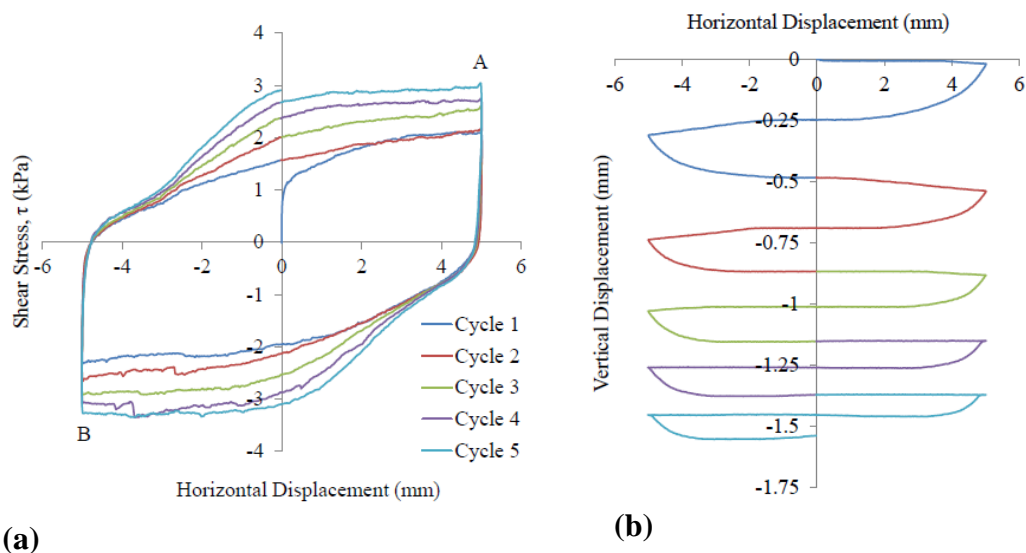


Figure 7. Typical (a) Shear stress - displacement and (b) Settlement – displacement response at 0.1 mm/s shearing rate (White et al.,2012)

Boukpeti and White (2017) presented interface test results for two marine clays studying the effect of undrained and partially drained shearing and consolidation during and in-between shearing cycles on the axial pipe-soil resistance. In the cases of slow tests, the shear stress increased gradually until reaching steady state at large

displacements (Figure 8a). The drained interface resistance was taken as the residual stress reached at 40 mm.

Plotting the residual stresses of the tested soil as a function of the normal stresses (Figure 8b) showed that the failure envelope is slightly non-linear. As for the undrained tests, the shear stress showed a peak after small displacements followed by softening until reaching the residual constant stress (Figure 9). Regarding the effect of roughness, the undrained shear strength of the smooth interface was lower than that of the rough interface. In addition, the same consolidation hardening behavior was noticed as in the study of White et al. (2012).

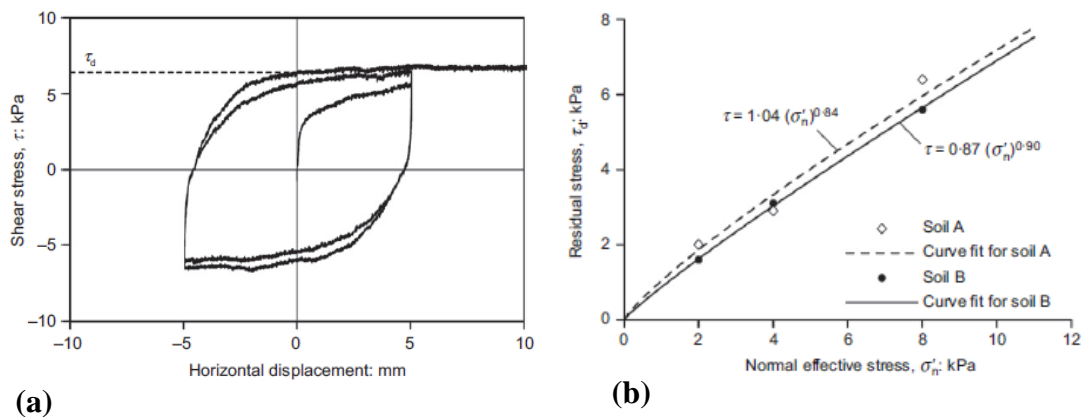


Figure 8. Drained Interface response: (a) Shear Stress - Displacement and (b) Residual Stress - Normal Effective Stresses (Boukpeti & White, 2017)

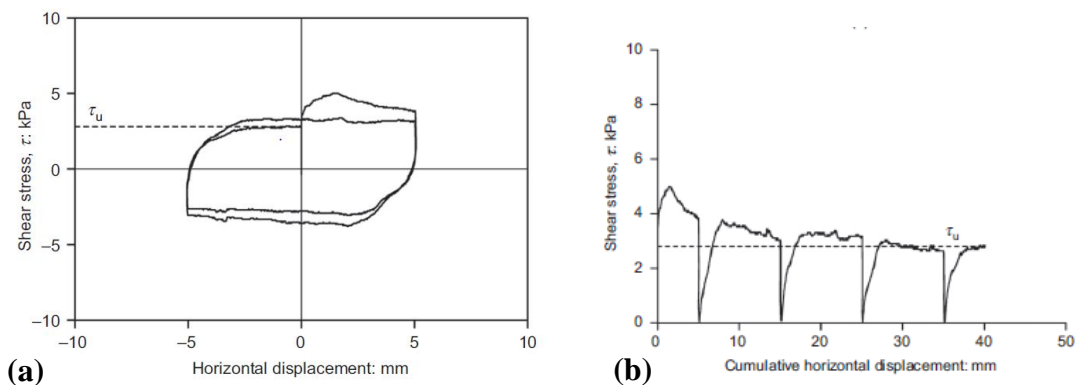


Figure 9. Undrained Interface Response: (a) (a) Shear Stress - Displacement and (b) Shear Stress – Cumulative displacement (Boukpeti & White, 2017b)

Westgate et al. (2018) collected data constituting more than 200 tests performed on several soft clays and pipeline coatings and suggested a site-specific test program using the interface direct shear device in order to get initial estimates of the axial pipe-soil interaction parameters. In addition, they summarized the key aspects of the interface behaviour as:

1. **General Trend:** an initial peak in resistance followed by a drop to a steady state with higher peaks generated by the rougher interfaces.
2. **Normally consolidated soils:**
  - **Smooth interface:** During undrained shearing, sample settlement is minimal but there is generation of positive pore water pressure that dissipates between cycles. The undrained resistance increases with cycles until reaching the drained limit.
  - **Rough interface:** The same response as on the smooth interface but the difference between the drained and the undrained resistance is much higher.
3. **Overconsolidated soils:** During undrained shearing, samples will slightly dilate with a generation of negative pore water pressure that dissipates between cycles. The undrained resistance decreases with cycles until reaching the drained limit.

Westgate et al. (2018) conclude that the modified interface direct shear device can provide accurate measurements of the axial interface resistance mimicking the real pipeline in-situ response. However, careful attention must be paid to reduce mechanical friction of the system as its impact at low effective stresses is important. Other limitations of this device are its relatively short horizontal displacement and its inability to measure pore pressures developed in the soil sample.

Modified torsional ring shear apparatuses have also been used for determination of the pipe-soil interface resistance particularly for quantifying the residual response as it permits unlimited shear displacements (Eid et al., 2015, 2019). Eid et al. (2015) modified a Bromhead type torsional shear device to run tests under low effective stresses (3-7 kPa). The lever system was replaced by a lightweight loading assembly, the force sensors were replaced by ones with a lower force range and higher accuracy, in addition to modifications of the specimen container to accept the soil-solid shearing (Figure 10). In addition, changes were made in compliance with the recommendations in Stark & Eid (1993) to reduce the side-wall friction of the container. Soils having a wide range of plasticity were tested against three types of interfaces to characterize the interface shear strength at large strains. Results have helped to develop some correlations to estimate the residual soil and interface shear strength at low effective stresses. The residual secant friction angle,  $\varphi'_r$ , was found to be dependent on the plasticity index of the soil,  $I_p$ , and can be described by equation (2.11). Another correlation (2.12) was also developed based on the interface results by Eid et al. (2015) that reveals the influence of roughness on the interface friction angle,  $\delta'_r$ .

$$\varphi'_r = 34^\circ e^{-0.014I_p} \quad (2.11)$$

$$\frac{\tan \delta'_r}{\tan \varphi'_r} = 0.7 R_a^{0.12} \quad (2.12)$$

The same device was used by Eid et al. (2019) to evaluate the drained peak and residual interface resistance under near-shore conditions where the normal stresses are

in a range of 10 to 25 kPa. It was found that the drop from the peak to residual strength depends on the soil plasticity index and interface roughness. These peak and residual strengths will be reduced when using rough interfaces and can be estimated using the same correlation (2.12) developed by Eid et al. (2015).

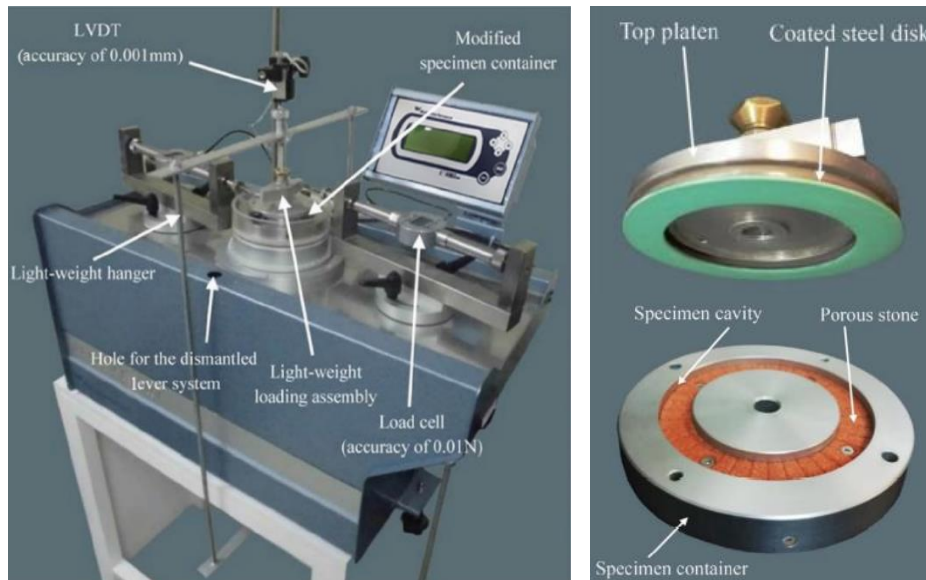


Figure 10. General view of ring shear apparatus (Eid et al., 2015)

Moving to the fabricated setups for low stress applications, the earliest one was the tilt table which relies only on gravity loading eliminating the friction errors resulting from mechanical systems ( Najjar et al., 2003; Najjar et al., 2007 and Pedersen et al., 2003), see Figure 11. Najjar et al. (2007) measured the drained residual strength of the clay-clay and clay-coating interface at effective normal stresses ranging between 1.7 and 5.8 kPa. For the tests that aimed at measuring the residual interface shear strength, the thickness of the soil specimen was 1.5mm, whereas for the ones that measure the internal residual shear strength of the clay, the thickness was 2.5 mm. The rate of shearing was slow enough to allow dissipation of water and ensure drained conditions,

with the time to failure taken as  $t_f = 50t_{50}$ . The resulting coating efficiency – defined as the interface residual strength with respect to residual strength of soil – ranged between 60% and 90%. A total of 54 tests led to the conclusion that the type of coating and composition of soil are the factors that affect the residual shear strength at the pipe-soil interface.



Figure 11. Tilt table frame and sliding of the plate at failure ( Najjar et al., 2007)

Another setup (known as the Cam-shear) similar to the direct shear test was introduced by Ganesan et al. (2014) (Figure 12). The main advantages of this apparatus are the possibility of testing directly offshore soil samples extracted from the site and shearing them to relatively large displacement, up to 190 mm. The used shear box was made of polytetrafluoroethylene (PTFE) to minimize the inherent friction in the system. Ganesan et al. (2014) conducted tests on reconstituted soft marine clays from west coast of Africa under undrained, partially drained and drained conditions against a smooth and a rough interface having a roughness of  $1.64 \mu\text{m}$  and  $67.44 \mu\text{m}$ , respectively. The tested clay samples were overconsolidated under effective stresses between 8 and 14 kPa in order to reach undrained shear strengths found in situ, and then sheared under normal stresses between 1 and 4.5 kPa. The authors focused on investigating the



drainage conditions occurring at both peak and end stages of the tests by using Gibson and Henkel approach and concluded that for the range of shearing rate used, the peaks can only be reached under partially drained or undrained conditions. Results showed that the response using smooth and rough interfaces are quite similar but higher roughness will induce higher peak and residual stresses. Figure 13 presents the linear correlations found by Ganesan et al. (2014) between the overconsolidation ratio, OCR, and the peak strength of the smooth and rough interfaces. The faster the shear rate and the higher the OCR, the higher the peak strengths which is associated to greater generation of negative pore pressures.

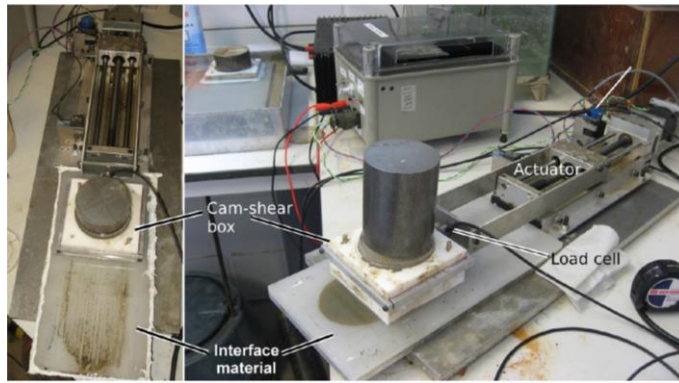


Figure 12. Photograph of Cam-shear test setup (Ganesan et al.,2014)

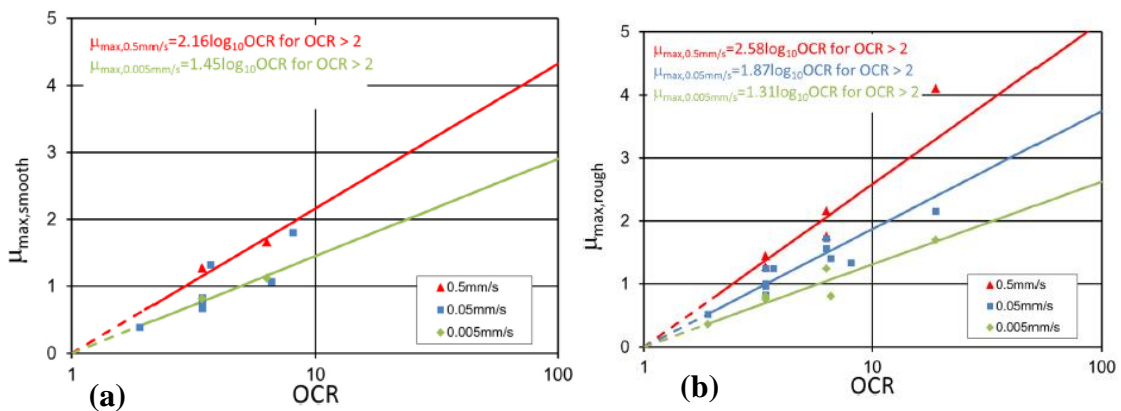


Figure 13. Peak friction coefficient in function of OCR for:(a) Smooth Interface and (b) Rough Interface (Ganesan et al., 2014)



The last element test apparatus that has been used to measure the interface resistance between pipes and soils is the Cam-Tor (Figure 14), which is a new torsional shear device developed at University of Cambridge in collaboration with BP and Fugro. The test setup allow for performng tests on intact and remoulded samples under normal stresses ranging from 2-40 kPa and at shearing rates between 0.0005 mm/s and 0.1 mm/s (De Brier et al., 2016; Kuo et al., 2015). De Brier et al. (2016) used the Cam-Tor device to investigate the effect of OCR, normal stresses and shearing rate on the resistance between a rough interface and soils from West Africa. They reported similar trends as in the study by Ganesan et al. (2014).

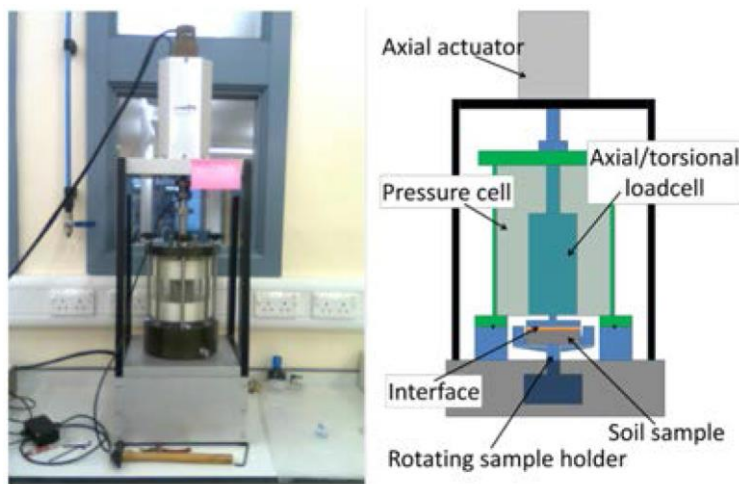


Figure 14. Photograph and Schematic diagram of the Cam-Tor machine (Kuo et al., 2015)

### 2.3.2 Model Tests

Two types of model tests have been used over the past ten years to investigate the pipe-soil interaction: the full scale tests (1g) and the small scale tests (centrifuge) (Boylan et al., 2014; Senthikumar et al., 2013; Shi et al., 2019; Smith & White, 2014; White et al., 2011;and Wijewickreme et al., 2014). The full-scale model simulates the

exact behaviour of in-situ pipelines since similar pipe shapes can be used, similar soil strengths can be achieved, and the pipe movement can be controlled and monitored. However, it requires a significant physical effort and consumes a lot of time. Centrifuge tests on the other hand are smaller in scale but can replicate the real pipe movement under comparable in-situ conditions in relatively less time due to scaling. Centrifuge facilities are however very expensive and available only in some major international institutions and research centers.

The first full scale model for investigating the pipe-soil interaction was built in the University of Cambridge as part of the SAFEBUCK JIP project (White et al., 2011). The model pipe was an 8m long plastic pipe that is 0.09 m in diameter. The pipe was placed on a reconstituted soft natural clay in a 10x0.3m bed and 0.4m in depth and was dragged axially in both directions at displacement rates that range between 0.001 mm/s and 5 mm/s, with different pause periods between the series of sweeps. Two pore pressure transducers were installed at the bottom of the pipe to study the effect of drainage and rate of loading on the axial interface resistance. The pipe (fully submerged) was free to move vertically and was dragged horizontally by an actuator through cables that ran over Teflon pulleys (Figure 15). A load cell was connected between the pipe and the cable to measure the horizontal force resistance, while vertical movement was recorded by two LVDTs placed on top of the pipe.

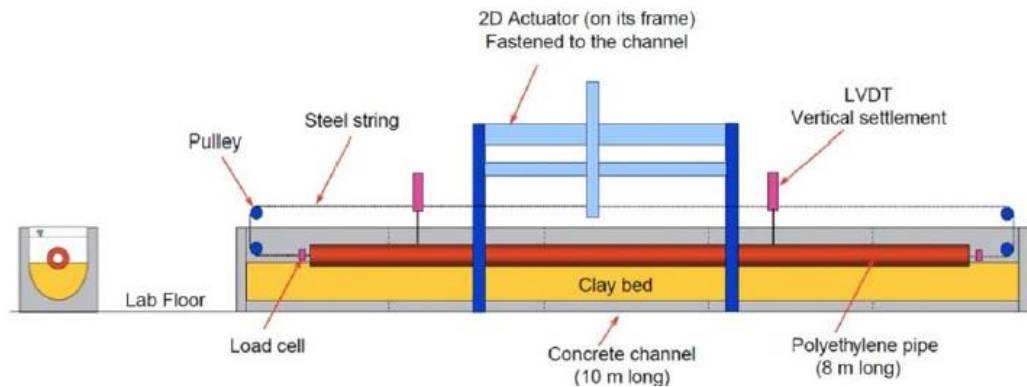


Figure 15. Schematic diagram of the model test in the University of Cambridge (White et al., 2011)

The authors argued that a high ratio of pipe length to diameter ( $L/D = 89$  in this case) is enough to consider the soil resistance at both ends of the pipe as negligible. White et al. (2011) tested natural sediments from West Africa's seabed using this model varying the pause periods and the shearing rates. They noticed that the peak-residual trend usually occurs during fast shearing accompanied with a generation of positive pore pressure and continuous pipe settlement. The peak resistance increases when the pause periods before shearing episodes are longer. During slow shearing, the resistance increases in a ductile manner. The resistance dependency on the shearing rate indicates that there is a transition rate that separates between the drained and undrained behaviour of the pipe-soil interface which was determined in this study. The resultant friction coefficients were not consistent with the adhesion factor,  $\alpha$  usually adopted in pipeline design.

Smith & White (2014) performed full scale pipe-soil interface tests at the Norwegian Geotechnical Institute (NGI) in Oslo. The test consisted of sweeping a model pipe of 1.4m in length and 120mm in diameter on a reconstituted glaciomarine

clay in a 3.4x1.75m bed on reconstituted natural clay from Onsoy. The pipe was penetrated initially to a depth of 0.3D and was then moved 150mm axially in each sweep at a displacement rate of 0.01mm/s with a pause period up to 43 hours between sweeps. The pipe was polypropylene coated, and sand blasted with an average surface roughness  $R_a$  of 21 $\mu$ m. 13 pore pressure transducers were placed at the bottom of the pipe to measure the excess pore pressures generated throughout the test. To remove the additional soil resistance due to end effects, the soil was scraped away manually from the ends of the pipe. Figure 16 shows a schematic diagram of the setup. Results indicated that the residual axial resistance increased by 80% after 13 sweeps along with an increase of the pipe embedment from 0.3D to 0.6D. This was also confirmed by the increase of the undrained shear strength of the soil beneath the pipe after comparing the T-bar results before and after the test. Taking into consideration the wedging effect and the generation of excess pore water pressure, the planar effective friction coefficient was approximately constant around 0.55 revealing that the interface friction angle is 29°. It was concluded that the undrained shearing on soft clay results in volumetric hardening of the clay beneath the pipeline and thus an increase in the axial interface resistance. However, this behaviour must be confirmed in future work for different shearing rates.

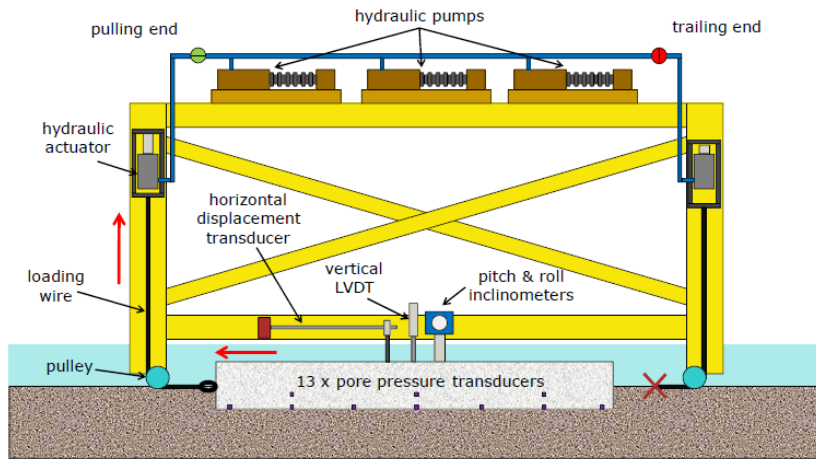


Figure 16. Schematic diagram of Smith and White (2014) setup.

The only available centrifuge test as carried out by Boylan et al. (2014) at the University of Western Australia (UWA) to examine the effect of soil drainage on the axial response between the pipe and the carbonate soil from the North West Shelf, Australia. The centrifuge testing presents a lot of advantages over the large-scale laboratory tests described previously. The in-situ shear strength profile of the soil can be precisely replicated, and tests can be performed within a realistic time period given the ability to scale time. The model pipe (140 mm in length and 20 mm in diameter) was placed in a 650x390mm “strongbox” with 325 mm in depth filled with soil. The pipe was attached to the loading arm through an S-shaped axial load cell to measure vertical forces and two bending strain gauges at the top of the loading arm to measure horizontal forces (Figure 17). Particles of fine-grained sand ( $d_{50} = 160\mu\text{m}$ ) were glued to the pipe to achieve the desired surface roughness. To remove the effect of the soil resistance at both ends of the embedded pipe when sheared, the soil was manually excavated before starting of the shearing phase.

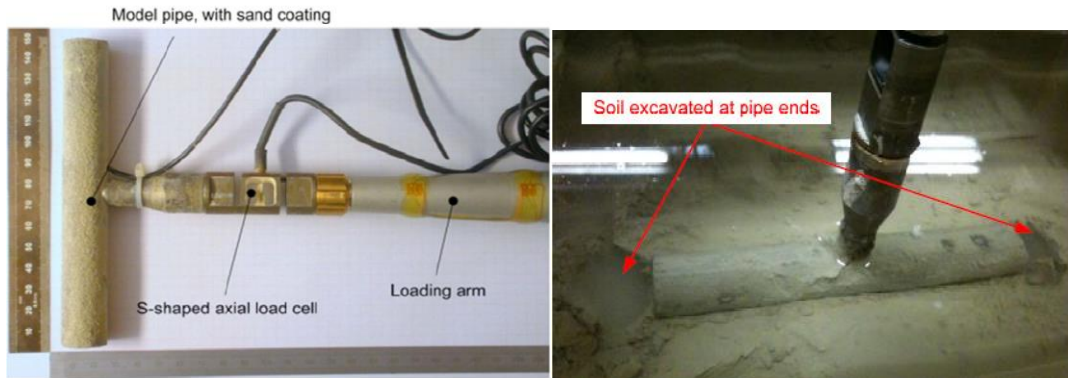


Figure 17. Assembled model pipe, S-shaped axial load cell and loading arm

Two testing procedures were adopted, each consisting of two shearing phases after the end of pipe consolidation:

- **Test A:** Constant shearing rate (2 or 0.2 mm/s) + Periods of consolidation
  - Phase 1: 24 cycles + 1000 s Pause Period
  - Phase 2: 42 cycles at 2 mm/s + No Pause Period
- **Test B:** Varied shearing rate (2/0.2/0.02/0.002 mm/s) + Periods of consolidation
  - Phase1: 7 cycles using 5 rates + 1000 s Pause Period
  - Phase 2: 97 cycles at 2 mm/s + No Pause Period

The resulting residual axial frictions are shown in Figure 18 for the constant rate and the variable rate tests. It is clear that the undrained resistance exceeded the drained resistance reached at slow shearing rate which indicated that the carbonate soil is dilatant with high friction angle of  $40^\circ$ . Cycles of shearing lead to a decrease of the residual resistance in both cases. In addition, the response initially showed a brittle peak followed by a resistance decay to reach a steady residual value in accordance with the generation of negative pore pressure. After accumulation of sliding displacement, consolidation periods and long time of shearing, the dilatancy effect lessens, peaks fade

away, no more negative pore pressure generation occurs until attaining the drained residual interface resistance. These results are the opposite of the ones found by Smith and White (2014) that showed a volumetric hardening behaviour for offshore clays from Onsoy due to the difference in soil properties and thus difference in the soil strength.

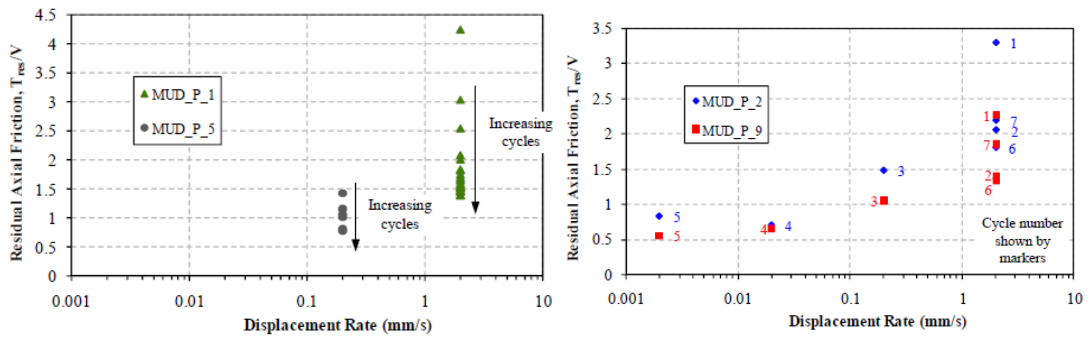


Figure 18. Residual axial friction: (a) Constant rate tests and (b) variable rate tests (Boylan et al. 2014)

Wijewickreme et al. (2014) introduced a new testing apparatus, the macro-scale interface direct shear apparatus, for determining the soil-solid drained shear strength at large displacement and under low effective normal stresses. The device is similar in concept to the conventional small-scale direct shear box but with the advantage of a larger interface shear area of  $3\text{m}^2$  ( $1.72 \times 1.75\text{m}$ ), and a large achievable shearing displacement of 1.2m (Figure 19). The shear displacement rates that were used in the study range from  $0.0001\text{mm/s}$  to  $1\text{mm/s}$  depending on the type of soil in use. The apparatus also comprises of 7 pore water pressure transducers mounted flush with the interface material in order to measure the excess pore water pressures and accurately determine the effective normal stresses. The functionality of the device was tested using four different soil types sheared against epoxy coated mild steel at effective stresses

between 3 and 7 kPa. The obtained trend and residual friction coefficients were very promising.

Eid et al. (2014) to assess the drained residual interface shear stresses as a function of the plasticity index of soils and to compare its results to the ones performed on the torsional ring shear where a good agreement was found between the two test mechanisms also used the device. Although the device was found to provide accurate measurement at large shear displacements, it was noticed that the peak stresses could not be accurately captured. One of the additional disadvantages of this device is the time consumed in the specimen preparation along with the significant physical effort needed.

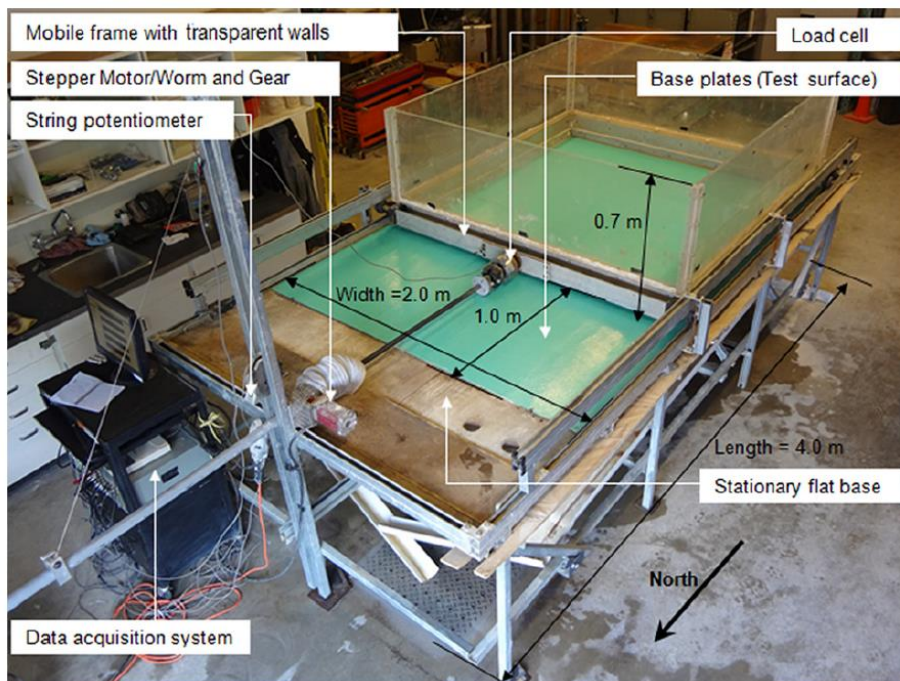


Figure 19. Photograph of the macro-scale interface direct shear test device (Wijewickreme et al., 2014)



### 2.3.3 *In-situ Tests*

In-situ testing offers the most realistic solution to characterizing the interface response of offshore pipelines. By adopting a geometry that is in line with the full-scale pipeline, an in-situ pipe model can accurately capture the pipeline behavior once it is laid down on the intact seabed. At shallow depths, sediments exhibit relatively high moisture contents and a characteristic structure/fabric that cannot be maintained in laboratory tests. In addition, a crust with relatively higher strength and stiffness characteristics can be found beneath the soft layer in some offshore locations. These conditions cannot be replicated in their laboratory and their influence on the axial pipe response can only be reflected in in-situ tests. Therefore, it is expected that in-situ axial interface pipe tests will provide more realistic measurements of the interface strength compared to all the above-mentioned laboratory and centrifuge testing mechanisms. Till date, very few tools are available for measuring the soil-pipe interaction in-situ (Ballard & Jewell, 2013; Hill & Jacob, 2008; Schneider et al., 2020; Stanier et al., 2015; White et al., 2011).

The Fugro SMARTPIPE is a sophisticated in-situ tool that was developed by Fugro (Geotechnical and Survey Services Company), BP (Major Oil & Gas Company), and the University of Cambridge to measure the axial and lateral pipe-soil interaction in the field. The full description of this tool is presented by Hill and Jacob (2008). It is a site investigation tool that is able to measure all the pipe-soil interaction parameters (axial and lateral) in addition to the estimation of the seabed shear strength. It can provide rapid results from infinite locations covering the pipeline footprint. The equipment comprises of a mini T-bar penetrometer and a model pipe (1200 mm long and 225 mm in diameter) mounted on a steel frame. The frame is deployed from a

vessel and is equipped with a settlement plate, a camera, roll and pitch sensor etc. The pipe consists of two end dummy sections that eliminate end effects and a central measurement section (776 mm long) that is connected to the two end parts by means of triaxial load cells to measure the vertical, lateral and axial forces acting on the central section. The pipe is actuated by a hydraulic system and is able to move axially at a rate that ranges between 0.005 mm/s and 1.15 mm/s, and laterally between 0.1 mm/s and 0.8 mm/s. Nine pore water pressure sensors are also attached to the bottom of the central pipe section to measure the change in excess pore water pressure during consolidation and shearing stages, and determine the effective normal stresses throughout the test. The pipe interface is polypropylene coated and has an average surface roughness of 5-10 $\mu$ m.

Figure 20 presents a detailed schematic view of the SMARTPIPE. The functionality of the SMARTPIPE was first tested in a shallow marine environment (Hill & Jacob, 2008). The quality of the generated data was assessed and compared to laboratory results. The results of the first deep water deployment of SMARTPIPE were presented by (White et al., 2011). The test consists of two shearing cycles at 0.04 mm/s followed by one cycle at 0.15 mm/s. A peak stress was found in the first sweep followed by a ductile behavior. The effective stress results were more consistent than those of total stresses indicating the importance of measuring the excess pore pressures during testing to understand the interface behavior.

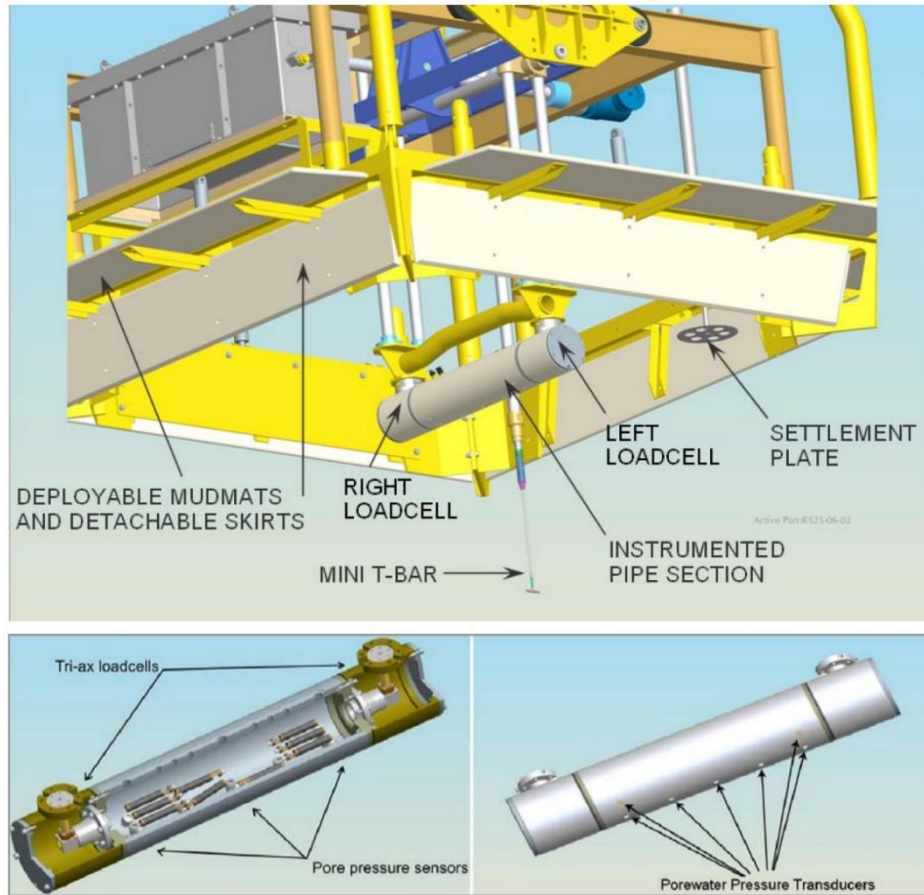


Figure 20. Schematic Detailing of SMARTPIPE (Hill & Jacob, 2008)

Ballard & Jewell (2013) investigated the effect of the pipe preloading on the interface resistance using the SMARTPIPE in offshore West Africa simulating the light pipeline weight change during hydrotest compared to the waterfilled conditions. The model pipe was first penetrated to a specified embedment and then left for three hours to consolidate under 0.4 to 0.5 kN/m vertical load. The vertical load was then reduced, and the axial shearing started at three different shearing rates (0.006, 0.045 and 0.35 mm/s).

A total of eight tests were conducted while varying the ratio between the consolidation vertical load and the load during axial movement,  $V_{\text{consolidation}}/V$

(overloading ratio), from 1 to 1.72. The peak-residual behaviour reported in the published literature was observed in all tests where the peak stress was mobilized at approximately 15 mm (Figure 21a). The peak and residual friction factors also decreased with normal stresses from 0.6 to 0.3 (Figure 21b). Another dependency on the overconsolidation ratio was spotted where the peak friction increased from 0.4 to 0.6 along with the increase of this ratio from 1 to 1.7 due to the reduction of the excess pore pressure and thus the increase in the effective stresses.

This indicated a similarity between the undrained shear strength response and the undrained interface response leading to the development of equation (2.13). This equation gave reasonable estimates of the peak and residual friction factors sheared under undrained conditions with  $\mu_{V=V_{consolidation}}$  of 0.37(peak) and 0.3 (residual), respectively and  $m = 0.9$ .

$$\mu_{V < V_{consolidation}} = \mu_{V=V_{consolidation}} \left( \frac{V_{consolidation}}{V} \right)^m \quad (2.13)$$

All the SMARTPIPE deployment tests available until now proved its efficacy in estimating the pipeline design parameters under different testing conditions. Nevertheless, the fact that it is vessel-dependent makes it very expensive. Moreover, although the model pipe can be actuated by displacement-rate control or load-controlled mechanisms, the results and observations from the tests showed that the hydraulic system failed to maintain constant vertical loading throughout the tests. One solution to such problems can be through the use of a detachable reaccessible test rig that would render the test vessel-independent (Hill & Jacob, 2008).

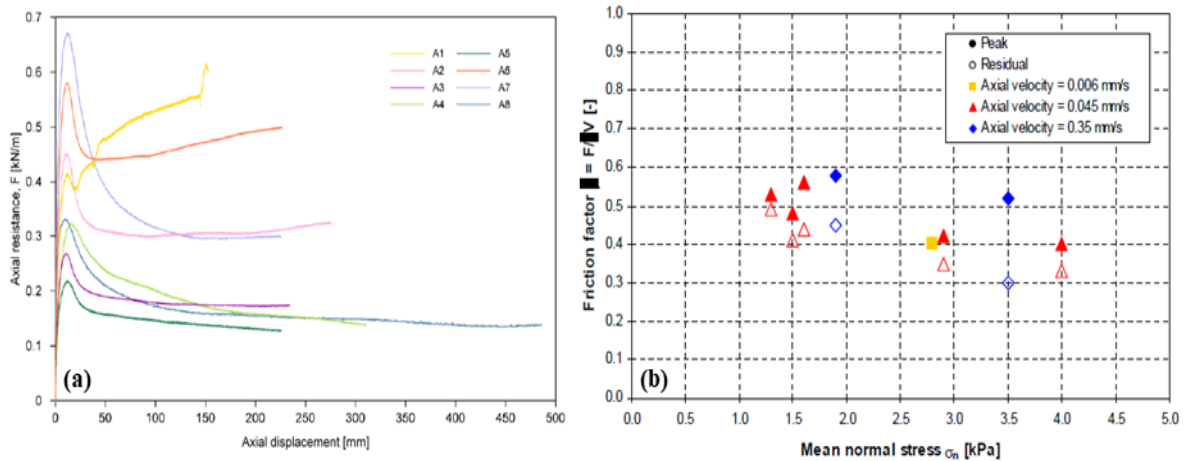


Figure 21. The interface axial response from (Ballard & Jewell, 2013): (a) Axial resistance vs displacement and (b) axial friction factor vs normal stress.

Stanier et al. (2015) proposed a device that aims at measuring the pipe/soil drained interface resistance. In principle, the concept involves dragging a tool on the seabed and measuring the friction mobilized between the tool and soil. The movement of the tool is controlled by an ROV (Remotely Operated underwater Vehicle) or by an electrical or hydraulic cylinder if the ROV is fixed in place (Figure 22).

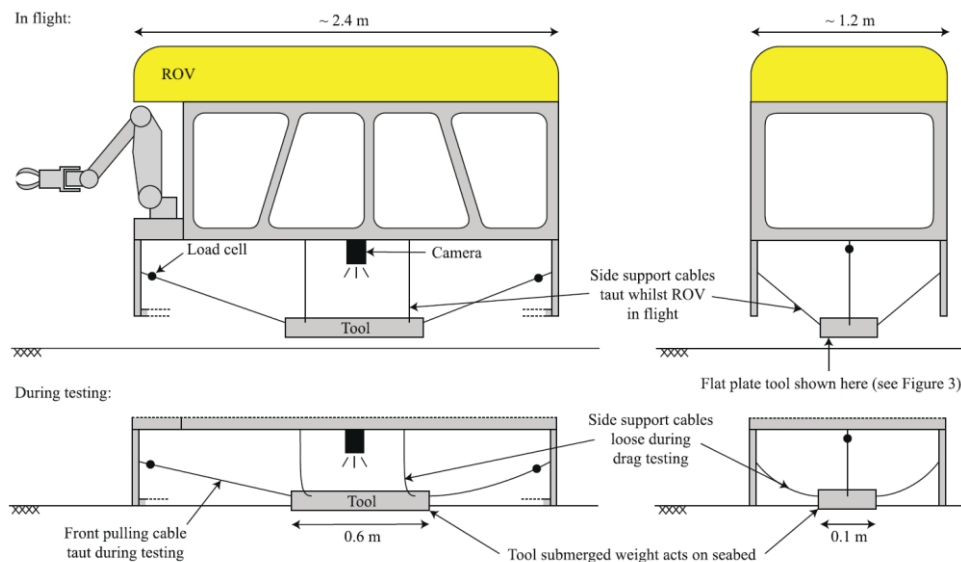


Figure 22 - Schematic of ROV-based drag test concept.

The sliding resistance is recorded by an attached load cell. Although the concept involves in-situ testing, all the reported tests in the study were conducted in the laboratory on dry sand and using three tools sandblasted to the same surface roughness: flat steel plate, steel pipe and steel chains. The tests were performed in a 2x2m pit with a thickness of 0.3m of dry silica sand, and under effective normal stresses between 4.8 and 6.6 kPa. An interpretation procedure is proposed to correct the results for the effect of the soil's passive force generated at the face of each embedded tool while dragging.

The limitations of this device are (1) the tool is dragged with an inclination angle which results in a non-uniform normal stress underneath it, and thus imprecise friction measurement, and (2) the tool is dragged using a displacement rate of 50mm/s, and if the tool were to be actuated by an ROV thruster, it is difficult to reach slower constant displacement rates. While this fast rate of shearing might be adequate for testing sands, much slower displacement rates are needed for tests on clays, particularly if drained conditions are targeted. Third, the analyses of the results to determine the interface resistance is not straightforward due to the need for a mathematical interpretation technique to account for the passive pressure at the ends and the shape effects of the test artifacts.

Recently, Schneider et al. (2020) introduced a new "Pipe-like" penetrometer apparatus to measure the strength, consolidation and the frictional properties of offshore sediments within a box-core sample. In concept, the apparatus consists of two novel box-core-sized penetrometers, the hemiball and toroid, having the same shape as the pipelines and equipped with pore pressure transducers, a load cell and an actuator with two degrees of freedom (Figure 23).

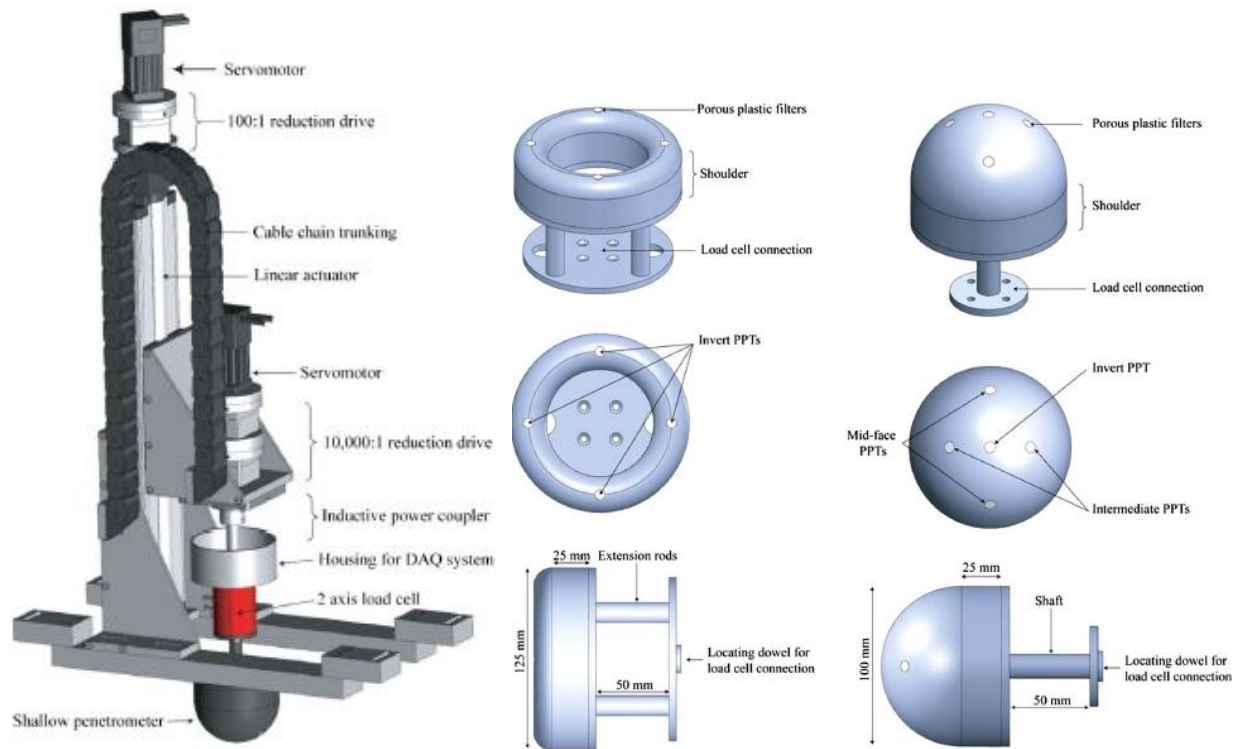


Figure 23. The "Pipe-like" penetrometer apparatus detailing (Schneider et al., 2020)

The setup can be fixed on a box-core to perform all the desired tests directly after the extraction of the soil sample on the deck of a survey vessel. Schneider et al. (2020) described in detail the design of each mechanical part of the apparatus in addition to the calibration of the sensors and custom-built wireless DAQ used to acquire live data. The basic test protocol comprises of four main stages:

1. Penetration stage: the probe will penetrate to a target vertical penetration load or to a desired embedment under undrained conditions.
2. Dissipation stage: under a constant vertical load, the excess pore pressures are allowed to dissipate until reaching the desired degree of consolidation, the coefficient of consolidation,  $C_v$  can be estimated.

3. Rotation stage: the probe can be rotated at either a fast rate or a slow rate with intervening dissipation periods to estimate the undrained and drained friction angles.
4. Penetration/extraction stage: an additional penetration of the probe can be done to a higher depth to capture the shear strength variation of the sediments.

Furthermore, a proof of concept test was performed in a kaolin clay box of 2 kPa strength to assess the apparatus functionality. The results were consistent with the ones performed in the interface direct shear box. Schneider et al. (2020) succeeded in building a very efficient testing setup that delivers quick and reliable results eliminating interpretation assumptions. Conversely, the minimum pressure range that can be applied is about 5 kPa whereas in offshore application lower pressures can be encountered. While this technique has been presented as an option for testing the pipe-soil interaction in a box core within an offshore vessel, the proposed setup cannot be used to perform an in-situ interface test under water.

## **2.4 Design approaches**

Appropriate prediction models for the axial pipe-soil interaction must be developed to help designers mitigate all the issues related to pipeline walking, buckling, geohazards and hydrodynamics. The key parameter for the pipeline design is the limiting resistance during axial movement which depends on the soil type, drainage conditions, and loading cycles. By analogy with the pile design, the  $\alpha$  (total stress) and  $\beta$  (effective stress) approaches were first adopted in analyzing axial pipe-soil interaction



problems. Given the advancement in experimental testing in the last two decades, a new much more complicated framework has been established, taking into consideration all the factors affecting the axial pipe-soil response.

#### **2.4.1 $\alpha$ and $\beta$ approaches**

Basically, both approaches are similar to the techniques used in estimating the shaft resistance on driven piles in clay. The alpha method predicts the axial soil-pipe resistance,  $F$ , assuming that the pipeline movement is fast enough to ensure undrained conditions using equation (2.14).

$$F = \alpha S_u A_s \quad (2.14)$$

Where  $S_u$  is the undrained shear strength of the soil sediments,  $A_s$  is the pipe-soil contact area and  $\alpha$  is the adhesion factor. These parameters require the identification of the pipeline embedment to calculate  $A_s$  and the in situ  $S_u$  profile to get the average undrained shear strength. Thus, this method could account for the undrained shear strength changes following the laying process and the interface roughness of the pipeline but it ignores the effect of the pipe submerged weight. White et al. (2011) reported on the indicative values of  $\alpha$  that can be used in design:

1. For peak resistance:  $\alpha = 1$
2. For residual resistance:  $\alpha = 1/S_t$  which is the inverse of the soil sensitivity

Nevertheless, the rate of the pipeline movement in actual loading conditions could be sufficiently slow preventing the generation of pore pressures and thus ensuring that failure occurs under drained conditions. In this case, the beta method must be adopted which is an effective stress method. The fully drained axial resistance can be expressed as equation (2.15).

$$F = \mu \xi V \quad (2.15)$$

Where  $\mu$  is the pipe-soil interface friction coefficient with  $\mu = \tan \delta$ ,  $\delta$  is the interface friction angle, and  $\xi V$  is the sum of the normal stresses around the pipe accounting for the wedging effect by the factor  $\xi$ . In case of the presence of pore pressures,  $\Delta u$ , the contact stresses have to be taken as the effective stresses. Equation 2.15 must then be adjusted to include the excess pore pressures. The axial resistance may then be estimated as:

$$F = \mu \xi V (1 - r_u) \quad (2.16)$$

Where:

$$r_u = \left( \frac{\Delta u}{\sigma_n} \right)_{average} \quad (2.17)$$

The above-mentioned methods can only deliver a single value of the pipe-soil axial resistance depending on the assumed drainage condition. They fail to capture the real pipe response through its whole operational time where a peak-residual response is expected, and a change of strength can occur after cycles of movement as noticed by White et al. (2011).

#### **2.4.2 Pipe-Soil Interaction Framework**

White et al. (2012) and Hill et al. (2012) used a set of data from in situ tests (Box Core, T-bar, SMARTPIPE), onshore model tests (small and large model) and laboratory tests (tilt table and interface shear box) to calibrate a theoretical framework

for assessing the axial pipe-soil resistance. The framework includes four main elements: (1) effective normal stress, (2) drainage conditions, (3) interface roughness and (4) wedging effect as shown in Figure 24. Boukpeti and White (2017) added a quantitative analysis of the consolidation process occurring either during shearing or between shearing cycles based on critical state soil mechanics concepts. The effect of such consolidation process and loading history on both the peak and residual axial resistance was also highlighted by Low et al. (2017) who suggested a detailed calculation procedure for the estimation of the interface strength throughout the pipeline operational life. The variations of the axial resistance with respect to all the elements introduced by these studies are presented in this section.

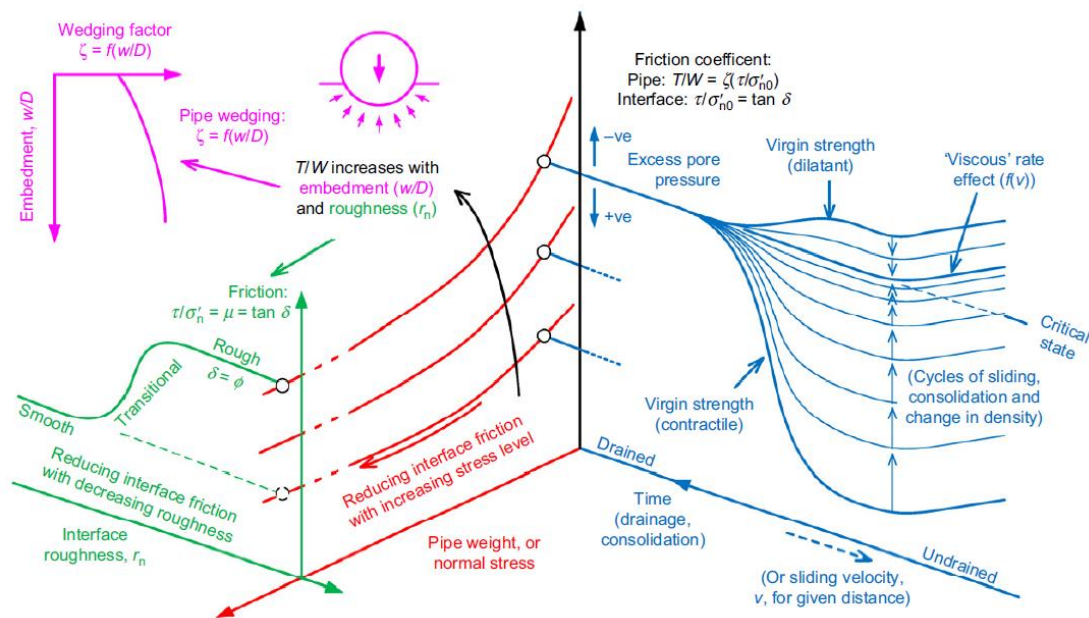


Figure 24. Mechanism controlling axial pipe-soil resistance (Boukpeti & White, 2017)

#### 2.4.2.1 Interface roughness

Westgate et al. (2018) gathered the data for more than 200 tests on clay soils at different interface roughness. It was shown that the drained and undrained interface

friction factors increased with interface roughness. There is a critical roughness representing the transition from smooth to rough interfaces and thus separating between the failure mechanisms occurring along the clay-pipe interface or internally through the clay. The data showed that this transition roughness is between 2 to 10  $\mu\text{m}$  (Figure 25).

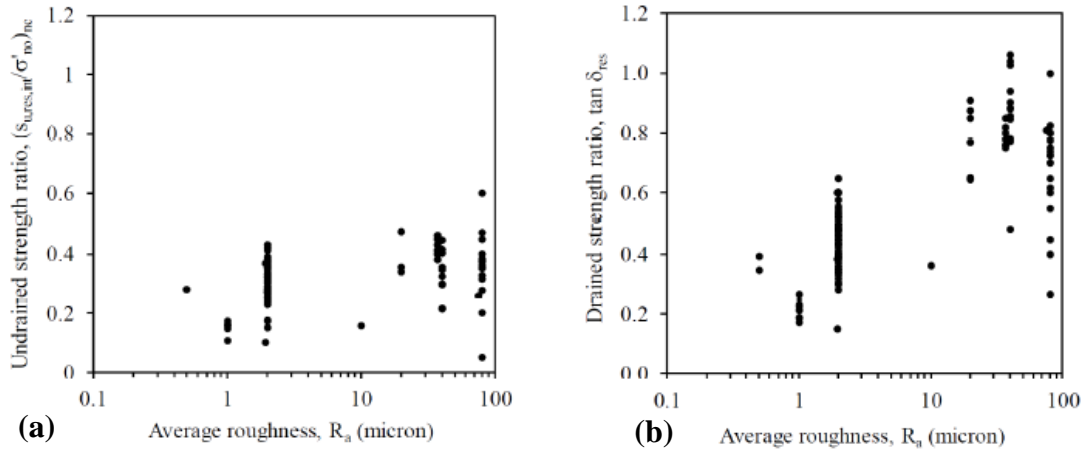


Figure 25. Shear strength ratio variation with interface roughness under: (a) undrained conditions and (b) drained conditions (Westgate et al., 2018).

#### 2.4.2.2 Effective normal stresses

Interface friction coefficients have been shown to decrease with effective normal stresses  $\sigma'_n$ , defined as the ratio between the submerged pipe weight,  $W'$  corrected by the wedging factor,  $\xi$  over the contact area.

The drained interface failure envelope was demonstrated to be slightly non-linear in the low normal stress range. Boukpeti and White (2017) proposed a power law relationship to describe this non-linearity.

$$\tau_d = a(\sigma'_n)^b < \mu_{max}\sigma'_n \quad (2.18)$$

Where  $a$  and  $b$  and  $\mu_{max}$  are constants that vary with the type of soil and the interface roughness.  $\mu_{max}$  is the maximum limit of the stress ratio  $\tau_d/\sigma_n$ , to avoid unrealistic friction coefficients as  $\sigma'_n$  approaches zero. Figure 26 shows the power law fitted by Boukpeti & White (2017) for both clays tested in the interface direct shear box.

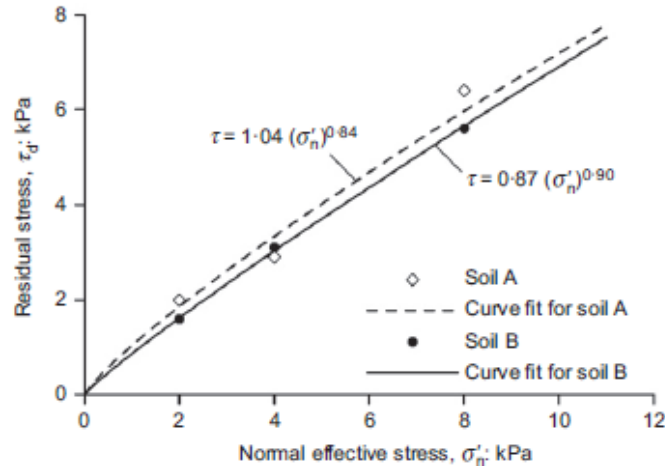


Figure 26. Power law function developed by Boukpeti & White (2017)

#### 2.4.2.3 Drainage conditions:

The drained interface resistance,  $F_{res}$ , is the residual/steady resistance reached after large pipe movement and it is controlled by the interface friction angle,  $\delta_{res}$ , enhanced by the wedging effect. It is usually expressed as:

$$F_{res,d} = \xi W' \tan \delta_{res} \quad (2.19)$$

Where  $W'$  is the submerged pipe weight and  $\delta_{res}$  can be estimated from laboratory tests.

The undrained residual axial resistance is mainly controlled by the pipe-soil contact effective stress level and history created by the precommissioning stages (flooding, hydrotest, dewatering). These processes will modify the pipe weight and the induced excess pore pressures and thus change the effective stresses applied on the

seabed. Such variation was included in the estimation of the undrained residual axial resistance by Low et al. (2017) and Westgate et al. (2018) as:

$$F_{res,u} = \xi W' \left( \frac{S_u}{\sigma'_{n0}} \right)_{nc} \left( \frac{W'_{max}}{W'} \right)^m = \left( \frac{S_u}{\sigma'_{n'}} \right)_{nc} \left( \frac{\sigma'_{n,max}}{\sigma'_{n0}} \right)^m \sigma'_{n0} A_s \quad (2.20)$$

Where  $S_u$  is the interface undrained shear strength in case of normally consolidated soil,  $W'_{max}$  is the previous maximum pipe weight,  $W'$  is the current pipe weight and  $m$  is equivalent to the plastic volumetric strain ratio in Cam Clay or SHANSEP overconsolidation index and usually ranges between 0.5 to 1 (Westgate et al., 2018).

In some cases, the interface response may be neither fully drained nor fully undrained. The displacement rate may permit some degree of consolidation during shearing leading to a continuous process of generation and dissipation of excess pore pressure. Other phenomena can also occur known as the episodic consolidation caused by the intermittent pipeline movement. Thus, the soil will be sheared under undrained conditions followed by consolidation periods. These different conditions throughout the pipe operational life will definitely change the state of stress around the pipeline and the resulting residual axial resistance. Boukpeti & White (2017) and Low et al. (2017) used critical state soil mechanics concepts to track the axial resistance variation (Figure 27a). Two scenarios can be differentiated for (1) initially normally consolidated soil and (2) initially overconsolidated soil.

For the first case, starting from the wet side of the critical state, the partially drained and undrained shearing cycles will lead to the generation of positive pore pressures and thus a decrease of the effective normal stresses. The excess pore pressure will dissipate either during partially drained shearing or afterwards during the

consolidation periods. Meanwhile, the soil will contract and densify. After repeated cycles of shearing and consolidation, the operational axial resistance will increase and finally converge towards the drained critical value. The blue curve in Figure 24 illustrates this “consolidation hardening” that was observed by Ballard & Jewell (2013) using the in-situ SMARTPIPE and by Boukpeti & White (2017) and White et al. (2012) using interface direct shear tests (Figure 28a).

For the second case, starting from the dry side of the critical state, negative pore pressures are expected during these shearing stages which will gradually dissipate. The soil will thus swell and soften. Therefore, the operational axial resistance will thus decrease with cycles until reaching the drained value (Figure 27b). This is known as the “consolidation softening” which was captured by Boylan et al. (2014) as indicated in Figure 28(b).

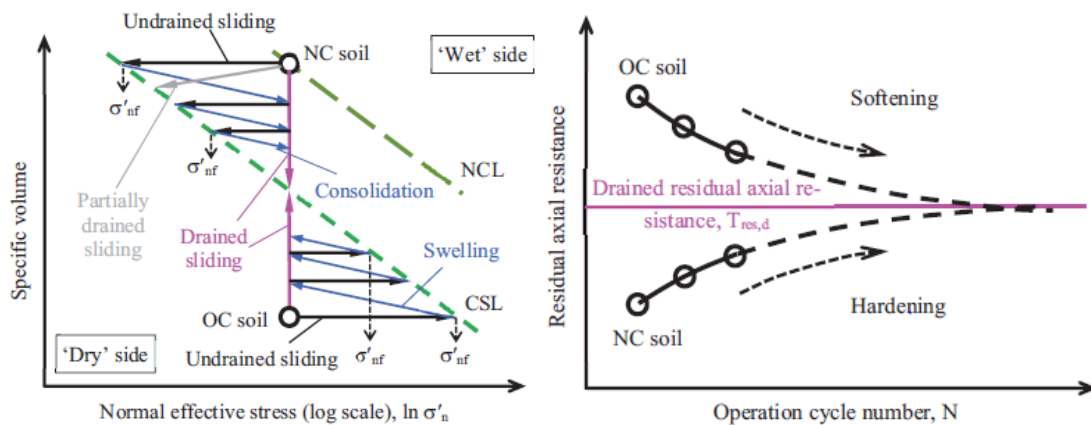


Figure 27. (a) Critical state model to capture the effective stress variation with shearing cycles and (b) The residual axial resistance change with number of cycles (Low et al., 2017).

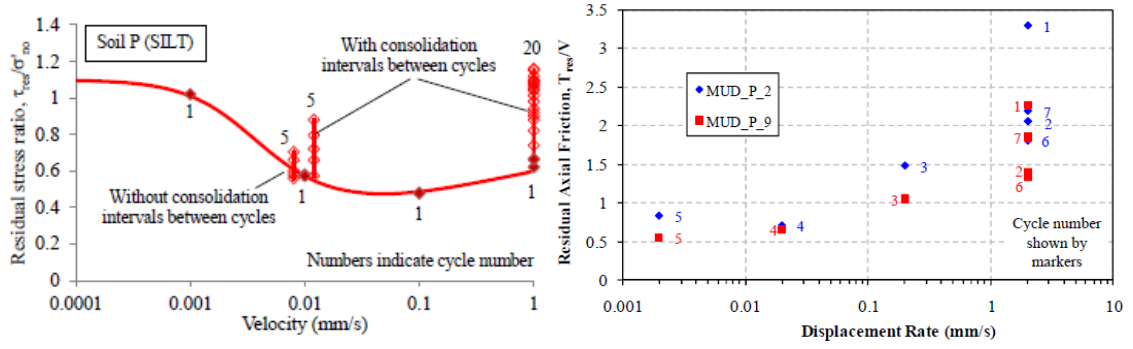


Figure 28. Residual stress ratio variation with shearing rates for : (a) Normally consolidated clay (White et al., 2012) and (b) Overconsolidated clay (Boylan et al., 2014)

The degree of dissipation of excess pore pressure during these episodic processes is related to the consolidation properties of soils, the time of shearing or of pause,  $t$ , and the drainage path. It can be calculated using equation (2.21)

$$U = 1 - e^{-\ln 2 \left( \frac{T}{T_{50}} \right)^n} \quad (2.21)$$

Where  $T = C_v t / D^2$ ,  $C_v$  the coefficient of consolidation of the soil,  $D$  is the pipe diameter, and  $T_{50}$  is 0.05 for axial pipe displacement and 0.005 for the pause period (Randolph et al., 2012). Knowing the degree of consolidation, the effective stress level at the end of each cycle,  $\sigma'_{nf}$ , can be estimated and thus the operational axial resistance can be calculated using equation 2.22 as proposed by Low et al. 2017.

$$T_{res,op} = \mu_{int,res} \sigma'_{nf} A_s \quad (2.22)$$

The presented calculation method can be calibrated using site-specific soil element tests or model tests, else the response of different soil and pipeline operational conditions can be extrapolated using the theoretical framework. This will help to narrow the estimated range of friction coefficients and reduce the predictions uncertainties.



## CHAPTER 3

### DRAINED AXIAL PIPE-SOIL RESISTANCE USING TILT TABLE AND DIRECT SHEAR TESTS

#### 3.1 Introduction

The increasing cost of high-pressure high-temperature offshore pipelines has pressed researchers to improve their design models in an effort to reduce project costs without compromising safety. The most critical design issues relate to excessive pipeline deformations that could lead to pipeline buckling and walking due to thermal expansion and contraction during operation. In order to mitigate such risks, the axial pipe-soil interface forces must be reliably quantified to incorporate/account for the pipeline interface roughness, the appropriate low normal stress levels imposed by the pipeline weight, and the rate of the pipeline movement.

Several researchers developed laboratory testing equipment specifically devised for the measurement of pipe-soil interface interaction at low normal/applied stresses. These include interface direct shear (IDS), cam-shear, torsional shear, and tilt table test devices (Najjar et al. 2007; White et al. 2012; Hill et al. 2012; Eid et al. 2015; Kuo et al. 2015; Boukpeti & White 2017; Westgate et al. 2018) . Other investigators built laboratory pipe model test setups that simulate field conditions ( White et al. 2011;Senthilkumar et al. 2013; Smith & White 2014; Boylan et al. 2014; Wijewickreme et al. 2014 and Shi et al. 2019) or devised field setups for measuring the axial pipe-soil resistance in situ ( Hill & Jacob 2008 ; White et al. 2011; Ballard & Jewell 2013 ; Stanier et al. 2015 and Schneider et al. 2020).

Laboratory element tests make up the largest share of test methodologies adopted to estimate the soil-soil and soil-interface resistances in the low pressure range, while minimizing cost and time. Such methodologies were utilized effectively to identify factors that govern the interface resistance, including the pipe roughness, rate of shearing, normal stress and soil composition.

Hill *et al.* (2012), White *et al.* (2012), Boukpeti and White (2017), Low *et al.* (2017) and Westgate *et al.* (2018) adapted and modified conventional interface direct shear devices to allow for reliable interface testing at low confining pressures while performing repeated cycles/reversals to reach residual conditions. The custom-fabricated devices allowed for the investigation of the effects of drainage conditions, consolidation during and in-between shearing episodes and over-consolidation ratio on the interface resistance (White *et al.* 2012 and Boukpeti and White 2017). Westgate *et al.* (2018) collected data consisting of more than 200 IDS tests on several soft clays and pipeline coatings and showed that the interface failure envelope in the low stress range tends to be nonlinear and independent of the plasticity index.

Ganesan *et al.* (2014) used the Cam-shear device that applies exceptionally large shear displacements (reaching ~ 200mm) to investigate the effect of drainage conditions on the peak and residual interface shear resistance of reconstituted soft marine clays tested against smooth and rough interfaces. Kuo *et al.* (2015) and De Brier *et al.* (2016) introduced a torsional shear device (Cam-tor) that allows for performing tests on intact and remolded samples under normal stresses ranging from 2-40 kPa. Along the same lines, Eid *et al.* (2015) used a torsional shear device to test different soils against smooth and rough interfaces. The device was modified and adapted for low effective stress conditions (1 kPa to 5kPa) by reducing side-wall friction in compliance with the

recommendations of Stark and Eid (1993). Several correlations were developed to estimate the residual soil and interface shear strength at low effective stresses as a function of the plasticity index of the soil and the interface roughness. Eid *et al.* (2019) validated these correlations for cases tested in “the intermediate normal stress range” (10 to 25 kPa).

Najjar *et al.* (2003, 2007) and Pedersen *et al.* (2003) developed a tilt table device to measure the drained residual shear strength mobilized at the interface between several pipeline coatings and marine clays. In the tilt table device, the drained residual interface or soil shear resistances could be readily mobilized and accurately quantified since this frictionless device relies only on gravity loading and allows for the reproduction of low confinement conditions (1 to 6 kPa) and relatively large displacements (up to 50 mm). Soil specimens used in the tilt table tests are very thin (1.5 to 3 mm thick) leading to short testing durations while ensuring fully drained conditions and relatively high shear strains. A total of 54 tilt table tests led to the conclusion that the type of coating and composition of soil are the predominant factors that affect the residual shear strength at the pipe-soil interface.

The comprehensive background review conducted as part of the work presented in this paper indicated that the two most common laboratory testing approaches used for measuring the interface strength between pipelines and clays are the tilt table test and the interface direct shear test. To date, there are no published efforts that show direct comparisons between results from these two testing systems. Thus, the objective of this paper is to design and fabricate tilt table and interface direct shear testing setups that are capable of measuring the drained interface resistance between pipelines and clays and use these setups to study the effects of low effective normal stresses, type of pipeline

coating, and soil composition on the drained peak and residual clay-pipe interface response. The ultimate goal is to compare the results from tilt table and interface direct shear tests under identical interface and soil conditions and provide recommendations on the use and value of these two test alternatives in the design and testing of offshore pipelines.

## **3.2 Testing Materials**

### **3.2.1 Soils**

Three fine-grained soils were used in the testing program. These include low plasticity clay (LPC), high plasticity clay (HPC) and synthetic kaolinite (KAO) (Figure. 29). The index properties and grain-size distribution of these soils are presented in Table 4 and Figure 30 respectively. It should be noted that the LPC is a natural soil that includes 26% sand in its composition. This makes it an interesting soil to study given that most of the published interface tests at low confining pressure are limited to pure clays or sands. The HPC consists of a mixture of 25% bentonite and 75% fire clay by weight. Image scans for the LPC and HPC at a scale of 500  $\mu\text{m}$  are presented in Figure. 31 (a) and (b) respectively. The SEM images clearly show the presence of sand particles within the clay matrix for the LPC.

The grain diameter that corresponds to 50% passing ( $D_{50}$ ) was found to be 0.01, 0.002 and 0.0009 mm for LPC, HPC and KAO, respectively. Slurry samples were prepared by mixing the oven-dried samples at water contents equal to or greater than their liquid limits. The LPC was mixed at a water content of 29%, whereas the HPC and KAO were mixed at 100% water content. After mixing, each reconstituted sample is left in a sealed plastic bag for a minimum duration to equilibrate/hydrate before being

tested. A minimum of 18 hours standing time for the LPC and a minimum of 36 hours for the HPC and KAO were used, as per ASTM D3080.

Table 4. Properties of clays used in the experimental program

Soil	$G_s$	Size fraction, %			USCS	Atterberg limits, %			$D_{50}, \text{mm}$
		Sand	Silt	Clay		$LL$	$PL$	$PI$	
Low Plasticity Clay	2.63	26	36	38	CL	28.9	16.4	12.5	0.01
High Plasticity Clay	2.78	0	50	50	CH	83	29	54	0.002
Kaolinite	2.56	0	13.4	86.5	MH	65	39	26	0.0009

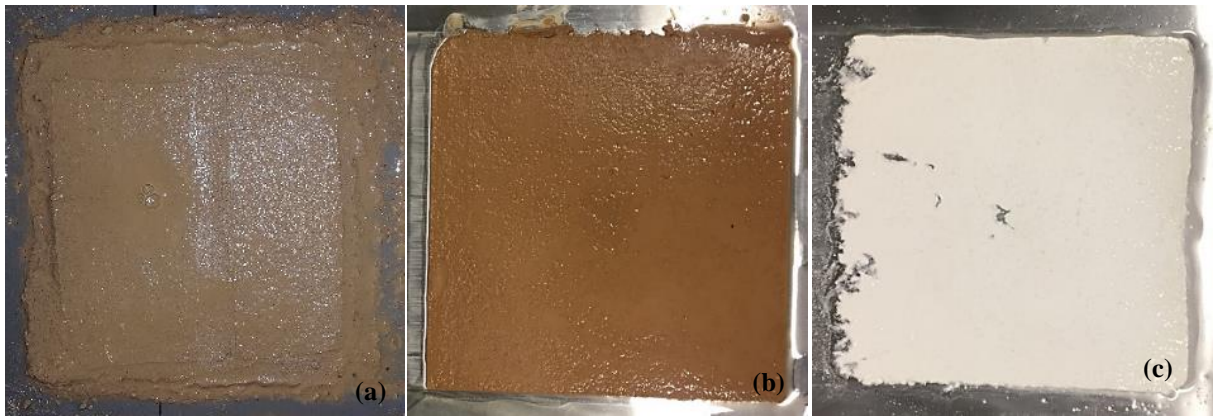


Figure 29 Tested soils: (a) Low Plasticity Clay, (b) High Plasticity Clay, and (c) Kaolinite

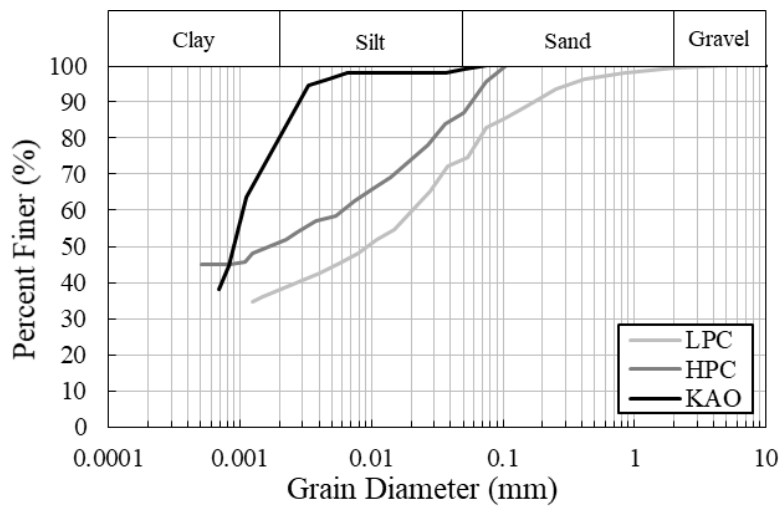
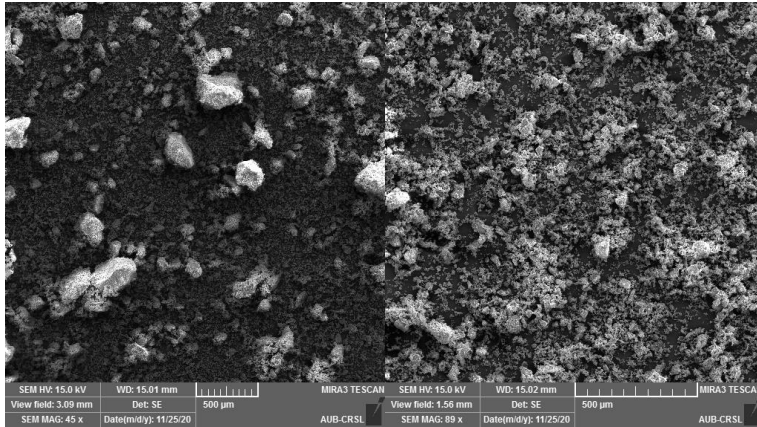
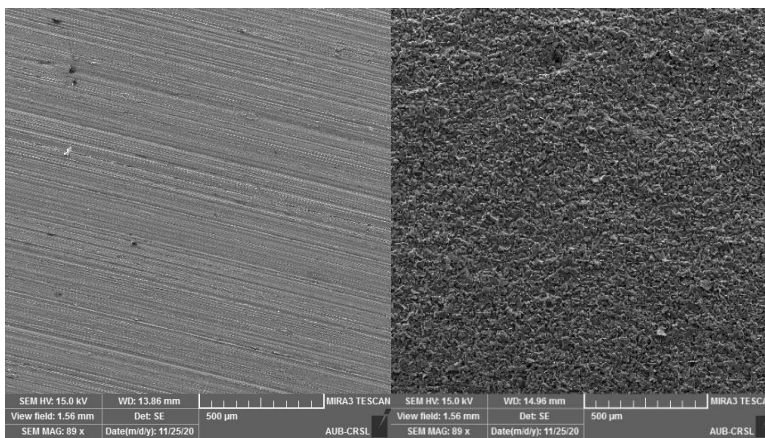


Figure 30. Gradation curves of the tested soils



(a) Low Plasticity Clay (LPC)      (b) High Plasticity Clay (HPC)



(c) Smooth Stainless Steel      (d) Rough Sandpaper

Figure. 31 SEM images of (a) LPC, (b) HPC, (c) Stainless Steel, and (d) Sandpaper

### 3.2.2 Interfaces

Interfaces of various roughnesses were used in the testing program (Figure. 31c, Figure. 31d, and Figure 32). The interfaces included plexiglass, stainless steel and sandpaper, with average surface roughness  $R_a$ , measured using a sensitive profilometer, of  $0.003 \mu\text{m}$ ,  $0.08 \mu\text{m}$  and  $3.5 \mu\text{m}$ , respectively. The plexiglass and stainless steel are referred to as the “smooth” interfaces in this paper and the sandpaper as the “rough” interface. For each interface material, 300x300 mm (tilt table tests) and 90x60 mm (interface direct shear tests) sheets were prepared to act as the solid interfaces on which the clay is sheared. In the case of the rough interface, sandpaper was glued to a plastic

sheet with epoxy resin to guarantee that no air bubbles are entrapped between the sandpaper and the lower plate and to prevent sliding of the sandpaper on the plate during testing.

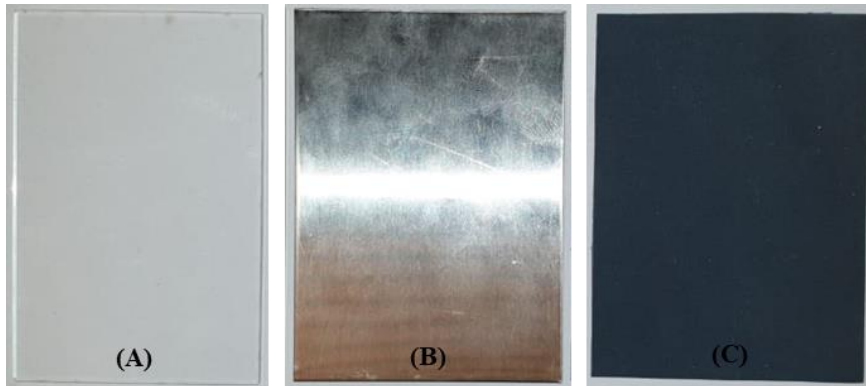


Figure 32. The 90x60 mm interfaces: (a) Plexiglass, (b) Stainless Steel, and (c) Sandpaper, fitted into the lower shear box of the interface direct shear apparatus

### 3.3 Interface direct Shear Testing

#### 3.3.1 Modified Direct Shear Apparatus

A conventional direct shear apparatus was modified to limit the mechanical friction in the system and be compatible with the stringent constraints of the low confining pressure application (Figure 33). The inherent system friction is mainly due to the box-interface sliding resistance, the weight of the shear box and the technique adopted to apply a normal load on the sample (level arm and eccentricity). Accordingly, and in an effort to reduce that potential source of error, the steel shear box was replaced by a custom-fabricated Teflon box that has a lighter weight and a much lower sliding resistance. Moreover, the conventional lever arm that is used to apply the normal stress was removed and replaced by dead weights that were applied directly on top of the sample via a frictionless custom-fabricated loading frame that ensures that the weights are perfectly centered and the applied normal stress on the soil sample is uniform. The lower half of the shear box was also fabricated from Teflon and designed to receive the

prepared interface plates. In a further effort to minimize friction between the upper and lower halves during shearing, four screws with Teflon caps were used to adjust the gap between the two halves. The modified interface direct shear setup was also equipped with a measurement and data collection system that guaranteed accurate readings of very low shear forces (Omega load cell with 0.05 N accuracy) and the vertical and horizontal displacements (LVDT with 0.001 mm accuracy). Figure 33 shows in details the modification made to the standard direct shear testing machine.

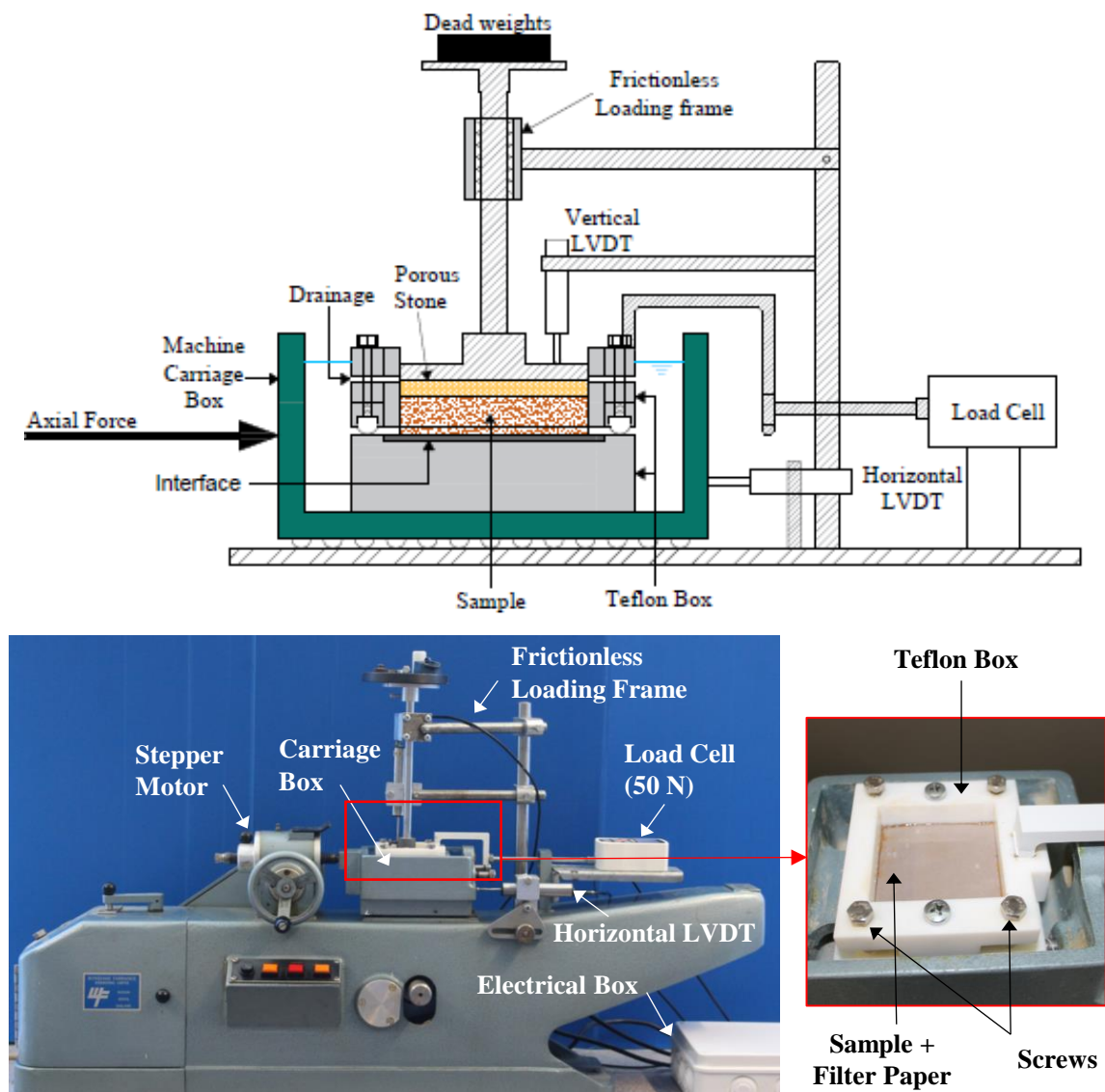


Figure 33. Modification made to the standard direct shear testing machine



### 3.3.2 Testing Procedure

The soil samples were prepared by thoroughly mixing the soil at the desired water content to ensure homogeneity. After completion of the required “stand period”, the mixed soil was transferred into the upper half of the Teflon shear box. A low friction oil was swabbed/applied to inside walls of the box sides to further minimize vertical friction. A filter paper and a porous stone were placed on top of the sample, along with the loading system and the LVDT measuring vertical displacements. Dead weights were then added on top of the loading arm to reach the desired confining pressure (1.7, 2.45, 4.26 and 6.1 kPa) and the monitoring of the consolidation phase started. Once the primary consolidation was completed, the screws were loosened and a gap of around 0.7 mm was created for the interface tests. For the tests aimed at measuring the internal strength of the clay, a gap having the maximum soil particle size was adopted.

The time to failure ( $t_f$ ) for drained conditions was computed as 50 times the time required for the sample to achieve 50% consolidation ( $t_{50}$ ), as per ASTM D3080. The shearing rate required to ensure fully drained conditions was then chosen to be smaller than  $R_d$  (mm/s) according to equation 3.1. Note that  $d_f$  (mm) in equation 3.1 is the estimated horizontal displacement at the peak shear stress.

$$R_d = \frac{d_f}{t_f} \quad (3.1)$$

Based on the consolidation data, the shearing rates were selected to be 0.00004 mm/s for interface tests and 0.00005 mm/s for the clay tests. The shearing phase was terminated when the reduction in the shear stresses with displacement stabilized, indicating the mobilization of the residual interface strength. Specimens that were sheared up to displacements as high as 10mm indicated that terminating the tests at

lower displacements (~ 3.0 mm) was sufficient for the purpose of estimating the residual strength of the slurry-consolidated remolded clay samples that were used in this study.

Despite the effort invested in modifying the direct shear setup to minimize friction, minor inherent friction persisted in the system. In order to quantify that residual friction in the modified setup, the shearing resistance between the upper and lower Teflon boxes was recorded without incorporating a soil sample. The resulting frictional resistance was 0.3 N at a shearing rate of 0.00004 mm/s. In addition, the friction between the soil and the inside walls of the box was quantified as the difference between the force read by a load cell placed beneath the soil sample and the dead weights that were applied to the top of the specimen. Despite the modifications made to the test setup, results indicated a reduction of about 5% to 11% in the applied normal stress as a result of vertical wall friction (Table 5). To account for (1) friction between the upper and lower Teflon boxes and (2) residual friction between the soil and inner sides of the Teflon box, a force of 0.3 N was subtracted from the measured shear force during the shearing stage and the nominal applied normal stress was reduced accordance with the data in Table 5.

Table 5. Measured percent reduction in normal stress due to friction in the box

Normal stress, kPa	Reduction in Normal Stress (%)		
	LPC	HPC	KAO
1.7	11	5-6	5-6
2.45	11	5-6	5-6
4.26	9	5-6	5-6
6.1	7	5-6	5-6

### **3.4 Tilt Table Testing**

#### **3.4.1 Tilt Table Apparatus**

A tilt table was fabricated to measure the drained residual pipe-soil interface strength. The apparatus is composed of a 450x450 mm Plexiglass plate hinged to the base at one side and attached to a manual gear through a cable on the other. The plate is lifted by rotating the gear and a maximum inclination angle of 45° can be read on the curved vertical plate as shown in Figure 34. Interfaces with a size of 300x300 mm are typically fixed on the plate using four screws except for the sandpaper that is glued to a thin plastic sheet using epoxy and then fixed to the tilt table. After placing the soil and applying the target normal stress, the tilt table is submerged inside a Plexiglass water bath to ensure full sample saturation during testing.

#### **3.4.2 Testing Procedure**

The tilt table soil specimen consisted of a 2-mm thick layer of soil spread over the interface with an area of 150x150 mm that matches the size of the steel loading plate used to apply the desired normal stress (Figure 34b). The consolidation phase was then initiated by placing the loading plate on top of the soil. Once 95% of the consolidation was achieved under the weight of the loading plate, the whole setup was placed inside the water bath and dead weights were added on top of the loading plate with a specific offset from the center to reach a uniform normal stress, while minimizing eccentricity (Figure 34c). This offset of the center of gravity of the load was created by attaching spacers of different thicknesses to the loading plate.

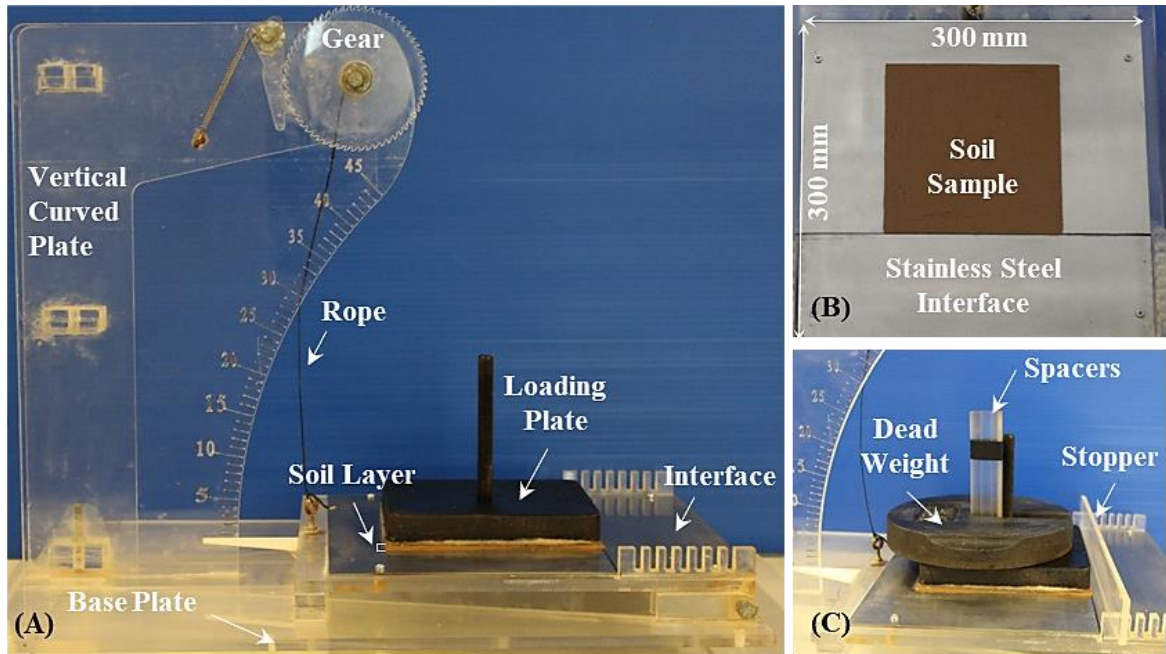


Figure 34. (a) Tilt table test setup, (b) 2mm clay specimen, and (c) Additional loading

One trial test was done for each normal stress to select the offset distance that ensures a uniform normal stress on the sample at failure. The sample was then allowed to achieve a degree of consolidation of 95% under the applied normal stress. The time needed was calculated as:

$$t_{95} = \frac{T_{95}H^2}{c_v} \quad (3.2)$$

Where:

$$T_{95}=1.129$$

$c_v$ = coefficient of consolidation obtained from the consolidation phase of the IDS tests at the same normal stress ( $\text{mm}^2/\text{s}$ )

H = sample thickness

After consolidation, shearing was initiated by lifting the Plexiglass plate slow enough in order to allow any generated excess pore water pressures at the interface to

fully dissipate. The rate of shearing was selected so as to maintain a more-or-less constant level of deformation and to ensure fully drained conditions (Najjar et al. 2007). The inclination increments were 5°, 3°, 2° followed by 1° increments until slippage occurred. From the trial test, a preliminary estimate of the failure angle can be obtained. Thus, an approximate number of inclination increments can be set. Based on this number, the minimum waiting time at each increment can be deduced by dividing the time to failure  $t_f$  by the number of increments. Once the sample slips, a stopper rod will block its displacement at 10 mm. Afterwards, the plate was lowered 10° and left for 10 min and the whole procedure was repeated 7 times until 70 mm of total shear displacement were attained. The last slippage angle was considered as the residual interface angle ( $\alpha$ ) and the corresponding effective normal stress and the shear stress at failure can be calculated using equations 3.3 and 3.4, respectively. Figure 34 below shows the slipping phase at failure.

$$\sigma' = \frac{W'}{S} \cos (\alpha) \quad (3.3)$$

$$\tau' = \frac{W'}{S} \sin (\alpha) \quad (3.4)$$

Where:

- a.  $W'$  = Submerged weight on the sample (sum of the loading plate and the dead weights) in kg
- b.  $S$  = area of the sample,  $\text{mm}^2$

Figure 34 shows the slipping phase when performing a tilt table test

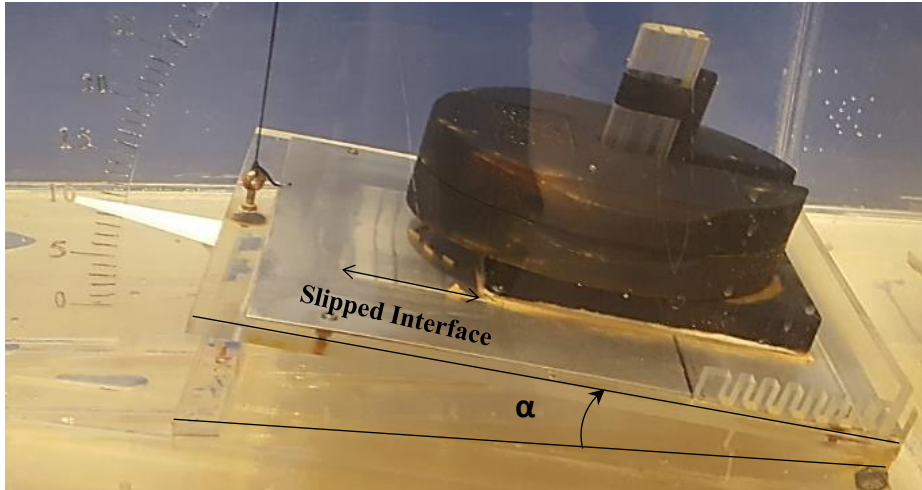


Figure 35. Slipping phase at failure

### 3.5 Testing Program

One of the main objectives of this study was to investigate whether the drained residual interface strength can be fully mobilized and reliably measured using interface direct shear test devices that are adapted for low confinement applications. Typical direct shear setups are limited by sample size, inherent mechanical friction of the device itself, and the maximum displacement which can be imposed in any given direction. Since the-tilt table device eliminates the negative effects of mechanical friction and allows for larger shear strains under fully drained conditions, it could be argued that tilt table test results can be used as a reference for comparison when it comes to the drained interface strength. Comparisons between tilt table and direct shear results on the same soils and interfaces could shed light on whether the reduction of friction and the adoption of very slow shearing rates in modified direct shear devices may render interface direct shear testing as the simpler, but equally reliable, test methodology.

In an attempt to answer that question, 18 tilt table and 30 interface and internal direct shear tests were performed at low confining pressures ranging from 1.7 to 6.1

kPa, using three interface types and three soil types. Aside from achieving a comparison between the tilt table and the direct shear tests, results of the experimental program were used to supplement the literature with data on the dependency of the clay-solid interface resistance on the normal stress, and the influence of the interface roughness and soil composition on the drained interface strength.

### **3.6 Experimental Results and Discussion**

#### **3.6.1 Direct Shear Tests**

In this section, the results pertaining to the direct shear tests on the clay and the clay-solid interfaces are presented. The time-settlement response of the clay specimens during the consolidation phase is recorded and analyzed to determine the compressibility and rate of consolidation of the clays. The response of clay and clay-solid interfaces during the shearing phase is then analyzed to quantify the shear stress versus horizontal displacement relationship and determine the drained peak and residual shear strengths as a function of the applied normal stress, clay type, and interface roughness. The results of the interface direct shear tests are then discussed in the context of published work to shed light on the effectiveness and applicability of available correlations that aim at predicting the drained interface shear response of clay-solid interfaces for offshore pipeline applications in the low confinement range.

##### **3.6.1.1 Consolidation Response**

Figure 36 shows representative consolidation curves measured in clay/clay (Figure 36a) and clay/interface (Figure 36b and Figure 36c) direct shear specimens at a

representative normal stress of 4.26 kPa. Results clearly indicate that the consolidation response depends on the composition of the soils, the fines content, and their plasticity. The high plasticity clay (HPC) exhibited the highest compressibility and the largest  $t_{50}$  value, leading to the lowest average coefficient of consolidation,  $c_v$  (Figure 36 and Figure 37b). The low plasticity clay (LPC) exhibited the lowest compressibility, which was linked to the presence of 26% sand in its composition (Figure 36). The limited number of tests that were conducted on the industrial kaolinite (KAO) at a normal stress of 4.26 kPa (Figure 36 and Figure 37c) indicated that the KAO exhibited an intermediate compressibility and a relatively high average coefficient of consolidation, which is in line with its classification.

A clearer representation of the variation of  $c_v$  with normal stress, clay type, and test type (clay, clay/steel, or clay/sandpaper) is presented in figure 9. Results indicate that irrespective of the clay type, the coefficient of consolidation  $c_v = 0.196 \frac{H^2}{t_{50}}$  that is back-calculated from the consolidation stage of interface tests is higher than that calculated from clay/clay tests. The average values of  $c_v$  in the clay-sandpaper tests were 2.6 times higher than  $c_v$  in the clay-clay tests for the LPC, 1.8 times higher for the HPC, and 1.5 times higher for the KAO. This indicates that horizontal drainage could be occurring at the clay-sandpaper interface.



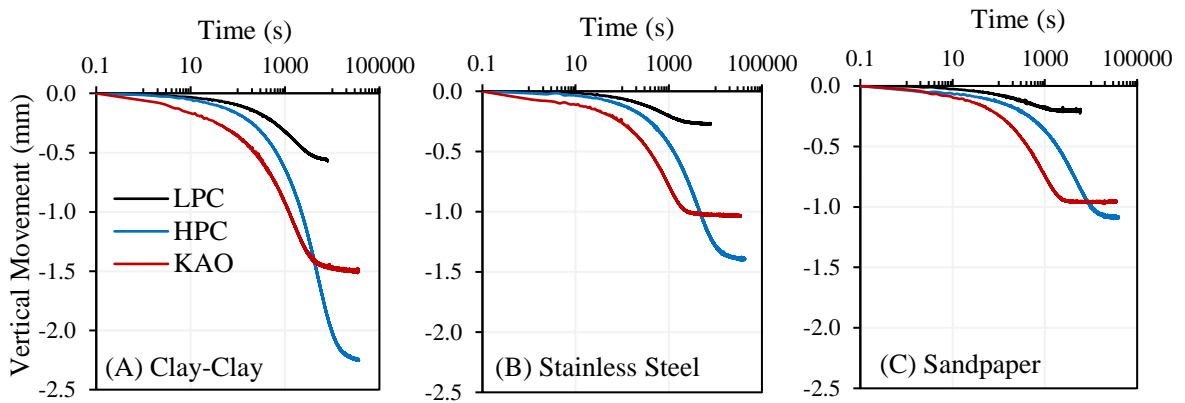


Figure 36. Consolidation curves for (a): clay-clay and clay-interface tests: (b): clay-stainless steel, and (c): clay-sandpaper at a  $\sigma'_n$  of 4.26 kPa

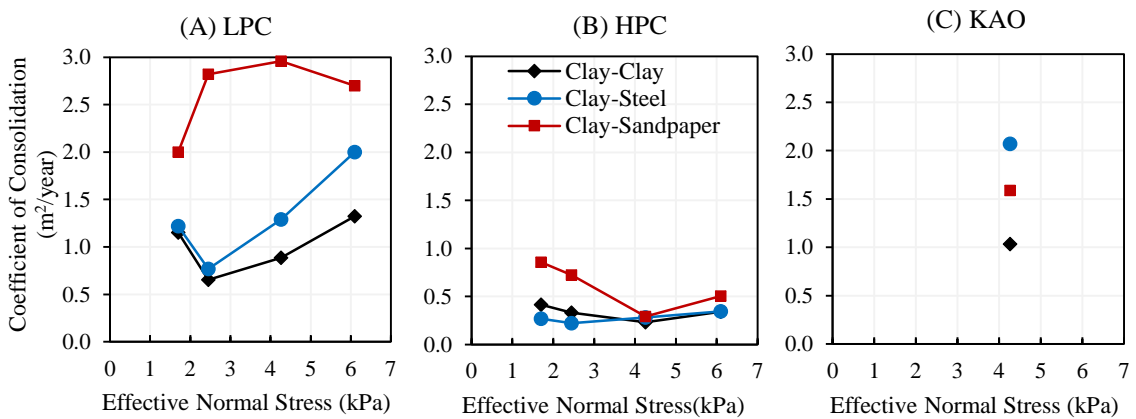


Figure 37. Variation of coefficient of consolidation with effective normal stress for (a): LPC, (b): HPC, and (c) KAO

Note that differences between  $c_v$  in clay-clay and clay-interface tests seem to narrow down (for LPC) or even disappear (for HPC) when the smooth steel interface is used. This indicates that the mechanism that seems to be facilitating horizontal drainage at the clay/pipe interface is a function of the roughness of the pipe interface and is affected by the applied normal stress.

### 3.6.1.2 Shear Response (Clay-Clay and Clay-Interface)

Direct shear tests were conducted on clay specimens to determine the shear strength of the clay at low confining pressure. The rate of shear was selected to ensure fully drained conditions based on the observed  $t_{50}$  values. Results are presented in Figure 38 and include the variation of the shear stress with horizontal displacement, peak and residual failure envelopes, and variation of the secant friction angle (peak and residual) with the logarithm of the normal stress. An investigation of the stress–displacement curves leads to several observations.

First, the LPC was observed to exhibit peaks at horizontal displacements in the order of 2 to 3 mm, in contrast to the HPC which exhibited a more ductile response with the peaks delayed to displacements of 5 to 7 mm. After the peaks, the LPC exhibited a softening response which ultimately stabilized at shear stresses corresponding to residual secant friction angles that were 3 to 5 degrees smaller than the peak angles. The HPC exhibited a complex post peak response that yielded residual secant angles that were only 2 degrees smaller than the peak.

Second, the observed failure envelopes were nonlinear with the nonlinearity being more visible in the LPC. The nonlinearity is evidenced in the reduction in the drained residual secant friction angle (average reductions of 23 and 8% for the LPC and HPC, respectively) as the normal stresses increased from 1.7 to 6.1 kPa. This nonlinearity was noted in previous studies (Skempton 1985; Stark and Eid 1994 and Najjar *et al.* 2007) for clays sheared at low stresses.

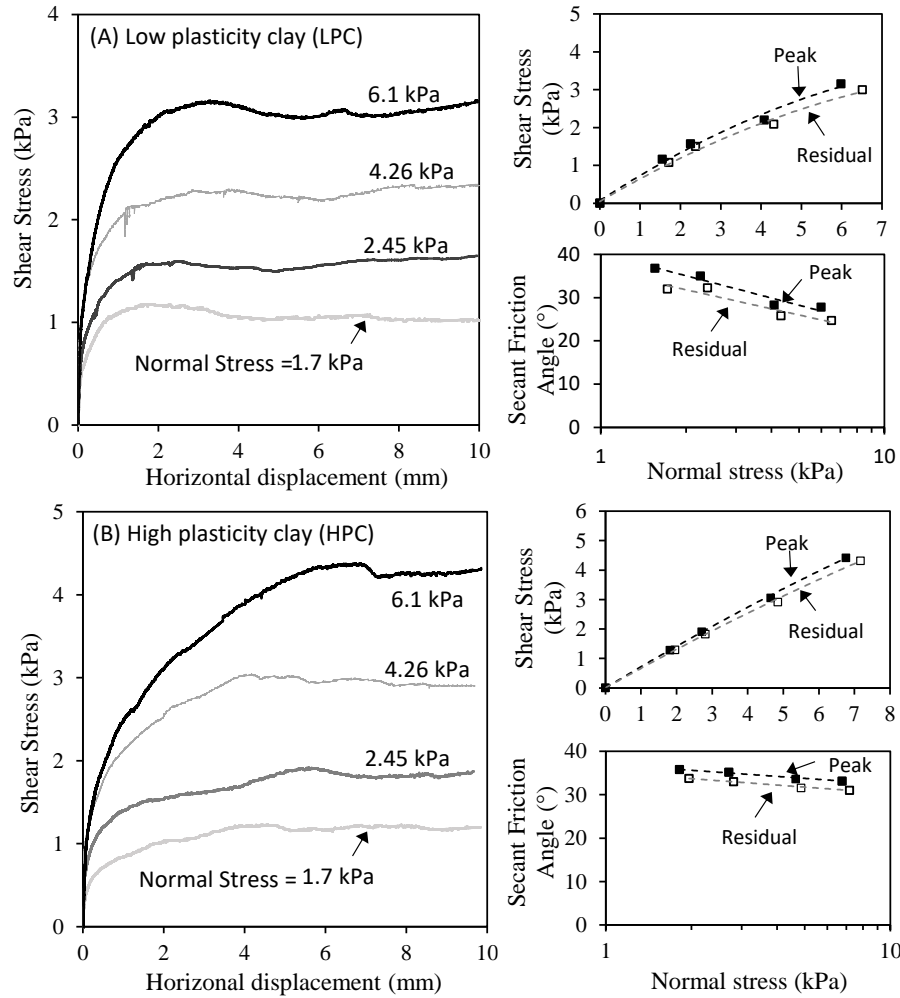


Figure 38. Results of the clay-clay direct shear tests on LPC and HPC soil

Third, a comparison between the HPC and LPC results indicates that the drained residual secant friction angle was highest for the HPC and lowest for the LPC, with a maximum difference of about 6 degrees at the highest normal stress. This difference in soil strength is related to differences in clay content and mineralogy in addition to the presence of sand (LPC).

Results of the interface direct shear tests are presented in Figure 39 and Figure 40 for the clay-steel (smooth interface) and the clay-sandpaper (rough interface) tests,

respectively. For the smooth interface, results show a relatively “brittle” interface response, with the peak interface stress being mobilized at very small displacements (~ 0.5 mm), irrespective of the soil type. However, the post peak response of the LPC was different than that of HPC, with the low plasticity clay achieving residual conditions at relatively low displacements compared to the high plasticity clay (Figure 39).

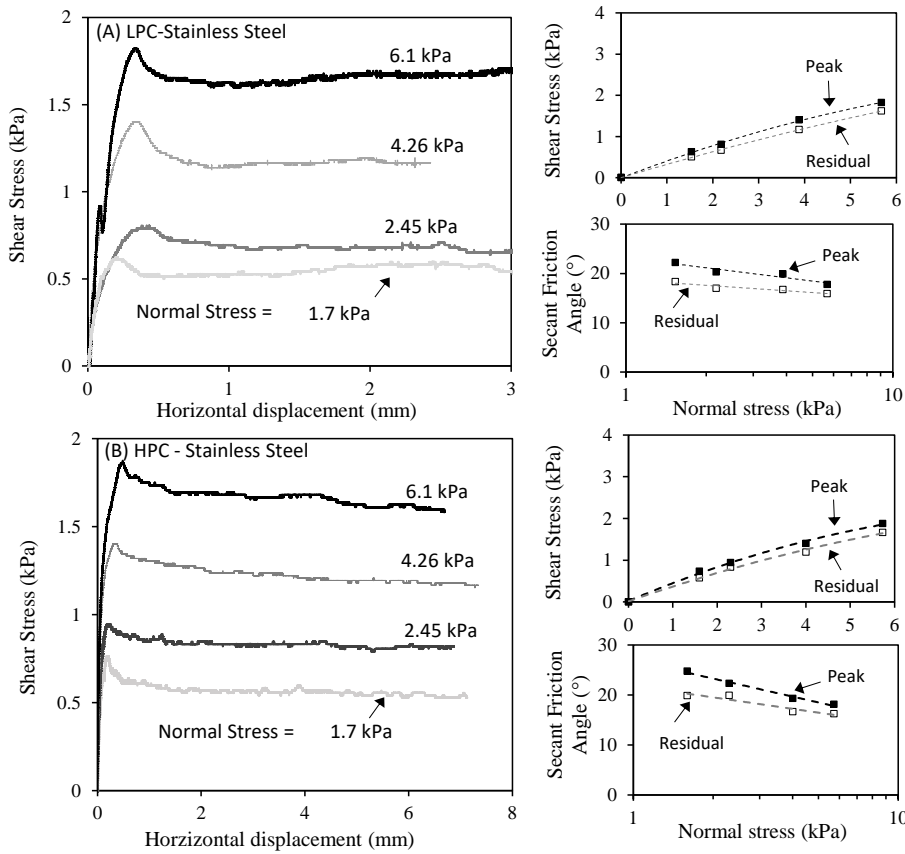


Figure 39. Results of the clay-solid direct shear tests on LPC and HPC with stainless steel

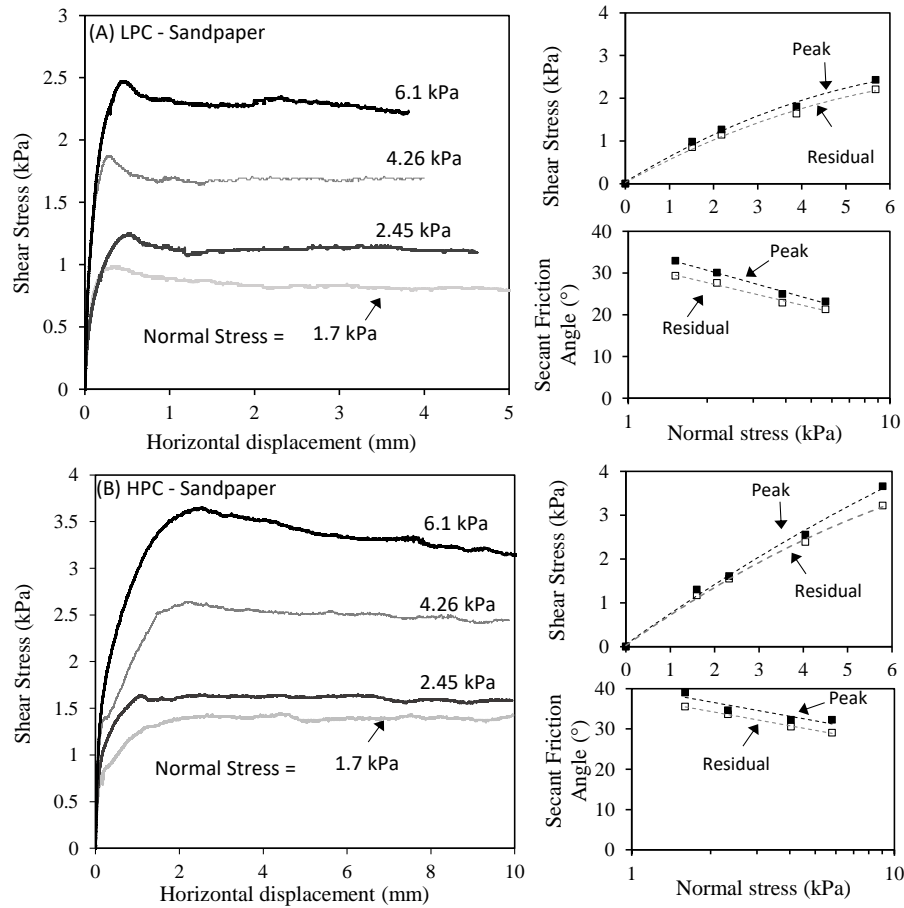


Figure 40. Results of the clay-solid direct shear tests on LPC and HPC with Sandpaper

For the rough interface (Figure 40), additional displacements were needed to mobilize the peak resistance, particularly for the case of the HPC. In summary, the interface direct shear tests show that relatively small displacements are needed to reach the residual state compared to the clay-clay tests. These observations are in line with published work on the residual strength of clay-solid interfaces in the typical stress range (ex. Lemos and Vaughan 2000).

The peak and residual drained interface secant friction angles were estimated as the arc tangent of the ratio of the shear stress to the effective normal stress at peak and large displacements, respectively. As in the case of the clay-clay tests, the drained

failure envelope and the variation of the secant interface friction angle with the logarithm of the normal stress (Figure 39 and Figure 40) clearly portray the nonlinearity in the failure envelop. A detailed discussion of the interface direct shear results is presented in the following section.

### **3.6.2 Discussion of Direct Shear Results**

#### **3.6.2.1 Non-Linearity in the Strength Envelope**

Nonlinearity in the drained shear strength envelope of clay-solid interfaces is a major factor that impacts the design of shallow offshore pipelines. The degree of non-linearity in the strength envelope is best represented and quantified through the variation of the secant friction angle with the logarithm of the applied normal stress (Figure 41).

Results on figure 41 indicate that drained residual friction angles measured for the smooth interfaces with the (a): HPC and (b): LPC are comparable, ranging between 21° (lowest normal stress) to 16° (highest normal stress). In the interface tests involving rough sandpaper, the residual friction angles were higher with clear differences observed between the low and high plasticity clays. In the HPC, the rough interface mobilized the full internal drained shear strength of the clay with secant residual friction angles of 33° at the lowest normal stress of 1.7 kPa, decreasing to about 29° at the highest normal stress of 6.1 kPa. This was not the case in the LPC where the residual friction angles remained within 85% of the clay-clay residual strength, while decreasing from 29° to 21° as the normal stress increased from 1.7 kPa to 6.1 kPa, reflecting strong non-linearity in the interface shear strength envelope. These differences in the responses of the rough interface with the LPC and HPC will be discussed in the following

sections. It should be noted here that the results pertaining to the Plexiglass interface are not presented since they yielded responses that were almost identical to the smooth stainless steel interface.

Alternatively, the nonlinear relationship between the residual shear strength and the effective normal stresses can be described/approximated by a power law function. Modeling drained residual failure envelopes for clay-solid interfaces with non-linear functions (ex. equation 3.5) was proposed in the literature by Boukpeti and White (2017), Najjar et al. (2007) and Westgate et al. (2018). The power law is described by the two parameters  $a$  and  $b$  such that

$$\tau = a\sigma'_n{}^b \quad (3.5)$$

Simple linear regression was used to back-calculate  $a$  and  $b$  for the interface direct shear tests conducted in this study. The resulting nonlinear failure envelopes and the corresponding best-fit  $a$  and  $b$  parameters for the power-law function are presented in Figure 42. Also shown in Figure 42 are the lower bound (10<sup>th</sup> percentile) and upper bound (90<sup>th</sup> percentile) ranges for drained residual interface shear strength envelopes that were published by Westgate et al. (2018) based on a comprehensive database of 200 IDS tests.

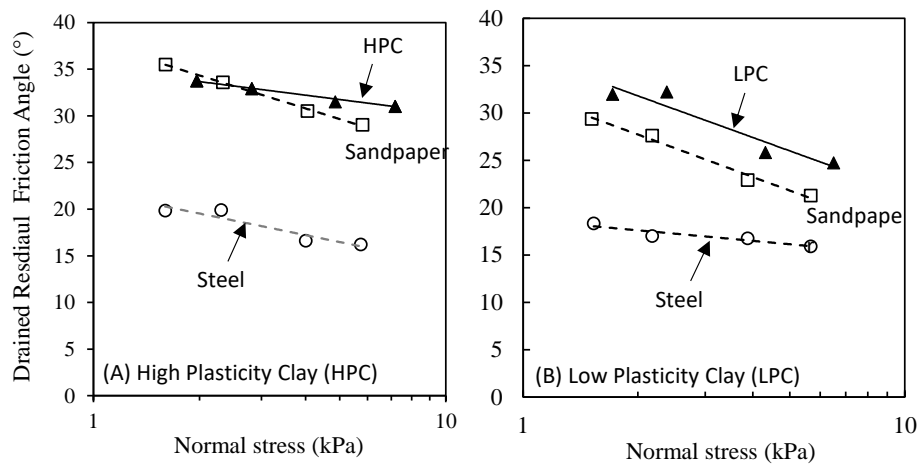


Figure 41. Variation of the drained secant residual friction angle with the logarithm of the normal stress for (A) HPC and (B) LPC

Results on Figure 42 lead to three main observations: (1) the failure envelopes for the rough interface tests (for both LPC and HPC) fall within the range of the Westgate et al. (2018) data, while the failure envelope of the smooth interface was lower than the 10<sup>th</sup> percentile curve; (2) the optimum values for the parameter “*a*”, which is indicative of the relative strength of the interface decreased from 0.78 (HPC) and 0.56 (LPC) in the rough interface to a relatively low value of 0.40 (HPC and LPC) for the smooth interface; and (3) an optimum “*b*” value of 0.8 captured the non-linearity in the interface drained failure envelopes, which is comparable but slightly smaller than the average *b*-value of 0.9 recommended by Westgate et al. (2018) for the IDS database, indicating that the envelopes in this study are slightly more curved.

It should be noted that the “*a*” value of 0.40 for the smooth interfaces tested in this study is slightly smaller than the 10<sup>th</sup> percentile “*a*” value of 0.44 recommended by Westgate et al. (2018). This difference is attributed to the fact that the minimum interface roughness in the cases analyzed in the Westgate et al. (2018) database was 0.8



$\mu\text{m}$ , which is one to two orders of magnitude higher than the roughness of the smooth interfaces tested in this study ( $0.003 \mu\text{m}$  for Plexiglass and  $0.08 \mu\text{m}$  for stainless steel).

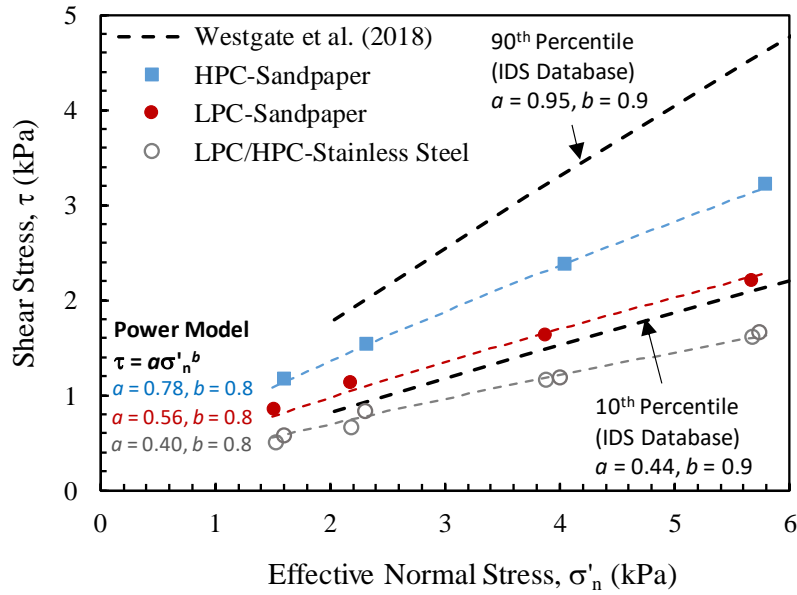


Figure 42. The nonlinear failure envelopes and the corresponding best-fit  $a$  and  $b$  parameters for the power-law function for all interfaces

### 3.6.2.2 Effect of Roughness

The interface roughness is a key factor in defining the clay-pipe interface shear strength and the interface efficiency ( $E$ ), which is defined as the ratio of the interface friction ratio ( $\tan\delta$ ) to the friction ratio for the clay ( $\tan\phi$ ). Results on Figure 39 to Figure 42 clearly show that an increase in roughness (from  $0.08 \mu\text{m}$  for steel to  $3.5 \mu\text{m}$  for sandpaper) led to a  $5^\circ$  to  $14^\circ$  increase in the interface friction angle depending on the soil type. The variation of the drained residual interface friction ratio ( $\tan\delta_{\text{res}}$ ) with roughness is presented in Figure 43 for the interface direct shear tests. Shown on the same figure are the trends observed between ( $\tan\delta_{\text{res}}$ ) and interface roughness in available published studies (Westgate et al. 2018 and Eid et al. 2015).

Results from published studies (Figure 43) indicate that a transition between “smooth” and “rough” interface behavior initiates at a threshold roughness of about 1 to 2  $\mu\text{m}$ . This threshold is supported by results from interface tests conducted in Tsubakihara et al.(1993), Lemos and Vaughan (2000) and Najjar et al.(2007). Such a transition is related to the governing failure mechanism when the soil is sheared against each interface. When the soil is sheared against a smooth interface (such as stainless steel or Plexiglass), a clean failure surface is generally observed at the interface indicating that the failure plane occurred along it. Such an interface response was clearly observed in the interface tests conducted between the HPC and LPC and the stainless steel or Plexiglass interfaces as indicated in Figure 44a. On the other hand, when the soil is sheared against a rough interface (as in the case of sandpaper), a combined failure mechanism develops at the interface and within the soil at some depth leading to a complex shear failure where clay particles stick to the rough interface, pushing the shear zone from the interface into the clay matrix (Figure 44b). In this case, the interface strength will be mainly governed by the clay properties, and the interface strength ratio may approach that of the soil, depending on the roughness.

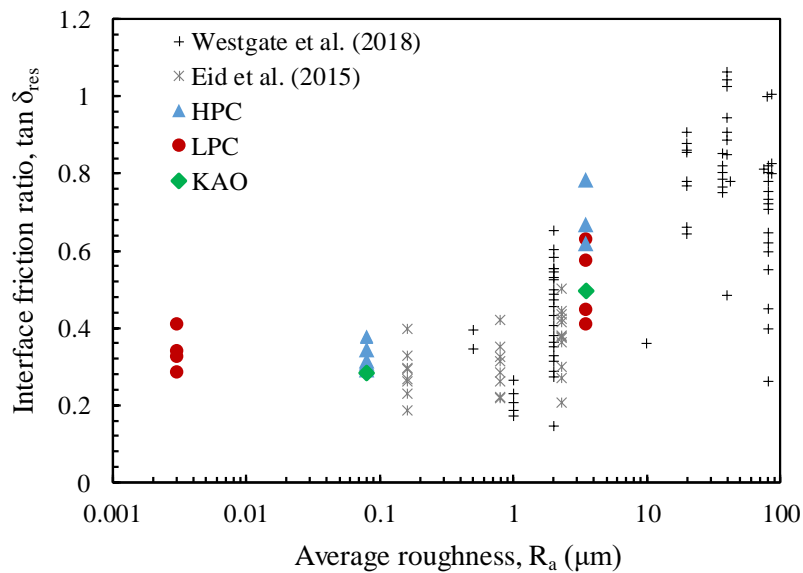


Figure 43. The variation of the drained residual friction ratio with the roughness

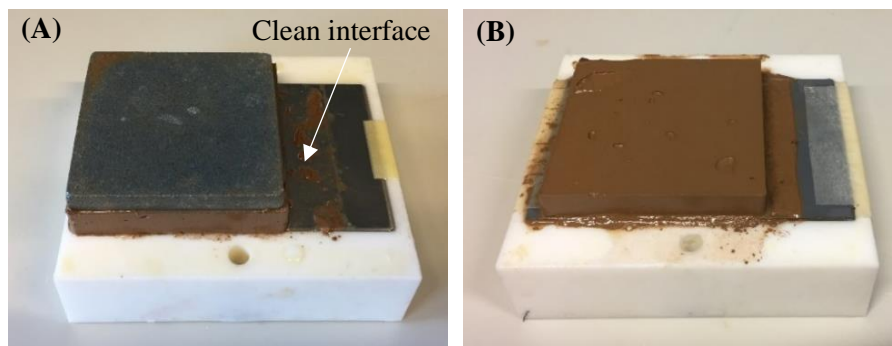


Figure 44. Failure mechanism of HPC on the (a) Stainless Steel and (b) Sandpaper

Lupini et al. (1981) reported that smooth interfaces promote the “sliding” shearing mode as they limit the interference between comparatively “massive” clay particles, forcing the development of shear zones between the interface and the oriented clay particles. Evidence of the “smooth” interface response can be found in the “brittle behavior” observed for both HPC and LPC once sheared against the smooth interfaces (Figure 39), in contrast with the somewhat “turbulent” mode observed for the clay-clay tests (Figure 38). In the case of sandpaper, the shearing mode changed to turbulent for

HPC indicating that the failure occurred in the soil matrix (Figure 40b). The corresponding residual interface efficiency was close to 1.0 in the HPC in contrast to slightly lower residual interface efficiencies (0.83 to 0.9) in the case of the LPC, which portrayed a combined sliding/matrix mode of failure.

In Figure 43, a comparison between the interface residual friction ratios reported in this study and those published in Eid et al. (2015) and Boukpeti et al (2017) indicates that the friction ratios are consistent with the results reported in Eid et al. (2015) for tests with natural clays sheared against mild steel and epoxy coated steel coatings using the ring shear device. The residual friction ratios were also in line with (but slightly lower than) those reported in Boukpeti et al (2017) and White et al. (2012), which mainly involved rough pipeline coatings tested against marine soils with typically higher drained shear strengths due to the presence of micro-skeletal remains (Hill and Jacobs, 2008 and Najjar et al. 2007) in their composition.

It should be noted that the drained residual interface coating efficiency ( $E_{res}$ ) calculated for the LPC, HPC, and KAO ranged from 0.5 to 0.65 for the smooth interfaces and from 0.82 to 1.0 for the rough sandpaper. Interestingly, the drained “peak” interface coating efficiency ( $E_{peak}$ ), which is defined as the peak interface friction ratio ( $\tan\delta_{peak}$ ) to the peak friction ratio of the clay ( $\tan\phi$ ), was comparable to the drained residual interface coating efficiencies ( $E_{res}$ ) for all soils and interfaces tested in this study (Figure 45). This indicates that the coating efficiency could be considered to be an independent parameter that is not significantly affected by the assumed level of deformations in the analysis of interface direct shear tests.

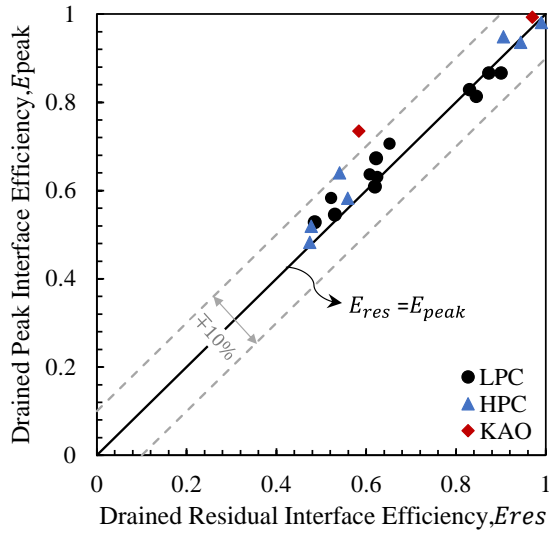


Figure 45. Comparison between peak and residual interface efficiencies

### 3.6.2.3 Effect of Soil Type

The effect of clay type on the clay-clay and clay-solid shear stress response for LPC, HPC, and KAO is shown in Figure 46 for a representative normal stress of 4.26 kPa. As expected, results for the clay-clay tests (Figure 46a) clearly indicate that the drained shear response is affected by the soil type. It is interesting to note however that the differences exhibited in the clay/clay response are practically eliminated when the HPC, LPC, and KAO are tested against the smooth interface (Figure 46c), indicating that differences in plasticity, fines content, and composition do not seem to have any significant effect on the interface response. On the other hand, the results of the rough interface tests (Figure 46b) at this normal stress clearly exhibit an intermediate response which seems to be affected by the clay type/characteristics.

A better understanding of the interface resistance of clay-solid interfaces requires a deeper investigation of the effect of soil type and composition on the interface response. Previous attempts were made to relate the residual interface strength to either

the liquid limit, plasticity index or clay content (Stark and Eid 1994; Najjar et al 2007, Eid et al. 2015 and Lemos and Vaughan 2000). Other studies investigated the effect of the same factors on the residual internal strength of the clay (Stark and Eid 1994; Lupini et al. 1981; Ramsey *et al.* 1998 and Jardine *et al.* 2005).

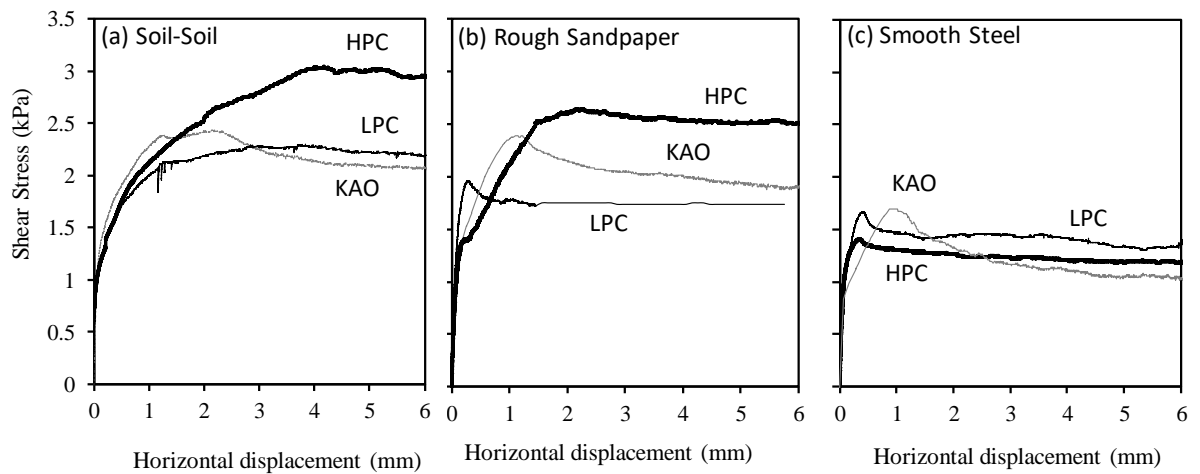


Figure 46. Internal and Interface Shear Stress Responses for LPC, HPC and KAO for (a): soil-soil, (b): rough sandpaper and (c): smooth steel

Stark and Eid (1994) reported an inversely proportional nonlinear relationship between the drained residual strength of the clay and its liquid limit and clay fraction. Ramsey *et al.* (1998) and Jardine *et al.* (2005) also reported a decrease in the clay strength with increase in the plasticity index. The main concern is that existing correlations were generated from tests in the high normal pressure range. Najjar et al. (2007) and Westgate et al. (2018) presented evidence that existing correlations may not be extrapolated to the low stress range with certainty.

Figure 47a shows the drained residual friction angle of the clays tested in this study with data from Najjar *et al.* (2007) and White *et al.* (2012) and the Eid *et al.* (2015) correlation with plasticity index. Although the data at relatively low plasticity

indices (LPC and KAO) follows the Eid et al. (2015) trend, the data for the HPC shows higher friction angles that do not follow the decreasing trend (Figure 47a). Similar observations can be made on the interface data presented on Figure 47b with the IDS dataset collected by Westgate et al. (2018). The drained residual interface strength does not show a clear trend with plasticity index, particularly for the smooth interfaces. For the rough interface, the data shows a slightly increasing trend with plasticity index and does not follow the trend observed in Westgate et al. (2018). The scatter in the data indicates that the plasticity index alone does not explain the variations observed in the drained residual strength of clays and clay-solid interfaces at low normal stresses.

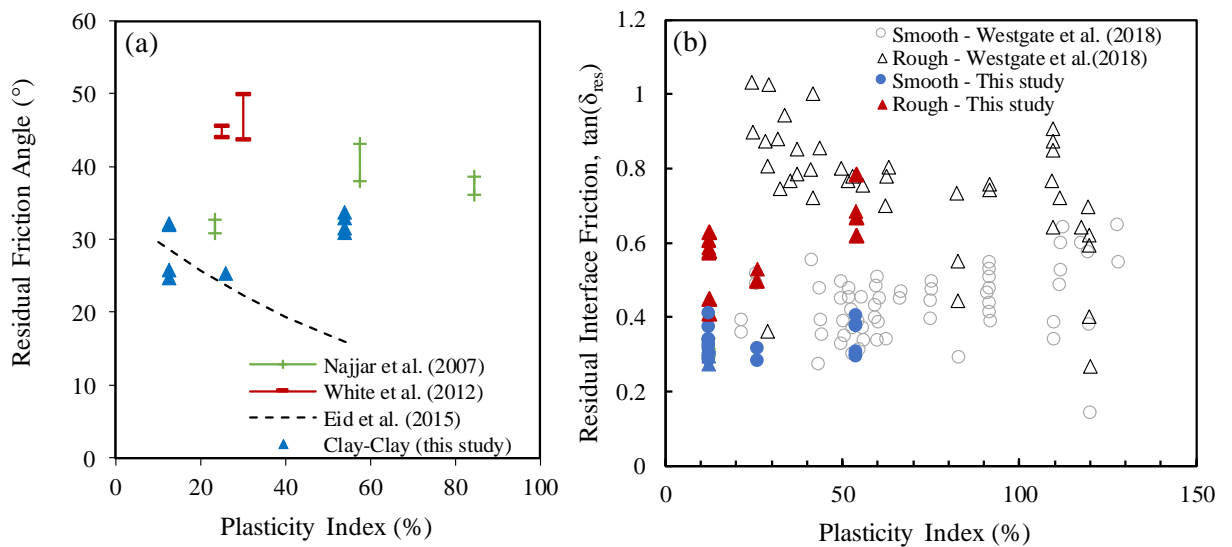


Figure 47. Effect of Plasticity Index on (a) residual clay and (b) residual interface strength

#### 3.6.2.4 Combined Effect of Roughness and Soil Type

In order to combine the effects of interface roughness and soil type, Eid et al. (2015) studied the correlation between the residual interface efficiency ( $E_{res}$ ) and the normalized interface roughness  $R_a/D_{50}$ , with  $R_a$  being the average interface roughness and  $D_{50}$  the mean grain size of the soil. Normalizing  $R_a$  with  $D_{50}$  was proposed by

Uesugi and Kishida (1986) and Oliphant and Maconohie (2007). The normalized roughness is a simple mathematical parameter that could model the interaction occurring between the soil particles and the coating asperities at the micro scale. Figure 48 presents a series of SEMs that portray the roughness of the steel and sandpaper interfaces relative to the LPC and HPC at a scale of about 50 microns. The figure clearly illustrates the contrast between the roughness of the steel and the sandpaper interfaces and shows the presence of “large” sand particles in the low plasticity clay (LPC).

The  $E_{res}$  versus  $R_a/D_{50}$  data compiled by Eid et al. (2015) is plotted on Figure 49 with the ranges of the residual interface efficiencies measured in this study for each  $R_a/D_{50}$  case encountered. The normalized roughness ranged from a minimum of 0.0003 (Plexiglass with LPC) to a maximum of 4.0 (Sandpaper with KAO).

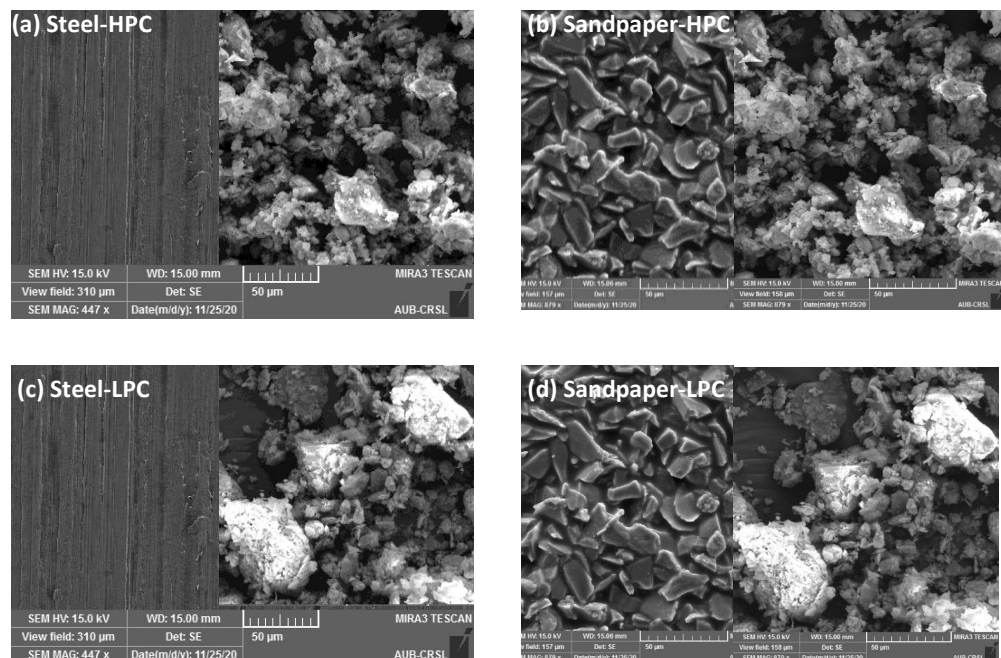


Figure 48. Contrast between the smooth and rough interfaces and the LPC and HPC



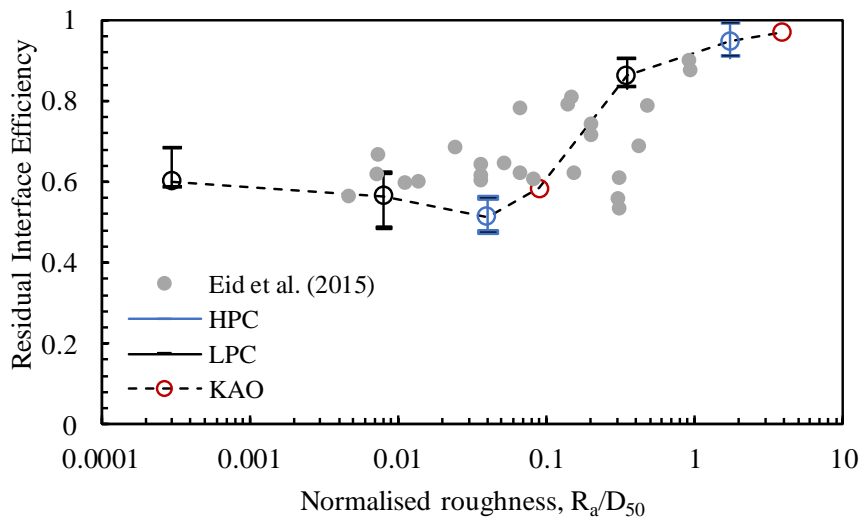


Figure 49. Variation of the residual interface efficiency with the normalized roughness

Results on Figure 49 provide a rational explanation of the trends observed in the previous section, particularly with regards to the higher interface strengths/efficiencies observed in the HPC and KAO compared to the LPC when tested against the rough interface. For these cases, Figure 49 shows that the  $R_a/D_{50}$  ratios were higher than 2, indicating that the failure mechanism was governed by failure within the soil matrix rather than at the interface, leading to an  $E_{res}$  that approached 1.0. On the other hand, the normalized roughness for sandpaper with LPC is an order of magnitude smaller ( $R_a/D_{50} \sim 0.35$ ), which may explain its relatively lower interface efficiency of 0.85. For normalized roughness values that were less than 0.1 (all soils with smooth interface), results show that the interface efficiency was relatively constant, with minimum values ranging from 0.55 to 0.6.

The data on Figure 49 shows that the results reported in this study are in line with the general trend that is defined by the data collected in Eid et al. (2015) despite the larger scatter that is exhibited that set. The scatter can be attributed to factors such as particle shape, gradation, or soil fabric (White et al., 2012). Other considerations that

may have affected the response could include factors related to the interface itself (such as the interface hardness, yield strength, and composition). These soil and interface parameters were not taken into consideration in the analysis of the data, given the limited number of tests.

### 3.6.3 Comparison between Tilt Table and Interface Direct Shear

#### 3.6.3.1 Tilt Table Results

Residual interface friction angles were also determined from the tilt table tests at maximum displacements on the order of 70mm. Figure 50a and Figure 50b show the failure mechanism of the low plasticity clay (LPC) on the smooth stainless steel and rough sandpaper interfaces, respectively. A clean interface is observed when the soil slipped on the smoother stainless steel interface indicating that the failure plane was along the interface. In the case of the rough interface, some clay particles adhered to the sandpaper after soil slippage indicating a combined failure mechanism which involves interface and soil-soil shearing. As in the case of the interface direct shear tests, this interface response is highly related to the interface roughness, where the transition from pure interface to a within-soil failure initiates at a roughness of about 2  $\mu\text{m}$ .

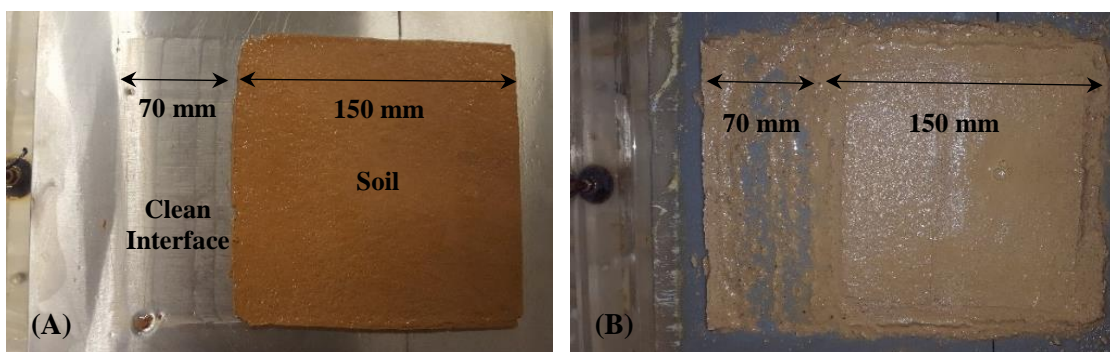


Figure 50. Failure mechanism of the Low Plasticity Clay on: (a) the Stainless Steel and (b) the Sandpaper

Figure 51 illustrates the variation of the drained residual secant friction angle with the logarithm of the effective normal stress at failure for all clay/interface combinations as obtained from the tilt table tests. In the HPC and LPC, the Mohr-Coulomb failure envelopes of the smoother interfaces (Plexiglass and Stainless Steel) were found to be curved at low normal stresses, as indicated by the reduction in the secant friction angle with normal stress. However, the tilt table tests that were conducted with the rough sandpaper interface and the LPC indicated that the failure envelope did not exhibit the same level of non-linearity with minor reductions in the secant friction angle at larger normal stresses. In fact, at the largest normal stress of 6.1 kPa, the interface friction angle measured for the LPC-Sandpaper interface exceeded the internal secant friction angle of the clay itself, a response which is not considered to be realistic.

One explanation for this response is that the geotextile that is under the loading plate could have interacted with the rough sandpaper interface preventing slippage of the soil on the rough interface. The presence of 26% sand in the composition of the LPC could have also contributed to this interaction which was also observed by Najjar *et al.* (2007) when testing rough interfaces in a tilt table setup with an offshore clay that included foraminifera. In Najjar *et al.* (2007) this problem was solved by redesigning the setup of the loading plate and replacing the geotextile under the loading plate with a punctured smooth geomembrane.

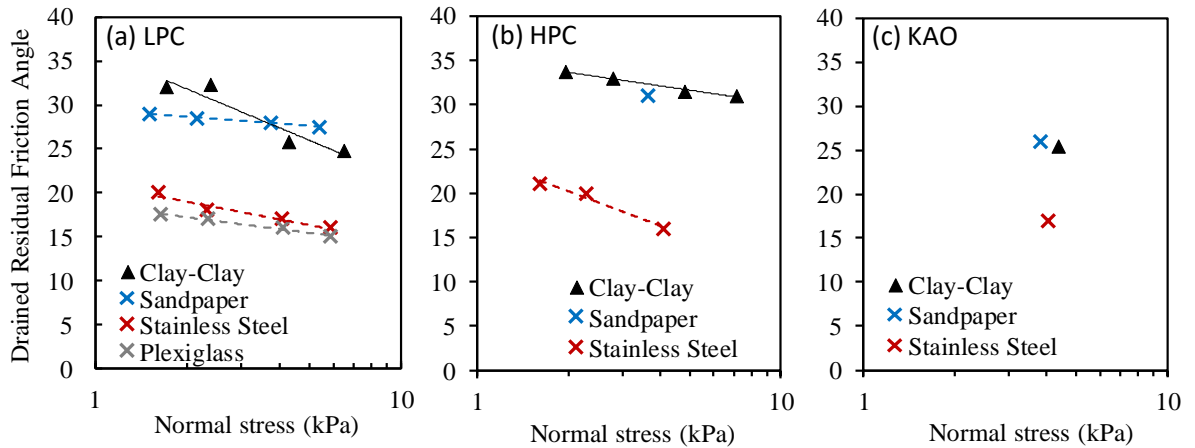


Figure 51. Drained residual friction angles of (a): LPC, (b): HPC, and (c): KAO sheared against all interfaces using the tilt table

### 3.6.3.2 Tilt Table v/s Interface Direct Shear

A direct comparison between the drained residual interface friction angles obtained from tilt table and direct shear testing is shown in Figure 52 for each interface type. Also shown on the figure are the residual friction angles of the clay as determined from the direct shear tests. Results for the smoother steel interface indicate that the two testing methodologies resulted in more-or-less similar residual secant friction angles independent of the clay type. For the tests conducted with rough sandpaper, results on Figure 52 indicate that excellent agreement exists between the tilt table and interface direct shear tests for the HPC and KAO. For the LPC clay (Figure 52a), results from the two testing methodologies showed a significant discrepancy in the residual secant friction angles at relatively larger normal stresses (4.26 kPa and 6.12 kPa), with the friction angles determined from the tilt table tests being larger than those determined from the direct shear tests. For these cases, although the two testing methodologies produced more-or-less similar residual friction angles at normal stresses less than 2 kPa (around 27 to 29 degrees), the results of the tilt table tests did not show a steep reduction

in the residual secant friction angle with normal stress as did the interface direct shear results.

The differences between the drained residual failure envelopes observed in the two test methodologies for the case of LPC with rough paper are clearly presented in Figure 53. As mentioned previously, the possible interference of the geotextile with the rough interface in the tilt table tests conducted at the higher normal stresses could have led to the mismatch observed. Future work will investigate in a dedicated testing program whether the relatively high interface friction angles for sandpaper at higher normal stresses may be attributed to such an interaction.

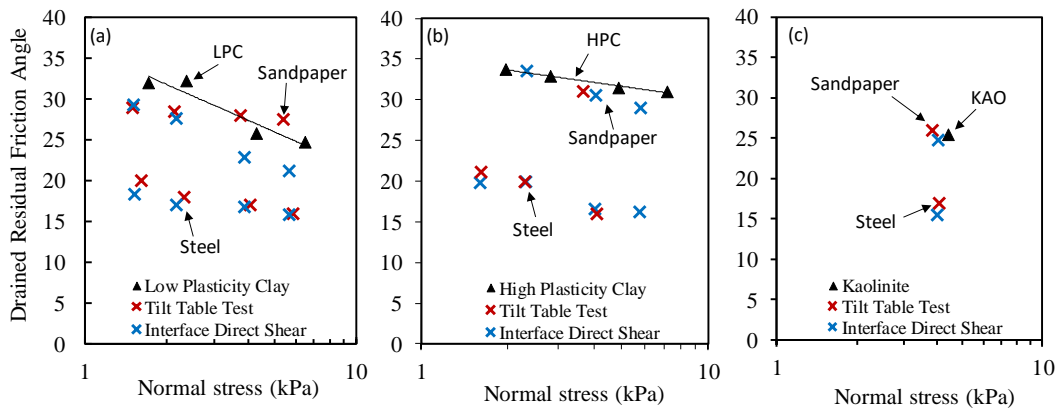


Figure 52. Comparison between the residual friction angles measured in the tilt table and direct shear setups for (a) LPC, (b) HPC, and (c) Kaolinite

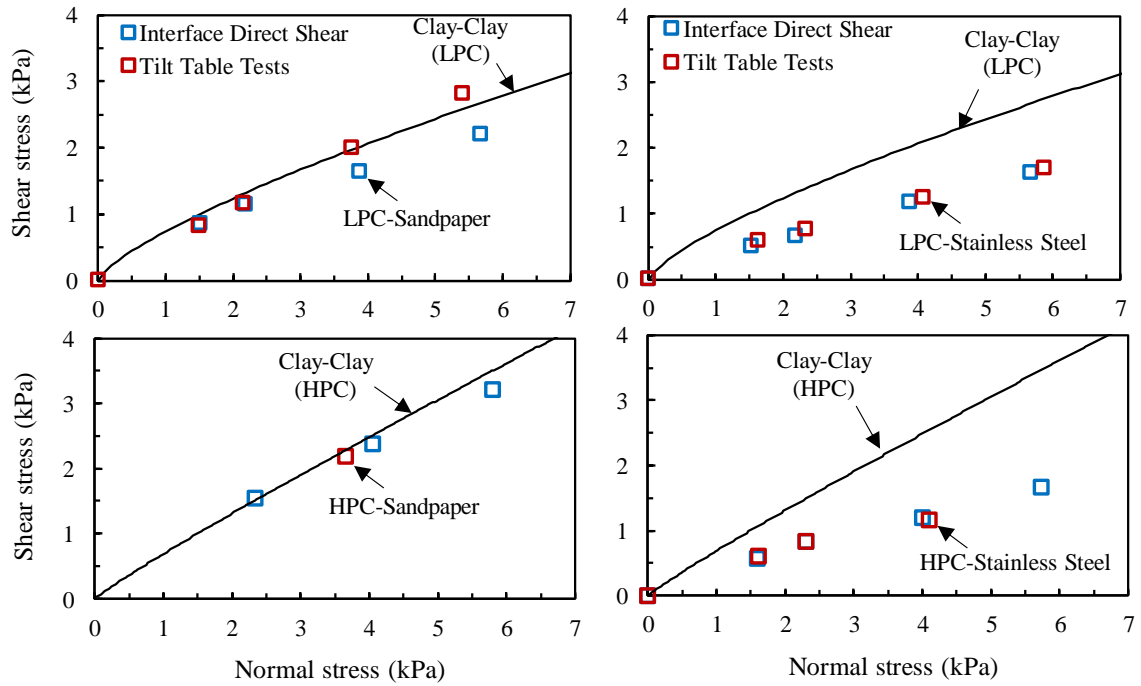


Figure 53. Comparison between the failure envelopes from tilt table and direct shear setups

Figure 54 presents the results of all the tilt table and interface direct shear tests conducted in this study at low normal stresses. Also plotted is the equality line (1:1 slope) in addition to two lines representing a discrepancy of plus or minus 10% in the measured friction angles. Results show a reasonable agreement between the tilt table and the interface direct shear results. The residual friction angles are approximately within 5% of each other, except for the two tests of the LPC sheared against the sandpaper at relatively high normal stresses, which are currently considered as outliers. These results support the validity of using interface direct shear tests to determine the residual interface friction angle at low confining pressure, provided that the test setup is adapted to low pressure testing and modified to eliminate mechanical friction.

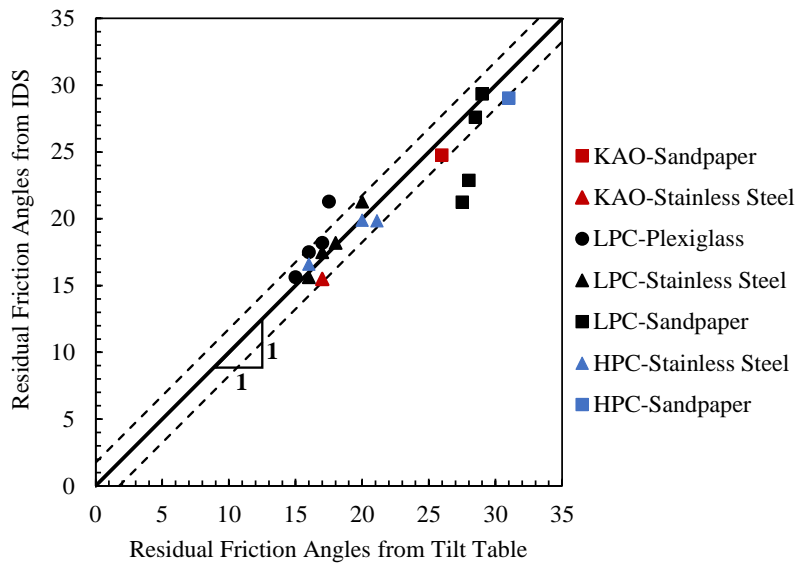


Figure 54. Comparison between the interfaces residual angles from tilt table and interface direct shear tests

It should be noted that the above conclusion is associated with a major limitation that needs to be clarified before generalizing the findings to all clay specimens and interfaces. This limitation is related to the fact that all of the specimens that were tested in this study are normally consolidated remolded specimens that were prepared from a slurry. The internal structure of slurry-consolidated remolded specimens is already destroyed and can be significantly different than the internal structure of clays that are deposited in the field. Although relatively small shear displacements (1 to 3 mm) were required in the interface direct shear tests to achieve residual conditions in the remolded clays, higher displacements may be required to push undisturbed clay specimens to residual conditions, necessitating shear reversals in the direct shear setup. No reversals were needed in this work to reach the residual condition. The tilt table device has the advantage of enforcing larger shear displacement without the need for reversals during shearing.

### 3.7 Conclusions

The axial pipe-soil interface resistance is a key parameter in the design of HPHT pipelines. Determining it using laboratory small element testing is widely acknowledged, with the Interface Direct shear and the Tilt Table being the two most common used setups in this regard. This study aimed at comparing test results obtained using both setups with identical interfaces and soil type. The following conclusions can be drawn from a total of 48 tests performed:

The interface direct shear results at low normal stresses proved to be convenient for characterizing the clay-clay and clay-interface stress-displacement response, allowing for the determination of the peak and residual strength envelopes. Moreover, the consolidation phase of the interface direct shear tests provided valuable information regarding the drainage conditions, leading to the conclusion that the interface/coating roughness may play a role in accelerating the rate of consolidation due to possible drainage that is occurring at the level of the interface.

Based on the direct shear test results, it can be concluded that the drained residual failure envelopes for the clays and the clay-solid interfaces were nonlinear and could be modeled by a simple power model. The measured residual interface friction angles were found to be highly correlated to the interface surface roughness, particularly when the roughness was normalized with the mean grain size. The measured residual and peak coating efficiencies were relatively similar ranging between 45% and 99% for the three interfaces tested.



A comparison between the tilt table and interface direct shear tests indicated that residual interface friction angles obtained from both setups are almost identical for the case of smooth interfaces (plexiglass and stainless steel).

For the case of the rough interface (sandpaper), the residual friction angles were comparable for the high plasticity clay (HPC) and kaolinite (KAO). However, the interface direct shear tests appeared to give conservative results compared to the tilt table tests for the case of low plasticity clay at normal stresses above 3 kPa. This might have been due to a possible adverse interaction between the geotextile (under the loading plate) and the rough interface in the tilt table device particularly at larger normal stresses. Further tests are required to investigate this phenomenon.

In line with observations that were published in some studies involving low normal stresses, no specific trend was observed between the drained clay-clay and clay-interface strength and the plasticity index of the clay.

The comparison between both setups suggests that using the Interface Direct Shear machine for determining the drained residual pipe-soil interface resistance is a practical and reliable testing alternative, provided that the conventional direct shear setup is properly modified to reduce mechanical friction and make it amenable to low pressure testing.

## CHAPTER 4

### A NOVEL IN-SITU SETUP: DESIGN AND PROOFING

#### 4.1 Introduction

Over the past decades, significant efforts have been made to reliably estimate the axial resistance of the pipeline throughout its operational life using different testing techniques, which include laboratory element tests, model tests and in-situ tests. A framework was also developed by researchers to capture the sensitivity of the axial resistance to different testing conditions, drainage conditions, normal stresses, interface roughness, and loading history. Such framework/models could be calibrated based on site-specific soil properties, and used in guiding the design of the pipeline against operational loads. As a result, sensible mitigation strategies relating to pipeline walking and buckling can be determined. Despite early promising results, further improvements are needed, particularly in reference to site-specific in-situ testing using cost-effective testing apparatuses, which have yet to be developed.

Although in-situ testing is known to be the most reliable technique for measuring the axial pipeline resistance, the available specialized field equipment are currently limited to the Fugro SMARTPIPE and the “pipe-like” penetrometer. Fugro SMARTPIPE applications are relatively expensive due to the dependence of the system on the vessel and other unresolved technical issues related to the ability to maintain a constant vertical load throughout testing. The “pipe-like” penetrometers are not suitable for in-situ applications since they can only be used on samples extracted by a box core and they are not yet to be deployed in any offshore project. Moreover, the tool of

Stanier et al. (2015) that consists of an ROV that simply pulls the pipe section has major limitations related to mobilization of passive pressure and the inclined forces applied to drag the tool. Such limitations lead to the need for complicated correction procedures in order to obtain an estimate for the net axial resistance.

The objective of the work presented in this chapter was to address the need for developing a *new in-situ, cost-effective* apparatus for measuring the axial pipeline resistance. A new test setup is proposed that directly addresses the limitations of previously studied systems, with particular focus on eliminating the problem of passive stresses generated at the pipe ends, and delivering a cost-effective setup for conducting the in-situ interface test. A laboratory proof of concept experimental setup that could be adapted/automated in future work to become an autonomous field apparatus was designed, produced, and tested. The scope of the work presented is limited to the design and validation of the basic mechanisms/components of the proposed in-situ test setup. Preliminary validation tests in a soft clay bed are reported which could be considered as a proof of concept at this stage of the project. The preliminary pipe-clay interface interaction results are compared to results from tilt table and interface direct shear tests on similar clay and interface coating and under comparably low confining stress levels. In order to help with, the interpretation of results, a ball penetrometer apparatus was designed, built, and calibrated to measure the obtained undrained shear strength measurements through and at various locations across the clay bed.

## **4.2 Design of the in-situ setup**

### **4.2.1 Concept**

The test setup was envisaged to combine the advantages of: (1) the tilt-table device (minimizing system friction error effects) and (2) the interface direct shear setup (ability to conduct displacement-controlled tests with minimal eccentric loading), while eliminating the limitations of the *in-situ* tests (need to control the vertical stress using external load control mechanisms). More importantly, the main objectives/design constraints of the proposed test setup were to overcome the limitations related to passive earth pressures that are generated at the ends of the pipe sections, the non-uniform stress distribution beneath the tested pipeline section, and the relatively high testing costs. Another significant goal involved building a model that can mimic the actual pipeline movement and that can be “easily/remotely” and eventually, autonomously deployed in different locations to effectively characterize the pipe-soil interface.

### **4.2.2 Design Model**

The schematic of the apparatus prototype is presented in Figure 55. The prototype is comprised of a semi-circular 1-m long half-pipe with a diameter of 160mm. The pipe section is constituted of five independent stainless-steel sheets that are folded into half-pipes of different lengths (50, 200 and 350 mm). During the consolidation stage, the 5 pipe sections are connected by lateral screws to a common 1-m long aluminum bar as shown in the top view in

Figure 56. The screws pass through 30-mm thick plastic spacers and connect to the aluminum bar to ensure that the bar is perfectly centered and that the 5 pipe sections act as a rigid body to apply a uniform vertical stress along the pipe length once the setup is laid on the clay surface.

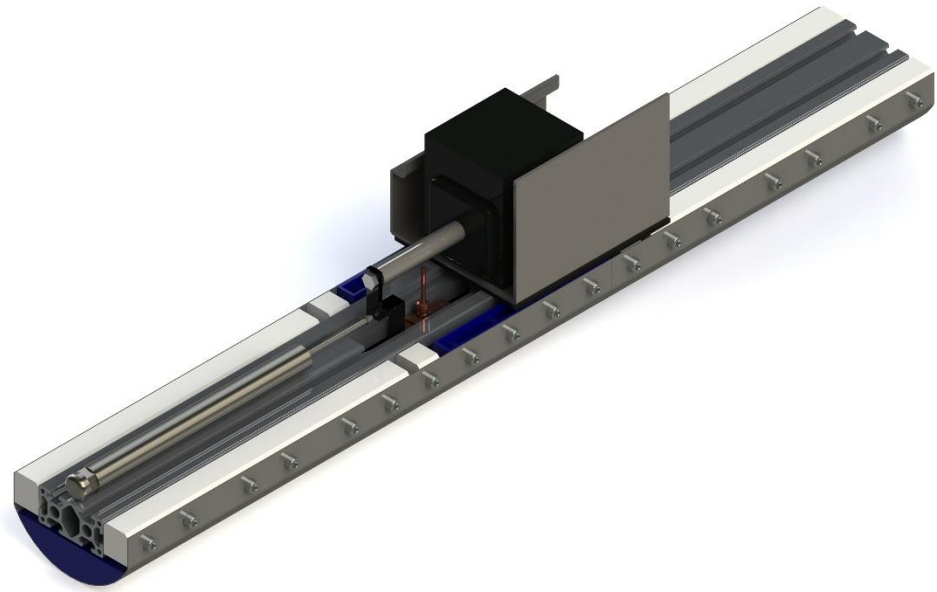


Figure 55. 3D view of the in-situ setup

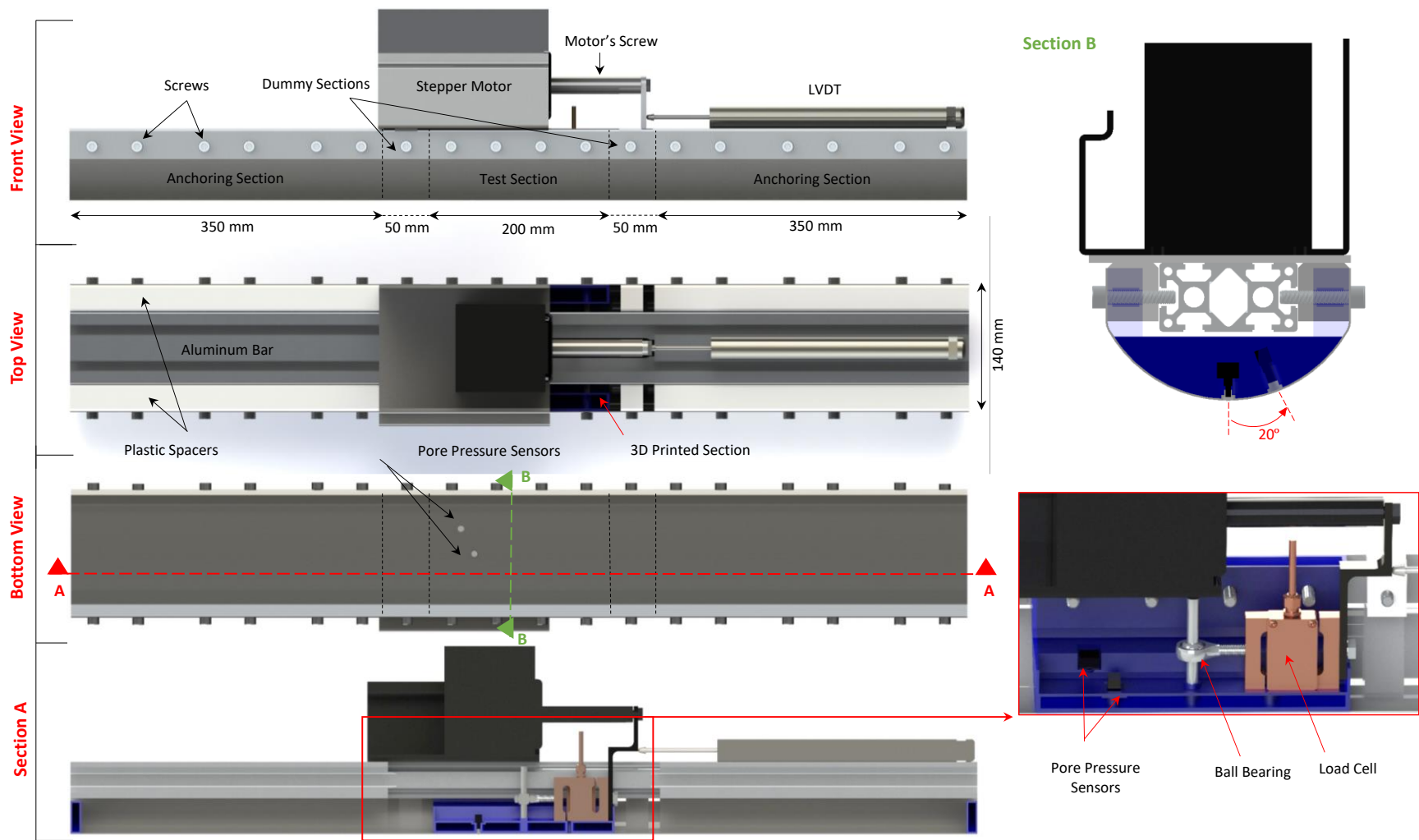


Figure 56. In- situ setup model using SOLIDWORKS.

At the completion of the consolidation stage, each pipe section takes on a specific role that was designed to allow for and facilitate the displacement-controlled shearing process: (1) The central pipe section which is 200 mm long will function as the main test section that will be displaced axially during shearing; (2) The two adjacent 50mm-long sections are dummies that will be removed prior to the test, thus creating a path that would allow for the lateral displacement of the central section without subjecting it to any passive resistance on either end; (3)The 350mm pipe sections at the two ends of the pipe function as “anchoring” sections that would provide the necessary reactions needed to displace the central test section. Prior to the commencement of shearing, the screws connecting the central pipe section and the two dummies to the central aluminum bar are removed. The shearing mechanism is provided via a stepper motor that is firmly supported on the rigid aluminum bar. It allows for different shearing rates, thus ensuring the option of performing the tests under either drained (“very slow”), partially drained or undrained conditions test (“fast”). The range of possible test speeds given the motor selected is  $1.67 \times 10^{-7}$  mm/s to 0.22 mm/s.

During the consolidation stage, the weight of the motor (93 N) is distributed to all pipe sections and constitutes a major part of the applied normal stress. In the shearing phase, and after detaching the central test section and the two dummy sections from the aluminium bar, the weight of the motor shifts to the 350-mm pipe sections at the two ends. Once the central test section is detached from the Aluminium bar, it will function as an independent pipe that is subjected the soil beneath it to a normal stress governed by its own weight. A major constraint that guided the design of the central test section was that its weight had to be selected to produce the same normal stress that was initially applied by the 1-m long connected pipe and assembly during the consolidation



process. This would prevent further consolidation, or swelling, of the test section upon detachment from the system. To achieve this objective, a 3D-printed box (Figure 57) was fabricated and filled with lead shots and fitted inside the stainless steel pipe. It is important to note here that the nature/type of the interface material exposed at the middle section of the pipe could be replaced for testing purposes as needed thus allowing the study of different types of pipe surface materials..

The motor that was used to control the horizontal deformation of the test section allows for a maximum displacement of 40 mm which corresponds to 20% of the length of the test section. The moving screw of the motor is connected to the central test section and to an S-shape load cell (capacity of 10 kg) using a rigid steel plate (Figure 1). The load cell is in turn connected to the middle of the 3D printed section by a spherical bearing allowing for free vertical motion. The unrestrained vertical motion in conjunction with the spherical bearing will allow the test section of the pipe to move freely in a vertical plane. Additionally, the connection will only allow horizontal forces to act on the test section while no other force (vertical or lateral) is transmitted to it. A linear vertical displacement transducer (LVDT with a 50 mm stroke) is fixed on the aluminium bar to measure the horizontal displacement of the tested part. A target and a checkerboard are fixed on the tested part and the dummies/anchor sections to track any motion of the setup in different directions using a computer vision approach. Two pore pressure sensors are fitted inside the test section at two different locations to measure the induced excess pore pressures during the various testing stages (

Figure 56- Section B).

It should be noted that once the setup was assembled, minor weights were added, as needed, to adjust its centre of gravity, and thus prevent tilting in any given direction. The total weight of the setup when all the system components are connected together is 206 N. The weight of the test section when detached from the aluminium bar is around 41 N. The actual normal stress that is acting on the pipe-soil interface, including the wedging effect, is not known beforehand since it is governed by the final embedment of the pipe after consolidation. The normal stress range could however be estimated to be between 1 and 4.0 kPa. Figure 58 shows the built setup.

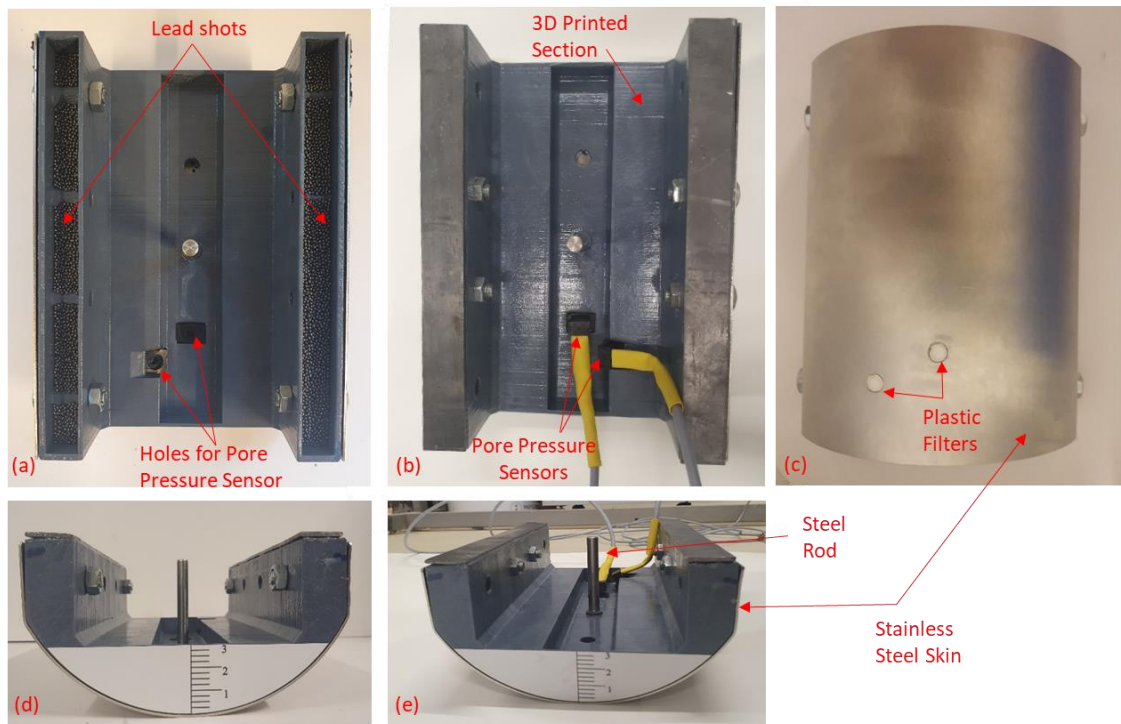


Figure 57. 3D Printed mid-section: (a, b) top view, (c) bottom view and (d, e) front view.

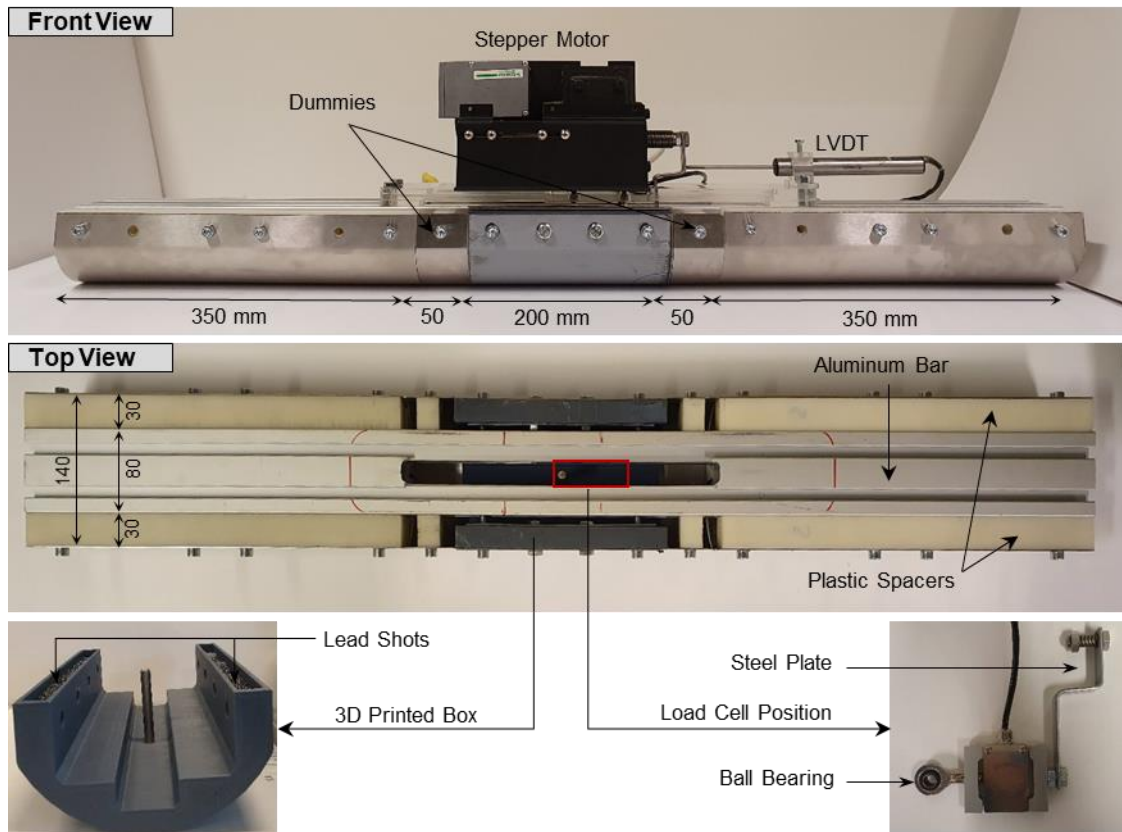


Figure 58. Schematic of the in-situ setup.

### 4.3 Instrumentation

#### 4.3.1 Load Cell

The load cell is directly connected to the test section and the motor screw and measures the resistance experienced by the test section as it is pushed axially. An S-shaped load cell from Applied Measurements LTD of a capacity of 25 kg (DDBSM) was used. The load cell range covers the expected levels of shear forces. The load cell calibration was checked/confirmed by using standard known weights before testing began.

### **4.3.2 LVDT**

A linear Variable Differential Transformer sensor (LVDT) was fixed on the setup to measure the axial movement of the test section. The chosen LVDT (LD600-OMEGA) had a 50 mm total stroke and high accuracy to capture minimal displacement especially during very slow/drained tests.

### **4.3.3 Pore Pressure Sensor**

The Honeywell pressure sensor (26PCAFA6G) with a 7 kPa maximum capacity was used to record the generated excess pore pressure during the pipe lay-down stage, the consolidation stage and the shearing stage. The maximum pore pressure expected during testing should not exceed the maximum applied normal stress induced by the setup weight once it touches the clay bed, which is around 4.5 kPa. As such the pressure range of the sensor is deemed acceptable and has some reserve capacity.

In order to prevent any clogging of the pressure sensor by soil particles and to ensure that only the water pressure will be read, plastic filters made of hydrophilic ultra-high molecular weight (UHMW) polyethylene porous sheets with a pore sizes on the order of 35  $\mu\text{m}$  were used to separate between the soil and the sensor port (from Scientific Commodities Inc.). This filter was fitted inside a 3D printed cap that could be perfectly placed at the sensor's port. Both were fitted with a rubber membrane to prevent any water infiltration (Figure 59). The void space between the sensor and the soil was filled with de-aired water to provide consistent pore pressure readings as recommended by Schneider et al. (2020). Full saturation of the system was ensured by vacuum-saturating the filter sheet inside a pressure cell up to 100 kPa..

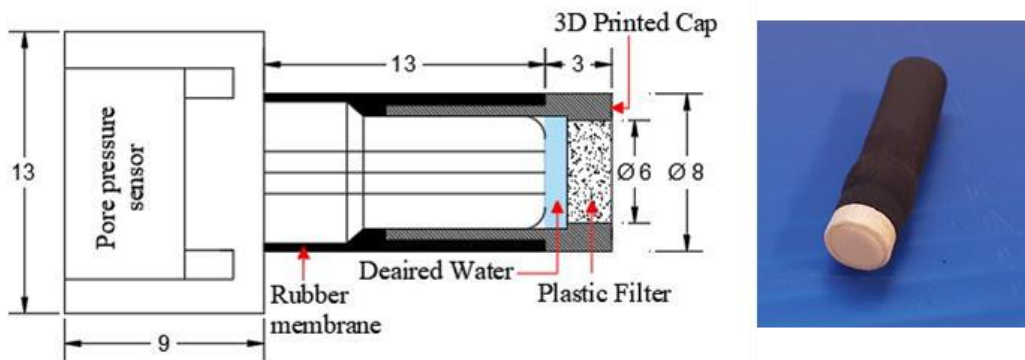


Figure 59. Pore pressure sensor and cap

The sensor was first tested and calibrated by comparing its voltage readings to the height of a water column created directly above it (Figure 60). This was achieved by placing the sensor inside a rubber tube and fitting it at the bottom of a graduated burette. The water was added gradually to specific levels and then the sensor readings were recorded. The test was done several times with and without the filter cap. Figure 61 shows the calibration graphs proving that the sensor was very sensitive, its readings repeatable and able to read low pressures with high accuracy.

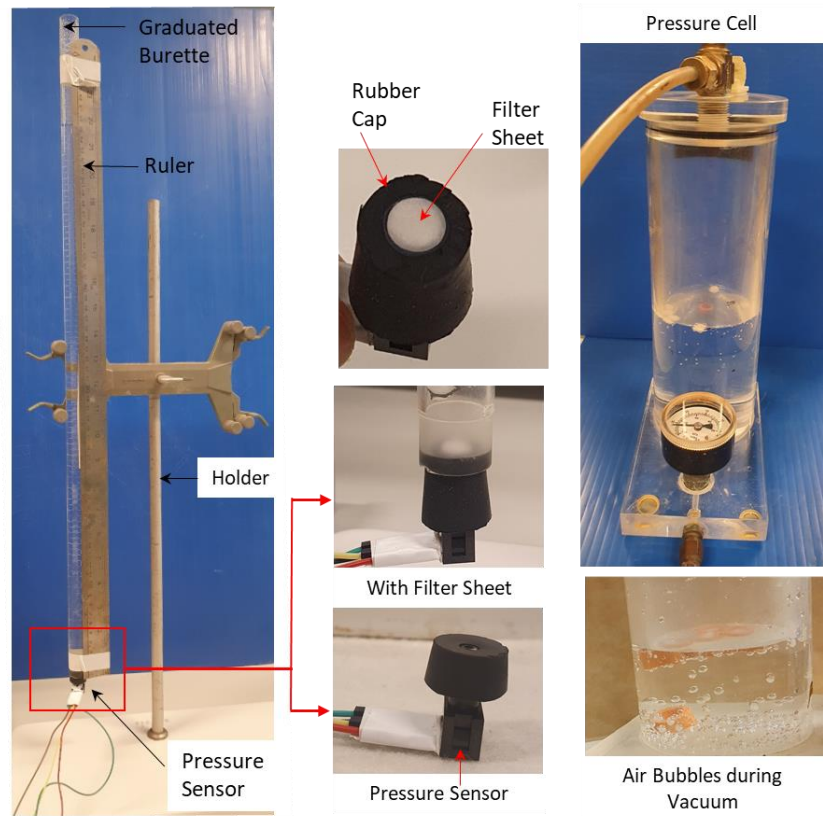


Figure 60. Calibration setup of the pore pressure sensor.

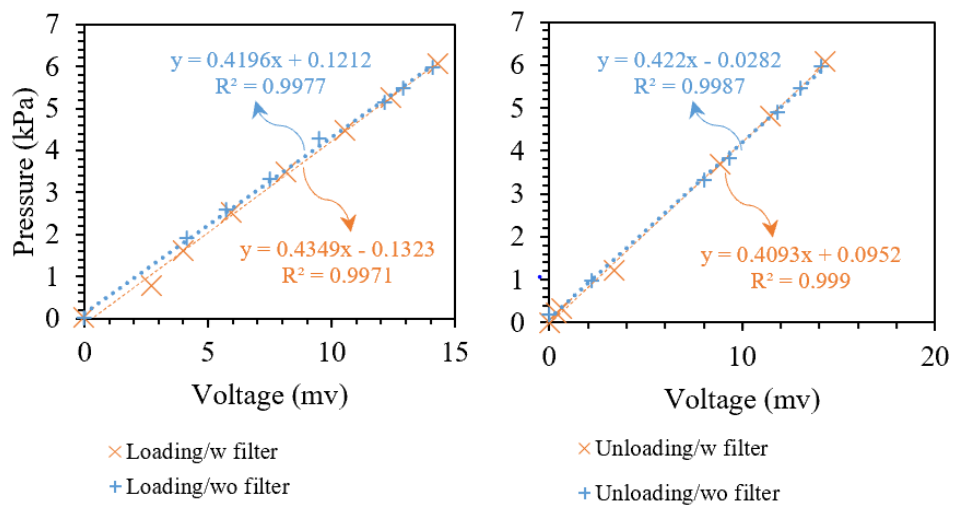


Figure 61. Calibration curves of the pressure sensor.

#### ***4.3.4 Digital Camera and Computer vision approach***

The proposed computer vision-based approach for real time displacement measurement consisted of a GoPro-Hero 7 camera and planar patterns attached on the surface of the object to be tracked. The processing algorithms include camera calibration, object tracking, and real displacements calculations.

##### **4.3.4.1 Camera Calibration**

The camera should be fully calibrated to get all the geometric information of the camera parameters and the lens distortion parameters. Camera parameters can be classified into two different groups: the intrinsic and the extrinsic parameters. The intrinsic parameters define the geometric and optical characteristics of the camera, while the extrinsic parameters describe the rotational and translational information of the image coordinate system in pixels relative to a predefined object coordinate system. The camera calibrator application in Matlab was used to accomplish that task. Images of a checkerboard pattern having a square size of 40 mm were taken at different orientations relative to the camera from a distance roughly equal to the distance from the camera to the setup that will be targeted during the interface tests. All images were then transferred to Matlab and then calibrated using the camera standard model. The camera parameters were then calculated and saved to be used in accounting for the effects of lens distortion from the images obtained during the interface testing.



#### 4.3.4.2 Object Tracking

In our application, two patterns were used to track the motion of the test section and the whole setup in each stage: (1) a checkerboard fixed on the test section and (2) a circle divided into four sectors, two of which are black, attached to each anchoring section. The points of interest, whose trajectory will be tracked, are the centroids of the circles which are also corner points between the sectors. The tracking algorithm consists of detecting the checkerboard first and then getting the corresponding rotation and translation matrices. The difference between the translation matrices of the current processed image and of the first image is in fact the test section displacement at that stage. From the rotation matrix, the rotation angles can be deduced to check whether the test section is rotating in any of the three directions. Regarding the second pattern, a region of interest will be manually selected around the pattern in the first iteration which facilitates the detection of the point of interest using Harris corner technique by selecting the strongest corner in that region. Then, the anchoring sections' displacements can be computed using the extrinsic parameters acquisition method (the rotation and translation matrices of the checkerboard in the first image). The flow chart of this approach is shown in Figure 62.

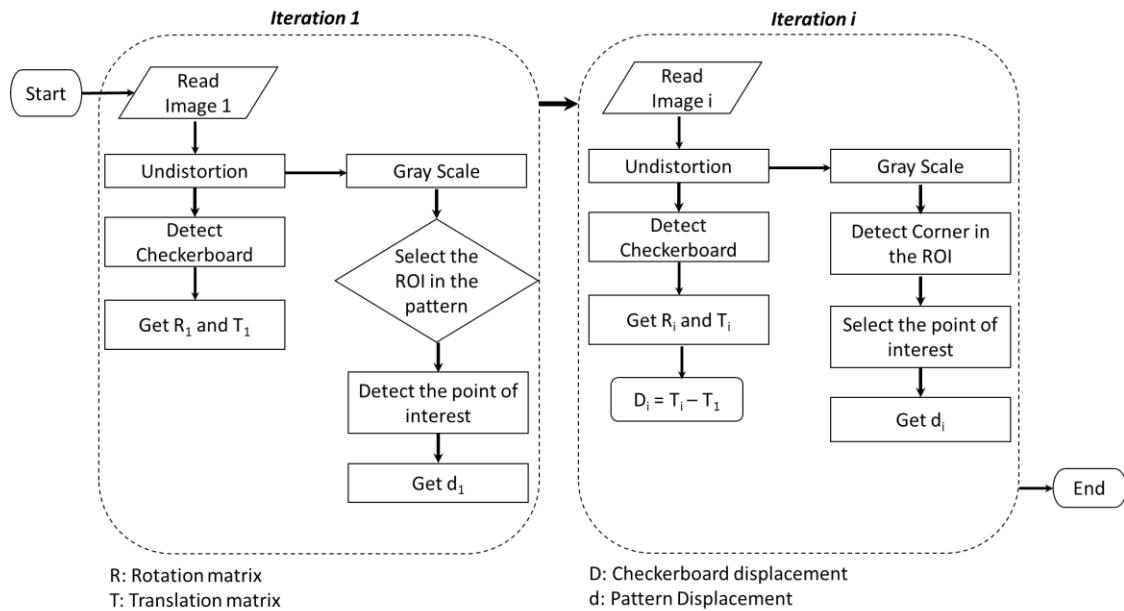


Figure 62. Flowchart of computer vision-based displacement measurement.

#### 4.3.4.3 Validation Test

A simple experiment was done to verify the accuracy and reliability of the proposed computer vision-based measurement approach. A checkerboard and one pattern were glued to a steel plate that was fixed to the base of a moving frame. The displacement of this base can be controlled and measured by an LVDT. Another pattern was fixed on the frame directly to check whether its displacement will remain constant. The base position was then increased from 0 to 13mm while taking images. Figure 63 shows the frame with the patterns with some details of the point of interest detection procedure. The comparison between the LVDT readings and the displacement of all the patterns shows that the method is accurate with a maximum error of 0.11 mm (Table 6).

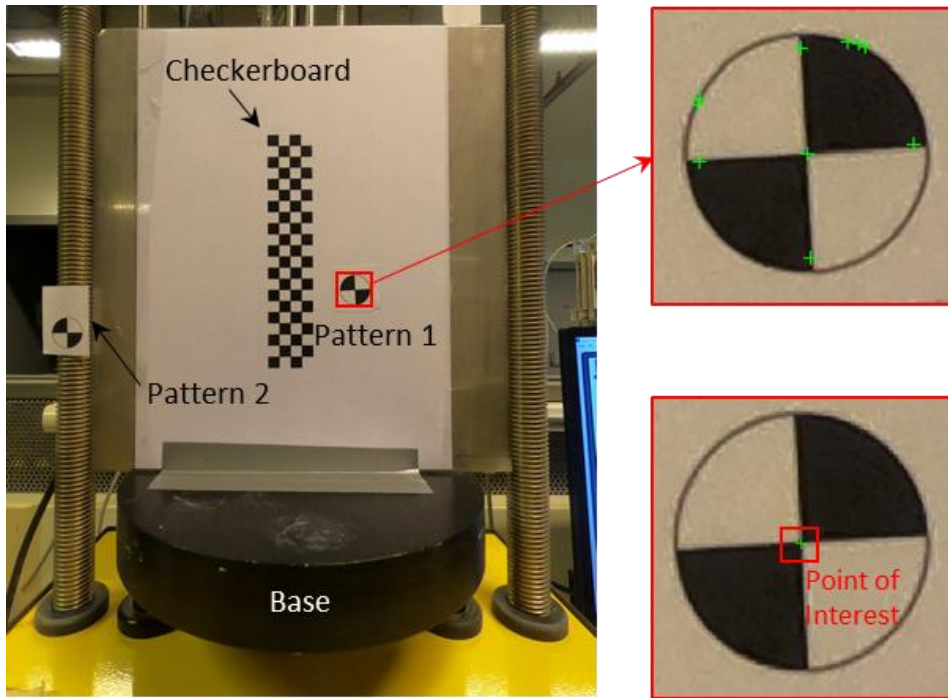


Figure 63. Validation Test: Patterns on the frame and detection procedure

Table 6. Comparison between the LVDT and patterns displacements.

LVDT	Checkerboard		Pattern 1		Pattern 2	
	Displacement	Error	Displacement	Error	Displacement	Error
0	0	0	0	0	0	0
1.977	1.988	-0.011	2.144	-0.167	0.046	0.046
2.992	3.022	-0.030	3.111	-0.119	0.076	0.076
13.009	13.080	-0.071	13.074	-0.065	-0.021	-0.021
Average	NA	-0.038	NA	-0.117	NA	0.033

#### 4.4 Data Acquisition

Live data during testing from the load cell, pore pressure sensors and LVDT was continuously streamed through a cDAQ from National Instruments that is able to acquire data on 4 different channels with high accuracy. In order to reduce the signal

noise, shielded cables were used for all sensors. A LABVIEW-based software was created to process and display the measurements in real-time directly on the computer screen.

#### **4.5 Validation Tests**

A preliminary testing program was designed and implemented at an early stage in the project to test the functionality of the novel test setup and identify any problems or limitations that could pose a risk on the implementation of the final test schedule that was envisioned for the research study. In particular, the objectives of the preliminary validation tests were to:

1. Assess the functionality of the proposed system
2. Check the practicality of removing the dummy sections once the setup consolidates into and is embedded within the soft clay bed
3. Assess the quality of the data obtained from the various sensors and monitoring devices
4. Identify required modifications to improve the setup
5. Confirm the stability of the system (anchoring sections), particularly during the shearing stage

The clay bed preparation, testing procedure, and preliminary results of this preliminary validation test are presented in the following sections. At this stage, the setup was not equipped with pore pressure sensors and the vertical displacements of the test section were not monitored.

#### ***4.5.1 Preparation of the Clay Test Bed***

In preparation for running the preliminary validation tests, a soil test bed was formed from a slurry and consolidated under a constant normal pressure of around 1.5 kPa for a period of about 5 months. The soil test bed consisted of oven-dried low plasticity clay (LPC), already used in earlier parts of our study for tilt table and direct shear tests. The dried soil was mixed with tap water to a water content of 40%, corresponding to 1.4 times its liquid limit. A 300 mm thick layer of this mix was placed in a 1.1x1.2x0.5m steel tank underlain by a 100 mm gravel layer separated by a geotextile filter fabric. The consolidation process of the clay slurry was completed in three stages: (1) under the soil own weight for 10 days, (2) under a pressure of 0.7 kPa for 20 days and (3) under a pressure of 1.4 kPa for 140 days. The clay bed was loaded using rigid steel plates to ensure a uniform pressure distribution and was inundated with water during all stages to avoid any desiccation. Drainage of pore water was permitted in the horizontal and vertical directions via geotextile sheets placed at the tank sides and between the clay and the gravel. Two valves installed on the lower side of the tank guaranteed the evacuation of water during the consolidation. An LVDT was fixed in the middle of the tank to record the consolidation settlement. Figure 64 shows all the preparation steps of the clay bed.

At the end of consolidation, the clay bed settled around 35 mm. The main portion of the recorded settlement (around 30mm) occurred under the own weight of the slurry and after the application of the 0.7 kPa normal stress. Figure 65(a) shows the consolidation curve of the last phase which involved the application of a normal stress~ 1.4 kPa, during which a settlement of approximately 5 mm was reached. Although primary consolidation of the soil bed was not yet fully completed by 140 days, a

decision was made to remove the dead weights and initiate the validation test trials under the pipe section. Soil samples were extracted from the bed once the steel plates were removed and the average water content was measured to be 31.8% (compared to an initial water content of 40%). Subsequently, the model pipe was laid down on the bed surface and allowed to consolidate under its own weight. This phase was completed and terminated after three days as shown in Figure 65(b). The total pipe embedment at that point,  $z$ , was 5.5 mm which is the sum of settlements from the seating phase (2 mm) and the consolidation phase (3.5 mm shown in Figure 65(b)). This result was confirmed by graduated scales that were placed at the pipe edges to monitor the embedment of the pipe at the two ends.

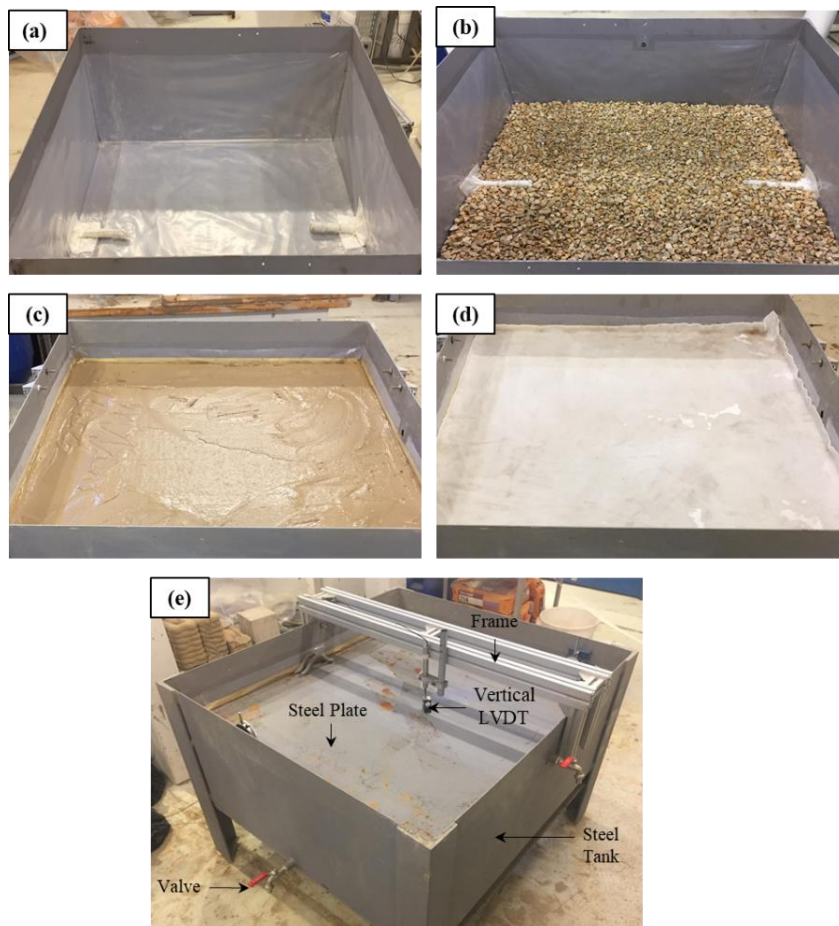


Figure 64. Clay Bed Preparation Steps: (a) Empty bed, (b) Gravel layer, (c) Filled with clay, (d) Covered with geotextile and (e) loaded by steel plates

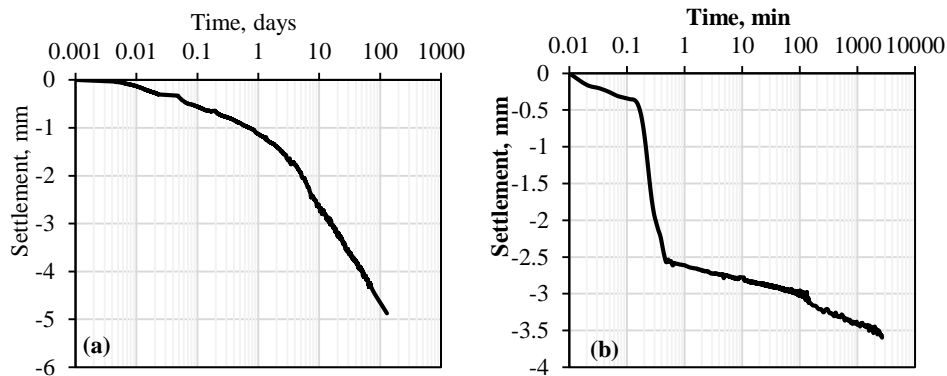


Figure 65. Consolidation curves of (a) the clay slurry under 1.4 kPa and (b) the pipe section under an estimated normal stress of about 3.55 kPa

#### 4.5.2 Testing Procedure

The setup was tested on the soft clay to validate its practicality and performance. The test aimed at measuring the residual drained interface strength between a stainless steel pipe/interface and the clay. First, the 1-m model pipe section was slowly placed on the soil surface and the settlements were recorded via an LVDT fixed on a horizontal frame that was connected to the tank. Consolidation of the pipe was allowed for three days following “touchdown”. Upon the termination of consolidation, one of the 50 mm dummy pipes was carefully removed, and the test pipe was separated/detached from the aluminum bar by removing the screws connecting the test section to the bar. The shearing phase was then initiated, and the test pipe section was axially displaced over the clay at a shearing rate of 0.00015 mm/s to ensure fully-drained conditions. The shearing stage lasted for 7 days during which three sweeps each consisting of an imposed movement of 25 mm, were executed. Figure 66 shows the model in the clay bed after consolidation and prior to the initiation of the shearing phase. Note the clean soil path created indicating that the goal of obtaining no soil accumulation ahead of the pile section to be displaced, and thus avoiding the formation of passive soil pressures,

was attained.. It is worth mentioning that every effort was made during dummy removal and bed preparation to prevent any soil surface disturbance.

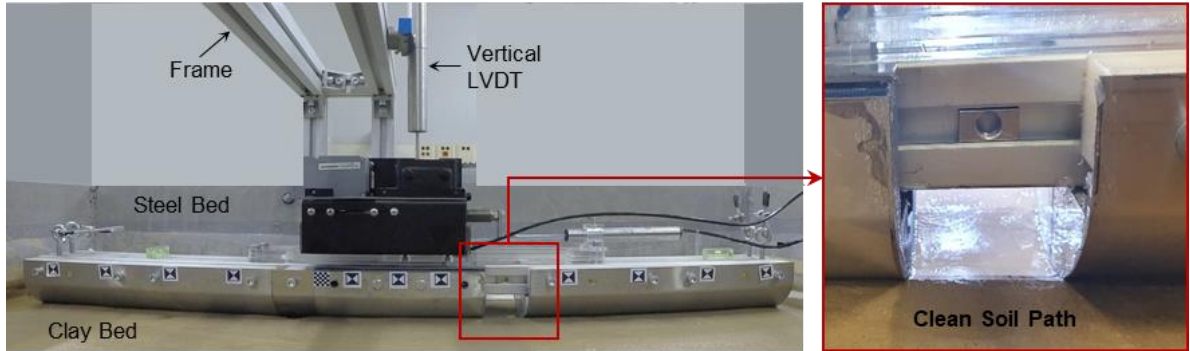


Figure 66. The setup inside the clay bed before shearing initiation

#### 4.5.3 Preliminary Results

As recommended by White and Randolph (2007), the normal stress around the pipe surface should be calculated taking into consideration wedging effects. The corresponding corrected normal stress was estimated using equation 4.1 to be 3.55 kPa.

$$\sigma_n = \frac{\xi V}{\vartheta D} \quad (4.1)$$

Where V is the vertical force (weight of the pipe section),

$$D \text{ is the diameter of the pipe, } \xi = \text{wedging factor} = \frac{2\sin\theta}{\theta + \cos\theta\sin\theta}$$

$$\theta = \text{half-angle enclosed by the pipe-soil contact perimeter} = 1 - 2\frac{z}{D}$$

The time histories of the imposed axial displacement and the measured axial resistance during the different shearing cycles are presented in Figure 67. The first sweep showed a peak in resistance (18.8 N) after 1.5 mm of displacement followed by strain softening to a minimum strength (13.6 N) at a maximum displacement of 24 mm. During the reversal sweep, the interface resistance was observed to be slightly lower (17.7 N) than the first peak, yet slightly higher than the minimum resistance observed



prior to the reversal. This could be due to changes in the loading direction, which could have affected the orientation of clay particles leading to added resistance. In the final sweep, no signs of strain softening were observed with a maximum interface resistance of about 13.5 N (close to the first minimum resistance).

The variations of the interface friction coefficient, defined as the mobilized shear stress over the corrected normal stress,  $\tau / \sigma_n$ , and the corresponding interface friction angle are plotted as a function of the axial displacement in Figure 68. The peak friction coefficient was 0.44 for the first sweep which corresponds to an interface friction angle of 24°. The residual friction coefficient in the first sweep was 0.33, slightly decreasing to 0.31 in the third sweep. This corresponds to a residual interface friction angle of 18°. The values of friction coefficient are in the range of those measured *in-situ* (0.3 to 0.6) using the SMARTPIPE between soft clay offshore West Africa and polypropylene coatings (Ballard et al. 2013). They are closer to the lower bound of the range since the stainless steel, with a roughness of 0.1  $\mu\text{m}$ , is smoother than the polypropylene (roughness of 3  $\mu\text{m}$ ).

The interface friction angles/coefficients that were obtained with the proposed novel testing apparatus could be compared to results from direct shear and tilt table tests as published in Houhou et al. (2020) for the same soil and stainless steel interface and in the same range of normal stresses. The variation of the interface friction angles with normal stress as obtained from direct shear and tilt table tests is presented in Figure 69. Also plotted on the figure are the peak and residual interface friction angles that were measured in the novel test setup. Results on Figure 6 indicate that the residual interface friction angles are similar, but the peak angles are somehow different. These results are significant since they indicate that the first deployment of the proposed testing setup

resulted in reliable estimates of the residual drained interface resistance of the clay/stainless steel interface that was used in this study. Further tests were done at later stages of the project to validate the performance of the testing mechanism using different interfaces and varying shearing rates.

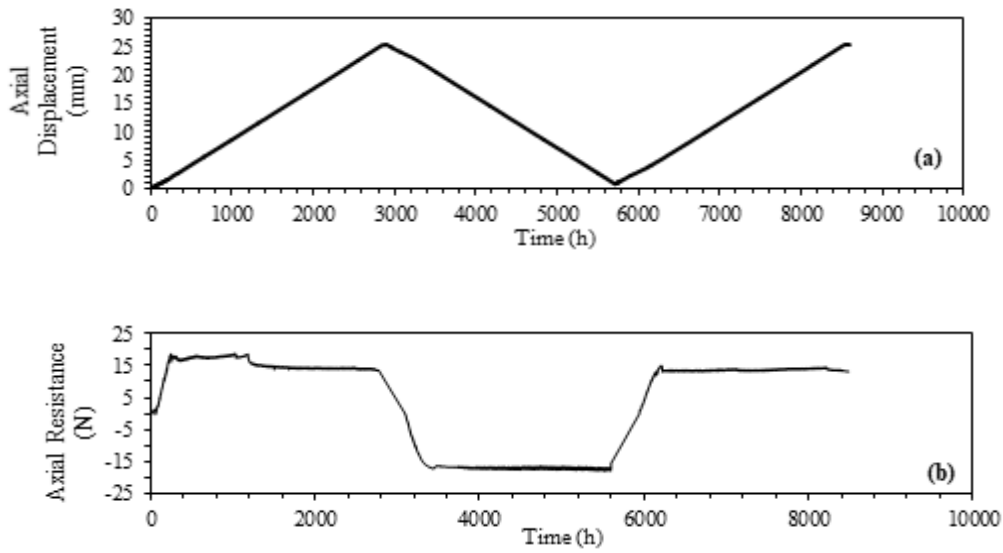


Figure 67. Time histories for (a) axial displacement and (b) axial resistance during test

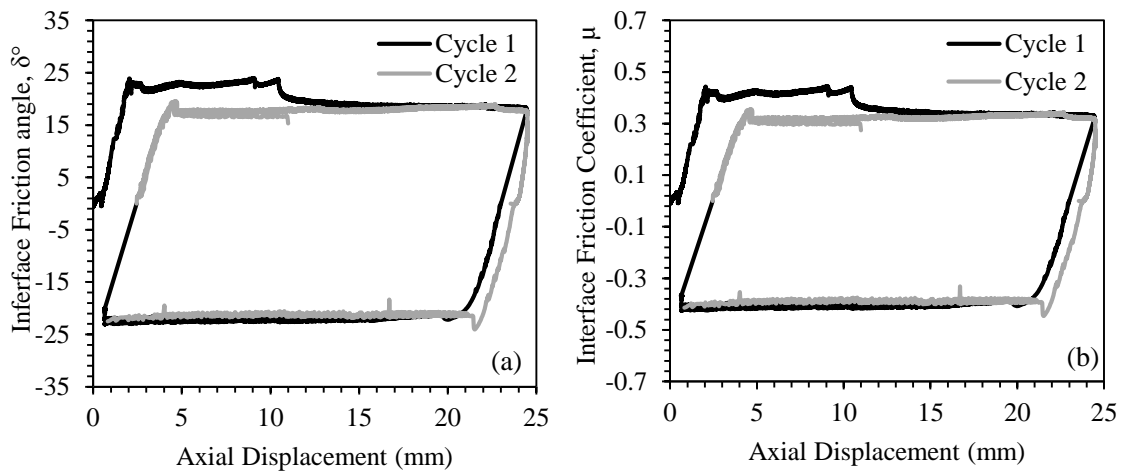


Figure 68. Variations of the mobilized interface friction angle and coefficient with displacement

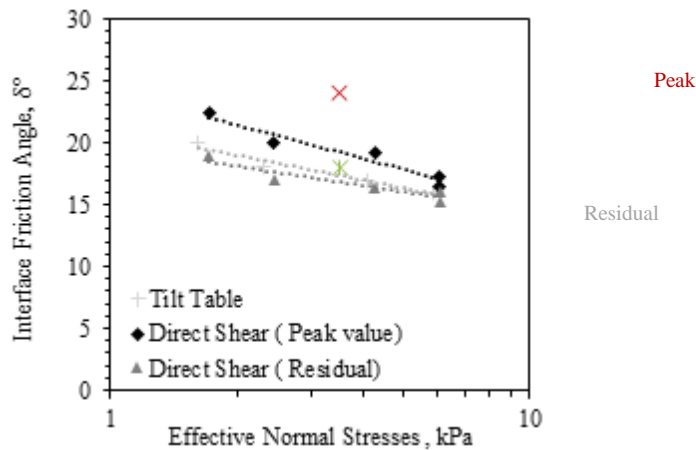


Figure 69. Comparison between interface direct shear and tilt table results and the model results

#### 4.5.4 Setup Improvements

Although the validation test was successful and yielded realistic interface resistance values, potential improvement to the test setup were implemented and consisted of adding the capability for measuring pore water pressures at the pipe/clay interface and including tools/means to enhance the overall measurement of the displacement/rotation of the test section during shearing. These capabilities allow for the collection of key information on the generation of pore water pressure and volume change during the shearing stages. More importantly, data from the pore pressure sensors would shed light on the dissipation of excess pore water pressure at all stages of testing and provide an indication of the drainage conditions during shearing. The computer-vision approach was adopted to identify the displacements of the test section while limiting direct contact with the test section. Displacements that are deduced from computer-vision analysis will indicate whether the soil is contracting or swelling as it is sheared. In addition, the load cell connection to the motor's screw needed to be replaced with a stiffer plate in order to further ensure full rigidity of that part of the setup.

In addition to improvements to the apparatus it was clear that an accurate and detailed characterization of the clay bed was necessary for the proper analysis of the pipe/clay interface test results. In particular, there was a need to determine the undrained shear strength of the clay in the test bed to use it as a reference when analyzing pipe/clay interface response under “fast” loading conditions. Since the clay in the bed was prepared from a slurry and consolidated under a relatively small normal stress, the range of the undrained shear strength in the 30-cm deep bed is expected to be very small. This renders conventional shear strength testing methodologies (triaxial, direct shear, etc.) ineffective in characterizing the shear strength in the bed. For similar conditions that are usually encountered in shallow seabed sediments, the ball penetrometer and vane shear tests have been proven to be effective and reliable testing methods for determining the undrained shear strength. As such, a miniature ball penetrometer was designed, fabricated and calibrated to be used in the subsequent characterization of the test bed. The miniature ball penetrometer was calibrated against undrained shear strength values that were measured from a laboratory vane setup that will be described in the following section together with the ball penetrometer design, fabrication and calibration.

#### **4.6 Shear strength of soft clay using miniature ball penetrometer, vane shear, UU triaxial tests and direct shear tests**

The undrained shear strength of the clay used in this research study was investigated and explored over a range of conditions through an extensive and comprehensive laboratory testing program. The tests adopted for the measurement of the undrained strength included ball penetrometer tests, vane shear tests, UU triaxial

tests and direct shear tests. The triaxial and direct shear tests were conducted to estimate the  $c/p$  ratio of the clay while the vane shear tests were conducted to evaluate and calibrate the resistance factor,  $N_{\text{ball}}$  of the ball penetrometer. The end aim for the generation of the well calibrated resistance factor was to use it when interpreting ball penetrometer tests that would be carried to determine the in-place shear strengths through and throughout the clay test bed.

#### ***4.6.1 Preparation of Element Soil Samples***

The low plasticity clay (LPC) was mixed at 60% water content using a large high rotational speed mixer. The clay slurry was scooped and placed inside plexiglass boxes (200 x 200 x 200 mm or 120 x 120 x 200 mm) in layers. Top and bottom drainage was allowed to facilitate the consolidation of the slurry. The clay was then left to consolidate under its own weight for 24 hours. Afterwards, deadweights were added at the top of the samples to apply the desired normal stress (ranges from 1.45 to 2.3 kPa) and left for 7 days to ensure that the consolidation phase was completed. Some boxes were left to consolidate for more than 7 days. Table 7 summarizes the applied normal stresses and the final water contents of the samples prepared. These samples were then tested using the ball penetrometer and the vane shear apparatuses.

As for the direct shear samples, the same mix was prepared and left for three hours before placing it inside the direct shear box to consolidate under the desired normal stress (10, 20, 30 and 40 kPa). A similar methodology was adopted for the triaxial tests. The mix was placed in prefabricated stiff PVC pipes 70 mm in diameter and 300 mm tall, which were sealed in a one-dimensional odometer setup.

Consolidation stresses (25, 38 or 49 kPa) were applied incrementally via a number of dead weights that were added based on a predetermined loading schedule. Subsequently, the 1D-consolidated samples were removed from the PVC pipes and trimmed to a final length of 140 mm, and placed in the triaxial chamber to be tested under UU triaxial conditions. It should be noted that the direct shear and triaxial tests were conducted at relatively large normal/confining stresses given the inherent limitations of the standard direct shear and triaxial setups.

Table 7. Properties for Vane and Ball Penetrometer Soil Specimens

<b>Boxes</b>	<b>Normal Stress, kPa</b>	<b>Initial water content, %</b>	<b>Final water content, %</b>
<b>Sample 1</b>	1.45	60	36-36.2
<b>Sample 2</b>	1.59	60	33-34.5
<b>Sample 3</b>	2.29	60	35.5-36

#### ***4.6.2 Miniature ball penetrometer apparatus***

As already discussed in the seabed characterization section of the literature review, the ball penetrometer is the most suitable method to measure the relatively low undrained shear strengths of soft clays, typical of those encountered in shallow marine sediments. Recently, a small-scale (miniature) ball penetrometer setup has been used to characterize the strength of a synthetic transparent soft clay in the laboratory (Ads et al., 2019). Such a miniature device is usually used to measure the shear strength of soils in centrifuge tests (e.g. Stewart and Randolph 1991; Lee et al. 2012). The miniature ball penetrometer is more practical for laboratory use as it requires smaller soil batches to eliminate possible boundary effects. In this project we fabricated and used a miniature ball penetrometer similar to the one presented in Ads et al. (2019).

In the absence of an ASTM standard, the design of the miniature ball penetrometer was based on the recommendations of Dejong et al. (2010). The penetrometer consists of a ball, a shaft, a linear actuator with position feedback (built-in potentiometer), and a load cell, all fixed to a rigid steel frame. The nominal ratio between the ball and the shaft areas was chosen as 10:1 with a shaft diameter of 6 mm and a ball diameter of 19 mm. The nominal penetration rate can be 3.8 to 5.7 mm/s which corresponds to 0.2D-0.3D per second.

The shaft of the penetrometer was attached to an S-shaped load cell (20 kg capacity) which is in turn was fixed to a linear actuator (full stroke of 250 mm) that pushes the ball penetrometer into the clay sample at a specified penetration rate. The rate of penetration was controlled by the input voltage of a variable power supply (0-24v). The linear actuator was attached at the center of a steel plate that is firmly fixed to four threaded rods 20 mm diameter and 1 m tall. This gave the setup a flexibility in choosing the exact position of the penetrometer at the intended test location across the clay bed. The end of the steel rods are welded to a steel base plate which can be either fixed on the frame above the steel tank of the clay bed or can simply stand on its own. The load cell and the built-in potentiometer outputs were transmitted to a cDAQ to be directly plotted on screen using a LABVIEW based software. Figure 70 shows the ball penetrometer apparatus while testing the clay bed or a clay sample prepared for that purpose.

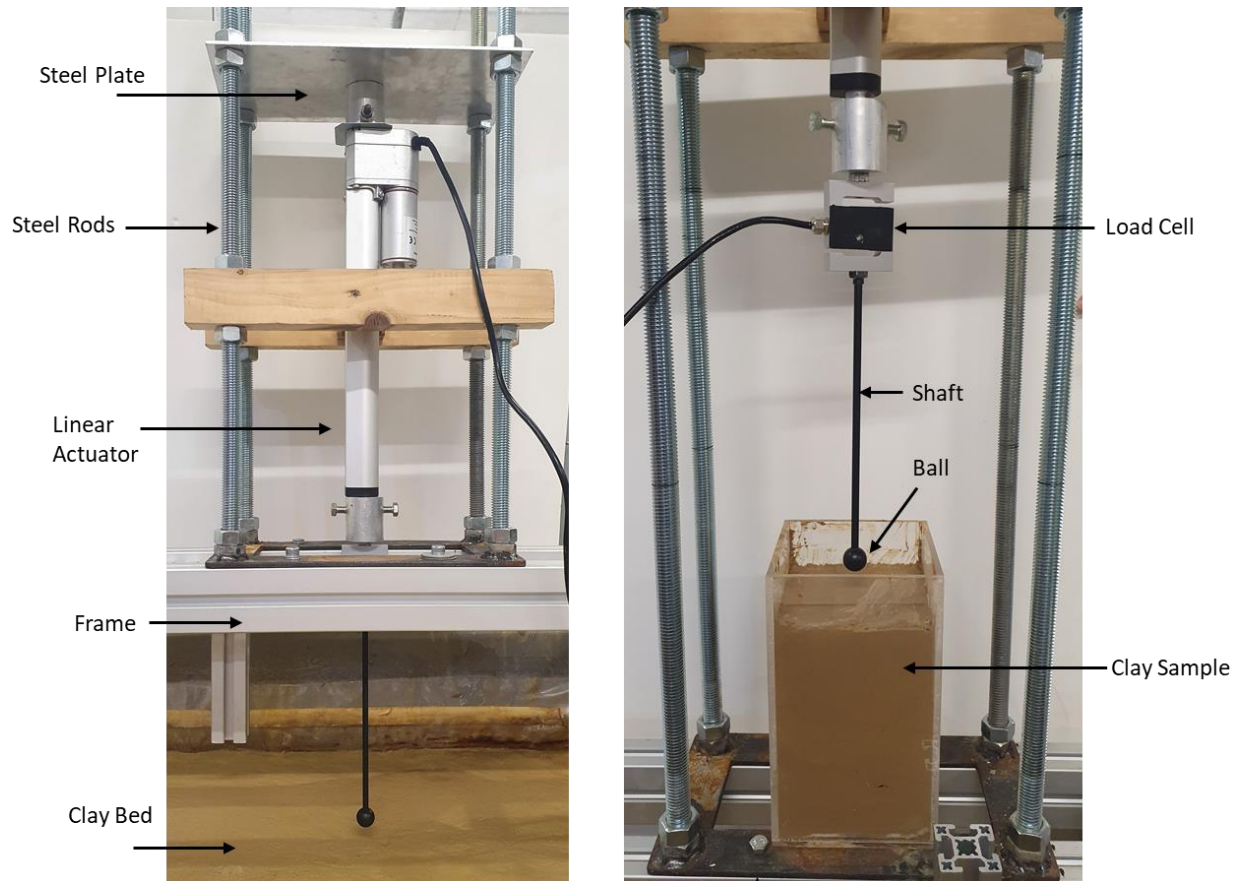


Figure 70. Ball Penetrometer Apparatus: (a) Fixed on the tank's frame to test the clay bed and (b) Testing a clay sample.

#### 4.6.3 *Vane shear apparatus*

The vane shear test is typically used to obtain estimates of the undrained shear strength of fine-grained soils. The test provides a rapid determination of the shear strength on undisturbed and remolded/reconstituted soils. The vane shear test involves inserting a four-bladed vane into an intact (or remolded) tube sample and rotating it at a constant rate to determine the torque required to cause shearing along a cylindrical surface defined by the geometry of the vane. This torque is then converted to a unit shearing resistance of the cylindrical surface area.



A motorized vane shear apparatus was manufactured according to ASTM standards D4648/D4648M. A four-bladed vane with H/D ratio of 2 (a diameter of 34.39 mm and a height of 68.78 mm) was used. The vane area ratio, computed based on Equation 4.2, was 6% which is less than the 10% limit recommended by the ASTM standard. The torque resistance was obtained by means of a torque transducer from NCTE having a maximum capacity of 2.5 N.m attached directly to the vane shaft (D=3mm). The upper shaft of the torque transducer was connected to a DC motor with a maximum speed of 2 rpm. The motor was mounted on a triaxial frame. The clay sample was held at the base of the frame, whose position could be controlled. The whole setup is shown in Figure 71.

$$V_A = \frac{4(R-r)e + \pi r^2}{\pi R^2} \quad (4.2)$$

Where  $V_A$  = Vane area ratio

$R$  = Radius of failure cylinder (in mm) = 17.195 mm

$r$  = Radius of vane shaft = 1.575 mm

$e$  = Vane blade thickness = 0.8 mm

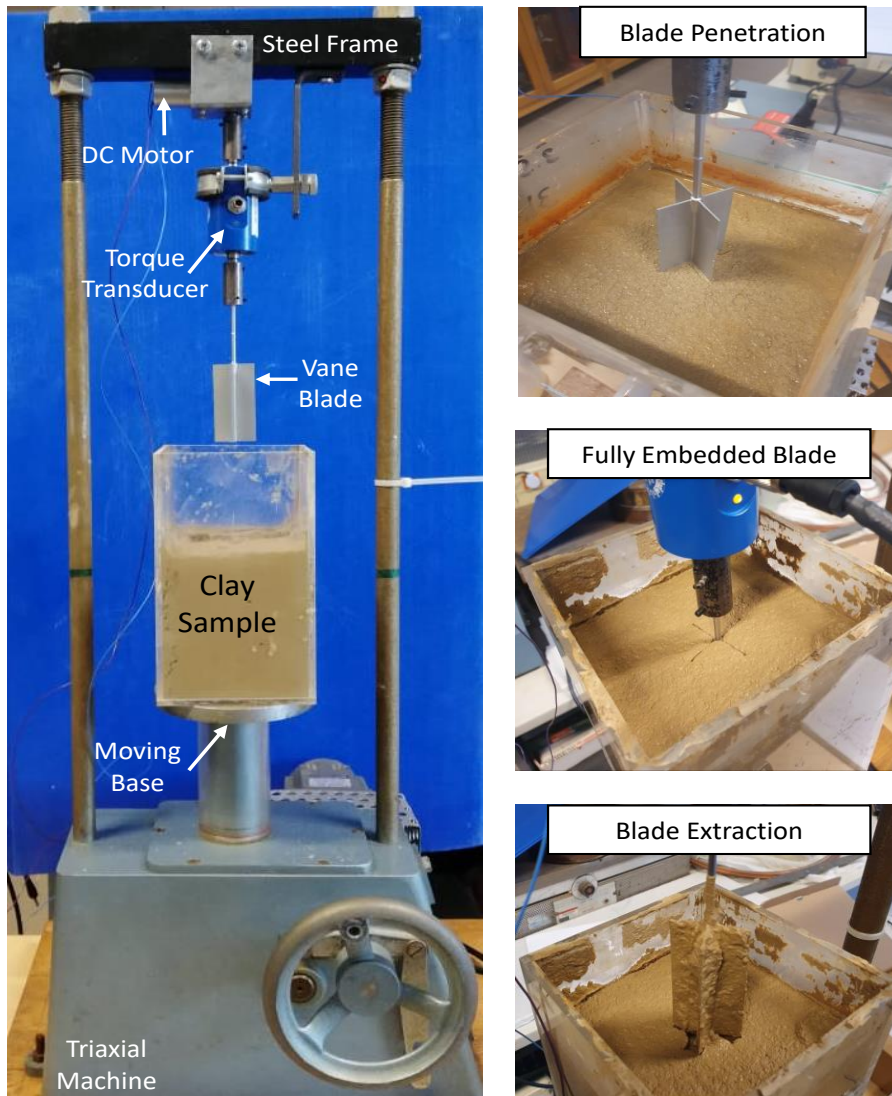


Figure 71. Vane shear apparatus and various testing stages.

#### 4.6.4 Testing Procedure

In the case of ball penetration tests, the ball was penetrated to a depth of 70 mm to 140 mm inside the clay samples at a rate of 3.8 mm/s, which corresponds to 0.2D per second. The resisting force,  $P$ , was recorded during penetration and extraction. Using  $P$ , the penetration and extraction resistances,  $q_{\text{ball}}$ , were computed as  $P/(\pi D^2/4)$ . These resistances are normally corrected for unequal pore pressure and overburden pressure effects (Chung and Randolph, 2004). However, testing shallow soil depths minimizes

these effects and thus no correction was needed (Low et al., 2008). The undrained shear strength of the soil could then be estimated from  $S_u = q_{ball}/N_{ball}$  where  $N_{ball}$  is the resistance factor of the ball penetrometer.  $N_{ball}$  was obtained by comparing the ball penetrometer results to the vane shear results conducted on identically prepared samples. Note that the water at the clay surface was first removed before penetrating the ball to prevent any water infiltration during the test that would cause additional soil softening.

For the vane shear tests, the vane blade was penetrated to a depth equal twice its diameter at a penetration rate of 1 mm/s by moving the frame base holding the soil sample upward. This depth secures that the top of the blade is embedded one diameter below the sample surface. After the vane had reached the testing depth, a 10 second waiting time was imposed. The motorised vane shear tests were then performed at a constant rate of 1.5°/s until reaching the first peak and then the rate was increased to 4.5°/s to get the remoulded strength. The interpretation of vane shear tests assumes that the soil shears as a cylinder. At failure (peak torque) the undrained shear strength is assumed to be fully mobilized around the vertical perimeter of the vane as well as along the horizontal planes comprising the two ends of the cylinder and thus could be calculated using equation 4.3.

$$S_u = \frac{T}{\frac{\pi D^2}{2} \left( H + \frac{D}{3} \right)} \quad (4.3)$$

A conventional direct shear apparatus was used to run the direct shear tests. However, the loading arm was replaced by a loading system that imposes dead weights directly on top of the sample, the same system described in Chapter 3. The modified direct shear device of Chapter 3 could not be used for these undrained tests since its

maximum shearing rate is 0.016 mm/s which leads to partially drained conditions. Thus, the undrained tests were performed using a VJ-Tech direct shear device at relatively high range of normal stresses (10-40 kPa) to reduce the effect of the system's friction on the shearing results. The soil mixed at 60% water content was placed inside the shear box, the dead weights were then added gradually to reach the desired normal stress (10, 20, 30 and 40 kPa) and then the soil was left to consolidate. After the completion of consolidation, a 1-mm gap was created and the sample was sheared at the highest shearing rate of 0.2 mm/s.

The unconsolidated undrained (UU) tests were performed according to ASTM-D2850 recommendations. The 1D consolidated samples were subjected to a confining pressure of 50 kPa in the triaxial chamber and then left for 10 min to stabilize under this pressure. Subsequently, the samples were axially loaded at a constant rate of axial deformation (1%/min) until reaching 15% axial strain while continuously recording the axial load. No drainage was permitted during the application of the confining pressure nor during the compression phase. It is worth mentioning that the samples were one-dimensionally consolidated at relatively high pressures (25 kPa and above) in order to minimize the effect of sample disturbance during preparation and subsequent testing. Samples consolidated at lower pressure would be very soft and would fail during the sample preparation stage.

#### 4.6.5 *Estimation of the undrained shear strength of clay and c/p ratio*

The stress-rotation responses from the vane shear tests are shown in

Figure 72. It is clear that the shear stress increased to reach a peak and then decreased rapidly at a rotation rate of 1.5°/s. The peak stress values correspond to the undrained shear strength,  $S_u$ , which varies between 0.64, 0.72 and 0.67 kPa for sample 1, 2 and 3, respectively. The shear stress values at the end of the vane shear tests indicated that the remoulded strength of the three samples,  $S_{ur}$ , is the same and equal to 0.45 kPa. As such and as expected the sensitivity of the low plasticity clay,  $S_u/S_{ur}$  is relatively low and ranges between 1.5 to 2.

The results of the “undrained” direct shear tests are presented in Figure 73. The shear stress increased with displacement and reached a peak and then slightly decreased after 8 mm of shearing at all stress levels. The undrained shear strength was estimated to be the maximum stress reached during the test. It varied from 2.7 to 14.65 kPa as the normal stress was increased from 10 kPa to 40 kPa. However, it is expected that the response during shearing was not fully undrained as all samples contracted during shearing as shown in Figure 73. This was expected since the drainage could not be controlled using the direct shear device even if the shearing rate is so fast. Drainage could only be prevented by varying the normal stress while maintaining a constant sample thickness and this is can only be done using a simple shear device.

As for the undrained triaxial tests, the variation of the deviatoric stresses with the axial strain is shown in Figure 74. The samples that were one-dimensionally consolidated at 38 and 49 kPa had the same shearing reponse where a steady state was reached after 3% axial strain. For the sample that was one-dimensionally consolidated to 25 kPa, a peak was reached at 15% axial strain indicating a more ductile response. The

corresponding undrained shear strengths were calculated as half of the deviatoric stress at failure to be 9.25, 8.75 and 4.7 kPa for samples that were one-dimensionally consolidated at 49, 38 and 25 kPa, respectively.

In order to compare the undrained strengths measured at different normal stresses and using different testing methodologies, all the measured undrained shear strength values were normalized with respect to the vertical effective normal stress as  $S_u/\sigma'_{vo}$ . These normalized values are also widely referred to as “c/p” ratios. For normally consolidated clays, Skempton (1957) suggested the c/p ratio could be related to the plasticity index following equation 4.4 which gives a ratio of 0.16 for the used low plasticity clay tested in this study. However, correlations that are similar to that presented in equation 4.4 might not be applicable for the clay tested in this study given that the clay contains 25% sand in its composition.

$$c/p = 0.11 + 0.0037 * PI \quad (4.4)$$

Table 8 summarizes the results from the three adopted testing methodologies. It is clear that the undrained direct shear tests resulted in high c/p values that were in the order of 0.34 due to the expected partially drained conditions during testing. On the other hand, the c/p ratios from UU tests ranged from around 0.19 to 0.23. The real c/p ratios for these specimens could be slightly higher than the reported values as a result of overestimating the vertical effective stress that the samples felt during one-dimensional consolidation in the PVC tubes. The effective stress at the bottom of the specimen could be reduced in the PVC tube as a result of internal friction between the soil and the tube. This has led to variation in the water content along the depth of the specimens, since the top of the specimen is expected to consolidate more than its bottom. Evidence of this

phenomenon is shown in the water content measurements, which show that triaxial specimens had higher final water contents than those of the direct shear tests at the same stress level  $\approx 40$  kPa (25.85 % compared to 23.11%). Another proof of the effect of clay/wall friction on the water content can be found in the specimens that were one-dimensionally consolidated in preparation for conducting the ball penetrometer tests. It was found that the resistance to ball penetration was high when the tests were conducted from the upper part of the specimen compared to tests that were conducted on the lower part, indicating non-uniformity in water content.

The results of the vane shear tests are presented in Table 1 and indicate that samples S1 and S2 yielded  $c/p$  ratio in the order of 0.45. This relatively high  $c/p$  ratio is explained by the fact that these two specimens were tested after more than 30 days of consolidation. For the only test that was done at 7 days (test S3), results indicated a more realistic  $c/p$  ratio of 0.29. Despite the fact that tests 1 and 2 were left for 30 days to consolidate, all three vane tests will be used in the calibration of the ball penetrometer since the ball penetration number  $N_{ball}$  is expected to be independent of the properties of the clay.

It can be concluded that the undrained shear strength of the clay in this study is affected by multiple factors including strain rate, drainage conditions, sample homogeneity, and shearing method (plane strain, triaxial, or torsional shearing). The results of the vane shear tests could be considered to be the most representative given that they were conducted at low confinement levels that are the closest possible to those that will be used in the full scale bed. In addition, the 20cm x 20cm test beds in which the vane shear tests were performed allow for equivalent ball penetrometer tests that could be done centimeters away from the vane tests. This will allow for the most

representative and realistic calibration exercise leading to the determination of reliable estimates of the ball penetrometer  $N_{ball}$  factor.

Table 8. Summary of vane shear, direct shear and UU tests.

Test	$\sigma'_v$ (kPa)	$S_u$ (kPa)	$c/p$	$w_{final}$ (%)
Vane shear	1.45	0.64	0.44	36.0
	1.58	0.72	0.46	35.0
	2.20	0.67	0.29	36.5
Undrained direct shear	10	2.7	0.27	28.7
	20	5.2	0.31	26.0
	30	10.7	0.35	24.2
	40	14.6	0.37	23.1
UU Triaxial	25	4.7	0.19	-
	38	8.7	0.23	25.8
	49	9.2	0.19	24.8

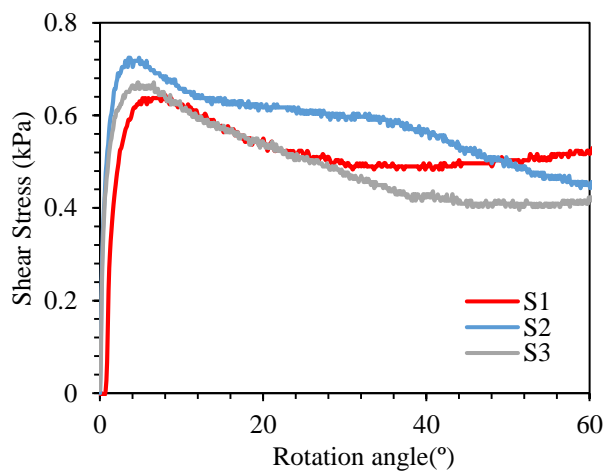


Figure 72. Stress-rotation responses from vane shear tests.



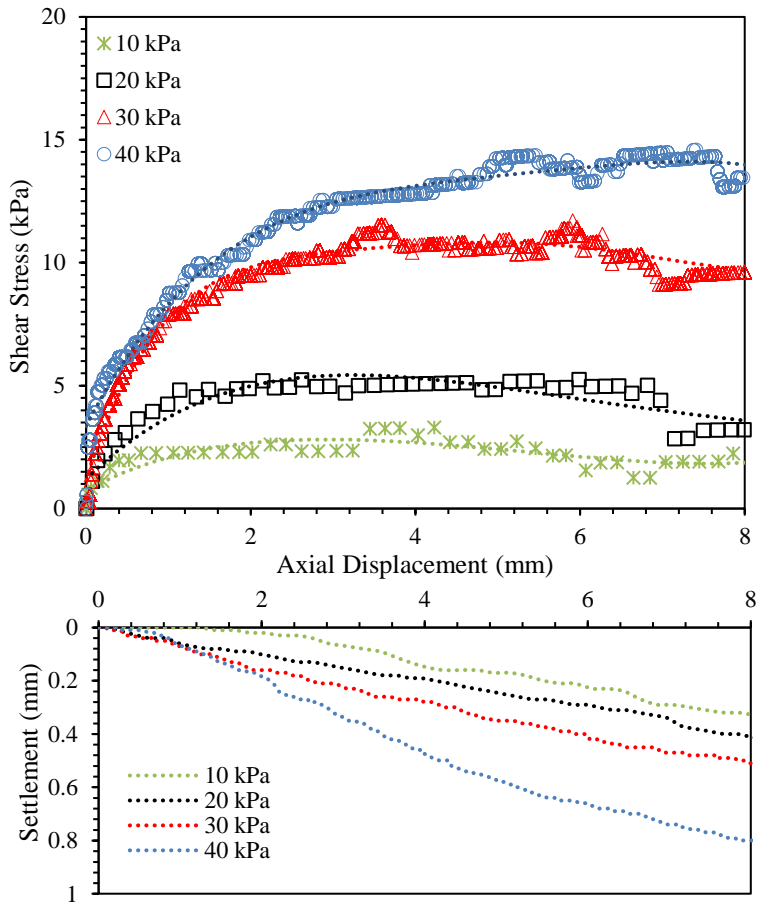


Figure 73. Undrained direct shear results: (a) Shear-stress responses and (b) Settlements.

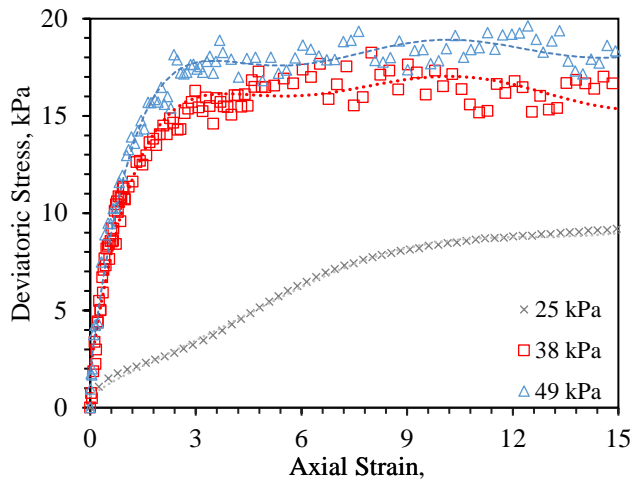


Figure 74. Deviatoric stress vs axial strain for UU-triaxial tests.

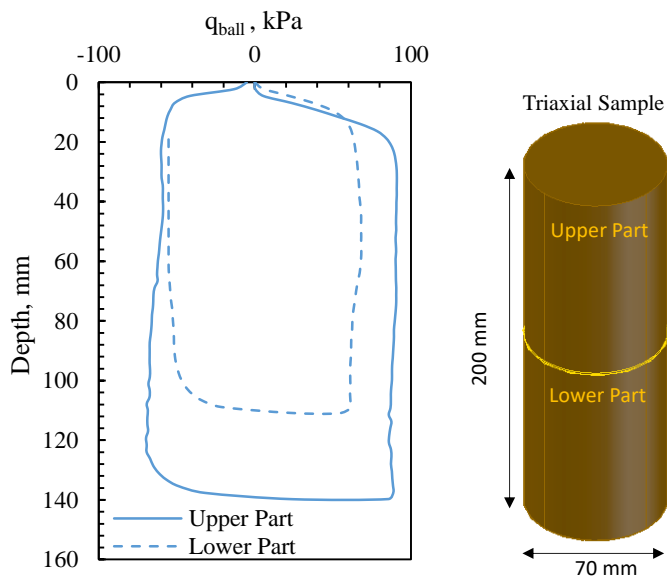


Figure 75. Penetration resistance for a 1D consolidated sample to 49 kPa.

#### 4.6.6 Evaluation of the resistance factor

Ball penetrometer tests were conducted in the three 20cmx20cm clay samples in which the vane tests were conducted. The ball penetration resistance profiles for the three tested clay samples are presented in Figure 76 and show similar profiles for the penetration resistance, with sample S1 giving a slightly higher resistance. The resistance value at the first 20 mm could be ignored since the ball was not yet fully submerged inside the clay. A slight increase in the resistance with depth could also be noticed. The average resistance values were 9.61, 9.16 and 8.81 kPa for samples S1, S2 and S3 respectively from 30 to 70 mm depth. Such small difference between the penetration resistances between the three samples indicates that they have practically the same shear strength. In addition, their water contents are comparable (Table 7). Although sample S3 was consolidated at higher stress (2.2 kPa), its relatively high water content is attributed to the fact that its consolidation stage lasted for 7 days compared to 30 days for the other

two specimens. The results confirmed that the designed ball penetrometer apparatus was successful and its measurements of sample “strength” were accurate and repetitive.

The penetrometer results are also aligned with the vane shear results that showed comparable undrained shear strength values for the 3 samples. Dividing these undrained shear strength values by the average ball penetration resistances gave the following resistance factor values,  $N_{ball}$  : 14.51, 12.85 and 13.2. These estimated  $N_{ball}$  values fall within the range of the worldwide database collected by DeJong et al. (2011), which shows  $N_{ball}$  factors between 8 and 16. Assuming that the friction coefficient between the steel ball and the clay is 0.3, the back-calculated  $N_{ball}$  values are close to the upper limit estimated theoretically by Einav and Randolph (2005). These  $N$  values are also close to the resistance factors estimated by equation (4) derived by DeJong et al. (2011) that ranged between 12.8 and 13.2.

$$N_{ball} = 13.2 - \frac{7.5}{1 + \left(\frac{q_{in}/q_{ext}}{1.9}\right)^{-20}} \quad (4.5)$$

Where  $q_{in}$  = ball resistance during penetration

$q_{ext}$  = ball resistance during extraction

As a result, an  $N_{ball}$  factor of 13.5 will be adopted in characterizing the variation of the undrained shear strength with depth in the full scale clay bed in which the pipe/clay interaction will be studied.

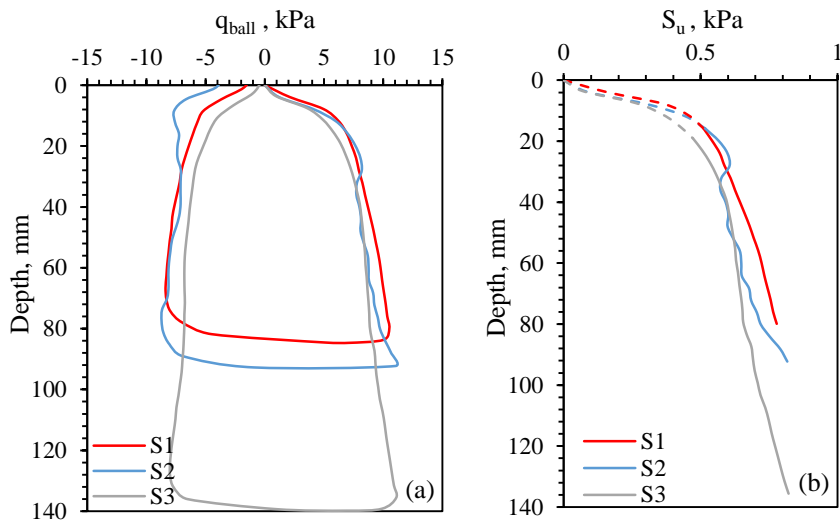


Figure 76. (a) Penetration Resistance Profiles and (b) undrained shear strength profiles with  $N_{ball} = 13.5$

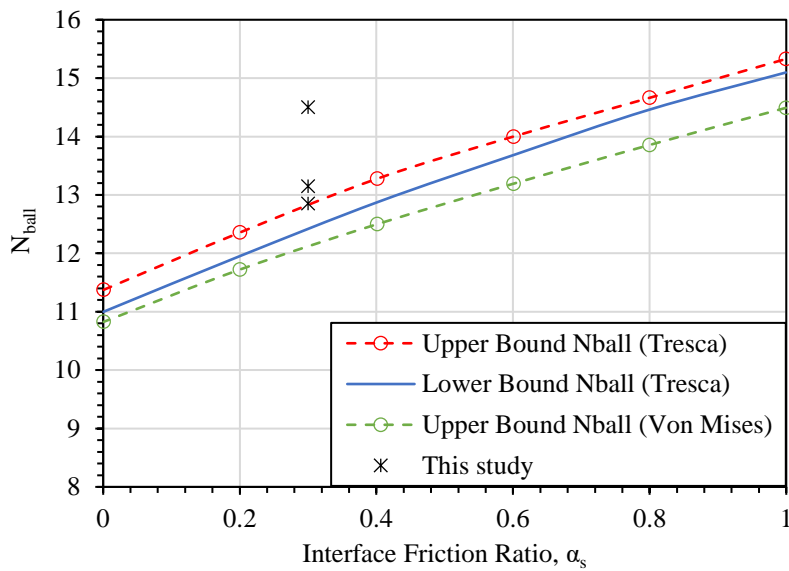


Figure 77. Theoretical  $N_{ball}$  factors.

#### 4.7 Conclusion

This chapter presents the design of a novel test setup that could eventually be adapted to measure the interface friction angle between pipelines and soils in the offshore environments. In the form that is presented in this thesis, the mechanism is in the early stages of development. The proposed test setup and the preliminary validation

tests that are reported could be considered to be a proof of concept at this stage of the project.

The proposed test setup minimizes errors due to passive resistance which typically develops at the end of test pipes in other existing test devices/systems. The setup also minimizes eccentricity or upward force components that could lead to complex variations in the normal stresses at the pipe-soil interface. More importantly, the setup relies on dead weights to apply the normal stress, eliminating the need for controlling the normal stress using costly loading systems that are currently used in other *in-situ* test setups (ex. SMARTPIPE). The main novelty in the proposed test setup is in the modular design of the pipe section which consists of 5 pipe segments that act as (1) main test section, (2) dummy sections that are removed to create a path for shearing, and (3) anchor sections that allow for producing the reaction needed for the motor to displace the test section.

A trial test on a normally consolidated clay was performed to check the adequacy and the practicality of the proposed setup. The results showed that the setup can produce realistic interface friction angles that are comparable to the ones available in the literature and the ones obtained from tilt table and interface direct shear tests on the same soil and interface. The fact that the used soil contains 25% of sand helped in capturing the drained interface response; however, for clays having a lower permeability, slower shearing rates should be adopted. Accordingly, it can be concluded that the proposed system is promising and could be adopted in measuring the interface response between offshore pipes and clays.

Further improvements must be implemented in the future to convert this setup into a fully independent field test setup. The challenges while moving in that direction involve designing a fully automated mechanical mechanism that could detach the test section and the dummy sections from the central aluminum bar without manual intervention. The other challenge is automating the process of removing the dummy sections in preparation for shearing. Finally, if the test setup is going to be deployed in offshore environments the motor and other parts of the system will have to be sealed within water-proofed chambers.

Finally, the design and calibration of a ball penetrometer apparatus were presented. Undrained direct shear tests, UU triaxial tests and vane shear tests were performed to estimate the undrained shear strength of the used soft clay. However, the vane shear proved to be the most reliable and its results were used to evaluate the resistance factor of the ball penetrometer.

## CHAPTER 4

### PIPE-SOIL RESISTANCE USING A NOVEL TEST SETUP

#### **5.1 Introduction**

The design of offshore pipelines is governed by the axial resistance between the pipe and the supporting and/or embedding soil. Under-estimation of the axial resistance will lead to low predicted compressive forces and excessive pipeline extension.

Conversely, an over-estimation of the axial resistance may imply high compressive forces and increased likelihood of lateral buckling, which will require costly restraining structures/provisions. In this context, the actual axial response is controlled by many factors such as the shearing rate, consolidation periods, roughness of the pipe-soil interface, and the expected normal stress level.

This chapter aims at investigating the efficiency and functionality of the proposed test setup under different test conditions. As such, the setup will be tested in the prepared clay bed under conditions that will enforce variable shear rates, different interface roughness, and different embedment levels. The results will also highlight the effect of each factor on the interface resistance.

#### **5.2 Experimental Program**

##### **5.2.1 Test Soil**

The clay bed that was used for conducting the preliminary tests reported in Chapter 4 was also utilized to implement the final testing program envisaged for this study. Following the preliminary tests in Chapter 4 and in order to ensure that the clay

bed remains saturated, an effort was made to continuously add water to the bed to maintain a 2-cm water cover above the mudline. Given the conditions prevailing at the time and which continue to date, and because of lockdown related limitations that prohibited the continuous watering operation, constant water levels could not be maintained, which resulting is loss of saturation in the upper/exposed parts of the clay bed..

Given the excessive time that would be needed to remold the whole thickness of the clay bed (30 cm) back into a slurry and consolidate it from scratch (requires 9 months), a decision was made to remold and reconsolidate the upper 5cm of the soil only (likely to have partially dried) in preparation for the implementation of the test program. Since the expected pipe embedment in the envisaged tests was restricted to less than 2.5cm, the interface shear tests will only involve clay in the upper 5 cms of the bed. As such, the decision to remold and reconsolidate the upper 5-cms of the bed only would result in significant time savings without affecting the objectives of the envisaged test program.

As a first step in reconstituting the upper 5-cm of the bed, water was added gradually for a period of 3 months to re-saturate the bed. The upper 5 cm of the bed were then manually mixed/remolded in preparation for consolidation under a 1.5 kPa pressure applied using the same steel plate originally used to consolidate the bed. The settlement of the bed was monitored with time as indicated in Figure 78. The final settlement after 45 days of consolidation was 4 mm (Figure 78). Samples taken from the clay bed after consolidation indicated a water content ranging from 28.5% to 30% in the upper 3 cm.



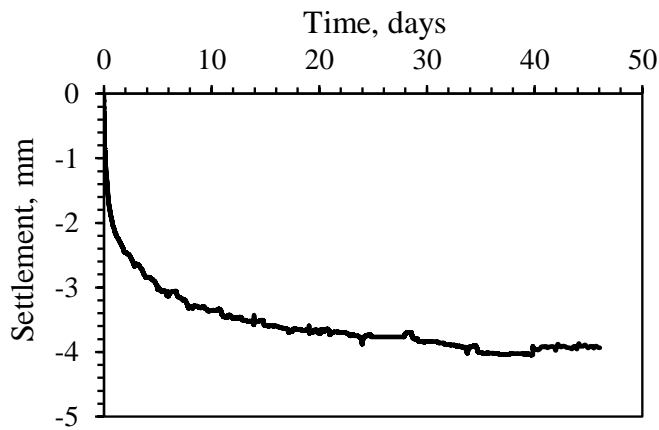


Figure 78. Consolidation with time after re-forming and loading the clay bed.

In order to characterize the shear strength of the clay in the thus prepared clay layer, three cyclic ball penetrometer tests were performed at 3 different locations to evaluate the undisturbed undrained strength, remolded undrained strength, and sensitivity of the clay. The ball penetrometer was initially penetrated to 220 mm depth at a rate of 3.8 mm/s. Then, 10 cycles of extraction and penetration were executed at the same rate over a fixed depth interval (120 mm to 180 mm) to measure the degradation of the shear strength upon repeated undrained cycles. The length of the cyclic interval was adopted as three times the ball diameter as recommended by DeJong et al. (2010).

The results of the three ball penetrometer tests are shown in Figure 79 and indicate that the penetration resistance curves are similar reaching a maximum of 28 kPa at 200 mm depth. The plotted penetration resistance is not corrected for unequal pore pressure and overburden pressure effects since such effects are expected to be negligible in 1g model tests (Low et al., 2008). The resulting undrained shear strength profiles are plotted in Figure 80c as estimated using a ball resistance factor,  $N_{\text{ball}}$ , of 13.5. These profiles confirm that the clay bed exhibits similar shear strength properties at the three

locations, especially for depths exceeding 50 mm, where all the curves converge to a common undrained shear strength of about 2 kPa (Figure 80c). The strength at the mudline could not be accurately measured, given that the results of the ball penetrometer can only be considered to be reliable when the ball is fully embedded in the soil. At an embedment depth of around 3cm from the mudline (minimum depth for which the results of the ball penetrometer may be considered to be reliable), the undrained shear strength is shown to vary between 1.7 and 1.85 kPa.

The measured undrained shear strength of the bed is higher than expected for a clay that was consolidated from a slurry at an effective stress of 1.5 kPa. Moreover, the water content of the clay in the upper 5 cms (~ average of 30%) is also considered smaller than expected for a normally consolidated clay. The virgin compression line for the clay under consideration indicates that the equilibrium water content at 1.5 kPa effective stress is expected to be between 33% and 35% (Figure 81) for a clay that is consolidated from a slurry.

These observations lead to the conclusion that the process of wetting, reconstituting, and reconsolidating the upper 5cms of the bed did not return the bed to a normally consolidated state. The reduced water content is indicative of the fact that the clay bed had contracted to a lower void ratio upon loss of saturation due to evaporation across the expose upper surface. The attempt to re-soak, reconstitute, and reconsolidate the bed was not successful at reproducing the virgin compression state. The final water content (~ 28% to 30%) and void ratio (~ 0.73 to 0.80) are smaller than those expected for the virgin compression state.  $e$ -log  $p$  curves from reconstituted specimens and more importantly from an undisturbed specimen that was extracted from the upper 30 mm of the clay bed (Figure 81) indicate that the water content of about 28% corresponds to a

pressure of 10 to 12 kPa if it were to be associated with the virgin compression line. As such, the clay in the bed is expected to behave as an over consolidated clay in subsequent interface tests.

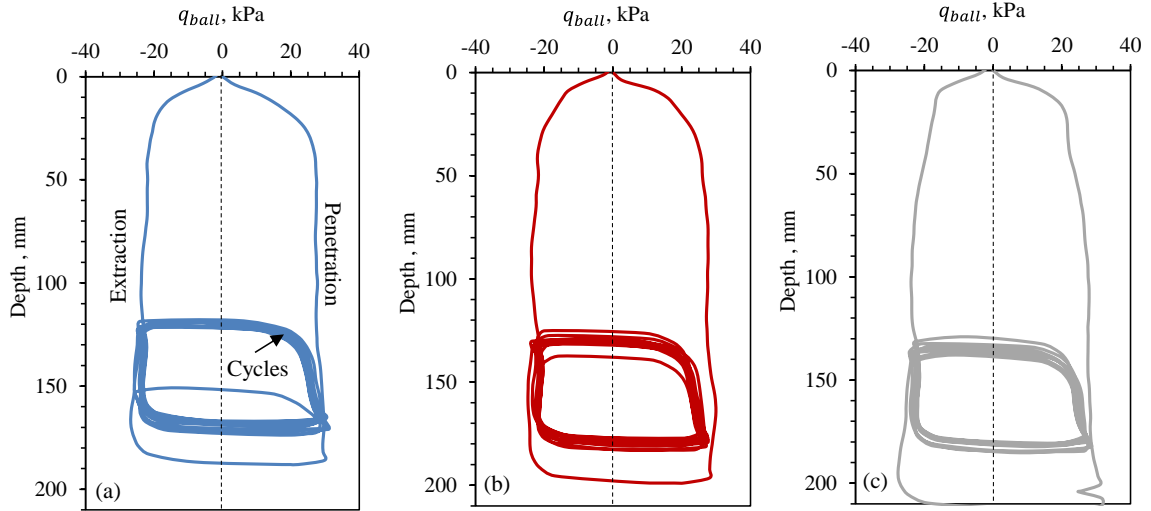


Figure 79. Measured penetration resistance at (a) Location 1, (b) Location 2, and (c) Location 3.

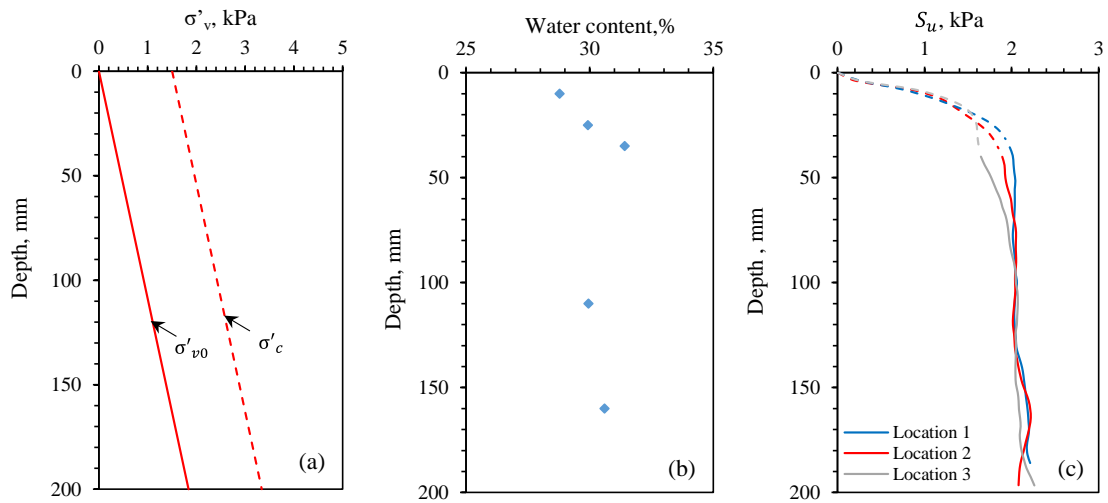


Figure 80. (a) Effective vertical stresses, (b) Water content and (c) Undrained shear strength variation with depth.

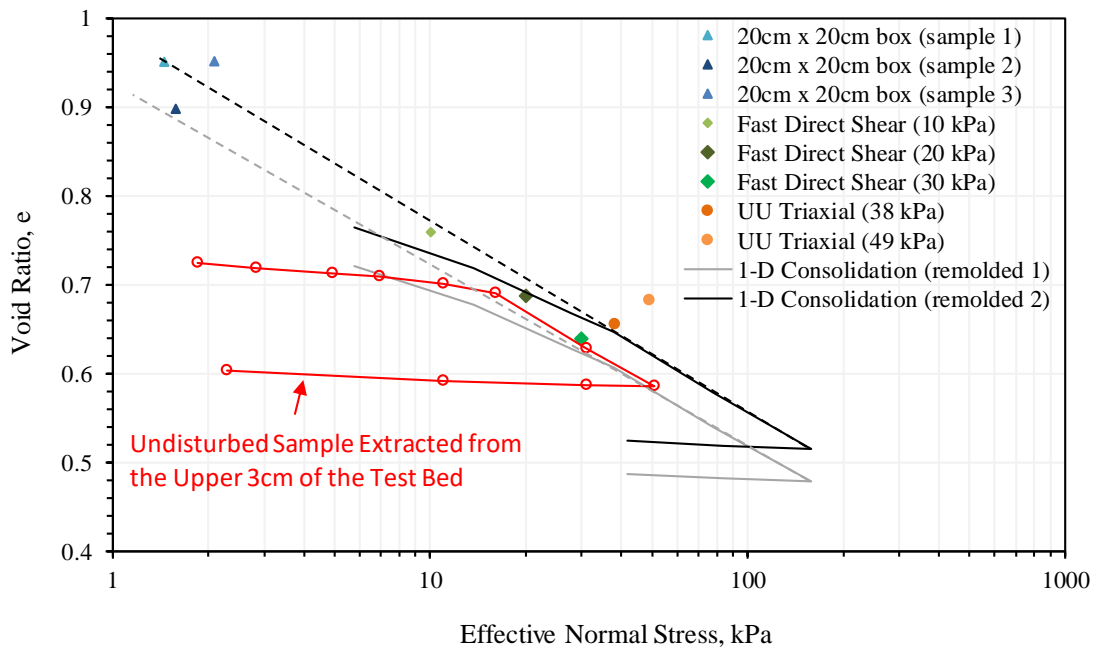


Figure 81. Compression curves of the tested clay.

Results of the repeated cyclic penetration tests (Figure 82a) indicate a slight degradation in the undrained shear strength with shearing cycles, which is in line with the low sensitivity of the clay. At the three locations, 5 cycles were enough to reach an average remolded ball resistance in the order of 22.5 kPa. This remolded resistance is defined as the average resistance observed during penetration and extraction after ten cycles. The normalization of the cyclic degradation data over the initial penetration resistance allows for a clearer comparison between the different locations. The three normalized curves were identical, indicating that the clay bed is homogeneous (Figure 82-b). The cyclic sensitivity defined by Boylan et al. (2014) as the inverse of the normalized penetration resistance is 1.26. However, the conventional soil sensitivity, known as the ratio of the undrained strength to the remolded strength, yielded values between 1.5 and 1.8, assuming that the remolded resistance factor,  $N_{ball,rem}$  is between 13 and 15 as recommended by Low et al. (2008). Therefore, the clay used has a low sensitivity and its softening rate is around 0.8.

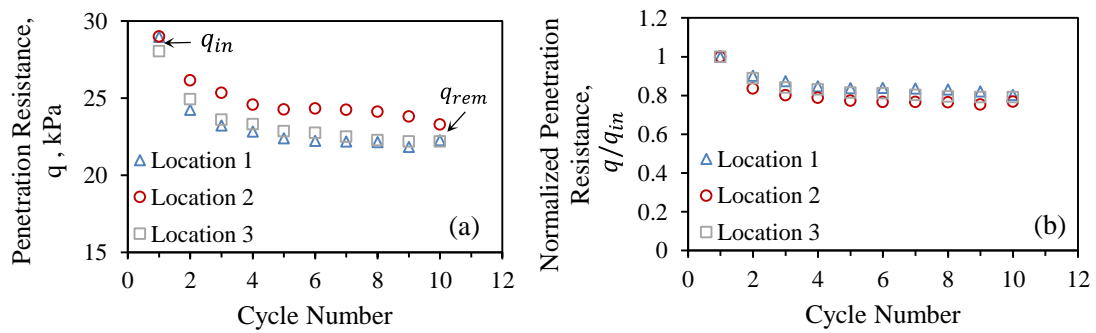


Figure 82. Cyclic curves: (a) Penetration resistance and (b) normalized penetration resistance.

### 5.2.2 Test Sequences

Two tests were performed on the clay bed to verify the functionality of the new test setup and the reliability of its results under different clay/pipe interface conditions. The tests aimed at measuring the drained and undrained clay/pipe interface resistance for smooth (stainless-steel) and rough (sandpaper) interface conditions. The applied normal stress, shearing rate, shearing cycles, pipe embedment, interface roughness, and waiting period between shearing cycles were varied in the test program. Each test is divided into three stages during which the embedment of the pipe was increased to change the normal stress level. The following procedure was followed for the stainless steel and sandpaper tests unless it is stated otherwise.

#### 1. Stage 1:

- a. **Consolidation Phase (Initial Embedment):** The 1-m long assembled test setup was placed on the clay bed and left to consolidate under its own weight until completing primary consolidation (generally 2 days). During this stage, the vertical settlement was monitored with time using a vertical LVDT placed on top of the model.

- b. **Shearing Preparation Phase:** the two dummy sections were removed, and the middle section was detached from the aluminum bar and left for half an hour for the pore pressures to stabilize.
- c. **Sequence 1 of axial shearing:** For the stainless steel interface, a total of 22 sweeps (30-35 mm of displacement in each) with a change of direction between successive sweeps were performed, while varying the shearing rate and the pause periods prior to shearing (Table 9). In the case of the tests with the sandpaper interface, only three consecutive fast shearing cycles were conducted in Stage 1 (Table 2).

2. **Stage 2:**

- a. **Penetration Phase (Second Embedment):** the setup was reassembled, and 27 kg of dead weights were added to it. It was then left to consolidate for 24 hours until full dissipation of excess pore pressures was achieved, at which point the loads were removed. After 2 hours of waiting time, the test section was detached as described in the shearing preparation phase. This phase aimed at increasing the pipe embedment, thus yielding a lower normal stress at the interface.
- b. **Sequence 2 of axial shearing:** 6 axial sweeps were performed at 0.2 mm/s and 0.00067 mm/s (Table 9) for the stainless steel interface and only a drained test for the sandpaper interface.

3. **Stage 3:**

- a. **Penetration Phase (Third Embedment):** after reassembling the setup for the second time, it was pushed downwards into the soil to an embedment of 15 mm using a jack and left for 12 hours to allow the pore

pressures generated to dissipate. Afterwards, the dead weights of 27 kg were added for 12 hours until the consolidation was complete. This stage was designed to further reduce the normal stress at the interface thus allowing for the determination of the failure envelope of the interface resistance from the results obtained at the three different normal stresses.

- b. Sequence 3 of axial shearing:** 12 sweeps were performed at 0.2 mm/s and 0.00067 mm/s as indicated in Table 9 for the case of stainless steel and Table 2 for the case of the sandpaper interface.

Table 9. Shearing sequence for the case of the stainless steel interface.

Shearing Sequence	Test Ref.	Cycles Number	Shearing rate(mm/s)	Waiting period prior to shearing (hours)	Cumulative Sweep number
1	F1-S1*	1-4	0.2	48	1-8
	F2-S1	5	0.2	24	9-10
	F3-S1	6-7	0.2	24	11-14
	F4-S1	8	0.2	24	15-16
	D1-S1**	10	0.00067	24	17-18
	D2-S1	11	0.00032	4	19-20
2	F1-S2	1	0.2	24	21-22
	F2-S2	2	0.2	4	23-24
	D1-S2	3-4	0.00067	12	27-28
3	F1-S3	1-2	0.2	48	29-34
	F2-S3	2	0.2	24	35-36
	F3-S3	3	0.2	24	37-38
	D1-S3	4	0.00067	12	39-40

\* F indicates “Fast” shearing, \*\* D indicates “drained” shearing

Table 10. Shearing Sequence parameters in case of sandpaper interface.

Shearing Sequence	Test Ref.	Cycles Number	Shearing rate(mm/s)	Waiting period prior to shearing (hours)	Cumulative Sweep number
1	F1-S1	1-3	0.2	0	1-6
2	D-S2	4	0.00067	24	7-8
3	D-S3	5	0.00067	48	9-10

### **5.3 Results from tests using the Stainless Steel Interface**

#### **5.3.1 Penetration and Consolidation Response**

##### **5.3.1.1 Initial Embedment (Stage 1)**

In Stage 1, the assembled 1-m long test setup was laid down on the clay bed and allowed to settle under its own weight. Settlement data indicated that upon “touchdown”, the setup exhibited an immediate settlement of 4.4 mm in less than 15 seconds. Concurrently, the pore pressure sensors along the pipe invert and at an angle of about 20 degrees exhibited excess positive pore water pressures of 4.8 kPa and 2.7 kPa, respectively (Figure 83a). The pore pressure measurements indicate that during pipe lay down, the setup weight ( $W$ ) is transferred to the clay at the contact zone through a concentrated force which induces high excess pore pressure at the invert. After 3 mm of pipe embedment, the pore pressure sensor at 20 degrees gets in contact with the soil and shows an increase in pore water pressure. The measured pore pressures at the two sensor locations indicate that the distribution of water pressure around the circumference of the pipe in the contact zone is not uniform, and is expected to range between zero at the edge of the pipe/clay contact zone and a maximum pore pressure at the pipe invert.

The dissipation of the excess pore pressure with the logarithm of time is presented in Figure 83b at the invert and the side of the pipe. The resulting pipe consolidation curve is also presented in Figure 83c. Results indicate that during the post-laydown consolidation, the pore pressures dissipated and the pipe settlement increased by about 0.5 mm (Figure 83c) over a time period of about 8 hours.

The magnitudes of the immediate and long term settlements of the pipe during and after laydown indicate a final pipe embedment of about 5 mm, divided between 4.5 mm of immediate settlement (undrained response) and 0.5 mm of consolidation



settlement (post laying of the pipe). The relatively low initial embedment of 4.5 mm is consistent with the normalized pipe setup weight of  $W/S_uD = 0.75$  which is small compared to the values usually encountered during pipe lay down (generally has a minimum of 1) in the field.

The final pipe embedment of 5 mm indicates that the effective normal stress at the clay/pipe interface is about 3.7 kPa including wedging effects as stipulated in equation (5.1).

$$\sigma_n = \frac{\xi W}{\theta D L} \quad (5.1)$$

Where  $W$  is the weight of the pipe (206 N),  $D$  is the diameter of the pipe,  $\xi$  is the wedging factor,  $\theta$  is the half-angle enclosed by the pipe-soil contact perimeter, and  $L$  is the length of the pipe (1 m). Figure 84 shows the setup inside the clay bed with the camera used to detect the patterns fixed on the setup.

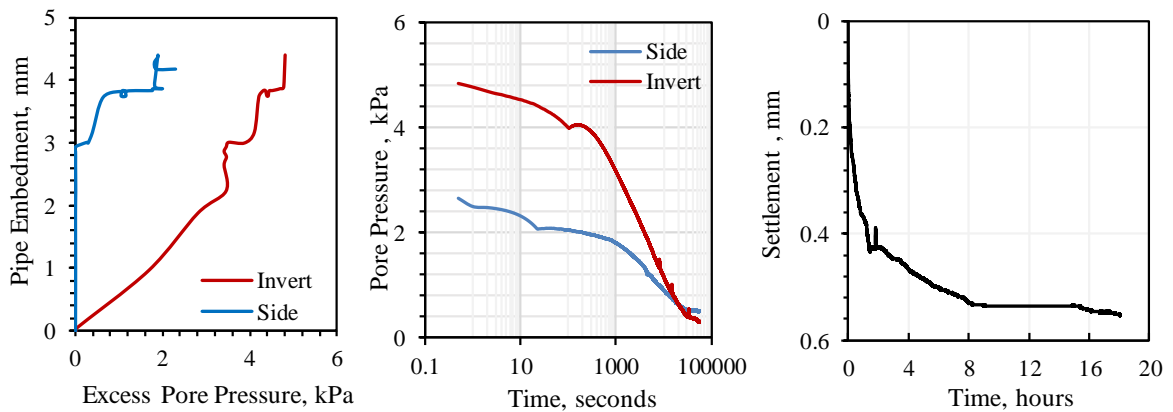


Figure 83. (a) Pore pressure measurements during pipe laying process, (b) dissipation of pore pressure post-lay, and (c) consolidation post lay.

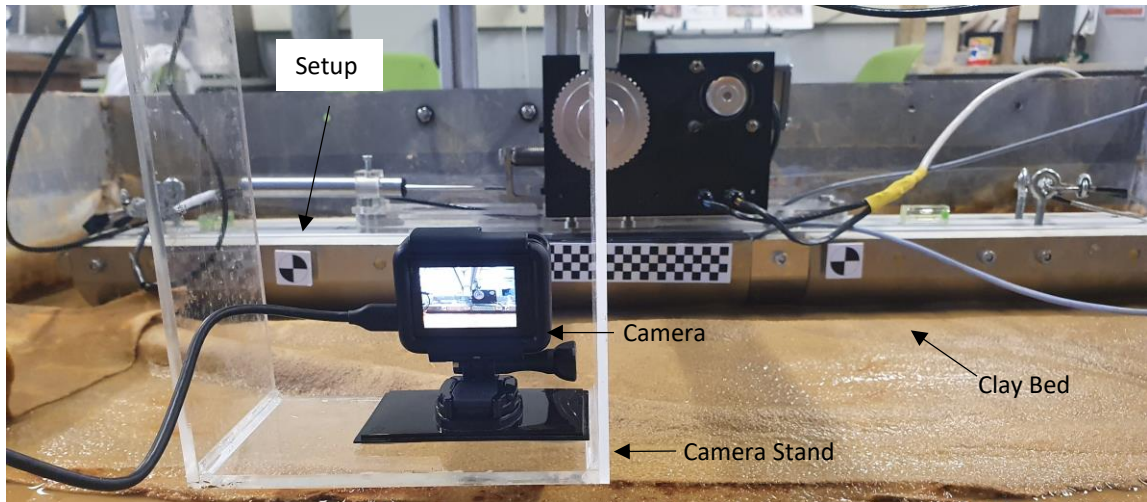


Figure 84. Setup after consolidation

#### 5.3.1.2 Second Embedment (Stage 2):

After completing the 20 sweeps of interface shear tests in sequence 1, the setup was reassembled and subjected to a dead weight of 27 kg to increase its embedment in the soil bed. The weights were added incrementally in order to prevent any rapid undrained failure of the soil which could lead to tilting of the pipe. Upon the application of the weights, the pore pressure sensors recorded an increase of 3.5 kPa at the invert and 2 kPa at the side. The excess pore pressures gradually dissipated over a period of about 24 hours as indicated in Figure 85. The settlement at the end of consolidation was 2.8 mm. Upon the removal of the dead weights, negative pore pressures in the order of -0.85 kPa were measured by the pore pressure sensors. These pore pressures dissipated in 3 hours as shown in Figure 86 and the soil underneath the pipe swelled by about 0.2 mm. The final pipe embedment at the end of this stage was about 7.7 mm, corresponding to a normal stress of about 3 kPa.

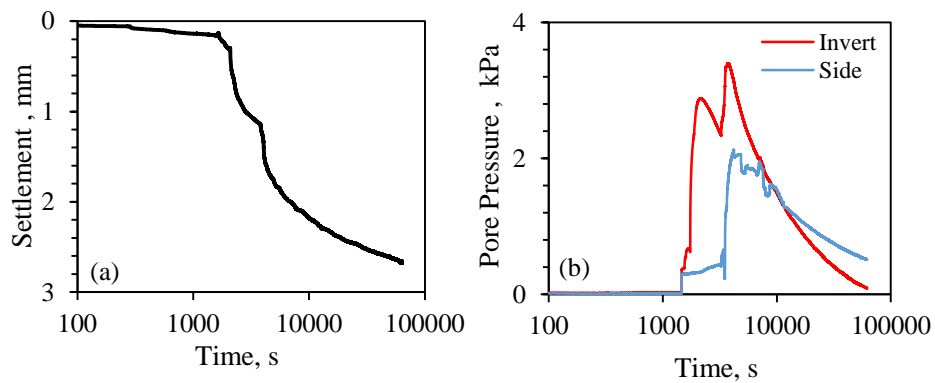


Figure 85. Variation of the pipe settlement and excess pore pressure with time during the second penetration and subsequent consolidation under dead weights of 27 kgs.

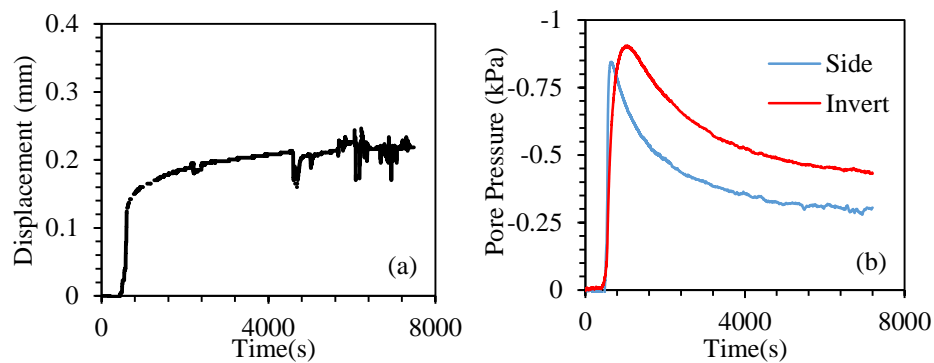


Figure 86. Variation of the pipe swelling and excess negative pore pressure with time upon pipe unloading.

### 5.3.1.3 Third Embedment (Stage 3):

After completing the 8 sweeps of interface shear tests in sequence 2, and since adding dead weights only induced additional settlements of 2.7 mm in Stage 2, a hydraulic jack was used in Stage 3 to push the pipe in the clay bed to a final embedment depth of approximately 20 mm. The motor was removed and a wooden bar was placed on the setup to act as a rigid member that would ‘uniformly’ transfer the load from the hydraulic jack to the pipe section. Dial gauges were placed on three corners of the pipe setup to monitor its displacements and ensure that the jacking operation is completed

without inducing tilting or rocking in any direction during undrained penetration (Figure 87).

During jacking, the pore pressure increased to 5.8 kPa at the invert and 2.2 kPa at the side. These excess pore pressures required about 12 hours to fully dissipate (Figure 88a). The pipe embedment at the end of primary consolidation was increased by 8 mm. Subsequently, the jacking system was removed and dead weights accounting for 27 kgs were added for a period of 24 hours (Figure 88b), in which an additional 1.2 mm of settlement was observed. Upon the removal of the dead weights, the pipe swelled about 0.2 mm, reaching a final net embedment of about 16.7 mm (Figure 89). This embedment level corresponds to about 0.1 D and results in a normal stress of about 2.1 kPa at the pipe/clay interface. At this embedment level, observations of the bed during and after testing indicated that berms formed adjacent to the pipe section as a result of pipe embedment. More importantly, when the dummy sections were removed, a clean and uniform shearing path that was required to eliminate passive resistance from the soil during shearing was created as shown in Figure 90.

Figure 91 shows the dissipation of the pore water pressure after each stage of pipe penetration. Results are presented as a function of (a) real time and (b) normalized time factor to be compared to the solution derived from elasto-plastic small-strain FEA models (Chatterjee et al., 2012) assuming a  $C_v$  of 2 m<sup>2</sup>/year. The excess pore pressures at the invert were normalized by the maximum excess pore pressure at the end of penetration referred to as  $\Delta u_{in}$ . Results on Figure 91b indicate that the dissipation of pore pressure is the fastest during Stage 1 and the slowest during Stage 3. The time needed to dissipate 50% of the excess pore pressure,  $t_{50}$  almost doubled from Stage 1 (0.68 h) to Stage 2 (1.2 h) and was 5.4 times higher (3.72 h) in Stage 3.

This response is expected given that the maximum drainage path increases as the pipe embedment depth increases, leading to increases in the required time for excess pore pressures to dissipate. The parameters used to plot the solution of Chatterjee et al. (2012) are the ones for a smooth interface and an embedment of 0.1D. Good agreement between the Chatterjee et al. (2012) solution and the dissipation curve of Stage 3 was observed since they both correspond to the same pipe embedment. The chosen  $C_v$  is slightly higher than the range of consolidation coefficients computed during direct shear tests in Chapter 3. This coefficient is expected to be even higher for Stages 1 and 2 since the dissipation was faster. A rough estimation indicated that  $C_v$  could have reached 40  $m^2/year$ . As such, the interface permitted enhanced drainage due its asperities and roughness (Jewell and Ballard, 2011). Such high values of  $C_v$  (in the order of 100  $m^2/year$ ) were also encountered by Ballard et al. (2013) and Jewell and Ballard (2011) in back-analyses using numerical models.

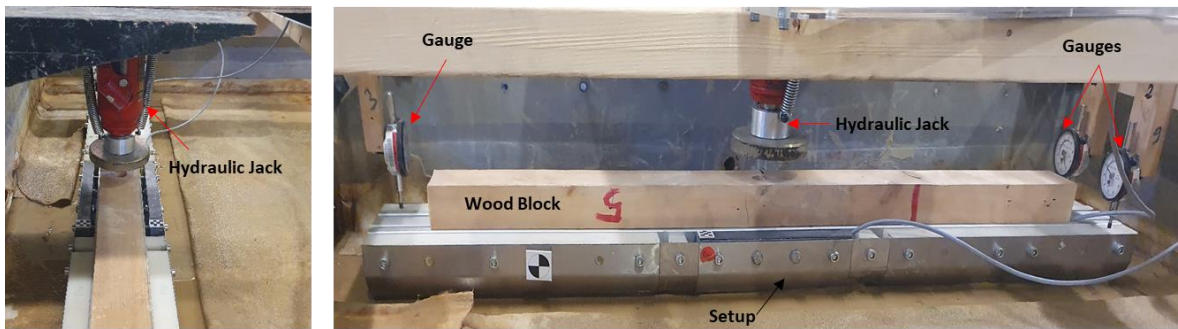


Figure 87. Undrained penetration stage of the setup using a hydraulic jack.

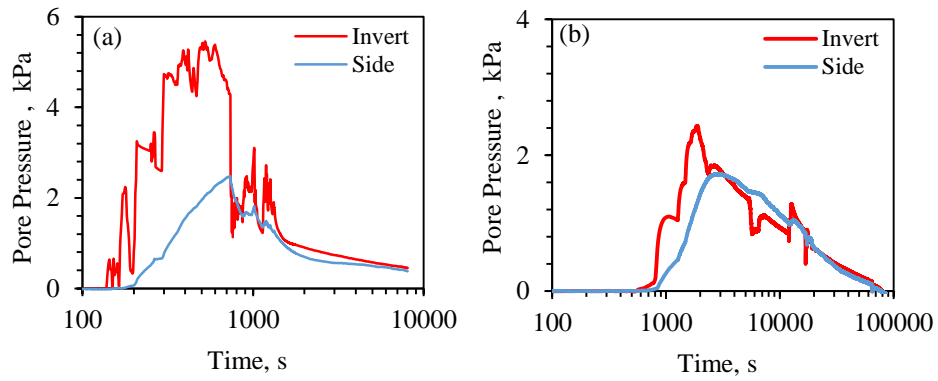


Figure 88. Pore pressures generation and dissipation during and after (a) undrained penetration and (b) application of dead weights in Stage 3.

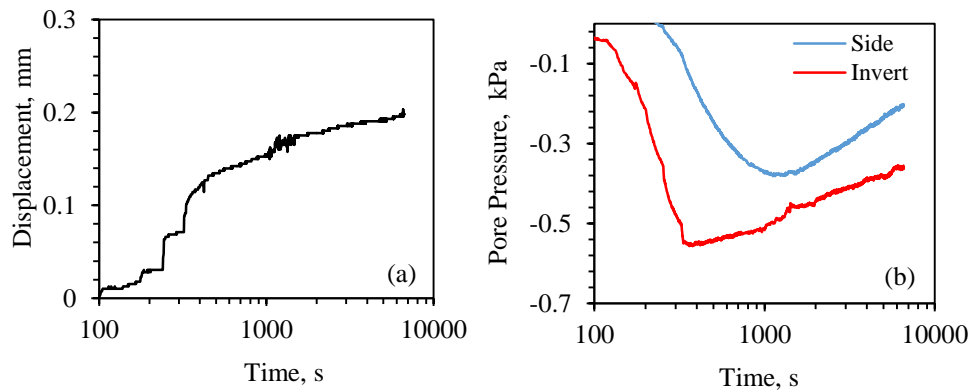


Figure 89. (a) Soil swelling and (b) pore pressure dissipation due to dead weight unloading in stage 3.



Figure 90. Soil berms around the setup and the created shearing path in Stage 3.

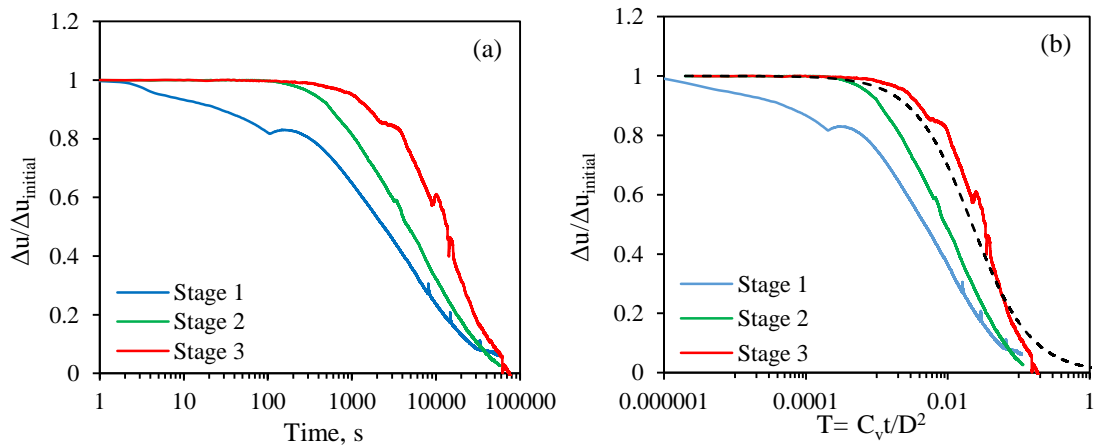


Figure 91. Dissipation time-histories of excess pore pressure at the pipe invert normalized by the initial excess pore pressure under applied load plotted against the time factor,  $T$  after pipe penetration in each stage.

### 5.3.2 Clay/Pipe Interface Resistance

#### 5.3.2.1 Sequence 1 – Pipe embedment = 4.8 mm

As mentioned in Section 2.3.1, the final pipe penetration in Stage 1 was about 5mm, leading to an applied normal stress of about 3.7 kPa at the pipe/clay interface. After the completion of consolidation, the dummy sections were removed and the test section was detached and left for two hours to equilibrate and dissipate any generated pore pressure during handling.

The first shearing sequence (F1-S1) consisted of 4 consecutive shearing cycles (8 sweeps) that were conducted with the smooth stainless steel pipe section at a relatively fast shearing rate (0.2 mm/s) to measure the “undrained” pipe/clay interface response. Each sweep consisted of a displacement of about 30 mm. Results for F1-S1 are presented in Figure 92 and show the mobilization of the interface shear stress and the generation of excess pore pressure at the side and invert of the test pipe section with axial pipe displacement.

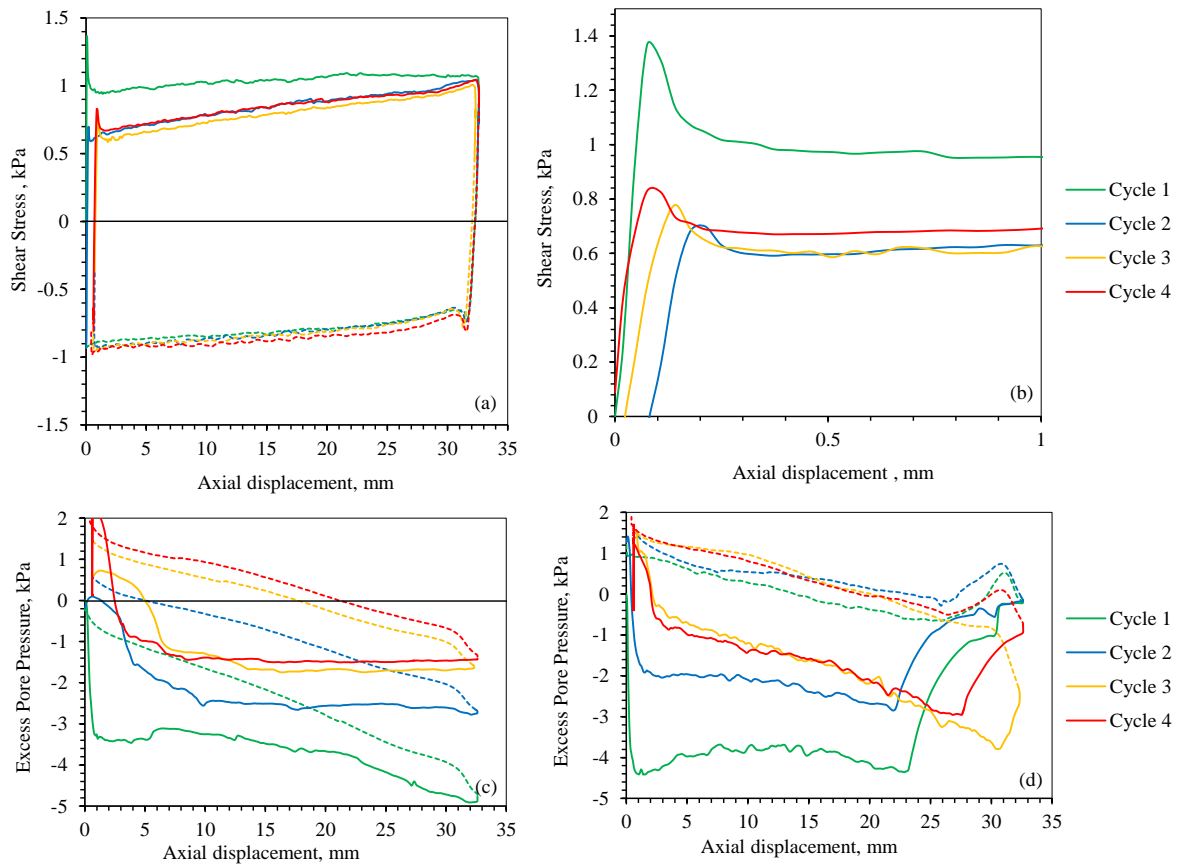


Figure 92. The axial response during F1-S1: (a, b) shear-stress variation, (c, d) excess pore pressures at the pipe invert and side.

Results on Figure 92a-b lead to several important observations:

- [1]. The interface shear stresses that were mobilized during “undrained” shear in all loading cycles exhibited a peak in the shear stress at relatively small pipe displacements (0.1 to 0.2mm). Following the peak, an abrupt reduction in interface shear stresses was observed leading to minimum observed shear stresses at displacements in the order of 0.3mm.
- [2]. The interface response exhibited in the first shearing cycle was unique compared to the remaining 3 additional cycles that followed. In the first



cycle, the pipe mobilized a significant proportion of the clay's undisturbed undrained shear strength, exhibiting a maximum interface shear resistance of about 1.4 kPa (compared to a clay/clay undrained strength of about 2.0 kPa). This relatively high interface resistance in the first loading cycle is almost twice that observed in the loading cycles that followed (maximum interface stress ranging from 0.7 to 0.85 kPa), indicating that clay remolding must have occurred at the interface in subsequent cycles.

[3]. The mobilized interface shear stresses clearly increased after a displacement of 1mm up to the maximum enforced pipe displacement (~33 mm). This increase in interface strength with axial displacement (particularly for cycles 2 to 4) could be attributed to multiple intertwined factors that will be discussed in the following paragraphs.

A more detailed investigation of the undrained interface response in the 4 continuous undrained cycles indicates that in the reversal sweep that followed the first sweep of the first cycle, a significant reduction in the maximum shear stress occurred (~0.7 kPa compared to 1.4 kPa in the first sweep). The second cycle showed a similar reduction in the mobilized interface strength (~0.69 kPa), but the third and fourth cycles showed slight increases in strength compared to the second cycle (0.75 kPa and 0.82 kPa, respectively). During these three cycles, the shear stresses dropped after the peak to almost the same minimum interface shear stress of 0.65 kPa (Figure 92-b). The reduction observed in the undrained interface shear resistance after the first cycle could be attributed to remolding of the clay under the pipe section and possible alignment of the clay particles at the clay/pipe interface. The consistent shear stress versus

displacement response that was observed in cycles 2 to 4 is a testimony of the ability of the novel test setup to produce results with a high level of repeatability, which is a very important metric in the assessment and evaluation of new testing systems in geotechnical engineering.

The excess pore pressure generated during shearing cycles is presented as a function of pipe displacement in Figure 92 (c, d). Results indicate that shearing at the pipe/clay interface generated negative pore pressures at the pipe invert and side during the first sweep of each cycle. These negative pore pressures confirm the over consolidated state of the clay at the clay/pipe interface. In general, results show that the magnitude of the generated excess negative pore pressure reduced with shearing cycles as a result of the cumulative shearing strains and associated remolding of the clay under the pipe. Moreover, results indicate that the negative pore pressure that were generated in the first sweep of every cycle dissipated gradually during the reversal sweep of that cycle, with relatively small positive pore pressure measured at the end of some reversal sweeps, particularly in Cycles 3 and 4.

To shed light on the generation of pore pressure during undrained shearing, the net excess pore pressures were calculated for the first sweep in each cycle and plotted on Figure 93. The net excess pore pressure is calculated as the pressure measured at a given pipe displacement minus the pressure at the beginning of that sweep (residual pore pressure from previous cycle). Results indicate that the largest negative excess pore pressures were generated during the first cycle, which partially explains the highest “undrained” interface shear strength observed for that cycle. In subsequent cycles, the excess negative pore pressure generation was reduced. The only exception is Cycle 4, which showed an increase in negative pressures compared to Cycles 2 and 3. This can

be explained by the fact that for Cycle 4, shearing was initiated 15 minutes after the completion of Cycle 3 and not directly after. This short unplanned waiting period between Cycles 3 and 4 was enough to dissipate some pore pressures at the clay/pipe interface, leading to slightly higher generation of negative pore pressure and improved shear resistance in Cycle 4 compared to Cycles 2 and 3.

Interestingly, measurements of pore water pressure at the sensor located on the side of the pipe section indicated that dissipation of the generated negative pore pressure started in the middle of the sweep, at pipe displacements ranging from 20mm to 30mm Figure (Figure 93-b). Such dissipation of pore water pressure was not observed at the pore pressure sensor located at the invert. The faster dissipation of pore water pressure in the side sensor is related to the shorter drainage path, given that the location of the sensor is closer to the clay surface. The shorter drainage path allowed for partial dissipation of pore pressures during shearing, despite the relatively fast shearing rate applied (0.2 mm/sec).

It should be noted that caution should be exercised before drawing conclusions about the pore pressure response along the full length of the clay/pipe interface. The complexity observed in the non-uniform generation of excess pore water pressure along the pipe section and its possible dissipation during the different cycles and sweeps, coupled with the limited number of pore pressure sensor used (measurement limited to one location along the pipe length), prohibit any in-depth analysis of the pore pressure response. Consequently, the results presented in Figure 93 should only be considered to be indicative of the local pore pressure response and should not be generalized and used to conduct any effective stress analysis to describe the clay/pipe interface shear resistance.

Finally, it should be noted that the complex pore pressure response that was observed at the two sensor locations could partially explain the increase that was observed in the undrained interface shear resistance at large displacement, particularly in Cycles 2 to 4. The gradual increase in interface resistance with pipe displacement in the last three cycles may be related to the generation of negative pore pressures and their dissipation. The observed increase in strength could also be attributed to additional passive resistance that could be mobilized at the front of the moving pipe section by a thin layer of clay that could have been dragged by the test pipe section during shear, particularly at large displacements. Figure 94 shows a snapshot of the clay that is left behind at the test section at the end of F1-S1.

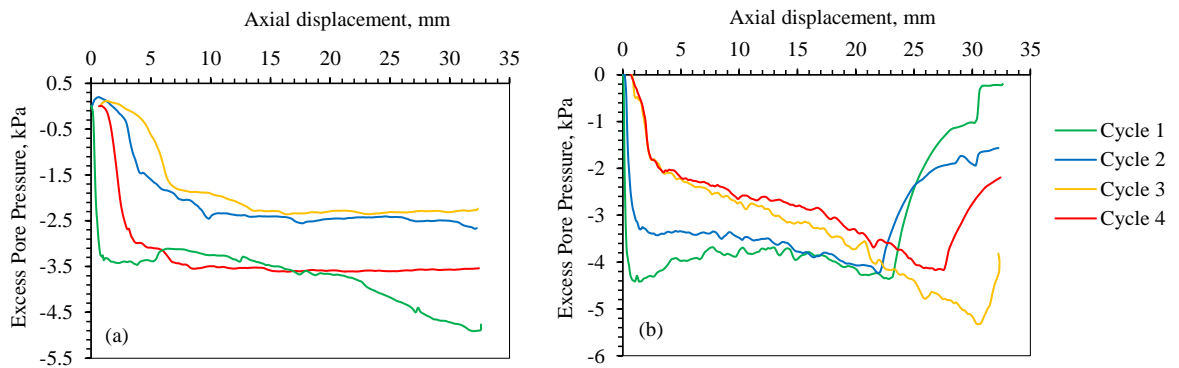


Figure 93. Net Pore Pressures during F1-S1 at the setup: (a) invert and (b) side.

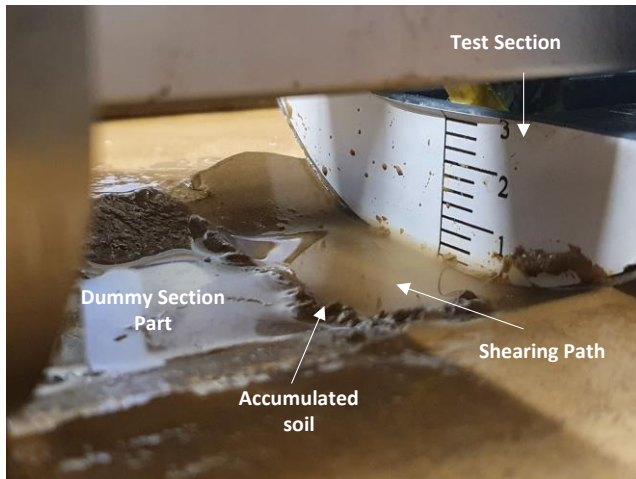


Figure 94. The accumulated soil pushed by the test section during shearing in a previous sweep

In order to investigate the robustness of the novel test setup and provide a quantitative measure of the stability of the test and anchoring section, an effort was made to measure the displacements of the test setup in the three directions during shearing using a GoPro camera that was fixed in front of the setup as shown in Figure 84.

For the undrained tests (F1-S1) that were conducted as part of sequence 1, the GoPro measurements indicated a total vertical displacement of about 3 mm at the end of the 4 shearing cycles. This global displacement is comprised of (1) the true vertical movement of the pipe section, and (2) rotational pipe movement that could have occurred in any of the three orthogonal planes. To isolate the true vertical pipe movement from any rotation-induced movement, the rotation angles of the test section were computed for the 4 cycles in F1-S1 using the GoPro measurements (see Figure 95).

Results on Figure 95 indicate that the pipe section has slightly rotated in all directions during shearing with a maximum rotation angle of about  $1.8^\circ$  in the x-

direction at the end of the 8 sweeps. The maximum rotation angles observed in the other two planes (y and z) are  $1.5^\circ$  and  $0.5^\circ$ , respectively. The orientation of the three orthogonal planes relative to the cross section of the pipe is presented in Figure 96 together with the assumed center of rotation. The measured rotation angles allow for correcting the global vertical movement that was observed in the GoPro images by subtracting from them the movements resulting from rotation of the pipe. The resulting vertical displacement provides a true representation of the actual net vertical movement of the pipe section as a result of volumetric changes (compression or expansion) in the clay being sheared under the pipe section.

The variation of the resulting net vertical displacement with pipe movement is presented in Figure 97. Results indicate that the net vertical pipe displacement is about zero, meaning that the soil under the test pipe did not settle nor swell during undrained shearing, which is expected for undrained loading conditions. However, the measured rotation of the pipe segment along the length of the pipe (y-axis) pointed to the possibility of having a moment acting on the test section when it is pulled axially. The observed rotation along the length of the pipe (although relatively small) produced a small degree of tilting in the pipe. Any possible moment that could be acting along the length of the pipe could affect the uniformity of the stress distribution under the pipe and may lead to additional compressive stresses along the front of the pipe and a reduction in compressive stresses at the back of the pipe. This potential non-uniform stress distribution may also push the soil at the front of the pipe downward and could explain minor clay dragging that was observed in front of the test pile section during shear.

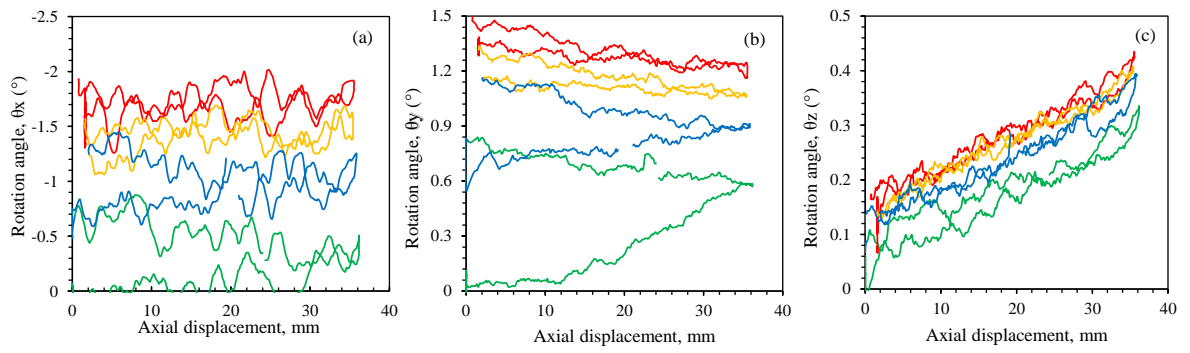


Figure 95. Rotation angles of the test section during F1-S1.

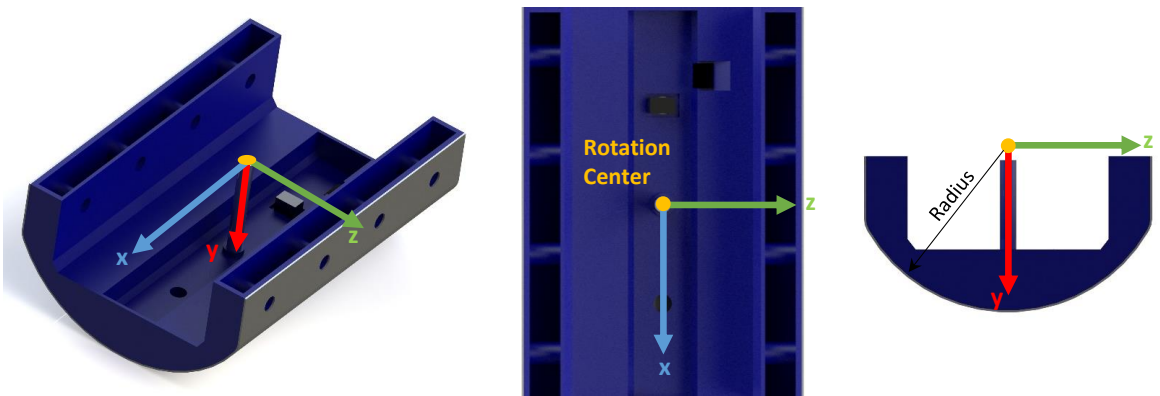


Figure 96. Position of the Center of rotation.

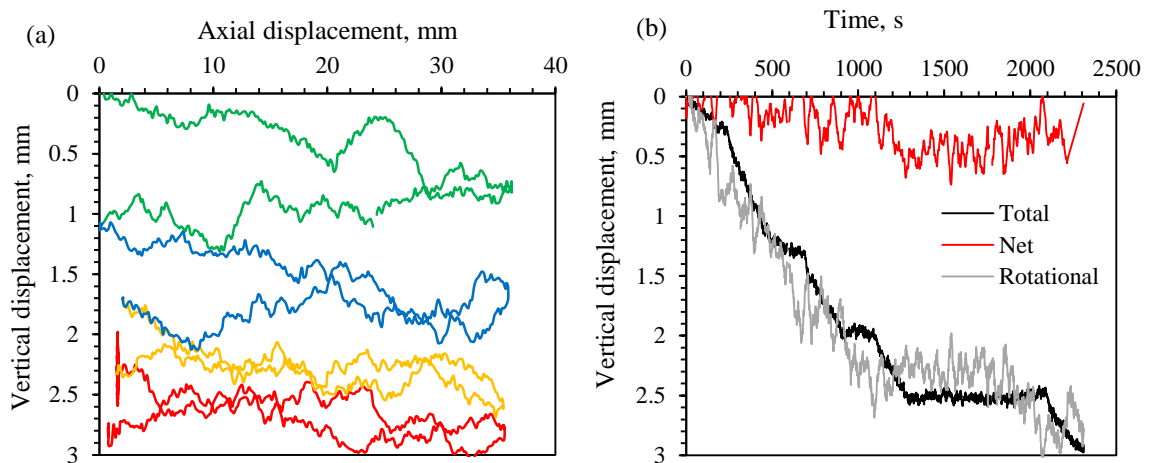


Figure 97. (a) Rotation displacement and (b) Net displacement of the test section (F1-S1)

Figure 98 shows a simulation of the potential effect of a moment on the stress distribution under the pipe section. Such a moment could be produced by possible lack of horizontality in the orientation of the pipe prior to shearing and from the small moment arm that constitutes the vertical distance that separates the center of mass of the test pipe section and the point of application of the horizontal load. The expected stress distribution at the pipe/clay interface due to the moment resulting from the maximum observed horizontal force (first cycle in F1-S1) and a moment arm of about 4 cm is presented in Figure 98.

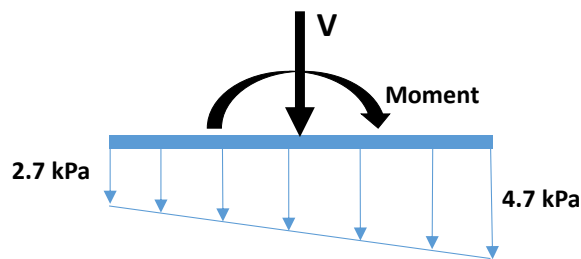


Figure 98. The normal stress distribution under the test section for the maximum applied load.

The existence of a possible moment could lead to a non-uniform stress distribution with a maximum stress of 4.7 kPa and a minimum stress of 2.7 kPa under the pipe (Figure 98). These stresses deviate slightly from the average normal stress of 3.7 kPa that is expected for the tests in Sequence 1. These deviations, however, are not expected to have a significant impact on the overall interface resistance which reflects the resultant of all the interface shear stresses at the pipe/clay contact area. However, the non-uniform stress distribution may have played a role in defining the pore pressure given that the pressure sensors were not located in the middle of the test section, but a distance of 5 cm from the edge. During shearing, changes in the normal stress at the location of the sensor as a result of a moment might translate into changes in pore water



pressure at that location. The moment will change directions during sweeps thus reversing the excess pore pressure generation between sweeps. In the absence of multiple pore pressure sensors along the pipe length, the possible impact of a moment on the pore pressure generation cannot be predicted with any degree of reliability. These observations reinforce the conclusion that the pore pressure readings during shear are considered indicative of the response and may not be used for an effective stress analysis.

For the purpose of completing the undrained interface tests in Sequence 1, three additional cycles of loading (F2, F3, and F4) were conducted, with a waiting time of 24 hours between cycles. The objective was to investigate whether the undrained interface response will exhibit any hardening or softening as a result of repeated cycles, with enough waiting time allowed for the dissipation of pore water pressure and full consolidation between cycles.

Results of undrained cycles F2, F3, and F4 are presented in Figure 99 and Figure 100. They indicate that the shear response and the excess pore pressure generation were approximately the same for all cycles. This observation shows that the undrained interface resistance for the over consolidated clay tested in this study did not exhibit strain hardening between repetitive loading cycles, despite the waiting time that was enforced. These results are expected since improvements in the undrained interface response as a result of repeated cycles with a waiting time have only been reported for normally consolidated soft clay in the published literature (Smith and White, 2014). For the over consolidated clay tested in this study, the lack of improvement in the interface response with repeated cycles is expected, particularly for the case involving a smooth

stainless steel interface where the failure/slip zone in which the shear strains are concentrated is expected to be relatively thin.

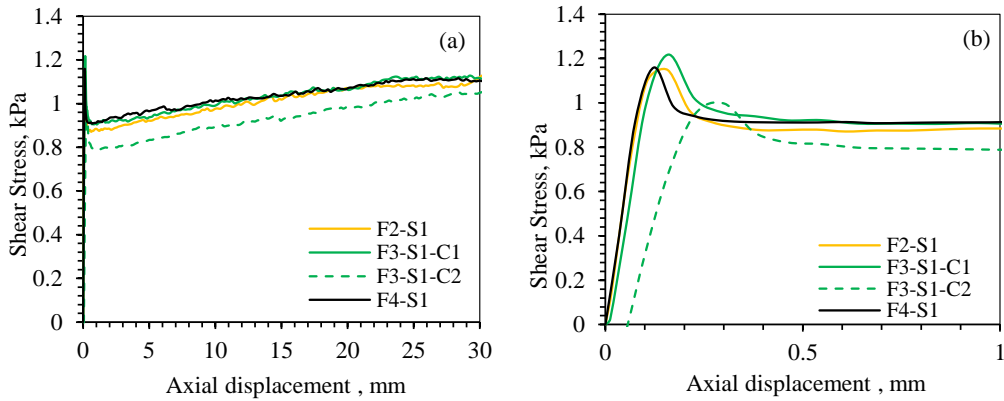


Figure 99. Shear response during undrained cycles F2, F3 and F4.

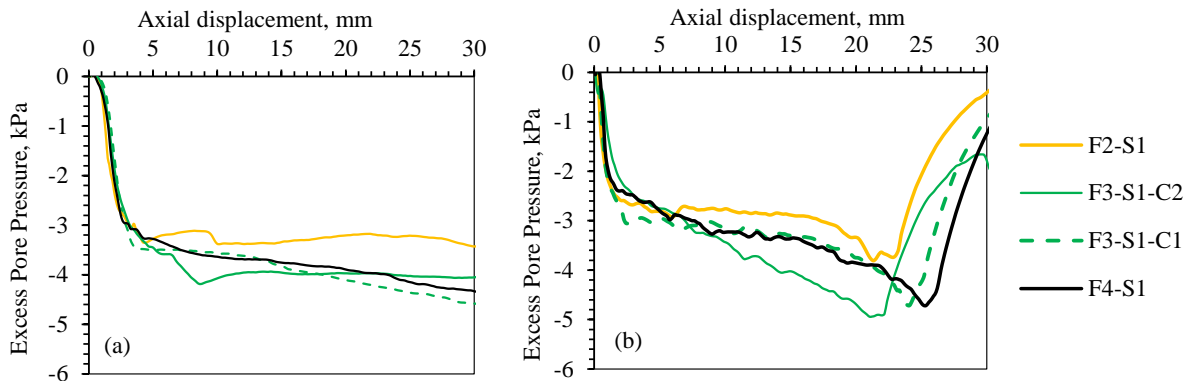


Figure 100. Pore pressures during F2, F3, and F4 at: (a) invert and (b) side of the test section.

Interestingly, the maximum observed interface shear stresses in F2, F3, and F4 (~ 1.2 kPa) exceeded the stresses measured in the last cycle of F1 (~ 0.82 kPa), indicating that the clay under the pipe benefited from the 24 hour waiting period in which the excess pore pressures dissipated to regain a proportion of its original shear strength. For test F3, an additional cycle was conducted immediately after the first cycle (no waiting time) to investigate whether a reduction in interface shear resistance may be observed. As expected, results on Figures 22 and 23 indicate that consecutive shearing cycles in F3 lead to a clear reduction in the measured interface shear stresses. During “undrained” cycles F2 to F4, the net vertical displacement of the pipe as indicated by

the GoPro data after correction was also close to zero. The rotation angles and the net displacements are presented in Appendix A.

Following the 16 undrained sweeps in cycles F1 to F4, the drained interface clay/steel response was measured in tests D1 (shear rate  $\sim 0.00062$  mm/s) and D2 (shear rate  $\sim 0.00032$  mm/s). Results of the drained tests are presented in Figure 101. The tests exhibited an identical interface shear stress versus displacement response with negligible generation of excess pore pressure during shearing. The shear stress reached a peak of about 1.15 kPa after about 0.4 mm of displacement which falls in the range of 0.3% to 0.8% of the pipe diameter as reported by Dendani et al. (2007). The peak stress corresponds to a drained friction coefficient of about 0.31 and a secant interface friction angle of  $17.5^\circ$ . After the peak, the shear stress decayed rapidly to a minimum value of 0.97 kPa (friction angle of  $15.2^\circ$ ) and remained more or less constant over the 25 mm of pipe displacement. This indicates that the residual shear stress was attained within the first 3 mm of displacement with no additional strain softening.

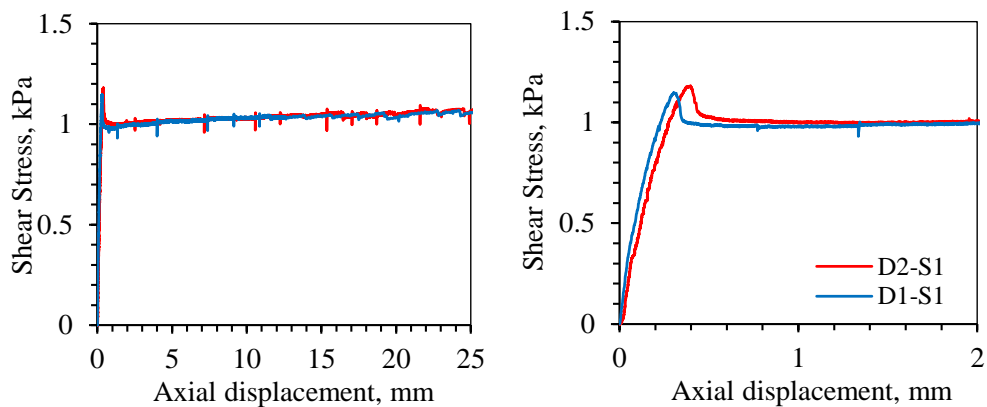


Figure 101. Drained clay/steel interface response during sequence 1.

In the literature, the peak friction factor,  $F/V$  ( $F$  being the peak axial force and  $V$  the weight of the test pipe) under undrained loading conditions are usually linked to the

waiting period between shearing cycles. Since the tests conducted in Sequence 1 involved several waiting periods (ranging from 1 second in back-to-back cycles of F1 to 24 hours in the cycles of F2 to F4), the ratio  $F/V$  was plotted in Figure 102a as a function of the waiting period prior to shearing. Results indicated that the higher the waiting time between cycles, the higher the peak friction factor. This trend was also noticed by White et al. (2011) from model tests on natural sediments from the seabed offshore West Africa.

On the other hand, repeated undrained shearing cycles with no waiting time are expected to remold the clay/pipe interface leading to reductions in the mobilized shear resistance compared to the peak resistance of the first cycle. The ratio of peak to minimum shear stress was computed for all tests and plotted against the number of cycles in Figure 102b. Results suggest a decreasing trend of peak to minimum ratio with the number of repeated shearing cycles. These results are expected given that the mechanism that governs the peak resistance of undisturbed clay is consolidation, whereas repeated undrained loading leads to progressive degradation in dilatancy and thus a reduction in resistance (Low et al., 2017).

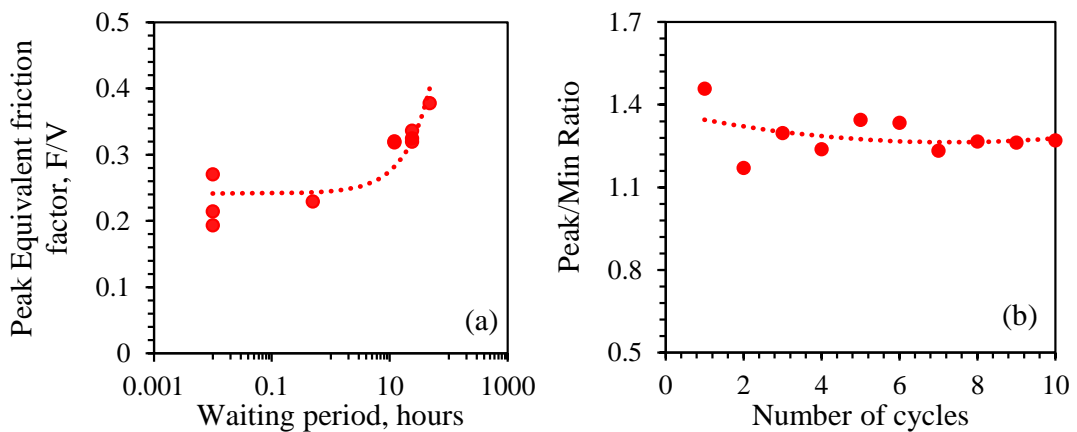


Figure 102. (a) Variation of peak friction factor with waiting period prior shearing cycle and (b) the Peak to minimum resistance ratio with shearing cycles.

### 5.3.2.2 Sequence 2 – Pipe embedment = 7.7 mm

The second sequence of tests with the smooth interface involved undrained and drained tests that were conducted after increasing the embedment of the pipe to 7.7 mm. This increased embedment and consequently larger contact area resulted in an effective normal stress of about 3.0 kPa at the pipe/clay interface. Two undrained tests (F1S2 and F2S2) and one drained test (D1S2) were conducted in this testing stage. A waiting time of 4 hours was enforced between the two fast/undrained tests.

The measured undrained interface response for tests in Sequence 2 (F1S2 and F2S2) is presented in Figure 103. For the first 5 mm of pipe displacement, the mobilization of interface shear stresses with deformation in F1S2 was relatively similar to that observed in the tests of Sequence 1. The peak interface stress was mobilized at very small displacements (0.6 to 0.7mm) and dropped to a minimum value at a displacement of 1 to 1.5mm. The mobilization of the maximum interface resistance was associated with significant generation of negative pore water pressure (Figure 103c, d) at both the pipe invert and side. The pore pressures reached relatively high values of about -6 kPa as a result of the overconsolidated clay's tendency to swell under the relatively low normal stress applied at the interface.

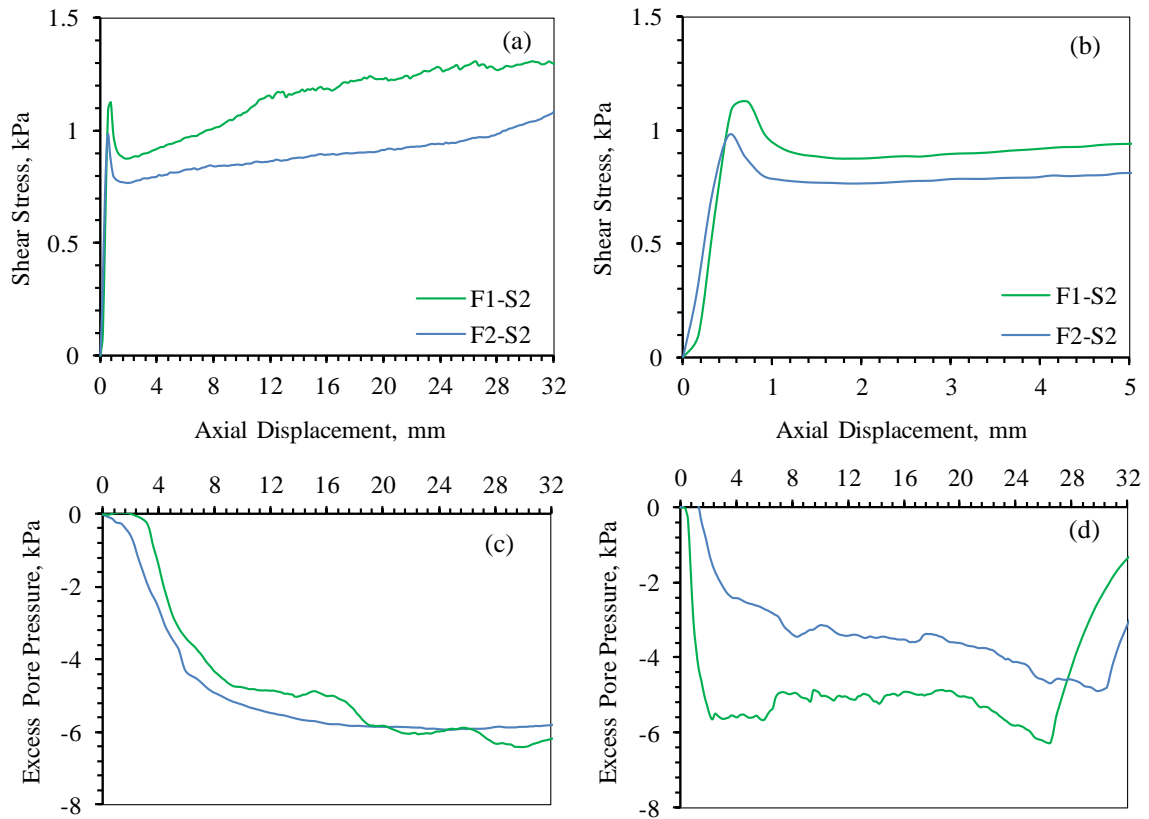


Figure 103. Undrained response in Stage 2: (a, b) shear stress variation and pore pressure generation at (c) the invert and (d) the side.

The second undrained cycle exhibited a 15% reduction in the peak and minimum interface shear resistance compared to the first cycle. As in the case of the undrained tests of Sequence 1, these results confirm the observation that the first cycle in any sequence will always mobilize the largest proportion of the undisturbed undrained shear strength of the clay at the clay/pipe interface compared to all subsequent cycles. The reduction in the undrained interface strength in the second cycle is consistent with the observed reduction in the magnitude of the excess negative pore water pressure at the sensor located on the side of the pipe (Figure 103d).

Results on Figure 103 show a complex shear stress versus displacement response at larger pipe displacements (greater than 10 mm), which is characterized by a

relatively steep increase in the shear resistance with displacement (F1S2). This increase in shear resistance was not observed in the subsequent undrained cycle performed after a waiting period of 4 hours (F2S2). The increase in interface shear resistance for F1S2 at large displacements could be attributed to the possible build-up of passive soil resistance in front of the pipe during shear, generation of excessive negative pore water pressure at the interface, or non-uniform stress distribution under the pipe as a result of an overturning moment.

An analysis of the rotations of the pipe section during the undrained tests in Sequence 2 indicated that they were in the same range as those observed in Stage 1. The same methodology was used to correct the total vertical pipe deformation from the camera readings. After subtracting the rotation-induced displacement, the net vertical pipe movement was also found to be negligible (Appendix A).

Following the two undrained tests that were conducted in Sequence 2, a slow drained test (D1S2) was performed to measure the drained interface response and the associated effective interface friction coefficient and secant friction angle. The shear stress – displacement response (Figure 104) indicates that the drained peak interface stress ( $\sim 1.0$  kPa) was mobilized at a displacement of 0.8 mm and then dropped to a minimum value of about 0.85 kPa and remained almost constant till the end of the sweep (pipe displacement of 30 mm). The corresponding drained peak and residual interface secant friction angles are  $18.2^\circ$  and  $15.85^\circ$  respectively, assuming a  $\sigma_n$  of about 3.0 kPa. These drained interface friction angles are slightly larger than those observed for the drained tests in sequence 1, where the shallow embedment enforced a larger  $\sigma_n$  of about 3.8 kPa. This slight increase in friction angle between Sequence 1 and Sequence 2 could be attributed to the curvature in the drained effective interface Mohr-

Coulomb envelop in the small pressure range. This trend of increasing drained secant friction angle with a decreasing normal stress (due to additional pipe embedment) will also be observed in the drained tests of Sequence 3 as indicated in Section 1.3.2.3.

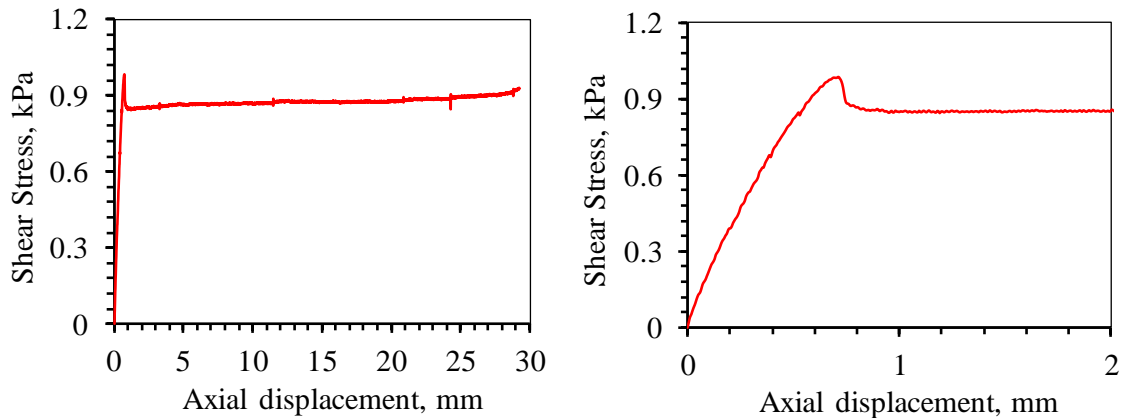


Figure 104. Drained interface response in Stage 2 ( $\sigma_n = 3.0$  kPa).

### 5.3.2.3 Sequence 3 - Pipe embedment = 16.7 mm

Upon the completion of tests in Sequence 2, the test setup was jacked into the bed at a pipe embedment of about 0.1 pipe diameter (~ 16 mm). Upon equilibration of the interface stresses at this pipe embedment ( $\sigma_n = 2.1$  kPa), 3 undrained (F1S3, F2S3, and F3S3) and 1 drained (D1S3) loading cycles were applied to quantify the interface resistance.

Results of the undrained interface tests in Sequence 3 are presented in Figure 105. For the first shearing cycle (F1S3) against virgin clay at the new embedment depth, the curve showing the mobilization of shear stresses with displacement indicated that the shearing process could have been mistakenly initiated while removing the dummy sections and disconnecting the screws that connected the test section to the anchor sections. This hypothesis is supported by observations during test preparation which



indicated that the process of removing the dummy sections for the case of Sequence 3 was more challenging compared to previous sequences since the pipe embedment and contact area between the pipe and the soil were higher.

It is hypothesized that these challenges in the dismantling process may have led to a premature shearing of the pipe against the clay by a fraction of a millimeter prior to the attachment of the load cell, preventing the detection/recording of the undrained peak resistance of the first cycle. The recordings from the load cell indicate that the shear stress in F1S1 initiated at a maximum value of about 0.85 kPa at zero displacements and did not show any signs of a drop with additional displacements as was the case for all other tests conducted in this study. It is thus anticipated that the 0.85 kPa is the minimum shear stress and that the peak shear stress for this particular sweep is a larger value that remains to be unknown.

In an attempt to recapture the “missing” peak, another cycle of undrained shearing was initiated immediately after the first cycle. However, results from the repeated cycle indicated a lower peak interface shear stress of 0.72 kPa, which immediately dropped to a minimum value of 0.57 kPa upon further shearing. The two additional undrained cycles (F2S3 and F3S4) which were conducted after a waiting time of 24 hours exhibited a similar interface response despite the waiting time. These results further confirm that the undrained response of the first shear cycle for the over consolidated clay tested in this study is always superior to any subsequent undrained cycle, irrespective of the waiting time between cycles.

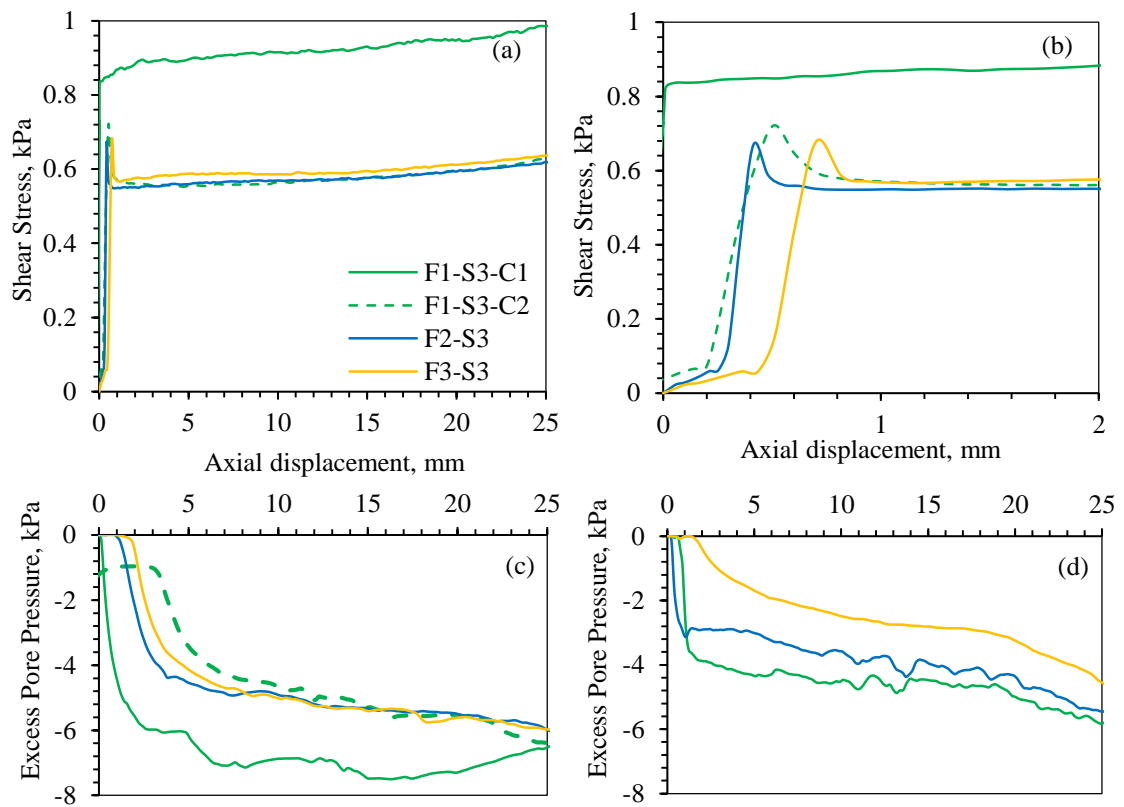


Figure 105. Undrained response in Stage 3: (a, b) shear stress variation and Pore pressure generation at (c) the invert and (d) the side.

Following the undrained cycles, a slow drained test (D1S3) was performed to measure the drained interface response and the associated effective interface friction coefficient and secant friction angle. The shear stress – displacement response (Figure 106) indicates that the drained peak interface stress ( $\sim 0.72$  kPa) was mobilized at a displacement of 0.5 mm and then dropped to a minimum value of about 0.6 kPa and remained almost constant till the end of the sweep (pipe displacement of 25 mm). The corresponding drained peak and residual interface secant friction angles are  $19^\circ$  and  $16.2^\circ$  respectively, assuming a  $\sigma_n$  of about 2.1 kPa. These drained interface friction

angles are slightly larger than those observed for the drained tests in sequences 1 and 2 ( $\sigma_n \sim 3.0$  to  $3.8$  kPa) due to curvature in the failure envelope.

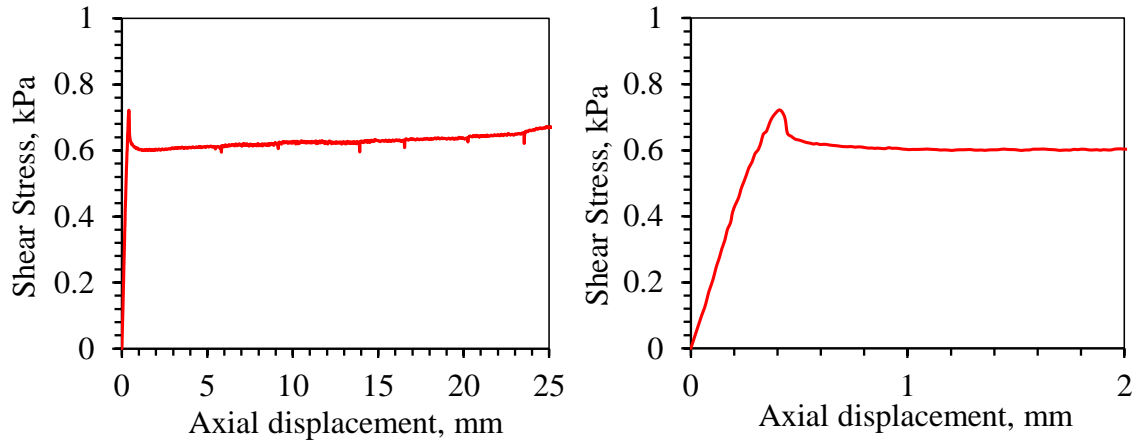


Figure 106. Drained interface response in Stage 2 ( $\sigma_n = 2.1$  kPa).

#### 5.3.2.4 Effect of Embedment/ Normal stress on the Pipe/Clay Interface Resistance

The tests that were conducted at different levels of pipe embedment allow for determining the sensitivity of the peak and minimum interface resistance to the effective normal stress at the pipe/clay interface. Figure 107 shows a schematic of the pipe embedment and the associated confinement levels in each of the three stages. Aside from the different normal stresses at the interface, changes in pipe embedment result in different levels of contact stresses and thus degrees of overconsolidation of the clay under the pipe: Assuming that the previous maximum consolidation pressure of the clay in the bed is approximately 12 kPa (Figure 81), the different normal stresses at the interface result in OCRs that range from about 3.0 in the case of the shallow embedment and about 6.0 for the case with the largest embedment. The combination of effective normal stress at the interface and the associated OCR is expected to govern the response of the interface under drained and undrained shearing.

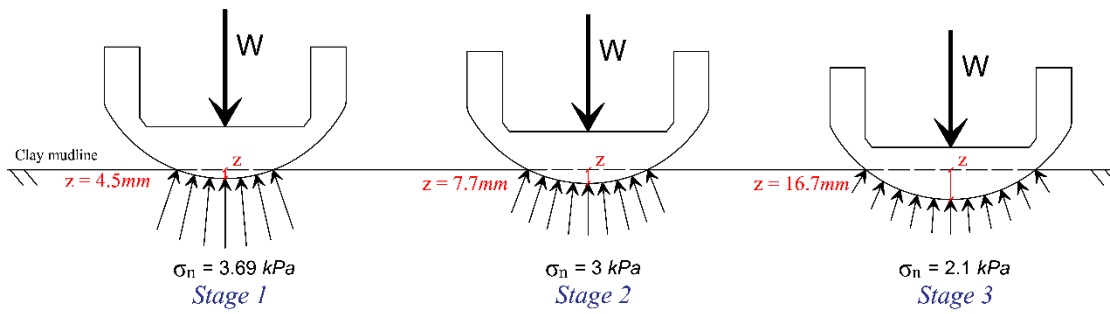


Figure 107. Visual of the Pipe Embedment for the three Stages of Testing

The effect of normal stress and OCR on the undrained interface response in the first shearing cycle (virgin clay) of every Stage is presented in Figure 108. Results indicate that the peak undrained interface resistance increases with an increase in the effective normal stress at the interface. This could be attributed to the smaller void ratio or water content that is expected under the larger normal stress. However, it is clear that the effect of the normal stress on the undrained interface response becomes negligible for the “minimum” interface resistance at larger displacement as the interface is sheared to the steady state.

Further investigation of the curves in Figure 108 indicates that the degree of overconsolidation of the clay under the pipe immediately before the shearing stage could have an effect on the generation of negative pore water pressure during interface shearing. It is clear that the cases involving the higher OCR and the lowest effective normal stress exhibited the highest generation of negative pore water pressure due to the enhanced tendency for dilation during shear and the low level of confinement.

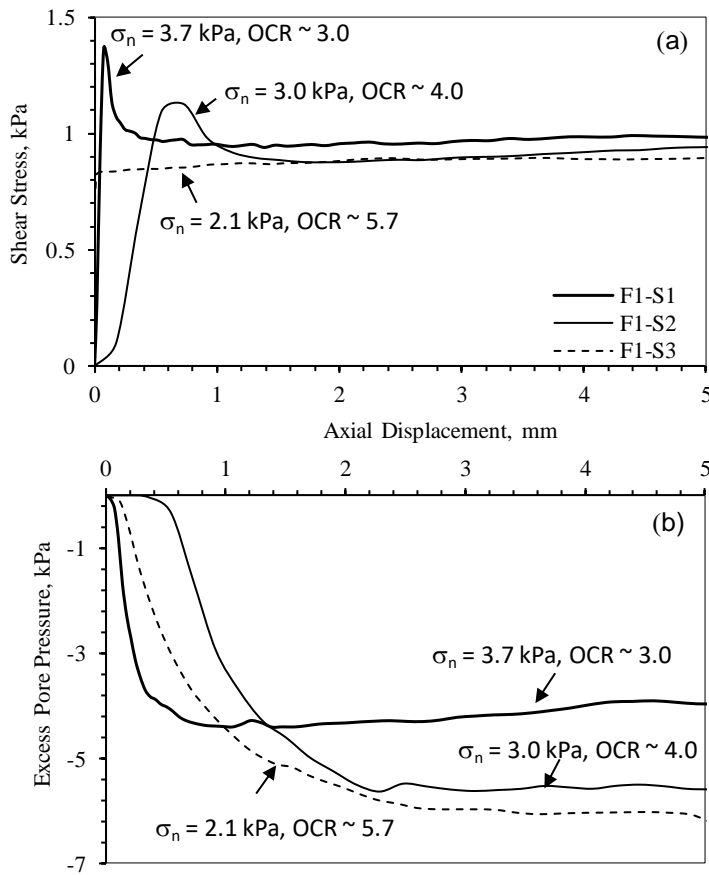


Figure 108. Comparison between the Undrained Interface Responses of the Smooth Pipe at Different Embedment Levels (Stage 1 to Stage 3)

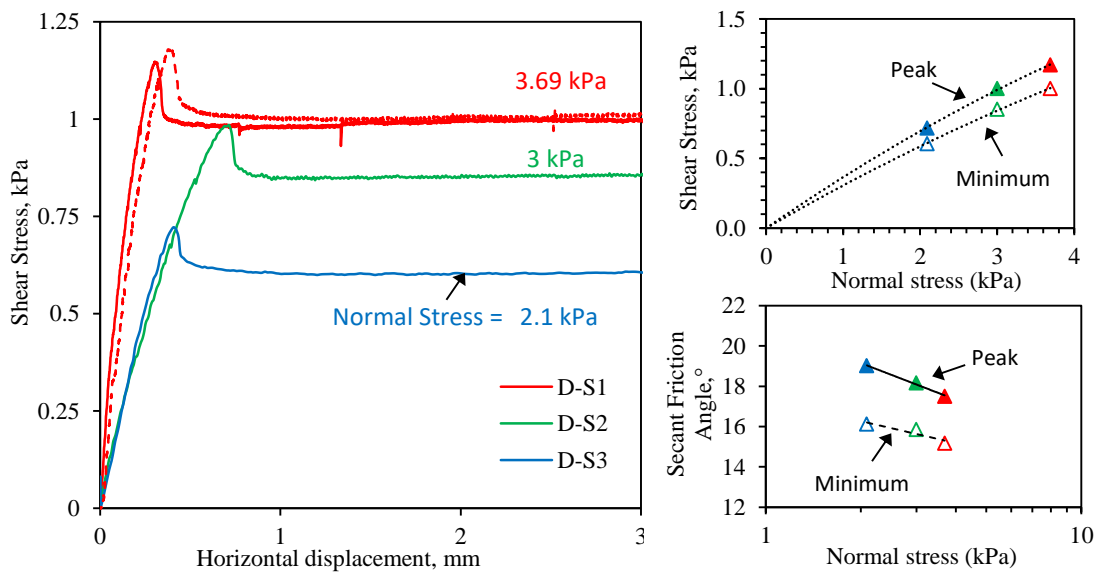


Figure 109. Comparison between the Drained Interface Responses of the Smooth Pipe at Different Embedment Levels (Stage 1 to Stage 3).

Results of the drained interface shear tests that were conducted in the different testing stages are plotted on Figure 109. Results clearly show that the drained interface resistance (both peak and minimum) increases with the effective normal stress at the pipe/clay interface. More importantly, the drained interface secant friction angles at each normal stress indicate a clear decrease (from 19 to 17.5 for the peak and 16 to 15 degrees) as the effective normal stress at the pipe/clay interface increases from 2.1 kPa to 3.7 kPa. These results further confirm that the drained Mohr-Coulomb failure envelop of the clay/pipe interface is curved in the low pressure range and that the curvature could be picked up and quantified using the novel proposed test setup.

The data collected in the testing program on the smooth interface was also used to assess the sensitivity of the axial friction factor to the different testing conditions. The axial friction factor for embedded pipes is defined as the ratio of the axial resistance,  $F$  to the normal force acting on the pipe,  $N$  which is in turn defined as the product of the pipe weight and the wedging factor  $\xi$  such that:

$$\mu_{\xi} = \frac{F}{N} = \frac{F}{\xi W} \quad (5.2)$$

The measured peak and minimum friction factors during undrained loading cycles in Stages 1 to 3 are plotted in Figure 102 against the shearing cycles and mean normal stress at the pipe/clay interface. The mean normal stress is defined as normal force acting on the pipe ( $N$ ) divided by clay/pipe contact area. Results on Figure 110 and Figure 111 indicate that the peak friction factor for the “first” undrained shearing cycle (shearing against virgin clay) is around 0.37, irrespective of the pipe embedment depth and the mean normal stress at the interface except for Stage 3 where the peak was not captured and it was assumed to be 0.4 (equal to the minimum stress measured).

Following the first cycle and upon repeated undrained loading, the peak friction factor decreases to values of about 0.32 as long as a waiting period of at least 4 hours is allowed between shearing cycles. This applies to shearing cycles in Stage 1, Stage 2 and Stage 3 and is thus independent of the normal stress at the interface. With repeated undrained cycles and as long as a waiting time is enforced, the peak and minimum friction factors reach relatively stable average plateau of about 0.32 and 0.25, respectively.

For shearing cycles that did not involve any waiting period, it is clear from on Figure 110 and Figure 111 that the peak friction factor reduced dramatically to values as low as 0.2. These relatively low “peak” friction factors approached the “minimum friction factors” that are reported in Figure 111b indicating that the effect of repetitive undrained loading without allowing a waiting period between cycles could bring the undrained friction factor to values that are consistent with the minimum reported friction factors. As mentioned previously, the reduction in undrained peak friction during consecutive shearing is attributed to the remolding of the soil without the ability to dissipate the excess pore pressures.

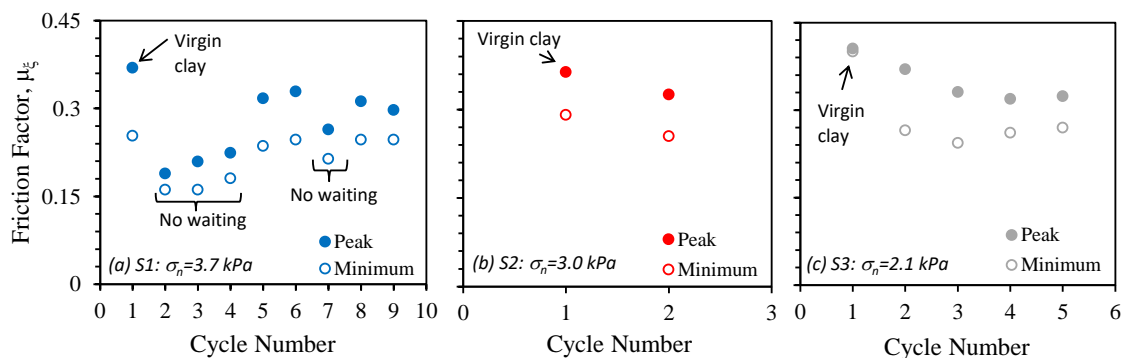


Figure 110. Variation of peak and minimum friction factors with shearing cycles during (a) Stage 1, (b) Stage 2 and (c) Stage 3.

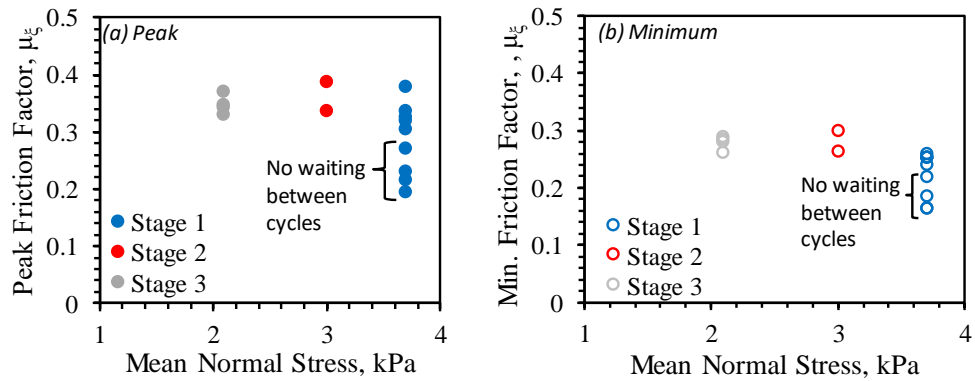


Figure 111. Effect of normal stress on: (a) peak friction factor and (b) minimum friction factor for Undrained Shearing Cycles

## 5.4 Results of Sandpaper interface testing

After completion of the different stages of the tests involving the stainless steel smooth interface, the test setup was removed, reassembled, and moved to a different test location on the clay bed. Before initiating any additional tests in the new location, rough sandpaper was fixed to the pipe test section in preparation for measuring the interface response for the rough surface under different testing conditions. The testing program that was implemented with the rough section is presented in Table 10. It is clear from Table 10 that the testing sequences and cycles adopted for the rough interface were limited to 5 cycles (10 sweeps) divided among 3 stages with different pipe embedment depths.

### 5.4.1 Penetration and Consolidation response:

Prior to initiating testing with the rough interface, the setup was moved to the middle of the clay bed, at a distance of about 300 mm from the location where the stainless steel interface was tested (Figure 112).



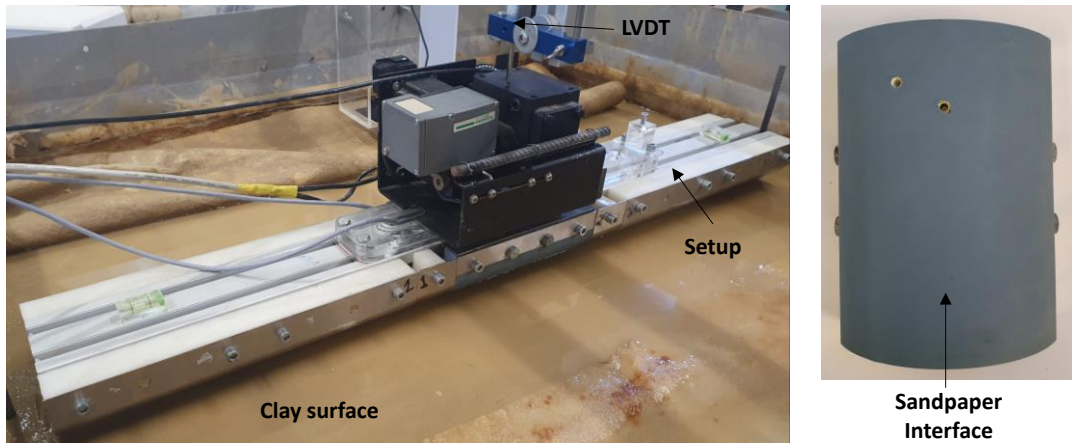


Figure 112. The setup placed in the middle of the clay bed during the second test and the sandpaper interface fixed around the test section.

For the first stage of loading, the pipe was allowed to consolidate as in the case of the smooth interface tests. The final embedment at the end of consolidation was only 2.8 mm as shown in Figure 113. The corresponding normal stress at the pipe/clay interface was relatively high (about 4.7 kPa) due to the limited contact area between the pipe and the soil. At such a small embedment, the pore pressure sensor at the side was not in contact with the soil and did not record any excess pore pressure and the pore pressure sensor at the invert was not functioning well. Thus, pore pressures measurements could not be reliably reported in Stage 1 testing.

The smaller initial embedment that was observed under the setup's own weight in the second test (rough interface) could be attributed to variations in the pipe laying process. Since the setup was placed manually on the soft bed, the force that was applied on the relatively small contact area during laying could not be controlled. Thus, any change in the rate of "penetration" (how fast the setup was placed) could eventually affect the pipe embedment. Another reason for the low penetration could be the higher

interface roughness, which has been identified in numerical models to produce higher penetration resistance during pipe laying (Chatterjee et al. 2012, Merifield et al., 2009).

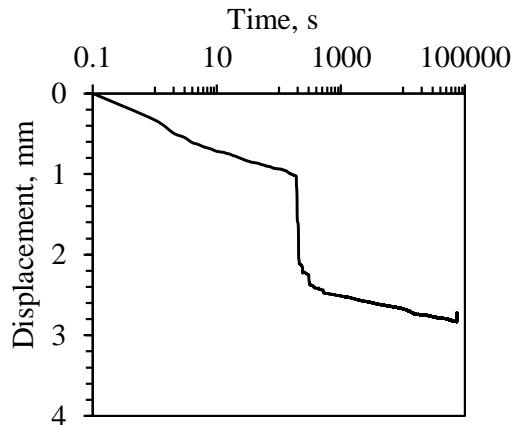


Figure 113. The settlement of the setup following pipe laydown in Stage 1.

During Stage 2, and after the application of the 27kg dead weight on the pipe, the embedment increased to 7.8 mm and the normal stress along the pipe/clay interface decreased to about 2.98 kPa. Positive excess pore pressure was detected by the pore pressure sensor at the side with a maximum of 1.67 kPa once all weights (27 kg) were added and then totally dissipated after 12 hours (Figure 114). Afterwards, the setup was unloaded and left for 2 hours to stabilize during which 0.16 mm of swelling was recorded (Figure 115).

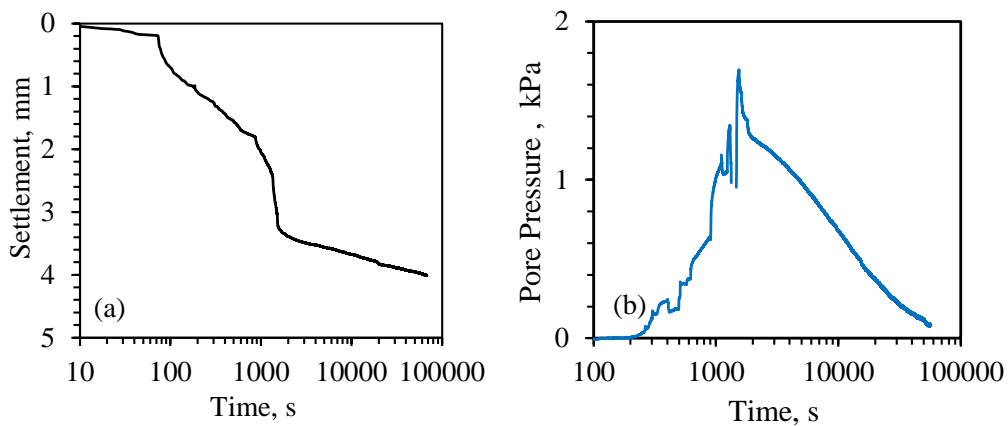


Figure 114. The settlement and the excess pore pressure observed during Stage 2 and the subsequent consolidation.

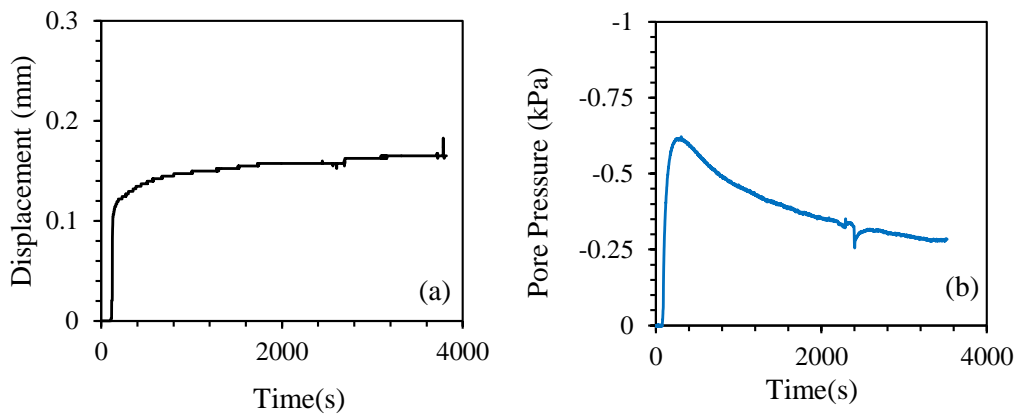


Figure 115. (a) Soil swelling and (b) negative pore pressure dissipation during unloading in Stage 2.

During stage 3, the setup was pushed into the soil using a hydraulic jack to an embedment of 21.75 mm and left to consolidate under an additional 27 kgs of loading. At the end of consolidation under the weight, an additional 0.5 mm of consolidation settlement was recorded (Figure 116). After removing the additional weights, negative pore pressures were measured along with 0.22 mm of rebound/swelling (Figure 117). In stage 3 testing with the rough interface, the final normal stresses at the pipe/clay interface was 1.85 kPa. A sketch showing the pipe embedment for the three stages of testing for the rough interface is presented in Figure 118.

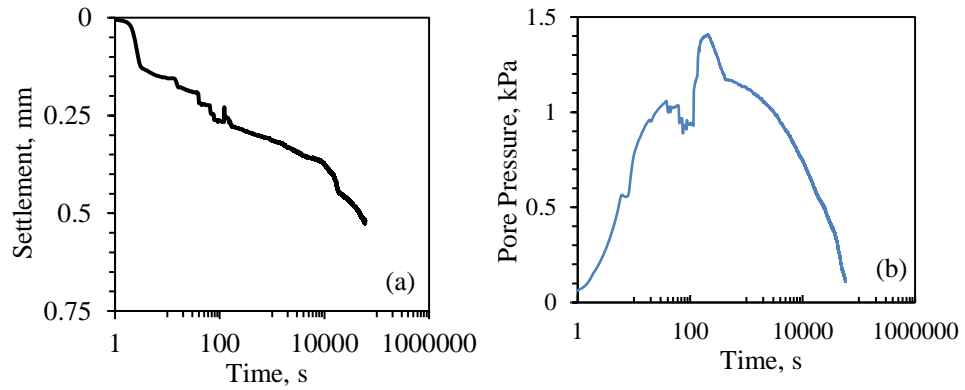


Figure 116. The setup settlement and the excess pore pressure during loading and the subsequent consolidation in Stage 3

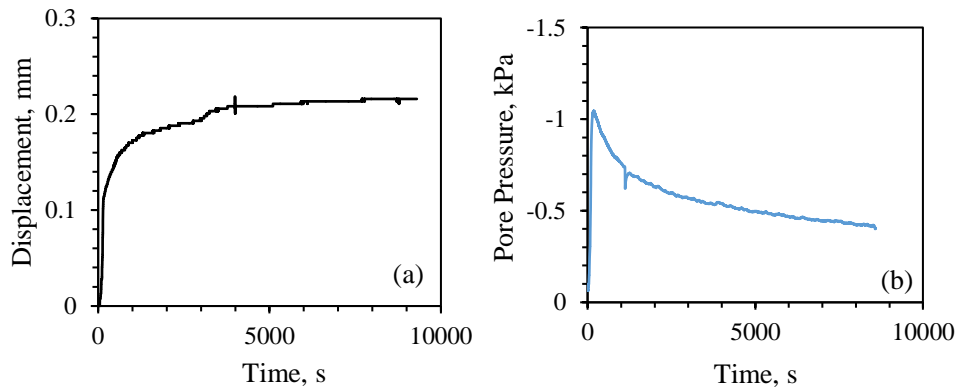


Figure 117. (a) Soil swelling and (b) pore pressure dissipation during unloading in Stage 3.

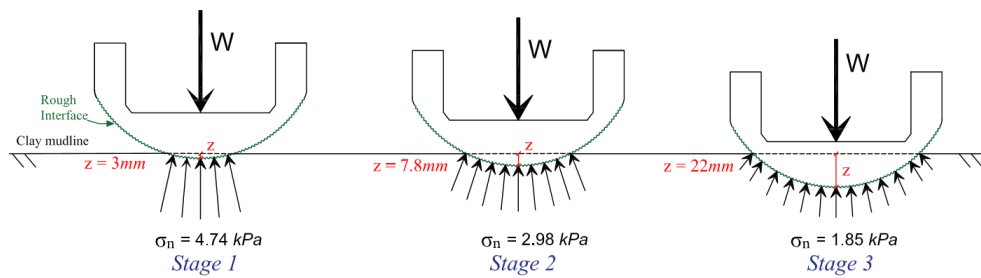


Figure 118. Embedment of Rough sandpaper interface in Stages 1 to 3

#### 5.4.2 Interface Response during Shear (Sandpaper)

Three consecutive undrained shearing cycles were performed during Stage 1 to measure the undrained shear strength of the sandpaper-clay interface. The shear stress versus displacement response in the three cycles is presented in Figure 119. The interface shear stress exhibited a relatively large peak (3.77 kPa) after 1.5 mm of pipe

displacement and then dropped to 2.48 kPa and remained more-or-less constant over the remaining 25 mm of the first cycle (Figure 119). This relatively large peak interface resistance indicates that the interface failure mechanism may have involved a clay/clay failure rather than a typical interface failure. The large roughness of the sandpaper interface coupled with visual observations of the failure mechanism during the test, point to the conclusion that the failure mechanism was internal to the clay and not at the pipe interface.

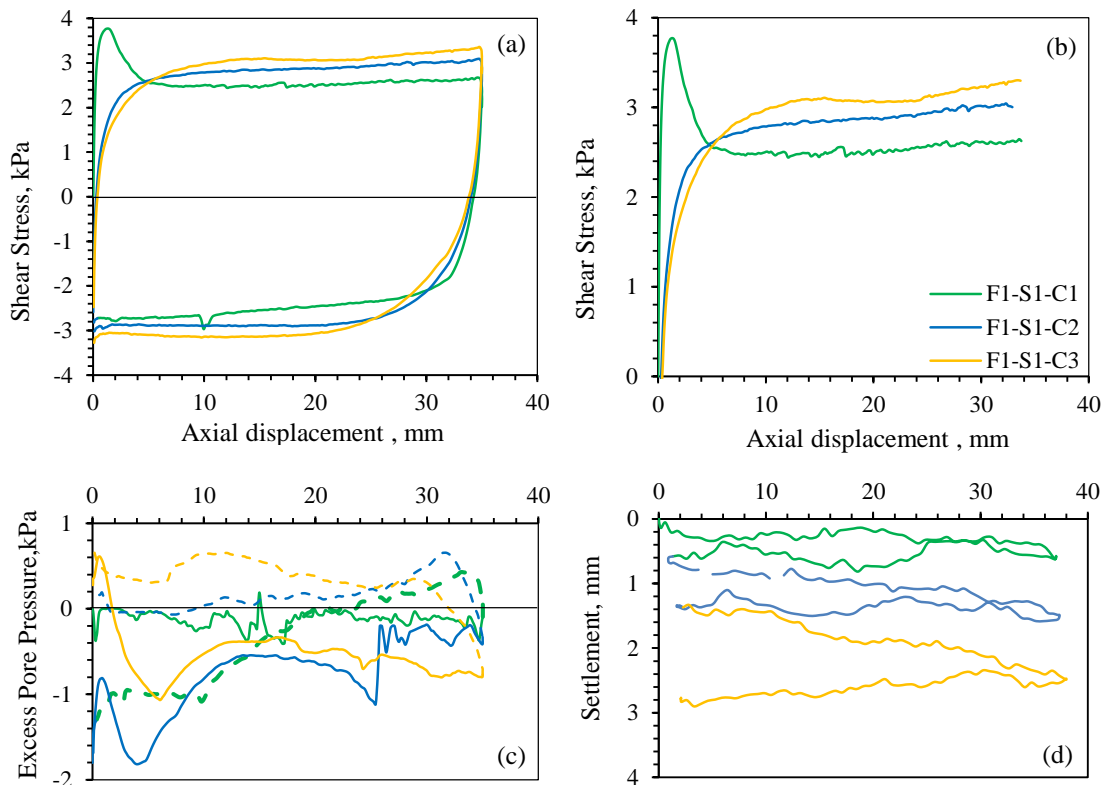


Figure 119. Undrained shear cycles results during Stage 1: (a, b) shear stresses, (b) pore pressure and (c) settlements

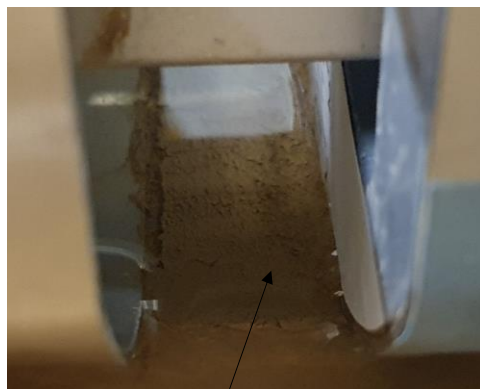
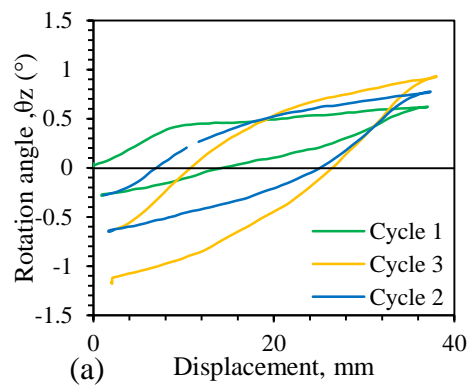
Surprisingly, the measured peak interface resistance of 3.77 kPa which was mobilized in Sweep 1 is almost double the undrained shear strength measured in the clay bed using the ball penetrometer at depths exceeding 30 mm (see Figure 80c). Since the interface test in Stage 1 was conducted at an extremely small embedment of 3mm,

the undrained shear strength in the clay at this extremely shallow depth may have been larger than expected and is “unknown”. A possible explanation of this observation is that the relatively large peak resistance may have been facilitated by partial drainage of pore pressure at the interface, given the proximity of the pipe/clay interface to the surface at a shallow pipe embedment of 3mm. The clay at the pipe interface in the seemingly “undrained test” may have mobilized its drained internal strength. A quick calculation indicates that if the drained friction angle of the clay is between 30 and 32 degrees as measured in the direct shear tests in Chapter 3, the drained interface resistance at a normal stress of 4.77 kPa could be above 3.0 kPa, explaining the high measured strength at the pipe/clay interface. The relatively low pore water pressures that were measured at the clay/pipe interface (Figure 119c) also support the possibility of drainage at the rough interface due to shallow embedment.

The two additional fast shearing cycles that were conducted after cycle 1 reflect a more ductile shear-stress versus pipe-displacement response which is governed by the absence of a peak at small pipe displacements and a clear reduction in the peak interface shear resistance compared to the first cycle on virgin clay. With repeated cycles, the shear stresses at large displacements improved by 0.5 and 0.6 kPa during cycle 2 and cycle 3, respectively. Since the clay was not allowed to consolidate during and between the three cycles (no waiting time), remolding of the clay as a result of repeated cycles may explain the observed response. White et al. (2017) report that the peak resistance commonly appears in the first cycle and then decays with additional shearing cycles.

An examination of the pipe section movements/rotations using the Go-Pro camera coupled with visual inspection of the test section during fast shearing lead to several observations that may also explain the relatively high resistance obtained in the

rough interface tests in Stage 1. Figure 120 presents the variation of the measured rotation angles ( $\theta_z$ ) with cycles of shearing. It is clear that the measured rotations in the z-direction (maximum of about 1 degree) were higher than those observed in the tests conducted with the smooth interface (maximum between 0.3 and 0.4 degrees) and continuously increased with increasing number of cycles. Pipe rotations along the z-direction are important because they could lead to non-uniform stresses under the pipe. The measured pipe rotations were validated through visual examination of the test section which showed a relatively higher level of clay dragging in front of the pipe during shearing (see Figure 120c).



(b) Sheared Soil



(c) Pushed Soil

Figure 120. (a) Rotation angle in the z-direction, (b) sheared soil, and (c) dragged soil in S1.

The rotations that were observed in the pipe section in the fast tests of stage 1 may be attributed to multiple factors: (1) the lack of confinement around the pipe due to the very small embedment level, rendering the pipe section more susceptible to rotations in all directions and (2) the possible generation of a rotating moment that could have produced additional compression on one end of the pipe, triggering additional dragging of soil at the moving end of the pipe, and contributing to the rotation observed. The added resistance that is provided by the unwanted passive resistance from the dragged clay may have contributed to the relatively high resistance that was observed at the clay/pipe interface in Cycle 1 and the possible slight improvement that was observed in the resistance in Cycles 2 and 3 at large pipe displacements. Any resulting moment is expected to be larger in the tests of the rough interface given the higher value of the applied shearing force. Figure 120b reveals the effect of the roughness on the sheared soil and the amount of soil pushed in Stage 1 (Figure 120c).

Given the rotations that were observed in the pipe in the fast cycles of Stage 1 and the obvious dragging of the soil, a decision was made to stop the testing at this level of embedment and to penetrate the pipe deeper into the bed prior to any additional testing. Moreover, to minimize the risk of not being able to measure the drained interface response (as was the case in Stage 1), a decision was made to limit the tests on the rough interface to drained tests so as to test the effectiveness of the test setup in determining the peak and residual drained interface friction angle for the pipe as it is sheared against the rough sandpaper. These drained tests will allow for a much needed comparison between the friction angles measured in the novel test setup and those measured in the drained interface direct shear tests that were conducted in Chapter 3 on the same soil and interface.



Based on the above, only drained interface tests were executed in Stage 2 and 3. Results from these tests are presented Figure 44. For stage 2 tests, the expected effective normal stress at the pipe-soil interface was about 2.98 kPa, reducing to a normal stress of 1.85 kPa in the drained test of Stage 3. Results on Figure 121 indicated a drained interface response that was characterized by peaks in the shear stress at pipe displacements in the order of 2mm and 3mm for Stage 2 and Stage 3 tests, respectively. Interestingly, the mobilized shear stresses decreased gradually with pipe displacement, reaching a residual condition at displacements in the order of 20 to 25 mm.

The resulting peak and residual drained secant friction angles were calculated as  $33.2^\circ$  and  $29.15^\circ$ , respectively for the test of Stage 2 (2.98 kPa) and  $39.82^\circ$  and  $31.5^\circ$ , respectively for the test of Stage 3 (1.85 kPa). The larger drained secant friction angles that were measured for the low confinement case of Stage 3 indicate that the novel test setup could help characterize the curvature in the Mohr-Coulomb failure envelop in the low pressure range, by simply increasing the pipe embedment without any additional change to the test setup. This advantage of the novel test setup will be invested in the future to provide an economical and efficient mechanism to determine the curved interface failure envelop through testing at one location in the seabed, but at slightly different embedment levels.

It is worth noting that the pipe rotations that were calculated in the drained shearing cycles indicated that the tendency for the pipe to rotate along its axis (in the z-direction) decreased by a factor of about 2 when the embedment of the pipe was increase from around 7mm in Stage 2 to around 22 mm in Stage 3 (see Figure 121b). This observation is important since it shows that higher confinement at the clay/pipe interface could lead to more stable testing conditions during shearing, leading to less

undesired rotations of the test setup, less soil dragging at the front of the pipe, and more reliable interface shear results.

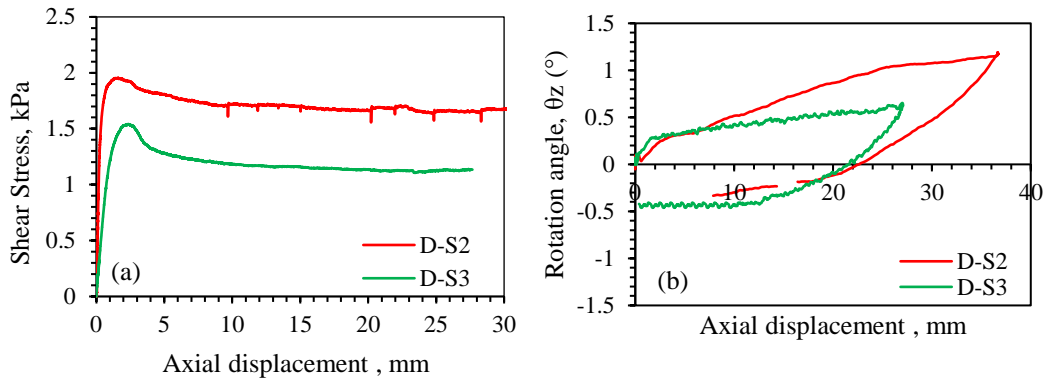


Figure 121. Drained response of the sandpaper-clay interface during Stage 2 and Stage 3 (a) shear stress versus displacement, and (b) rotation angle versus displacement.

To test the hypothesis of possible partial drainage that could have occurred during the fast tests of stage 1 due to the proximity of the pipe/clay interface to the surface at a shallow pipe embedment of 3mm, the shear-stress versus displacement curve that was measured for the first sweep in Stage 1 was added to the results of the drained tests in Stages 2 and 3 on Figure 122. Interestingly, results on Figure 122 could point to the possibility that the fast tests that were conducted in Stage 1 were already significantly “drained”. The response of the tests is very similar to that observed in the drained tests of Stage 2 and 3. Since the test was conducted with a relatively high normal stress of 4.74 kPa at the clay/soil interface, the peak shear stress observed in stage 1 was larger than those observed in Stages 2 and 3. The clay at the pipe interface in the seemingly “undrained test” of Stage 1 may have mobilized its drained internal strength.

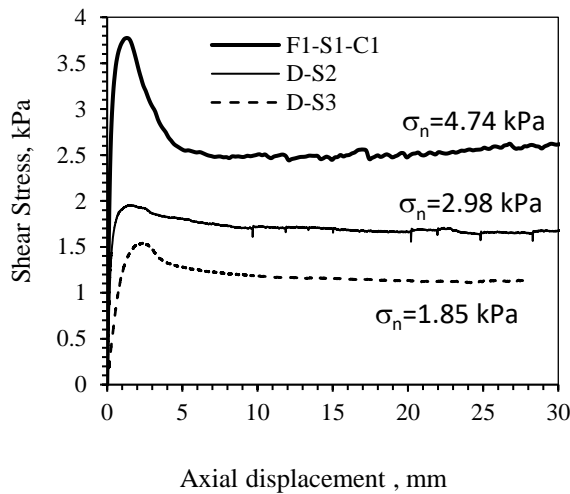


Figure 122. Comparison between the interface shear response in the “fast” test of Stage 1 with the responses observed in the drained tests of Stages 2 and 3.

### 5.5 Post-test penetration tests

Following the completion of the tests at location 1 (smooth tests) and location 2 (rough), the undrained shear strength profiles under the test section and the anchoring sections were measured using ball penetrometer tests as shown in Figure 123. A clear improvement of the undrained shear strength in a 60 mm thick clay segment (directly under the pipe) could be noticed due to the combined effect of pipe jacking, consolidation, and shearing. The hardened soil thickness extended from a depth of about 0.65D to a depth of 1 D and indicated shear strength that increased from an average value of 2 kPa prior to testing to values in the range of 2.5 kPa to 3.2 kPa following testing. In addition, measurements of water content from samples taken under the test setup indicated a significant reduction in water content compared to the values prior to testing. The water contents reduced from values in the order of 30% prior to testing to values as low as 26-28% after testing.

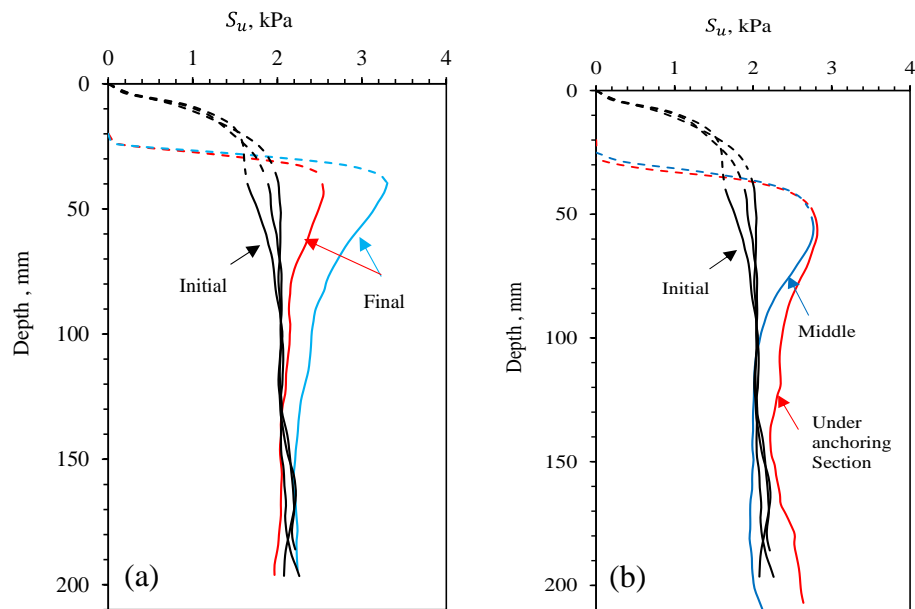


Figure 123. Ball penetrometer profiles before and after testing with (a) Smooth Interface and (b) Rough Interface.

## 5.6 Comparison between smooth and rough interface responses

The axial interface response depends on the interface roughness as already discussed in Chapter 3. As roughness increases, the interface resistance is expected to increase. Results from the novel test setup clearly indicated the effect of the pipe roughness on the mobilization of shear stresses and the generation of pore water pressure with axial displacement. To assess the impact of roughness on the interface friction, the variation of the interface friction factor with pipe displacement is presented on Figure 124 or the drained tests conducted on the smooth and rough interfaces for shearing Stages 2 and 3 (no drained tests were available for the rough surface in Stage 1).

Despite the slight variation in the applied normal stresses at the pipe-clay interface, the results clearly show that the smooth interface exhibited a relatively small drained peak friction factor ( $\sim 0.32$ ) which was almost half that observed for the rough

test interface in Phase 2 (~ 0.65) and almost a third of that observed in Phase 3 (~0.83). For the residual condition, the friction factor was also more than doubled for the rough interface cases. Similar results were also observed for the “fast” shearing tests as indicated in Figure 124 with the undrained friction factor for the rough interface being about 2.5 times larger than that in the smooth interface.

The pipe displacement at which the peak friction factor was mobilized also increased with the interface roughness of the pipe. Less than 0.5 mm displacement were enough to reach a peak resistance for the smooth interface compared to 1.7 - 2.5 mm (2.5%D) for the cases involving a rough interface. The other factor that also affected the mobilization distance is the pipe embedment as the peaks in Stage 3 tests were also shifted to the right.

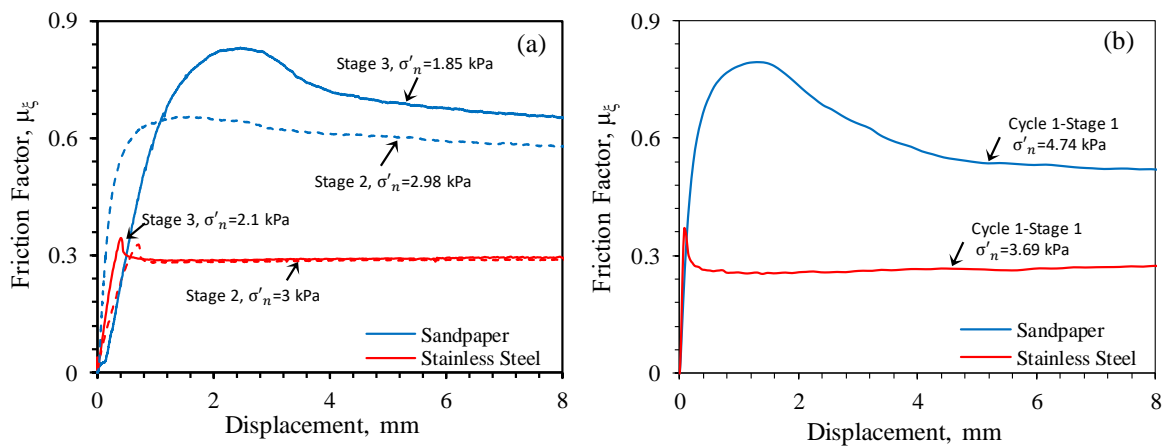


Figure 124. Friction factors variation for the sandpaper and stainless steel interfaces during (a) drained cycles and (b) undrained cycles.

### 5.7 Evaluation of the new test setup (comparison with interface direct shear)

In this section, the results of the drained interface tests that were obtained using the novel test setup by shearing a 20-cm long pipe section against the in-situ soil are compared to the drained results that were obtained from interface direct shear tests

conducted in a 10cm x 10cm direct shear box (Chapter 3). Both the model pipe tests and the small scale interface direct shear tests were conducted with the same clay type (LPC) and sheared against the same smooth stainless steel and rough sandpaper interfaces.

Graphs showing a comparison between the results of the interface direct shear tests and the novel model tests for the smooth and rough interfaces are presented in

Figure 125 (a,b). Results include the full shear stress versus displacement response and the variation of the drained secant interface friction angle with the logarithm of the effective normal stress at the clay/solid interface. Results for the secant friction angles are reported for both the peak stress condition and the residual/large deformation loading condition.

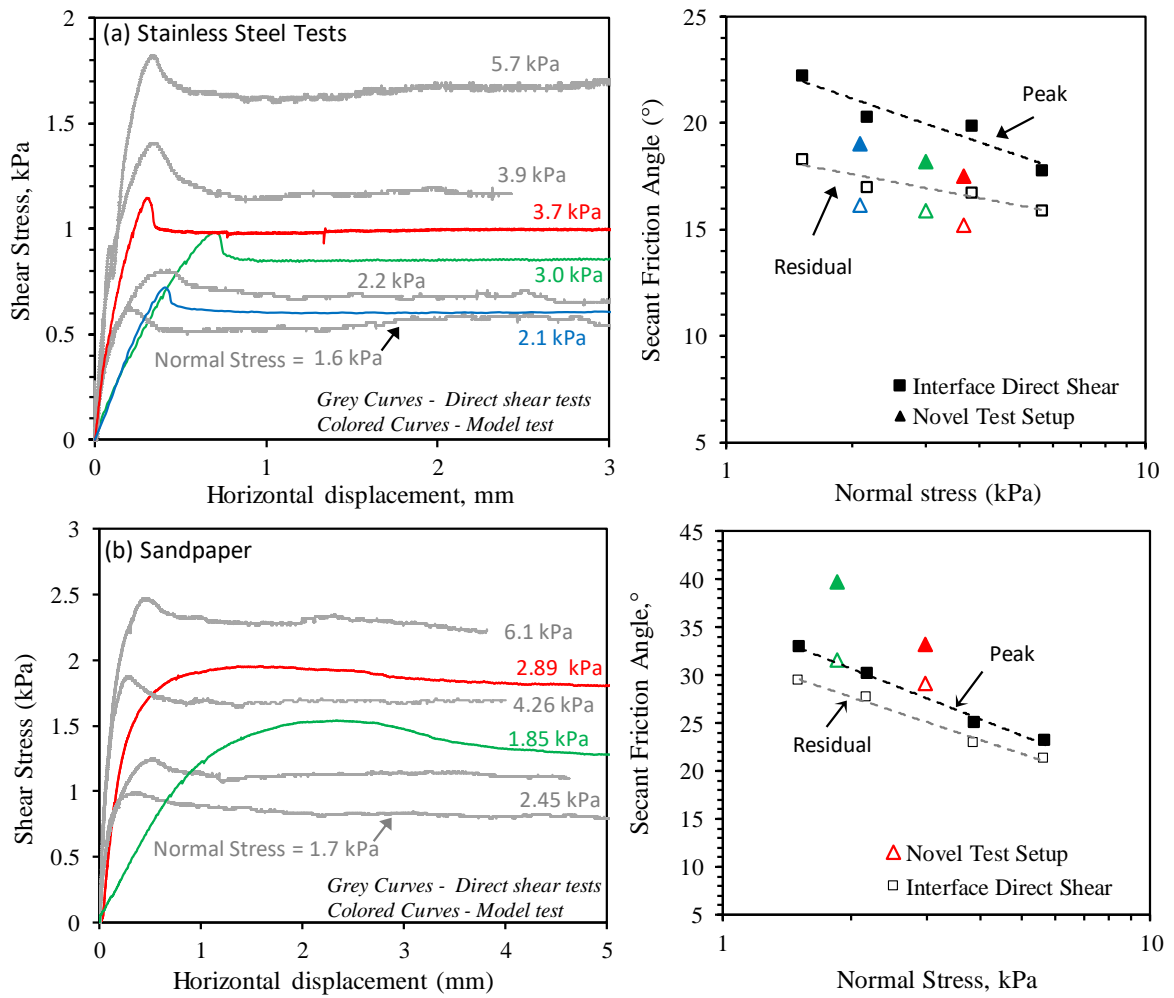


Figure 125. Comparison between the interface direct shear results and the novel pipe model interface test results.

For the tests conducted with a smooth interface, the overall interface shear stress versus horizontal displacement response shows a remarkable consistency between the two types of tests (direct shear versus model test) considering the significant differences in the test setups and the scale and geometric shape of the contact/area between the pipe and soil where the shearing is concentrated. This consistency in the overall measured response is indicative of the robustness of the novel testing setup that was adopted in conducting the pipe model shear tests on the clay bed.

A one to one comparison between the drained interface secant friction angles that were measured in the two test methodologies indicates that for the smooth interface (Figure 125a), the peak and residual friction angles that were measured in the model tests were slightly lower than those determined from the interface direct shear tests. Although both methodologies resulted in friction angles that decreased linearly with the logarithm of normal stress, the friction angles from the model tests were about 2 degrees smaller. One explanation for the lower peak and residual strengths in the case of the model tests is that the drained tests in all smooth model tests were conducted following a number of undrained cycles and sweeps that would enforce significant deformations and strains along the pipe/clay interface. Conversely for comparison, the interface tests conducted in the direct shear box only involved 3mm of shear displacement.

For the tests conducted with the rough interface (Fig. 125b), the shear stress versus pipe displacement curves in the novel model test setup exhibited a response that diverged from the results of the rough interface direct shear tests. The drained peak interface shear stresses that were mobilized at the model pipe/clay interface were 50% larger than those measured in the direct shear tests at a similar normal stress. More importantly, the shape of the shear stress versus displacement curves in the interface direct shear tests pointed to a mode of failure that is controlled by interface slippage (brittle failure with an early peak in stress) while the curves of the model pipe tests reflected a more-or-less ductile clay/clay failure, which was confirmed visually during the actual tests. These differences in response translated into differences in the measured peak and residual interface friction angles in the two test setups, with the model tests exhibiting friction angles that were clearly higher.



To confirm that the mode of failure observed in the pipe model tests was reflective of a clay/clay failure, the results of the rough model tests were plotted on

Figure 126 with the direct shear results of the tests conducted on the clay only (internal clay/clay tests). Interestingly, the rough interface response in the model tests was very consistent with the direct shear clay/clay direct shear response. The remarkable consistency in the shear-stress versus displacement response translated into a clear agreement between the peak and residual interface friction angles measured in model pipe tests and the clay/clay friction angles measured in the direct shear (

Figure 126). This consistency is clearly demonstrated in Figure 51 which shows secant friction angles at the peak and residual conditions separately for the smooth, rough, and clay/clay strengths.

These results confirm the observation that the mode of failure in the model tests involving the rough interface were governed by a clay/clay failure. This observation poses a question mark on the validity of the results of interface direct shear tests for clays sheared against rough surfaces. The main limitation of the direct shear test is that shearing is forced along a predetermined thin shear zone in the gap between the two sides of the box. This limitation is not present in the case of the pipe model tests that mimic the real response of the pipeline in the field, whereby the failure zone at the pipe/clay interface is not artificially restrained by the test setup. In the model tests, the thickness of the shear zone and the resulting location of the shear plane are governed by the interface roughness and the clay particle arrangement at the shearing zone. The validity of interface direct shear tests with rough interfaces will need to be verified in

the future with additional tests involving different types of soils and different pipe roughness.

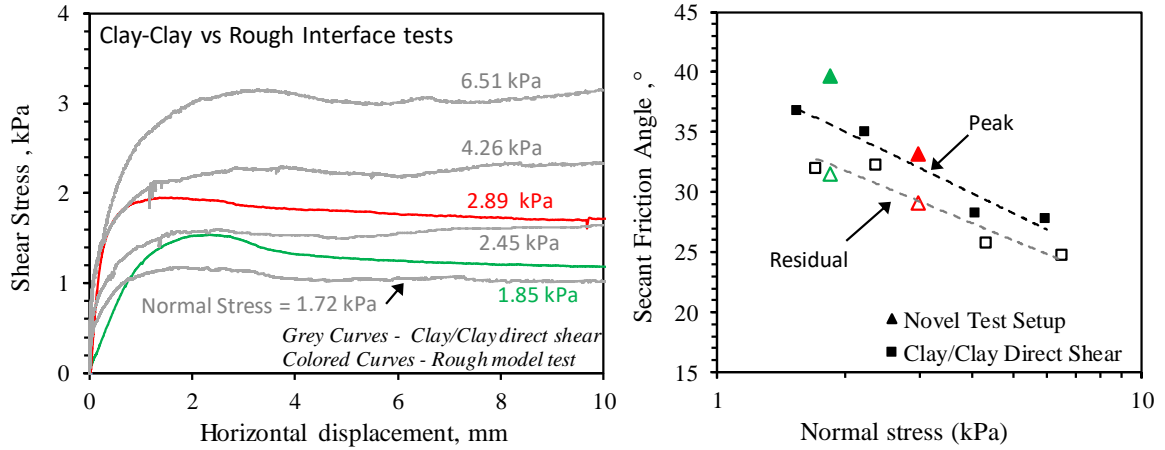


Figure 126. Comparison between the clay/clay internal strength (direct shear) and the interface tests with the novel rough pipe model.

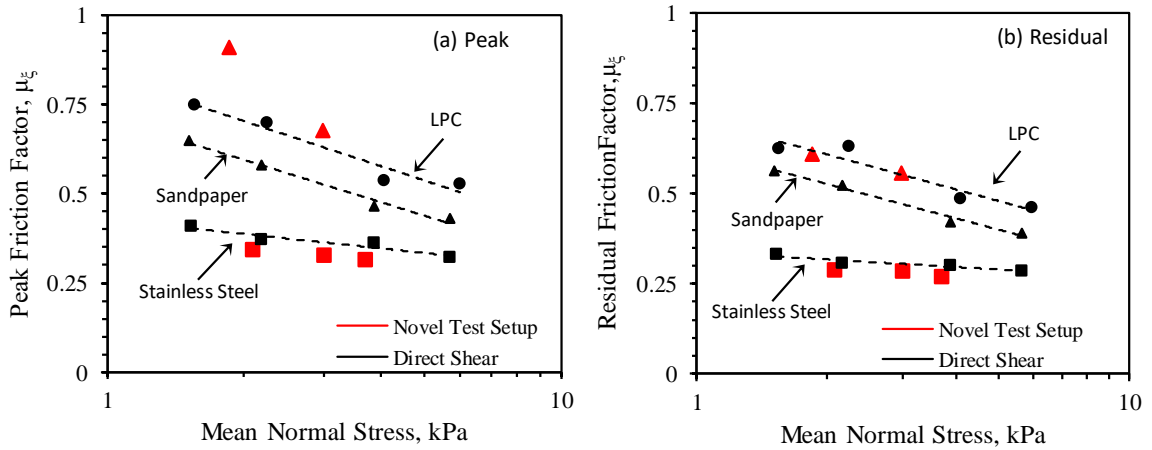


Figure 127. Peak and residual drained friction factors from interface direct shear and the novel pipe model tests.

It should be noted that in the case of offshore pipelines, the pipes are subjected to large deformations that would render the residual friction factor a key parameter in design. The peak friction factor is of lesser importance but still plays a role in defining the global pipeline response at the initiation of buckling. Thus, the reliable and cost-effect evaluation of the peak and residual interface fraction factors is a major objective

and challenge for current testing systems. The proposed setup has been proven to be a reliable testing option in achieving this objective.

As shown in

Figure 127, the setup yielded reliable friction factors for both the stainless steel and the sandpaper interfaces. For the case involving smooth interfaces, results show repeatable and reliable results that are consistent with those measured in an interface direct shear setup that has been customized to eliminate the effects of friction in the test device so as to produce reliable estimates of the interface friction response in the low pressure range. Such direct shear machines are not common except in a limited number of research institutions in the world. For the more realistic case that involves a rough interface with a surface roughness that is in line with those typically adopted in offshore pipelines, results from the novel pipe model testing setup portrayed an interface failure mechanism that involved an internal clay/clay failure. On the other hand, the interface direct shear tests produced interface results with a slightly lower interface resistance indicating a different model of failure. Even with these significant differences in response, the drained residual friction angles that were measured with the rough model pipe were only about 10% larger than the residual friction angles measured in the interface direct shear tests.

Moreover, the proposed novel pipe testing setup was proven to reliably capture the effect of drainage conditions and rate of loading on the on the interface resistance. The setup allows for conducting continuous shearing cycles in two directions and allows for forcing waiting time between cycles to allow for pore pressure dissipation. More importantly, by increasing the pipe embedment at the same location in the same bed, the effect of normal stress on the interface response could be investigated. This allows for

determining the curvature in the interface Mohr-Coulomb failure envelope from one testing location in any future field application. Finally, the limited number of pore water pressure sensors that were incorporated in the model pipe section allowed for monitoring the generation and dissipation of pore water pressure at the interface at all stages of testing, which included pipe penetration, consolidation, and shearing. The number of pore pressure sensors along the pipe length and along the cross section of the pipe could be increased in the future to allow for a more representative and comprehensive investigation of the pore pressure generation/dissipation and its variation along the pipe length. Such pore pressure measurements would be key for making decision all stages of testing including (1) marking the full dissipation of pore pressure and the end of consolidation (2) reflecting the field coefficient of consolidation of the clay under the pipe, and (3) reflecting the degree of overconsolidation of the soil (positive versus negative pore pressure generation during shear), and (4) indicating non-uniform distribution of pressure under the pipe as a result of a potential overturning moment.

## **5.8 Conclusion and Recommendations**

In this chapter proof of concept tests for the proposed in-situ model test setup were conducted to assess and explore its potential to accurately estimate the pipe-soil interface design parameters. The setup was tested under different testing conditions inside a soft clay bed. The results were promising and confirmed the practicality and functionality of the setup and opened the path towards some improvements that are still needed to optimize testing effectiveness. The following conclusions have been reached:

1. The interface response was adequately captured by the novel in-situ setup during drained and undrained shearing. Based on the testing conditions, the peak and the residual resistances were successfully measured.
2. The drained interface resistance could be reliably and repeatedly measured using the in-situ setup for a rough and smooth interface. In the case of the smooth interface, the resulting secant friction angles and residual drained friction factors compare favorably with the results of the direct shear tests performed on the same soil and the same interface.
3. Results from the rough tests indicated a failure mode that was internal to the clay, unlike the interface direct shear tests that indicated a forced clay/interface failure. This resulted in interface friction angles for the rough interface that were higher than those observed in the interface direct shear tests. This was attributed to possibility of formation of multiple failure planes in the in-situ pipe model tests where the sheared soil is not restraint as in case of the direct shear.
4. Under undrained conditions, the measured interface response was realistic. However, as the test section was free to move, it exhibited slight uncontrolled rotations in all directions when it was pushed fast, especially when the embedment was very small and when consecutive cycles were executed. Some soils were thus pushed during shearing and the pore pressure readings were complex. In case of drained conditions, the rotations were smaller and the movement was more controlled.
5. The pore pressures measurement were accurate during loading and consolidation steps which were used to calculate the consolidation coefficient of the soil and the ending time of consolidation.

6. The main advantages of the proposed setup is that it can provide quick results once it is implemented in-situ while accounting for soil structure and fabric that are usually destroyed during sampling.

Based on the above observations and explanations, some improvements and recommendations are proposed for a better performance of the proposed setup:

1. For rough fast interface tests, cyclic shearing is not recommended. The soil will be highly disturbed and the test section movements and rotations will accumulate, potentially affecting the accuracy and reliability of the measured undrained resistance.
2. In order to better control the test section movements, the moment acting on the test section should be minimized/eliminated. This could be done by either using a frictionless sliding connection between the test section and the load cell instead of the ball bearing connection or by lowering the connecting point.
3. Tests should be performed at higher embedment as the ones reached in Stage 3 to limit, confine, and restrain the test section during shearing.
4. Multiple pore pressure sensors should be incorporated in the pipe tests section at various locations to provide comprehensive data on pore pressure along the pipe. The pore pressure sensors should be kept saturated throughout the testing process.
5. Additional tests should be conducted in the future on normally consolidated clay (rather than over consolidated clay) while varying the shearing rate to detect the transition from undrained to drained conditions on the interface resistance.

6. The setup should be further improved to be implemented in-situ: it should be submersible and automatically controlled. Thus, the sensors and the motor should be waterproofed, a controlling system should be incorporated to impose the test section movements and remove the dummy sections.

Having tested the setup under different conditions, the following are the main interpretations of the axial interface response:

1. The factors that affect the interface resistances are: The normal stress, the roughness, the embedment, and the drainage conditions.
2. The failure envelope of the interface at low normal stress is curved.
3. The effect of the drainage conditions is clear on the decay from peak to residual that was more prominent during the undrained cycles.
4. The peak shear stress depends on factors other than the normal stress. These include the waiting period prior to shear, the shearing rate and the number of shearing cycles.

## CHAPTER 6

### CONCLUSIONS AND RECOMMENDATIONS

#### 6.1 Thesis findings

A novel in-situ tool has been proposed for measuring the interface resistance between pipelines and underlying soils in this thesis. A proof of concept experimental setup was designed and implemented. The prototype produced could be further developed as an automated and independent field test setup. The proofing tests conducted demonstrated the potential of the proposed in-situ setup as an advanced, innovative, cost-effective and reliable test alternative to quantify the pipe-soil interface resistance in-situ. In what follows some of the key findings and tasks achieved are presented:

A ball penetrometer apparatus was specifically designed and built to measure the undrained shear strength profiles across the clay test bed used in the pipe interface experiments. The ball penetrometer apparatus was calibrated by means of extensive tests. Undrained direct shear tests, UU triaxial tests and vane shear tests were performed to establish the undrained shear strength of the used soft clay. However, the vane shear proved to be the most reliable and its results were used to evaluate the resistance factor of the ball penetrometer.

While the main emphasis has been on designing and testing a prototype of the novel interface testing apparatus, some of the early work conducted as part of this thesis focused on comparing the results obtained from the two most common laboratory interface testing methods: the tilt table and the interface direct shear. This exercise was



critical given that these two methods are by far the most commonly used approaches when testing soil-interface resistance in the low-pressure range.

A tilt table device was designed and fabricated in the lab, while an already existing direct shear device was modified to limit the mechanical friction in the system and be compatible with the stringent constraints of the low confining pressure application. Both setups were used to test the drained clay-solid interface response for various soil compositions (high and low plasticity clay), interface roughness (smooth and rough), and ranges of normal stress. The comparison suggested that using the Interface Direct Shear machine for determining the drained residual pipe-soil interface resistance is a practical and reliable testing alternative, provided that the conventional direct shear setup is properly modified to reduce mechanical friction and make it amenable to low pressure testing. The residual interface friction angles obtained from both setups were almost identical for the case of smooth interfaces whereas the interface direct shear yielded conservative friction angle values for the case of rough interfaces.

Based on the direct shear test results, it was found that the drained residual failure envelopes for the clays and the clay-solid interfaces are non-linear and could be modeled by a simple power model. The residual interface friction angles are highly correlated to the interface surface roughness, particularly when the roughness is normalized with the mean grain size. The residual and peak coating efficiencies are relatively similar ranging between 45% and 99% in function of the interface roughness.

The concept, design, and fabrication of the in-situ setup were described in details in Chapter 4. The main novelty in the proposed test setup is in the modular design of the pipe section which consists of 5 pipe segments that act as (1) main test section, (2) dummy sections that are removed to create a path for shearing, and (3) anchor sections

that allow for producing the reaction needed for the motor to displace the test section. The proposed test setup minimizes errors due to passive resistance which typically develops at the end of test pipes in other existing test devices/systems. The setup also minimizes eccentricity or upward force components that could lead to complex variations in the normal stresses at the pipe-soil interface. More importantly, the setup relies on dead weights to apply the normal stress, eliminating the need for controlling the normal stress using costly loading systems that are currently used in other in-situ test setups (ex. SMARTPIPE). Once tested on normally consolidated clay for the first time, the setup produced realistic interface friction angles that are comparable to the ones available in the literature and the ones obtained from tilt table and interface direct shear tests on the same soil and interface.

The results of the proof of concept tests that comprised the use of variable shear rates, different interface roughnesses, and different embedment levels performed inside a clay bed were promising and demonstrated the practicality and functionality of the novel apparatus and opened the path towards some improvements that are still needed to optimize testing effectiveness. The drained interface resistance was reliably and repeatedly measured using the in-situ setup for a rough and a smooth interface. For the smooth interface, the resulting secant friction angles and residual drained friction factors compare favorably with the results of the direct shear tests performed on the same soil and the same interface. Results from the rough tests indicated a failure mode that was internal to the clay, unlike the interface direct shear tests that indicated a forced clay/interface failure. This resulted in interface friction angles for the rough interface that were higher than those observed in the interface direct shear tests. This was

attributed to possibility of formation of multiple failure planes in the in-situ pipe model tests where the sheared soil is not restraint as in case of the direct shear.

Under undrained conditions, the measured interface response was realistic. However, as the test section was free to move, it exhibited slight uncontrolled rotations in all directions when it was pushed fast, especially when the embedment was very small and when consecutive cycles were executed. Some soils were thus pushed during shearing and the pore pressure readings were complex.

In brief, the proposed novel pipe testing setup was proven to reliably capture the effect of drainage conditions and rate of loading on the interface resistance. The setup allows for conducting continuous shearing cycles in two directions and allows for forcing waiting time between cycles to allow for pore pressure dissipation. More importantly, by increasing the pipe embedment at the same location in the same bed, the effect of normal stress on the interface response could be investigated. This allows for determining the curvature in the interface Mohr-Coulomb failure envelop from one testing location in any future field application. Finally, the limited number of pore water pressure sensors that were incorporated in the model pipe section allowed for monitoring the generation and dissipation of pore water pressure at the interface at all stages of testing, which included pipe penetration, consolidation, and shearing.

## **6.2 Suggestion for future research**

This work has shown the advantages of the proposed in-situ testing setup for estimating the interface resistance. However, it revealed the need for the following improvements and some of the aspects that must be covered in future work.

### **6.2.1 Setup Improvements:**

- The setup must be converted into a fully independent field test setup. The challenges while moving in that direction involve designing a fully automated mechanical mechanism that could detach the test section and the dummy sections from the central aluminum bar without manual intervention. The other challenge is automating the process of removing the dummy sections in preparation for shearing.
- The setup is going to be deployed in offshore environments, the motor and other parts of the system have to be sealed within water-proofed chambers.
- In order to better control the movement of the test section, any resulting moments acting on it should be minimized or eliminated. This could be done by either using a frictionless sliding connection between the test section and the load cell instead of the ball bearing connection adopted for the prototype, or by lowering the connecting point.
- Multiple pore pressure sensors should be incorporated in the pipe tests section at various locations to provide comprehensive data on pore pressure along the pipe. Such pore pressure measurements would be key for making decision during all stages of testing including (1) marking the full dissipation of pore pressure and the end of consolidation (2) reflecting the field coefficient of consolidation of the clay under the pipe, and (3) reflecting the degree of overconsolidation of the soil (positive versus negative pore pressure generation during shear), and (4) indicating non-uniform distribution of pressure under the pipe as a result of a potential overturning moment.
- Pressure sensors should be added to the test section and the anchoring sections for an accurate estimation of the normal stresses acting along the pipe-soil interface.

Such measurements would also be used to estimate the penetration resistance upon setup laying down.

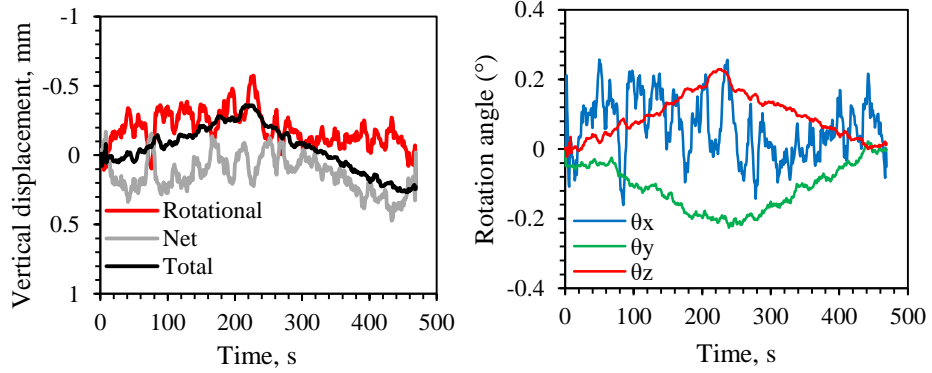
### **6.2.2 *Uncovered Aspects***

- The validity of interface direct shear tests with rough interfaces will need to be verified in the future with additional tests involving different types of soils and different pipe roughness.
- Additional tests should be conducted on a truly normally consolidated clay bed (rather than over consolidated clay) while varying the shearing rate to detect the transition from undrained to drained conditions on the interface resistance.
- Numerical simulations may be attempted and validated using the experimental data, and then used for additional parametric studies involving changes to all the key variables.

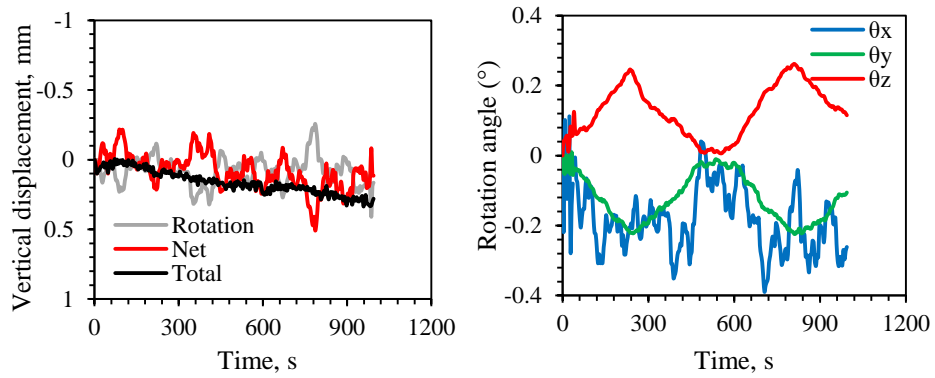
# APPENDIX A

## a. Vertical displacements and rotation angles during Stage 1 (Stainless Steel Interface)

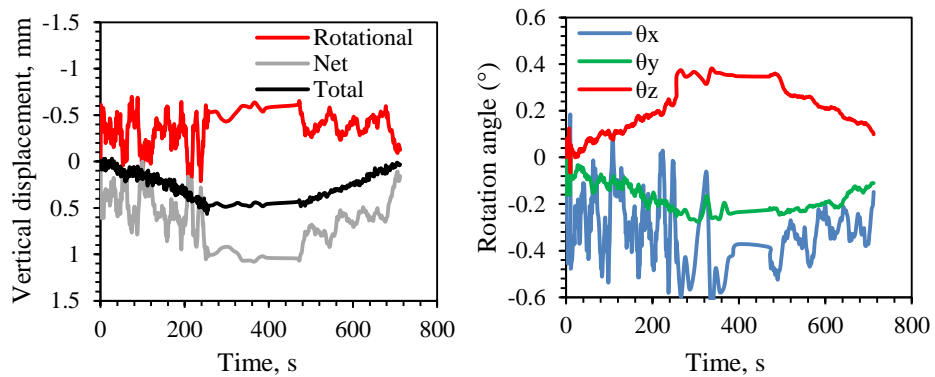
### 1. F2-S1



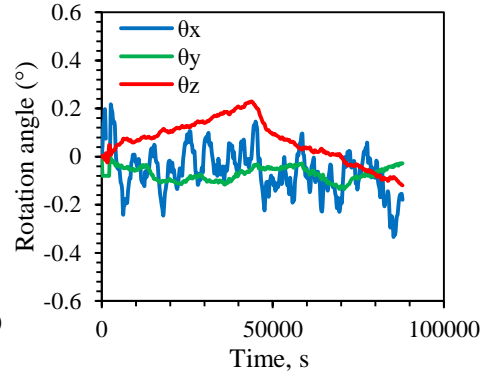
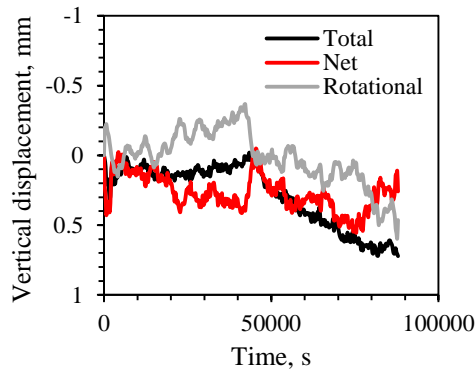
### 2. F3-S1



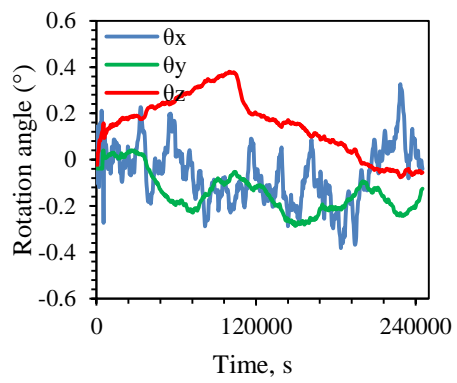
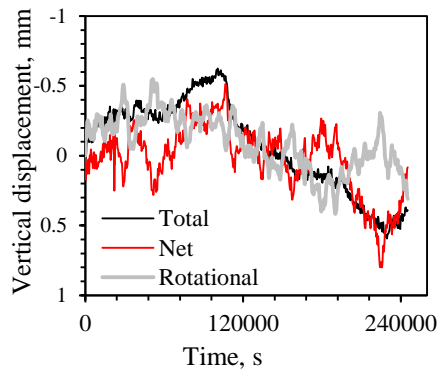
### 3. F4-S1:



#### 4. D1-S1

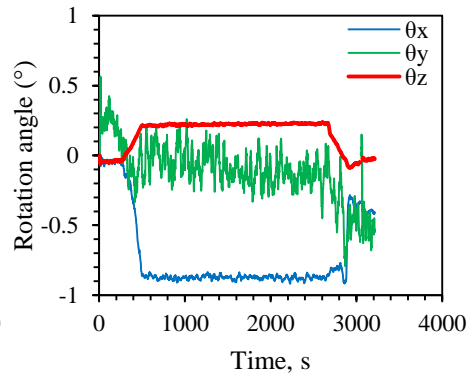
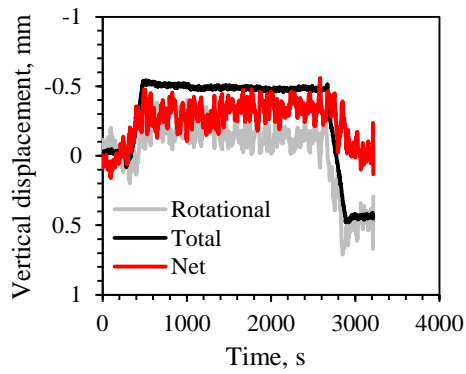


#### 1. D2-S1:

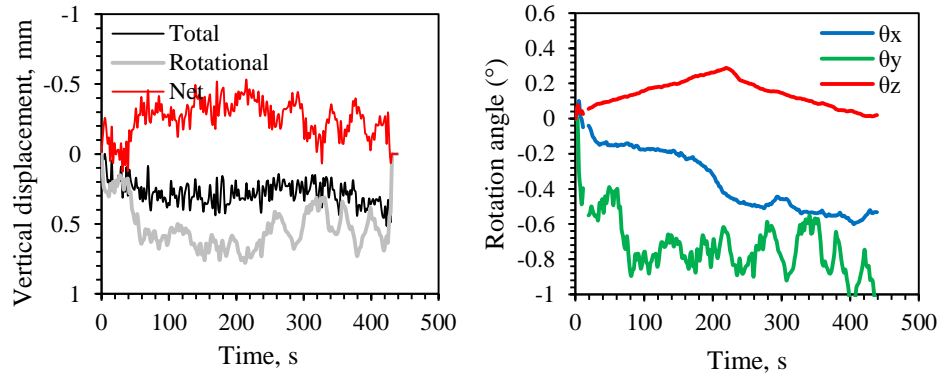


### b. Vertical displacements and rotation angles during Stage 2 (Stainless Steel Interface)

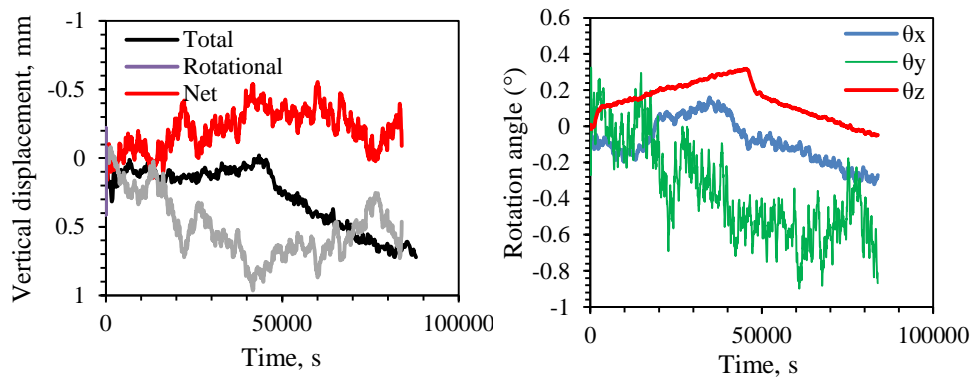
#### 1. F1-S2:



## 2. F2-S2

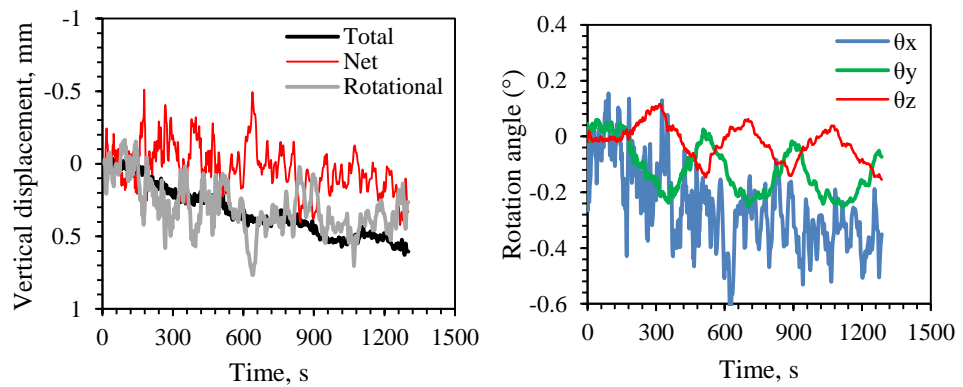


## 3. D-S2



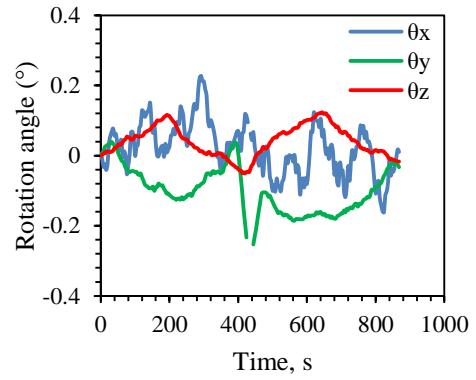
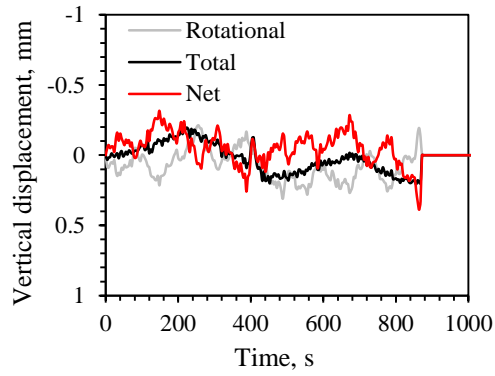
## c. Vertical displacements and rotation angles during Stage 1 (Stainless Steel Interface)

### 1. F1-S3

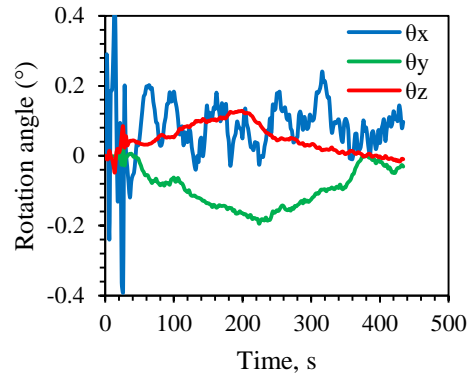
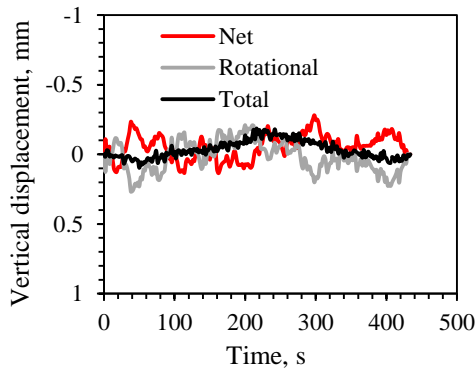




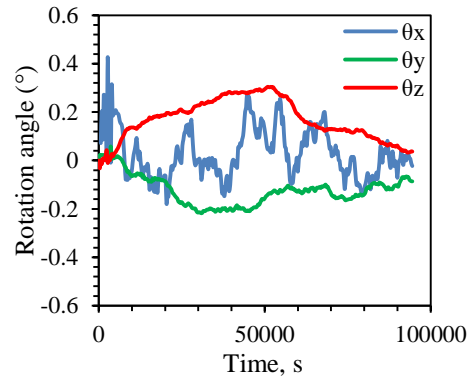
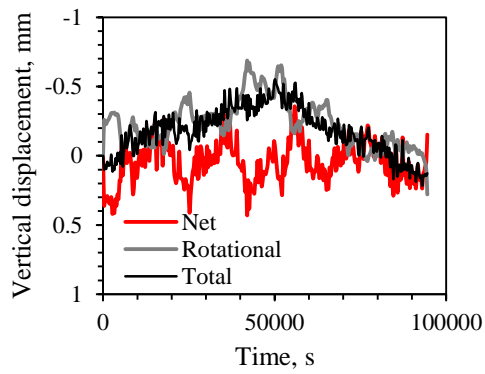
## 2. F2-S3



## 3. F3-S3



## 4. D-S3



## REFERENCES

- Ads, A, M. Iskander, and S. Bless (2019). Shear Strength of a Synthetic Transparent Soft Clay Using a Miniature Ball Penetrometer Test,” *Geotechnical Testing Journal* <https://doi.org/10.1520/GTJ20190020>.
- ASTM D4648 / D4648M-16, Standard Test Methods for Laboratory Miniature Vane Shear Test for Saturated Fine-Grained Clayey Soil, ASTM International, West Conshohocken, PA, 2016, [www.astm.org](http://www.astm.org)
- ASTM D2850-15, Standard Test Method for Unconsolidated-Undrained Triaxial Compression Test on Cohesive Soils, ASTM International, West Conshohocken, PA, 2015, [www.astm.org](http://www.astm.org)
- Aubeny, C. P., Shi, H., & Murff, J. D. (2005). Collapse loads for a cylinder embedded in trench in cohesive soil. *International Journal of Geomechanics*, 5(4), 320–325. [https://doi.org/10.1061/\(ASCE\)1532-3641\(2005\)5:4\(320\)](https://doi.org/10.1061/(ASCE)1532-3641(2005)5:4(320))
- Ballard, J.-C., & Jewell, R. (2013). *Observations of pipe-soil response from in-situ measurements*. May, 6–9. <https://doi.org/10.4043/24154-ms>
- Boukpeti, N., & White, D. J. (2017a). Interface shear box tests for assessing axial pipe-soil resistance. *Geotechnique*, 67(1), 18–30. <https://doi.org/10.1680/jgeot.15.P.112>
- Boukpeti, N., & White, D. J. (2017b). Interface shear box tests for assessing axial pipe-soil resistance. *Géotechnique*, 67(1), 18–30. <https://doi.org/10.1680/jgeot.15.p.112>
- Boylan, N. P., White, D. J., & Brunning, P. (2014). Seabed friction on carbonate soils: Physical modelling of axial pipe-soil friction. *Proceedings of the Annual Offshore Technology Conference*, 5(May), 3342–3358. <https://doi.org/10.4043/25398-ms>

- Brier, C. De, Geoconsulting, J. B. F., & A, D. C. T. S. (2016). *On the added value of advanced interface shear testing for pipeline walking mitigation*. 1–15.
- Bruton, D. A. S., Sinclair, F., & Carr, M. (2010). Lessons learned from observing walking of pipelines with lateral buckles, including new driving mechanisms and updated analysis models. *Proceedings of the Annual Offshore Technology Conference*, 3(August 2016), 1970–1981. <https://doi.org/10.4043/20750-ms>
- Bruton, D., Carr, M., & White, D. J. (2007). *The Influence Of Pipe-Soil Interaction On Lateral Buckling And Walking of Pipelines- The SAFEBUCK JIP*.
- Carr, M., Sinclair, F., & Bruton, D. (2006). Pipeline walking-understanding the field layout challenges and analytical solutions developed for the safebuck JIP. *SPE Projects, Facilities and Construction*, 3(3). <https://doi.org/10.2118/120022-pa>
- Chatterjee, S., Randolph, M. F., & White, D. J. (2012). The effects of penetration rate and strain softening on the vertical penetration resistance of seabed pipelines. *Geotechnique*, 62(7), 573–582. <https://doi.org/10.1680/geot.10.P.075>
- Chatterjee, S., Yan, Y., Randolph, M. F., & White, D. J. (2012). Elastoplastic consolidation beneath shallowly embedded offshore pipelines. *Géotechnique Letters*, 2(2), 73-79.
- De Brier, C., Ballard, J.-C., & Colliard, D. (2016). On the added value of advanced interface shear testing for pipeline walking mitigation. *Proc. Offshore Pipeline Technology Conf. Amsterdam, Feb. 24-25*, 1–15.
- Dejong, J., Yafrate, N., Degroot, D., Low, H. E., & Randolph, M. (2010). Recommended practice for full-flow penetrometer testing and analysis. *Geotechnical Testing*

*Journal*, 33(2), 137–149. <https://doi.org/10.1520/GTJ102468>

- Dendani, H., & Jaeck, C. (2007). Pipe-soil interaction in highly plastic clays. In *Offshore Site Investigation and Geotechnics: Confronting New Challenges and Sharing Knowledge*. Society of Underwater Technology
- Eid, H. T., Al-Nohmi, N. M., Wijewickreme, D., & Amarasinghe, R. S. (2019). Drained Peak and Residual Interface Shear Strengths of Fine-Grained Soils for Pipeline Geotechnics. *Journal of Geotechnical and Geoenvironmental Engineering*, 145(10). [https://doi.org/10.1061/\(ASCE\)GT.1943-5606.0002131](https://doi.org/10.1061/(ASCE)GT.1943-5606.0002131)
- Eid, H. T., Amarasinghe, R. S., Rabie, K. H., & Wijewickreme, D. (2014). Residual shear strength of fine-grained soils and soil–solid interfaces at low effective normal stresses. *Canadian Geotechnical Journal*, 52(2), 198–210. <https://doi.org/10.1139/cgj-2014-0019>
- Eid, H. T., Amarasinghe, R. S., Rabie, K. H., & Wijewickreme, D. (2015). Residual shear strength of fine-grained soils and soil–solid interfaces at low effective normal stresses. *Canadian Geotechnical Journal*, 52(2), 198–210. <https://doi.org/10.1139/cgj-2014-0019>
- Einav, I., & Randolph, M. F. (2005). Combining upper bound and strain path methods for evaluating penetration resistance. *International journal for numerical methods in engineering*, 63(14), 1991–2016.
- Ganesan, S., Kuo, M., & Bolton, M. (2014). Influences on Pipeline Interface Friction Measured in Direct Shear Tests. *Geotechnical Testing Journal*, 37(1), 20130008. <https://doi.org/10.1520/gtj20130008>

- Hill, A. J., White, D. J., Bruton, D. A. S., Langford, T., Meyer, V., Jewell, R., & Ballard, J. C. (2012). A new framework for axial pipe-soil resistance, illustrated by a range of marine clay datasets. *Offshore Site Investigation and Geotechnics 2012: Integrated Technologies - Present and Future, OSIG 2012, January*, 367–377.
- Hill, Andrew John, & Jacob, H. (2008). *In-Situ Measurement of Pipe-Soil Interaction in Deep Water*. May, 5–8. <https://doi.org/10.4043/19528-ms>
- IEA (2018), *Offshore Energy Outlook 2018*, IEA, Paris  
<https://www.iea.org/reports/offshore-energy-outlook-2018>
- Kuo, M., & Bolton, M. (2013). The nature and origin of deep ocean clay crust from the Gulf of Guinea. *Geotechnique*, 63(6), 500–509.  
<https://doi.org/10.1680/geot.10.P.012>
- Kuo, M. Y., Vincent, C. M., Bolton, M. D., Hill, A., & Rattley, M. (2015). A new torsional shear device for pipeline interface shear testing. *Frontiers in Offshore Geotechnics III - Proceedings of the 3rd International Symposium on Frontiers in Offshore Geotechnics, ISFOG 2015*, 405–410. <https://doi.org/10.1201/b18442-45>
- Kodikara, J., Barbour, S., & Fredlund, D. (1999). Changes in Clay Structure and Behaviour Due to Wetting and Drying. *Non-Serials*, 179–185.  
<https://search.informit.org/doi/10.3316/informit.730113752528813> (Original work published January 1999)
- Low, H. E., Randolph, M. F., Rutherford, C., Bernard, B. B., & Brooks, J. M. (2008). *Characterization of Near Seabed Surface Sediment*. <https://doi.org/10.4043/19149-ms>
- Lee, K. K., M. J. Cassidy, and M. F. Randolph. 2012. “Use of Epoxy in Developing

- Miniature Ball Penetrometers.”*International Journal of Physical Modelling in Geotechnics* 12, no. 3 (September): 119–128.  
<https://doi.org/10.1680/ijpmg.11.00016>
- Low, H., Ramm, M., Bransby, M., White, D., & Westgate, Z. (2017). Effect of through-life changes in soil strength and axial pipe-seabed resistance for HPHT pipeline design. *Proc. Int. Conf. on Offshore Site Investigation and Geotechnics. SUT, London.*, 675, 841–849.
- Lunne, T., Andersen, K. H., Low, H. E., Randolph, M. F., & Sjørusen, M. (2011). Guidelines for offshore in situ testing and interpretation in deepwater soft clays. *Canadian Geotechnical Journal*, 48(4), 543–556. <https://doi.org/10.1139/t10-088>
- Merifield, R. S., White, D. J., & Randolph, M. F. (2009). Effect of surface heave on response of partially embedded pipelines on clay. *Journal of Geotechnical and Geoenvironmental Engineering*, 135(6), 819-829.
- Najjar, Shadi S, Gilbert, R. B., Hall, C., & McCarron, B. (2003). *Omae2003- 37499*. 1–8.
- Najjar, Shady S., Gilbert, R. B., Liedtke, E., McCarron, B., & Young, A. G. (2007). Residual shear strength for interfaces between pipelines and clays at low effective normal stresses. *Journal of Geotechnical and Geoenvironmental Engineering*, 133(6), 695–706. [https://doi.org/10.1061/\(ASCE\)1090-0241\(2007\)133:6\(695\)](https://doi.org/10.1061/(ASCE)1090-0241(2007)133:6(695))
- Pedersen, R. C., Olson, R. E., & Rauch, A. F. (2003). Shear and interface strength of clay at very low effective stress. *Geotechnical Testing Journal*, 26(1), 71–78.  
<https://doi.org/10.1520/gtj11104j>
- Peuchen, J., Adrichem, J., & Hefer, P. A. (2005). Practice notes on push-in penetrometers

- for offshore geotechnical investigation. *Frontiers in Offshore Geotechnics, ISFOG 2005 - Proceedings of the 1st International Symposium on Frontiers in Offshore Geotechnics*, 973–979. <https://doi.org/10.1201/noe0415390637.ch117>
- Randolph, M. (2004). *Characterisation of soft sediments for offshore applications*.
- Randolph, M. F., & White, D. (2008). *Pipeline Embedment in Deep Water: Processes and Quantitative Assessment*. May. <https://doi.org/10.4043/19128-ms>
- Schneider, M. A., Stanier, S. A., White, D. J., & Randolph, M. F. (2020). Apparatus for measuring pipe-soil interaction behavior using shallow “Pipe-like” penetrometers. *Geotechnical Testing Journal*, 43(3). <https://doi.org/10.1520/GTJ20180293>
- Senthilkumar, M., Kodikara, J., Rajeev, P., & Robert, D. J. (2013). Axial pipe-soil interaction behaviour of offshore pipelines. *Australian Geomechanics Journal*, 48(4), 123–136.
- Shi, Y. M., Wang, N., Gao, F. P., Qi, W. G., & Wang, J. Q. (2019). Physical modeling of the axial pipe-soil interaction for pipeline walking on a sloping sandy seabed. *Ocean Engineering*, 178(February), 20–30. <https://doi.org/10.1016/j.oceaneng.2019.02.059>
- Smith, V. B., & White, D. J. (2014). Volumetric hardening in axial pipe soil interaction. *Proceedings of the Annual Offshore Technology Conference*, 2(March), 1611–1621. <https://doi.org/10.4043/24856-ms>
- Stanier, S. A., White, D. J., Chatterjee, S., Brunning, P., & Randolph, M. F. (2015). A tool for ROV-based seabed friction measurement. *Applied Ocean Research*, 50, 155–162. <https://doi.org/10.1016/j.apor.2015.01.016>

- Stark, T. D., & Eid, H. T. (1993). Modified Bromhead Ring Shear Apparatus. *Geotechnical Testing Journal, ASTM, 16*(1), 100–107.
- Stewart, D. P. and M. F. Randolph. 1991. “A New Site Investigation Tool for the Centrifuge.” In International Conference Centrifuge, 35–40. Rotterdam, the Netherlands: Balkema.
- Westgate, Z. J., White, D. J., & Randolph, M. F. (2013). *fine-grained soils*. 27(May 2012), 15–27.
- Westgate, Z. J., White, D. J., & Savazzi, M. (2018). *OTC-28671-MS Experience with Interface Shear Box Testing for Axial Pipe-Soil Interaction Assessment on Soft Clay*.
- White, D., Bruton, D. A. S., Bolton, M., Hill, A. J., Ballard, J.-C., & Langford, T. (2011). *SAFEBUCK JIP - Observations of Axial Pipe-soil Interaction from Testing on Soft Natural Clays*. September 2014. <https://doi.org/10.4043/21249-ms>
- White, D. J., Campbell, M. E., Boylan, N. P., & Bransby, M. F. (2012). A new framework for axial pipe-soil interaction, illustrated by shear box tests on carbonate soils. *Offshore Site Investigation and Geotechnics 2012: Integrated Technologies - Present and Future, OSIG 2012*, 379–387.
- White, D. J., & Cathie, D. N. (2011). Geotechnics for subsea pipelines. In *Frontiers in Offshore Geotechnics II - Proceedings of the 2nd International Symposium on Frontiers in Offshore Geotechnics* (Issue December 2015). <https://doi.org/10.1201/b10132-6>
- White, D. J., Clukey, E. C., Randolph, M. F., Bransby, M. F., Zakeri, A., Hill, A. J., & Jaek, C. (2017). The state of knowledge of pipe-soil interaction for on-bottom



- pipeline design. *Proceedings of the Annual Offshore Technology Conference*, 2, 969–995. <https://doi.org/10.4043/27623-ms>
- White, D. J., Hill, A. J., Westgate, Z. J., & Ballard, J. C. (2011). Observations of pipe-soil response from the first deep water deployment of the SMARTPIPE®. *Frontiers in Offshore Geotechnics II - Proceedings of the 2nd International Symposium on Frontiers in Offshore Geotechnics*, October, 851–856. <https://doi.org/10.1201/b10132-125>
- White, David J., & Randolph, M. F. (2007). *Seabed Characterisation And Models For Pipeline-Soil Interaction*.
- Wijewickreme, D., Amarasinghe, R., & Eid, H. (2014). Macro-scale direct shear test device for assessing soil-solid interface friction under low effective normal stresses. *Geotechnical Testing Journal*, 37(1). <https://doi.org/10.1520/GTJ20120217>
- Young, A. G., Honganen, C. D., Silva, A. J., & Bryant, W. R. (2000). Comparison of geotechnical properties from large-diameter long cores and borings in deep water Gulf of Mexico. *Proceedings of the Annual Offshore Technology Conference*, 1, 427–438. <https://doi.org/10.4043/12089-ms>

